

**Design and synthesis of renewable lipid-based nanocarriers with  
thermosensitivity for targeted drug delivery applications**

by

Huiqi Wang

A thesis submitted in partial fulfillment of the requirements for the degree of

Doctor of Philosophy

in

Bioresource and Food Engineering

Department of Agricultural, Food and Nutritional Science

University of Alberta

© Huiqi Wang, 2024

## ABSTRACT

Numerous drug molecules currently available on the market suffer from short half-life, *in vivo* instability, poor bioavailability, rapid degradation and inappropriate distribution. While nanocarriers have emerged as a promising solution to address these issues, the primary objective and challenge in modern medicine lie in achieving successful drug delivery in a targeted and controllable manner. Ongoing innovations are exploring the use of biocompatible, biodegradable, and sustainable materials for drug delivery. Among these, lipids, as naturally occurring biomolecules, have found extensive applications in the pharmaceutical industry. However, examples of utilizing fatty acids as hydrophobic building blocks to fabricate amphiphilic block copolymers for drug delivery are relatively scarce. This study aimed to synthesize and investigate thermoresponsive renewable lipid-based block copolymers, along with their bioconjugates with proteins, as a means of achieving effective anti-cancer drug delivery.

The self-assembly of amphiphilic macromolecules to form polymeric micelles is considered as one of the most potent drug delivery systems. In the first study, a stearic acid-based polymer, poly(2-methacryloyloxy) ethyl stearate (PSAMA), was synthesized by microwave-assisted reversible addition-fragmentation chain transfer (RAFT) polymerization, and it was subsequently utilized as a macro-chain transfer agent (CTA) to block copolymerize with N-isopropylacrylamide (NIPAM) to produce the thermoresponsive amphiphilic block copolymer PSAMA-*b*-PNIPAM. These block copolymers with variable hydrophobic block length self-assembled in aqueous media and formed spherical nanoparticles of ~30 nm with low critical micelle concentration (CMC). The hydrophobic model drug, carbamazepine (CBZ), was chosen to assess the micelles' performance as nanocarriers, achieving a loading efficiency of 31.6% into

PSAMA-*b*-PNIPAM micelles. The drug release displayed an obvious temperature-triggered response at body temperature, with a sustained and slow release lasting up to 84 h.

In the second study, the impact of fatty acid type on self-assembly and drug encapsulation was explored. Two distinct fatty acid-based polymers, poly(vinyl stearate) (PVS) and poly(vinyl laurate) (PVL), were synthesized as the hydrophobic segments for the polymeric micelles. The hydrophilic shell was formed using another thermoresponsive polymer, poly(N-vinylcaprolactam) (PNVCL), known for its excellent biocompatibility, biodegradability, and non-toxicity. By varying fatty acid types and adjusting hydrophilic/hydrophobic block lengths, the self-assembly behavior of the block copolymer (PVS/PVL-*b*-PNVCL) was found to be highly tunable in terms of morphology and particle size. Specifically, PVS-*b*-PNVCL micelles tended to form smaller, spherical structures (~80 nm) with an increase in hydrophilic block length, while both worm-like and spherical structures with an average size of 111 nm were observed when the repeating unit of PNVCL was 35. Notably, micelles made from PVL-*b*-PNVCL exhibited exclusive spherical morphology and larger particle sizes (130-145 nm) with a relatively broad size distribution. Additionally, PVS-*b*-PNVCL polymeric micelles demonstrated high drug loading capacity for anticancer drug doxorubicin (DOX), along with good serum stability, controlled drug release, favorable biocompatibility, and efficient *in vitro* uptake.

The third study outlined the development of a protein-polymer bioconjugate comprising bovine serum albumin (BSA) and a lipid-based thermoresponsive amphiphilic block copolymer (PVS-*b*-PNVCL). The resulting bioconjugates exhibited a well-defined structure, low cytotoxicity and commendable biocompatibility with different cell lines. In an aqueous environment, the amphiphilic BSA-polymer conjugates can self-assemble into vesicular compartment with a particle size of approximately 200 nm. DOX was effectively encapsulated into the conjugates with

a high loading capacity of 25.6%, demonstrating an effective *in vitro* antitumor activity and efficient cellular uptake. Notably, the lower critical solution temperature (LCST) of the bioconjugates was fine-tuned to around 40 °C through the integration of hydrophilic BSA. This temperature modulation facilitated targeted drug delivery to tumors, allowing enhanced therapeutic efficacy of the bioconjugates.

Overall, this PhD research highlights the potential for advancing smart drug delivery nanocarrier platforms by exploring renewable materials as hydrophobic building blocks. The findings hold promise for future advancements in biobased and biocompatible carrier systems in cancer therapies.

## PREFACE

This thesis contains original work done by Huiqi Wang, which is written according to the guidelines for a paper format thesis of the Faculty of Graduate Studies and Research at the University of Alberta.

The thesis consisted of six chapters: Chapter One provides a general introduction to the context, the hypothesis, and the objectives of the thesis. Chapter Two comprises a literature review covering several topics related to the thesis.

Chapter Three has been published as Huiqi Wang, Aman Ullah. (2022). “Synthesis and Evaluation of Thermoresponsive Renewable Lipid-Based Block Copolymers for Drug Delivery”. *Polymers*, 14(17), 3436. I am responsible for designing and conducting experiments, analyzing data, and drafting the manuscript. Dr. Ullah contributed to the conceptualization, manuscript review, editing, and manuscript submission.

Chapter Four has been published as Huiqi Wang, Lin Xu, Xing-Zhen Chen, Aman Ullah. (2024). “Tunable self-assembly of lipid-based block polymeric micelles with temperature-sensitive poly (vinylcaprolactam) shell for effective anticancer drug delivery”. *European Polymer Journal*, 206, 112795. I am responsible for conceptualization, designing and conducting experiments, analyzing data, and drafting the manuscript. Dr. Ullah contributed to the conceptualization, manuscript review, editing, and manuscript submission. Dr. Xu made contributions in performing cellular studies and analyzing data for cell experiments. Dr. Chen contributed to manuscript editing.

Chapter Five has been prepared as a manuscript for submission to peer-reviewed journal as Huiqi Wang, Xiaoling Deng, Xing-Zhen Chen, Aman Ullah. “Polymersomes prepared from

lipid-based protein-polymer conjugate with temperature-sensitivity for targeted drug delivery applications”. I am responsible for conceptualization, designing and conducting experiments, analyzing data, and drafting the manuscript. Dr. Ullah contributed to the conceptualization, manuscript review, editing, and manuscript submission. Xiaoling Deng made contributions in performing cellular studies and analyzing data for cell experiments. Dr. Chen helped in providing facilities for cellular studies.

Chapter Six provides an overall conclusion and outlines future directions for the studies discussed.

## **DEDICATION**

*To all scientific researchers who never say never.*

*Let's make a difference.*

## ACKNOWLEDGEMENTS

First and foremost, I would like to sincerely express my deep gratitude to my supervisor Dr. Aman Ullah for providing me the opportunity to pursue my Ph.D. and for his countless mentorship, support, encouragement, and guidance throughout the program. I would like to extend my deepest gratitude to Dr. Feral Temelli and Dr. Guanqun(Gavin) Chen for being my supervisory committee members and for their support, guidance, and constructive criticism of my research. I would like to thank Dr. Hongbo Zeng and Dr. Ravin Narain for accepting the invitation to serve as external examiners in my candidacy. I am also thankful to my defense external examiner Dr. Luyi Sun for sparing valuable time to read and evaluate my thesis.

I extend my sincere appreciation to Dr. Xing-Zhen Chen, Dr. Lin Xu, and Xiaoling Deng for their assistance in conducting the cellular studies, a crucial component of my research endeavors. I am grateful to Dr. Kacie Norton, Pinzhang(Priscilla) Gao and Dr. Xuejun Sun for their professional guidance and assistance in TEM imaging. I am thankful to Ereddad Kharraz for his mentoring and training in using different pieces of equipment. Additionally, my gratitude extends to the Chemistry NMR Laboratory, specifically Nupur Dabral and Dr. Mark Miskolzie, for their support in NMR spectroscopy. Special thanks go to Jing Zheng from the Chemistry Mass Spectrometry Laboratory for her unwavering help with MALDI-TOF MS analysis. I also would like to express my profound thanks to Gareth Lambkin for providing access to the centrifuge.

I am also thankful to my past and current labmates in Lab SAB-540: Dr. Muhammad Arshad, Dr. Muhammad Faisal Irfan, Dr. Yanet Rodriguez Herrero, Dr. Irum Zahara, Dr. Muhammad Zubair, Karen Lopez-Camas, Siti Amirah Binti Haji Yussof, Punita Upadhyay, Guojuan Xu and many more. I appreciate your help and assistance in my research. My heartfelt

appreciation goes to my friends, Dr. Jin Xie, Hungyi(Jonathan) Yang, Yueying Huang and Dr. Jing Zhou. Thank you for cheering me up, encouragement and company. Finally, my deepest gratitude goes to my parents and my grandparents for their endless love, trust, and encouragement throughout my life. Words cannot express my thanks for your immense support and encouragement.

## TABLE OF CONTENTS

<b>ABSTRACT</b> .....	<b>ii</b>
<b>PREFACE</b> .....	<b>v</b>
<b>ACKNOWLEDGEMENTS</b> .....	<b>viii</b>
<b>TABLE OF CONTENTS</b> .....	<b>x</b>
<b>LIST OF TABLES</b> .....	<b>xiv</b>
<b>LIST OF FIGURES</b> .....	<b>xv</b>
<b>LIST OF SCHEMES</b> .....	<b>xvii</b>
<b>LIST OF ABBREVIATIONS</b> .....	<b>xviii</b>
<b>CHAPTER 1. General Introduction and Thesis Objectives</b> .....	<b>1</b>
1.1 General introduction.....	1
1.1.1 Challenges and opportunities in drug delivery .....	1
1.1.2 Renewable lipid derived bio-based materials in drug delivery .....	3
1.2 Hypotheses .....	5
1.3 Objectives.....	5
1.4 References .....	6
<b>CHAPTER 2. Literature Review</b> .....	<b>11</b>
2.1 Amphiphilic block copolymer.....	11
2.1.1 Microwave-assisted RAFT polymerization.....	12
2.1.1.1 RAFT polymerization .....	12
2.1.1.2 Microwave-assisted synthesis.....	15
2.1.2 Self-assembling micelle behaviours .....	17
2.1.3 Applications in drug delivery .....	19
2.2 Protein-polymer bioconjugate .....	23
2.2.1 Synthetic approaches .....	24
2.2.2 Self-assembly of protein-polymer conjugates .....	27
2.2.3 Application as drug nanocarriers .....	28
2.3 Thermoresponsive polymeric materials in targeted drug delivery .....	29
2.3.1 Tumor-targeted drug delivery.....	31
2.3.2 Thermoresponsive polymers.....	33

2.3.3 Thermoresponsive micellar drug delivery systems .....	36
2.4 References .....	38
<b>CHAPTER 3. Synthesis and Evaluation of Thermoresponsive Renewable Lipid-based Block Copolymers for Drug Delivery .....</b>	<b>59</b>
3.1 Introduction .....	59
3.2 Materials and methods .....	62
3.2.1 Materials .....	62
3.2.2 Synthesis of 2-(methacryloyloxy) ethyl stearate (SAMA) .....	63
3.2.3 Synthesis of homopolymers.....	63
3.2.4 Synthesis of PSAMA- <i>b</i> -PNIPAM block copolymer .....	64
3.2.5. Characterization of polymers.....	65
3.2.6. Determination of critical micelle concentration (CMC).....	66
3.2.7. Micelle formation .....	66
3.2.8. Drug loading within micelles .....	66
3.2.9. <i>In vitro</i> drug release study .....	67
3.3 Results and discussion.....	67
3.3.1. Synthesis of block copolymer PSAMA- <i>b</i> -PNIPAM.....	67
3.3.2. Characterization of PSAMA- <i>b</i> -PNIPAM.....	70
3.3.3. Self-assembly study of PSAMA- <i>b</i> -PNIPAM.....	73
3.3.4. CMC determination .....	76
3.3.5. Drug loading and release behavior of block copolymer PSAMA- <i>b</i> -PNIPAM .....	77
3.4 Conclusions .....	80
3.5 References .....	81
<b>CHAPTER 4. Tunable Self-assembly of Lipid-based Block Polymeric Micelles with Temperature-sensitive Poly(vinylcaprolactam) Shell for Effective Anticancer Drug Delivery .....</b>	<b>89</b>
4.1 Introduction .....	89
4.2 Materials and methods .....	92
4.2.1 Materials .....	92
4.2.2 Synthesis of O-ethyl-S-(1-methoxycarbonyl) ethyldithiocarbonate (XA1) .....	93
4.2.3 Synthesis of PVS and PVL macro-CTA.....	93
4.2.4 Synthesis of PVS- <i>b</i> -PNVCL and PVL- <i>b</i> -PNVCL block copolymers.....	94

4.2.5	Characterization of the block copolymer.....	94
4.2.6	Preparation and characterization of micelles.....	95
4.2.7	Determination of critical micelle concentration (CMC).....	96
4.2.8	DOX encapsulation and <i>in vitro</i> release studies.....	96
4.2.8.1	Preparation of DOX-loaded micelles.....	96
4.2.8.2	Temperature-triggered release of DOX.....	97
4.2.9	Serum stability of the micelles .....	97
4.2.10	Cell experiments.....	98
4.2.10.1	Cell culture.....	98
4.2.10.2	Cell viability assay.....	98
4.2.10.3	Cellular uptake assay .....	98
4.3	Results and Discussion.....	99
4.3.1	Synthesis and characterization of PVS- <i>b</i> -PNVCL and PVL- <i>b</i> -PNVCL.....	100
4.3.2	Self-assembly behaviour of block copolymers.....	104
4.3.3	Drug encapsulation and <i>in vitro</i> temperature-triggered release of PVS/PVL- <i>b</i> -PNVCL .....	110
4.3.4	Stability of PVS- <i>b</i> -PNVCL in the presence of serum proteins .....	114
4.3.5	<i>In vitro</i> cytotoxicity of PVS- <i>b</i> -PNVCL.....	115
4.3.6	<i>In vitro</i> uptake of PVS- <i>b</i> -PNVCL in cellular models.....	116
4.4	Conclusions .....	118
4.5	References .....	119
<b>CHAPTER 5. Polymersomes Prepared from Lipid-based Protein-polymer Conjugate with Temperature-sensitivity for Targeted Drug Delivery .....</b>		<b>127</b>
5.1	Introduction.....	127
5.2	Materials and methods .....	130
5.2.1	Materials.....	130
5.2.2	Synthesis of S-2-(3-(pyridin-2-yl)disulfanyl)propyl propanoate)-O-ethyl xanthate (X2) .....	130
5.2.3	Synthesis of PVS and PVS- <i>b</i> -PNVCL with PDS functionality .....	131
5.2.4	Reduction of bovine serum albumin (BSA) and determination of free thiols using Ellman's assay .....	132

5.2.5	Conjugation of the reduced BSA to polymers.....	132
5.2.6	Thermally induced precipitation.....	133
5.2.7	LCST determination of the bioconjugates.....	133
5.2.8	Preparation of DOX-loaded BSA-polymer nanoparticles .....	133
5.2.9	Characterization.....	134
5.2.10	<i>In vitro</i> cell viability assay.....	135
5.2.11	Cellular uptake assay .....	136
5.3	Results and discussion.....	136
5.3.1	Preparation of pyridyl disulfide functional homopolymers and block copolymers ...	138
5.3.2	Preparation and characterization of BSA-PVS- <i>b</i> -PNVCL bioconjugates.....	141
5.3.3	Self-assembly behaviour of BSA-PVS- <i>b</i> -PNVCL bioconjugates.....	144
5.3.4	Thermoresponsiveness of bioconjugates.....	145
5.3.5	Drug-loaded protein-polymer bioconjugates.....	147
5.3.6	<i>In vitro</i> cytotoxicity of BSA-PVS- <i>b</i> -PNVCL conjugate .....	149
5.3.7	<i>In vitro</i> uptake of bioconjugates in cellular models .....	151
5.4	Conclusions .....	154
5.5	References .....	155
<b>CHAPTER 6. General Discussion and Future Directions .....</b>		<b>161</b>
6.1	General conclusions .....	161
6.2	Recommendations for future research.....	164
<b>BIBLIOGRAPHY .....</b>		<b>166</b>
<b>APPENDIX A: Supplementary Information of Chapter 3 .....</b>		<b>206</b>
<b>APPENDIX B: Supplementary Information of Chapter 4 .....</b>		<b>207</b>
<b>APPENDIX C: Supplementary Information of Chapter 5.....</b>		<b>212</b>

## LIST OF TABLES

Table 2.1. Different characteristics between microwave irradiation and conventional heating. ..	16
Table 2.2. Summary of polymeric micelle-based formulations in clinical trials. ....	20
Table 3.1. Microwave-assisted RAFT polymerization of PSAMA, PNIPAM and PSAMA- <i>b</i> -PNIPAM at 60 °C. ....	69
Table 3.2. Drug loading characteristics of CBZ-loaded micelles. ....	78
Table 4.1. Microwave-assisted RAFT polymerization of homopolymers and block copolymers at 60 °C. ....	104
Table 4.2. Characteristics of blank and DOX-loaded polymeric micelles. ....	106
Table 5.1. Microwave-assisted RAFT polymerization of PVS and PVS- <i>b</i> -PNVCL at 70 °C. ....	140
Table 5.2. Characteristics of DOX-loaded bioconjugates. ....	148

## LIST OF FIGURES

Figure 2.1. The higher-order morphologies formed by block copolymer amphiphiles as predicted by their packing parameter P in aqueous environment.(Adapted from Varlas et al. <sup>53</sup> ) .....	19
Figure 2.2. Selected polymers with LCST behaviour in aqueous systems. ....	36
Figure 3.1. <sup>1</sup> H NMR spectrum of (A) SAMA, (B) PSAMA and (C) PSAMA- <i>b</i> -PNIPAM. ....	71
Figure 3.2. GPC traces of block copolymer PSAMA- <i>b</i> -PNIPAM and its PSAMA macro-CTA. ....	72
Figure 3.3. FTIR spectrum of SAMA, PSAMA, PNIPAM and PSAMA- <i>b</i> -PNIPAM. ....	73
Figure 3.4. DLS distributions for PSAMA- <i>b</i> -PNIPAM in aqueous solution at 25 °C.....	74
Figure 3.5. TEM images of (a) PSAMA <sub>8</sub> - <i>b</i> -PNIPAM <sub>106</sub> ; (b) PSAMA <sub>12</sub> - <i>b</i> -PNIPAM <sub>121</sub> ; (c) PSAMA <sub>8</sub> - <i>b</i> -PNIPAM <sub>106</sub> micelle solution heated at 50 °C; (d) CBZ-loaded PSAMA <sub>8</sub> - <i>b</i> -PNIPAM <sub>106</sub> . .....	75
Figure 3.6. Plots of the intensity ratio I <sub>337</sub> /I <sub>333</sub> of pyrene excitation spectra versus logarithm of concentration for PSAMA <sub>12</sub> - <i>b</i> -PNIPAM <sub>121</sub> .....	77
Figure 3.7. Release profiles <i>in vitro</i> of free CBZ and CBZ drug-loaded micelles in PBS (pH 7.4) at 37 °C and 25 °C. ....	80
Figure 4.1. <sup>1</sup> H NMR spectrum of (A) PVS and (B) PVS- <i>b</i> -PNVCL.....	102
Figure 4.2. Plots of the intensity ratio I <sub>337</sub> /I <sub>333</sub> of pyrene excitation spectra versus logarithm of concentration of PVS- <i>b</i> -PNVCL. ....	105
Figure 4.3. TEM images of self-assemblies formed by (A) PVS <sub>18</sub> - <i>b</i> -PNVCL <sub>35</sub> ; (B) PVS <sub>18</sub> - <i>b</i> -PNVCL <sub>72</sub> ; (C) PVS <sub>18</sub> - <i>b</i> -PNVCL <sub>95</sub> ; (D) worm-like structures of PVS <sub>18</sub> - <i>b</i> -PNVCL <sub>35</sub> . ....	108
Figure 4.4. DLS distributions for PVS <sub>18</sub> - <i>b</i> -PNVCL <sub>35</sub> in aqueous solution at 25 °C and 37 °C..	110
Figure 4.5. TEM images of DOX-loaded PVS <sub>18</sub> - <i>b</i> -PNVCL <sub>35</sub> .....	112
Figure 4.6. Release profiles <i>in vitro</i> of free DOX and DOX-loaded micelles in PBS (pH 7.4) at 37 °C and 25 °C. ....	113
Figure 4.7. Fluorescence emission spectra (excitation at 570 nm) of NR-loaded PVS <sub>18</sub> - <i>b</i> -PNVCL <sub>35</sub> micelles incubated with 10% FBS. ....	114
Figure 4.8. Cell viability results for (A) HeLa and (B) HEK 293T cells treated with different concentrations of PVS <sub>18</sub> - <i>b</i> -PNVCL <sub>35</sub> .. ....	115
Figure 4.9. Effect of DOX-loaded PVS <sub>18</sub> - <i>b</i> -PNVCL <sub>35</sub> micelles on HeLa cell viability. HeLa cells were incubated with free DOX as control and DOX-loaded micelles for 24 h (A) or 48 h (B). ....	116
Figure 4.10. CLSM images (400 ×) of HeLa cells treated with DOX encapsulated into PVS <sub>18</sub> - <i>b</i> -PNVCL <sub>35</sub> micelles and free DOX for 4 h or 24 h.....	118

Figure 5.1. <sup>1</sup> H NMR spectrum of PVS and PVS- <i>b</i> -PNVCL.....	140
Figure 5.2. MALDI-TOF spectrum of (A) BSA and (B) BSA-polymer conjugate.....	142
Figure 5.3. SDS-PAGE electropherogram of BSA and bioconjugates. ....	143
Figure 5.4. DLS distributions of BSA and BSA-PVS- <i>b</i> -PNVCL in aqueous solution at 25 °C.....	144
Figure 5.5. TEM images of purified BSA-PVS- <i>b</i> -PNVCL self-assemblies.....	145
Figure 5.6. Plot of relative absorbance at 500 nm of PNVCL and BSA-PVS- <i>b</i> -PNVCL bioconjugate in aqueous solution as a function of temperature.....	146
Figure 5.7. DLS distributions of BSA-PVS- <i>b</i> -PNVCL in aqueous solution under different temperatures.....	147
Figure 5.8. TEM images of DOX-loaded BSA-PVS- <i>b</i> -PNVCL bioconjugates. ....	149
Figure 5.9. <i>In vitro</i> cytotoxicity of BSA-PVS- <i>b</i> -PNVCL conjugate with (A) HeLa and (B) HEK 293T cells after incubation for 24, 48, 72 h.....	150
Figure 5.10. CLSM images of free DOX and DOX-loaded BSA-PVS- <i>b</i> -PNVCL conjugates in HeLa cells at different incubation time.....	153
Figure S3.1. Temperature-dependent transmittance of PSAMA- <i>b</i> -PNIPAM in aqueous solution .....	206
Figure S4.1. GPC traces of PVS and PVL homopolymers.....	207
Figure S4.2. FTIR spectrum of PVS, PNVCL and PVS- <i>b</i> -PNVCL.....	208
Figure S4.3. TEM images of PVL <sub>16</sub> - <i>b</i> -PNVCL <sub>54</sub> .....	208
Figure S4.4. Temperature-dependent transmittance of PVS <sub>18</sub> - <i>b</i> -PNVCL <sub>95</sub> (1 mg/mL) in aqueous solution at 500 nm.....	209
Figure S4.5. Fluorescence emission spectra (excitation at 570 nm) of NR-loaded PVS <sub>18</sub> - <i>b</i> -PNVCL <sub>35</sub> micelles incubated in PBS solution.....	209
Figure S4.6. Effect of DOX-loaded PVS <sub>18</sub> - <i>b</i> -PNVCL <sub>35</sub> micelles on HEK 293T cell viability. HEK 293T cells were incubated with free DOX and DOX-loaded micelles for 24 h (A) or 48 h (B).. .....	210
Figure S4.7. CLSM images (1000 ×) of HeLa cells treated with DOX encapsulated into PVS <sub>18</sub> - <i>b</i> -PNVCL <sub>35</sub> micelles and free DOX for 4 h or 24h.....	211
Figure S5.1. <sup>1</sup> H NMR spectrum of S-2-(3-(pyridin-2-yl)disulfanyl)propyl propanoate)-O-ethyl xanthate (X2) .....	214
Figure S5.2. ATR-FTIR spectra of PDS-PVS and PDS-PVS- <i>b</i> -PNVCL .....	215
Figure S5.3. MALDI-TOF spectrum of PVS <sub>15</sub> - <i>b</i> -PNVCL <sub>55</sub> .....	216

## LIST OF SCHEMES

Scheme 2.1. The mechanism of RAFT homopolymerization (I and II) and block copolymerization (III).....	14
Scheme 3.1. Synthetic route for amphiphilic block copolymer PSAMA- <i>b</i> -PNIPAM via microwave-assisted RAFT polymerization.....	62
Scheme 4.1. Illustration of the synthetic route for block copolymer PVS/PVL- <i>b</i> -PNVCL via RAFT polymerization under microwave irradiation.....	100
Scheme 5.1. Synthetic route for BSA-PVS- <i>b</i> -PNVCL bioconjugate. ....	137

## LIST OF ABBREVIATIONS

<sup>1</sup> H NMR: Proton nuclear magnetic resonance spectroscopy	DMEM: Dulbecco's modified Eagle medium
ACVA: 4,4'-Azobis(4-cyanovaleric acid)	DOX: Doxorubicin
AIBN: 2, 2'-Azobisisobutyronitrile	DP: Degree of polymerization
ATR-FTIR: Attenuated total reflectance Fourier transform infrared	DTNB: 5,5'-Dithio-bis-(2-nitrobenzoic acid)
ATRP: Atom transfer radical polymerization	DTT: Dithiothreitol
BSA: Bovine serum albumin	DTX: Docetaxel
CBZ: Carbamazepine	EPR: Enhanced permeability and retention
CDP: 4-Cyano-4 [(dodecylsulfanylthiocarbonyl)sulfanyl]pentanoic acid	FBS: Fetal bovine serum
CLSM: Confocal laser scanning microscope	FDA: Food and Drug Administration
CMC: Critical micelle concentration	GPC: Gel permeation chromatography
CPT: Camptothecin	HEK: Human embryonic kidney
CRP: Controlled radical polymerization	LCST: Lower critical solution temperature
CTA: Chain transfer agent	MALDI-TOF MS: Matrix assisted laser desorption ionization-time of flight mass spectrometry
DAPI: 4',6-Diamidino-2-phenylindole dihydrochloride	MDR: Multidrug resistance
DLS: Dynamic light scattering	NIPAM: N-isopropylacrylamide
DMA: N,N-dimethylacrylamide	NMP: Nitroxide-mediated polymerization
	NR: Nile Red

NVCL: N-vinylcaprolactam

PCL: Poly( $\epsilon$ -caprolactone)

PDI: Polydispersity index

PDLLA: Poly(D, L-lactic acid)

PDS: Pyridyl disulfide

PEG: Polyethylene glycol

PEO: Poly(ethylene oxide)

PLA: Poly(lactic acid) (PLA)

PMMA: Poly(methyl methacrylate)

PPO: Poly(propylene oxide)

PS: Polystyrene

PSAMA: Poly(2-methacryloyloxy) ethyl stearate

PTX: Paclitaxel

PVL: Poly(vinyl laurate)

PVP: Polyvinylpyrrolidone

PVS: Poly(vinyl stearate)

RAFT: Reversible addition-fragmentation chain transfer

RDRP: Reversible deactivation radical polymerization

RES: Reticuloendothelial systems

ROS: Reactive oxygen species

SDS-PAGE: Sodium dodecyl sulfate polyacrylamide gel electrophoresis

TCEP: Tris(2-carboxyethyl)phosphine hydrochloride

TEM: Transmission electron microscopy

UCST: Upper critical solution temperature

# CHAPTER 1. General Introduction and Thesis Objectives

## 1.1 General introduction

### 1.1.1 Challenges and opportunities in drug delivery

Many pharmaceuticals on the market currently suffer from short half-life, *in vivo* instability, and rapid degradation. Besides, approximately 40% of both existing and preclinical therapeutic agents encounter issues related to poor water solubility,<sup>1</sup> hindering their effective diffusion and absorption into the bloodstream. Over the past century, substantial efforts have been invested in optimizing the pharmacokinetic properties of these drugs. The drug delivery technology began in 1952 with the introduction of the first controlled-release Spansule® capsule technology, which allowed for the 12-h delivery of dextroamphetamine following oral administration.<sup>2</sup> From then until the 1980s, the basic mechanism of controlled drug release was established, contributing mainly to the development of oral and transdermal controlled formulations.<sup>3</sup> Throughout this period, many other drug delivery technologies have been developed. In 1964, Alec D. Bangham discovered lipid vesicles, later known as liposomes, and their potential as a drug delivery system was first proposed in 1971.<sup>4</sup> The 1980s witnessed the expansion of drug delivery systems, with the development of diverse drug vehicles such as polymeric micro/nano- particles, polymeric micelles, dendrimers, hydrogels, and nanotubes. These systems are primarily polymer-based, offering enhanced drug solubility, improved body distribution, drug protection, and sustained drug release.<sup>5-10</sup>

Cancer has been a persistent challenge for human beings throughout the history. The nonspecific nature and high toxicities of chemotherapeutic drugs which impact both normal and

cancer cells entailed innovative solutions. The development of nanotechnology-based drug delivery systems offers a promising strategy for selective delivery of anticancer drugs to tumor sites. Since the 2000s, a significant research focus was directed toward developing nanosized targeted drug delivery systems to tumors. Moreover, with the advancement of the medical field, new generations of therapeutics based on proteins and peptides, nucleic acids, antibodies, and drug conjugates have emerged, bringing additional challenges to the existing drug delivery systems in terms of intracellular delivery requirements as well as therapeutic stability, bioavailability, and specificity. To address these challenges, drug delivery strategies have undergone evolution over the last three decades. Significant progress has been achieved by manipulating the physicochemical properties of nanoparticles to increase drug accumulation at the intended site of action.<sup>11-15</sup> Despite promising results in *in vitro* and animal studies, the translation of these nanocarriers into clinical productions, as indicated by the number of Food and Drug Administration (FDA)-approved drugs, has been limited. This can be attributed, in part, to the complexity of therapeutics involved and, on the other hand, to the challenge of predicting the *in vivo* behavior of drug delivery systems after administration and overcoming biological barriers.

In modern medicine, the primary focus of drug delivery remains on drug solubilization, controlled drug release, and drug targeting. To achieve successful drug delivery, carrier systems need to tackle the obstacles posed by both physicochemical and biological barriers, which still need to be solved in previous drug delivery systems. These challenges include large size and instability of therapeutic proteins and peptides, inefficient intracellular delivery, difficulty in achieving targeted and controlled drug release, and unclear systemic drug distribution issues.<sup>16,17</sup> The progress in drug delivery systems is a culmination of extensive experimentation and learning from repeated trials and errors. Achieving advancements demands a comprehensive understanding

and insights drawn from a range of scientific disciplines, including biology, chemistry, and polymer/materials science. Different drug delivery systems with peculiar characteristics can be elaborately designed and explored to ensure enhanced safety and biocompatibility. The development of advanced drug delivery systems with multifunctionality can be achieved by incorporating biological components, responsive polymers, imaging agents, innovative biomaterials, and implementing combination therapies.

### **1.1.2 Renewable lipid derived bio-based materials in drug delivery**

Polymeric materials play a pivotal role in the evolution of novel drug delivery systems due to their customizable and functional nature to meet specific requirements.<sup>18-20</sup> For diverse applications in biomedical fields, drug delivery systems must prioritize safety as a paramount concern. The utilization of biocompatible and biodegradable materials as drug nanocarriers offers several advantages, including prolonged circulation time, sustained release, improved therapeutic efficacy, reduced toxicity, and *in vivo* degradability.<sup>21</sup> Taking polymeric micelle as an example, they usually consist of biocompatible and biodegradable hydrophobic blocks such as poly( $\epsilon$ -caprolactone) (PCL), poly(lactic acid) (PLA) and poly(D, L-lactic acid) (PDLLA) covalently bound to a biocompatible hydrophilic block, typically polyethylene glycol (PEG).

As naturally occurring biomolecules, lipids have extensive applications in the pharmaceutical industry. Most FDA-approved drug delivery systems belong to the liposome or lipid-based formulations category. The frequently utilized lipid-based drug delivery systems include liposomes, solid lipid nanoparticles and nanostructured lipid carriers.<sup>22-24</sup> Despite their several benefits, lipid-based drug platforms face significant limitations, i.e., a short blood circulation time, *in vivo* instability, and relatively larger particle sizes due to their rigid lipid components, necessitating additional functional modifications. Another less-explored category,

lipid-core micelles formed by conjugates of phospholipids with hydrophilic polymers (such as PEG or polyvinylpyrrolidone (PVP)), has been reported to self-assemble in aqueous solutions and encapsulate poorly soluble drugs.<sup>25,26</sup> However, their efficiency to encapsulate drugs is restricted by the limited space within the hydrophobic core attributed to the two relatively short fatty acid acyls.

In response to the growing concern of environmental and health-related issues, the scientific community has shifted its focus toward utilizing renewable resources to substitute petroleum-based polymers in diverse industrial applications. The primary constituents of renewable plant oils are fatty acids which are mostly saturated and perform as chain terminators in the polymerization process. Nevertheless, it was noted that the reactive sites on the fatty acid structure, like carboxylic acid and alcohol open up diverse possibilities for functionalization and allow the production of novel bio-based monomers.<sup>27</sup> With the progress in polymer science, various polymers derived from renewable vegetable oil resources, including polyesters, polyurethanes, polyepoxides, and polyamines, have been synthesized through step growth polymerization or oxypolymerization.<sup>28,29</sup> More recently, advancements in controlled radical polymerization (CRP) techniques, such as reversible addition-fragmentation chain transfer (RAFT) or atom transfer radical polymerization (ATRP), have facilitated the production of well-defined fatty acid-based (meth)acrylate block copolymers.<sup>30-32</sup> Despite these strides, applications of fatty acid-based polymers have predominantly concentrated on coatings,<sup>33</sup> elastomers<sup>34</sup> or adhesives<sup>35</sup> with limited attention given to their potential biomedical applications as amphiphilic block copolymers for drug delivery.

## 1.2 Hypotheses

Based on the outlined challenges and perspectives, it was hypothesized that:

(i) Fatty acid residues from renewable resources could serve as effective hydrophobic core-forming components for the fabrication of controlled amphiphilic block copolymer through CRP techniques. The self-assembled polymeric micelles, formed from the amphiphilic block copolymers, are anticipated to exhibit a high drug loading capacity. This is attributed to the spacious core generated by the hydrophobic fatty acid residues, coupled with favorable biocompatibility and biodegradability.

(ii) The incorporation of hydrophilic thermoresponsive polymers is expected to facilitate temperature-triggered drug release, providing controlled and on-demand drug delivery properties.

(iii) It is feasible to prepare protein-polymer biohybrids which combine advantages from both biological biomolecules and multifunctional polymer materials by site-specific conjugation to create new advanced drug delivery systems for tumor targeting.

## 1.3 Objectives

This proposed research aims to prepare amphiphilic block copolymers composed of thermo-responsive polymers and renewable lipid-based polymers and develop block copolymer-protein bioconjugates for constructing safe, efficient, controlled and targeted drug delivery systems. The synthesized block copolymers and protein-polymer conjugates were characterized by proton nuclear magnetic resonance spectroscopy ( $^1\text{H}$  NMR), gel permeation chromatography (GPC), Fourier transform infrared (FT-IR) and matrix assisted laser desorption ionization-time of flight mass spectrometry (MALDI-TOF MS). Their self-assembly behaviours were characterized by critical micelle concentration (CMC), transmission electron microscopy (TEM) and dynamic light

scattering (DLS). Their efficiency as drug carriers were assessed with drug encapsulation, drug release and *in vitro* cellular studies.

The specific objectives of this study are listed as below:

1. Synthesis of amphiphilic block copolymer micelles containing N-isopropylacrylamide (NIPAM) and stearic derivatives by microwave-assisted RAFT polymerization for delivering hydrophobic drug carbamazepine (CBZ) (Chapter 3).
2. Synthesis of amphiphilic block copolymer micelles containing N-vinylcaprolactam (NVCL) and two distinct fatty acid moieties via microwave-assisted RAFT polymerization for delivering anticancer drug doxorubicin (DOX) (Chapter 4), and
3. Preparation of bioconjugate of bovine serum albumin (BSA) with amphiphilic thermo-responsive block copolymers via “grafting-to” strategy as a tumor-targeted drug delivery system (Chapter 5).

## 1.4 References

- (1) Tenchov, R.; Bird, R.; Curtze, A. E.; Zhou, Q. Lipid Nanoparticles from Liposomes to mRNA Vaccine Delivery, a Landscape of Research Diversity and Advancement. *ACS Nano* **2021**, *15*, 16982–17015.
- (2) Park, H.; Otte, A.; Park, K. Evolution of Drug Delivery Systems: From 1950 to 2020 and beyond. *J. Controlled Release* **2022**, *342*, 53–65.
- (3) Park, K. Controlled Drug Delivery Systems: Past Forward and Future Back. *J. Controlled Release* **2014**, *190*, 3–8.
- (4) Gregoriadis, G.; Ryman, B. E. Liposomes as Carriers of Enzymes or Drugs: A New Approach to the Treatment of Storage Diseases. *Biochem. J.* **1971**, *124*, 58.

- (5) Leong, K. W.; Langer, R. Polymeric Controlled Drug Delivery. *Adv. Drug Delivery Rev.* **1987**, *1*, 199–233.
- (6) Brannon-Peppas, L. Recent Advances on the Use of Biodegradable Microparticles and Nanoparticles in Controlled Drug Delivery. *Int. J. Pharm.* **1995**, *116*, 1–9.
- (7) Kataoka, K.; Kwon, G. S.; Yokoyama, M.; Okano, T.; Sakurai, Y. Block Copolymer Micelles as Vehicles for Drug Delivery. *J. Controlled Release* **1993**, *24*, 119–132.
- (8) Graham, N. B.; Mcneiu, M. E. Hydrogels for Controlled Drug Delivery. *Biomaterials* **1984**, *5*, 27-36.
- (9) Barth, R. F.; Adams, D. M.; Soloway, A. H.; Alam, F.; Darby1, M. V. Starburst Dendrimer-Monoclonal Antibody Immunoconjugates: Evaluation as a Potential Delivery System for Neutron Capture Therapy. *Bioconjugate Chem.* **1994**, *5*, 58–68.
- (10) Ghadiri, M. R. Self-Assembled Nanoscale Tubular Ensembles. *Adv. Mater.* **1995**, *7*, 675–677.
- (11) Li, Y.; Xiao, K.; Luo, J.; Lee, J.; Pan, S.; Lam, K. S. A Novel Size-Tunable Nanocarrier System for Targeted Anticancer Drug Delivery. *J. Controlled Release* **2010**, *144*, 314–323.
- (12) Sutton, D.; Nasongkla, N.; Blanco, E.; Gao, J. Functionalized Micellar Systems for Cancer Targeted Drug Delivery. *Pharm. Res.* **2007**, *24*, 1029–1046.
- (13) Kaneda, Y. Virosomes: Evolution of the Liposome as a Targeted Drug Delivery System. *Adv. Drug Delivery Rev.* **2000**, *43*, 197–205.
- (14) Sawant, R. M.; Hurley, J. P.; Salmaso, S.; Kale, A.; Tolcheva, E.; Levchenko, T. S.; Torchilin, V. P. “SMART” Drug Delivery Systems: Double-Targeted PH-Responsive Pharmaceutical Nanocarriers. *Bioconjugate Chem.* **2006**, *17*, 943–949.
- (15) Singh, R.; Lillard, J. W. Nanoparticle-Based Targeted Drug Delivery. *Exp. Mol. Pathol.* **2009**, *86*, 215–223.

- (16) Vargason, A. M.; Anselmo, A. C.; Mitragotri, S. The Evolution of Commercial Drug Delivery Technologies. *Nat. Biomed. Eng.* **2021**, *5*, 951–967.
- (17) Ezike, T. C.; Okpala, U. S.; Onoja, U. L.; Nwike, C. P.; Ezeako, E. C.; Okpara, O. J.; Okoroafor, C. C.; Eze, S. C.; Kalu, O. L.; Odoh, E. C.; Nwadike, U. G.; Ogbodo, J. O.; Umeh, B. U.; Ossai, E. C.; Nwanguma, B. C. Advances in Drug Delivery Systems, Challenges and Future Directions. *Heliyon* **2023**, *9*, e17488.
- (18) Grund, S.; Bauer, M.; Fischer, D. Polymers in Drug Delivery-State of the Art and Future Trends. *Adv. Eng. Mater.* **2011**, *13*, 61–87.
- (19) Hunter, A. C.; Moghimi, S. M. Smart Polymers in Drug Delivery: A Biological Perspective. *Polym. Chem.* **2017**, *8*, 41–51.
- (20) Englert, C.; Brendel, J. C.; Majdanski, T. C.; Yildirim, T.; Schubert, S.; Gottschaldt, M.; Windhab, N.; Schubert, U. S. Pharmapolymers in the 21st Century: Synthetic Polymers in Drug Delivery Applications. *Prog. Polym. Sci.* **2018**, *87*, 107–164.
- (21) Deng, C.; Jiang, Y.; Cheng, R.; Meng, F.; Zhong, Z. Biodegradable Polymeric Micelles for Targeted and Controlled Anticancer Drug Delivery: Promises, Progress and Prospects. *Nano Today* **2012**, *7*, 467–480.
- (22) Salvi, V. R.; Pawar, P. Nanostructured Lipid Carriers (NLC) System: A Novel Drug Targeting Carrier. *J. Drug Delivery Sci. Technol.* **2019**, *51*, 255–267.
- (23) Alavi, M.; Karimi, N.; Safaei, M. Application of Various Types of Liposomes in Drug Delivery Systems. *Adv. Pharm. Bull.* **2017**, *7*, 3–9.
- (24) Mehnert, W.; Mäder, K. Solid Lipid Nanoparticles: Production, Characterization and Applications. *Adv. Drug Delivery Rev.* **2012**, *64*, 83–101.

- (25) Gill, K. K.; Kaddoumi, A.; Nazzal, S. PEG-Lipid Micelles as Drug Carriers: Physiochemical Attributes, Formulation Principles and Biological Implication. *J. Drug Target.* **2015**, *23*, 222–231.
- (26) Joshy, K. S.; Snigdha, S.; Anne, G.; Nandakumar, K.; Laly, A., P.; Sabu, T. Poly (Vinyl Pyrrolidone)-Lipid Based Hybrid Nanoparticles for Anti Viral Drug Delivery. *Chem. Phys. Lipids* **2018**, *210*, 82–89.
- (27) Lomège, J.; Lapinte, V.; Negrell, C.; Robin, J. J.; Caillol, S. Fatty Acid-Based Radically Polymerizable Monomers: From Novel Poly(Meth)Acrylates to Cutting-Edge Properties. *Biomacromolecules* **2019**, *20*, 4–26.
- (28) Gaglieri, C.; Alarcon, R. T.; de Moura, A.; Bannach, G. Vegetable Oils as Monomeric and Polymeric Materials: A Graphical Review. *Curr. Res. Green Sustainable Chem.* **2022**, *5*, 100343.
- (29) Bonetti, R.; Parker, W. O. Insights into Polymerization of Vegetable Oil: Oligomerization of Oleic Acid. *JAOCS.* **2019**, *96*, 1181–1184.
- (30) Maiti, B.; Kumar, S.; De Priyadarsi. Controlled RAFT Synthesis of Side-Chain Oleic Acid Containing Polymers and Their Post-Polymerization Functionalization. *RSC Adv.* **2014**, *4*, 56415–56423.
- (31) Maiti, B.; De, P. RAFT Polymerization of Fatty Acid Containing Monomers: Controlled Synthesis of Polymers from Renewable Resources. *RSC Adv.* **2013**, *3*, 24983–24990.
- (32) Obeng, M.; Milani, A. H.; Musa, M. S.; Cui, Z.; Fielding, L. A.; Farrand, L.; Goulding, M.; Saunders, B. R. Self-Assembly of Poly(Lauryl Methacrylate)-*b*-Poly(Benzyl Methacrylate) Nano-Objects Synthesised by ATRP and Their Temperature-Responsive Dispersion Properties. *Soft Matter* **2017**, *13*, 2228–2238.
- (33) Rajput, S. D.; Hundiwale, D. G.; Mahulikar, P. P.; Gite, V. V. Fatty Acids Based Transparent Polyurethane Films and Coatings. *Prog. Org. Coat.* **2014**, *77*, 1360–1368.

- (34) Wang, S.; Vajjala Kesava, S.; Gomez, E. D.; Robertson, M. L. Sustainable Thermoplastic Elastomers Derived from Fatty Acids. *Macromolecules* **2013**, *46*, 7202–7212.
- (35) Vendamme, R.; Olaerts, K.; Gomes, M.; Degens, M.; Shigematsu, T.; Eevers, W. Interplay between Viscoelastic and Chemical Tunings in Fatty-Acid-Based Polyester Adhesives: Engineering Biomass toward Functionalized Step-Growth Polymers and Soft Networks. *Biomacromolecules* **2012**, *13*, 1933–1944.

## CHAPTER 2. Literature Review

### 2.1 Amphiphilic block copolymer

Amphiphilic block copolymers are composed of two or more incompatible polymer subunits, referred to as blocks, covalently linked into linear, branched or cyclic structures. The blocks are obtained by polymerization of different types of monomers, which typically have at least one hydrophobic monomer and one hydrophilic monomer. The resulting molecules composed of two (or more) distinct regions exhibit opposite affinities towards an aqueous medium. This ultimately leads to microphase separation and spontaneous organization to form a diverse set of nanoscale structures with defined sizes and morphologies.<sup>1,2</sup> The properties of these polymeric assemblies are strongly influenced by the chemical nature of the constituent block copolymer amphiphiles, and the techniques employed in their syntheses. To date, a multitude of amphiphilic block copolymers have been produced featuring a wide array of block combinations with well-controlled hydrophilic and hydrophobic block lengths via controlled radical polymerization (CRP) techniques, such as atom transfer radical polymerization (ATRP),<sup>3</sup> reversible addition fragmentation polymerization (RAFT)<sup>4</sup> and nitroxide-mediated polymerization (NMP).<sup>5</sup> The high diverse properties of amphiphilic block copolymers, combined with their distinctive “self-assembly” behaviours, have paved the way for their extensive utilization in various fields, including nanomedicine,<sup>6,7</sup> bioengineering,<sup>8,9</sup> sensing technology,<sup>10,11</sup> separation processes,<sup>12</sup> and catalysis,<sup>13</sup> etc. This PhD research focuses on the synthesis of amphiphilic block copolymers via microwave-assisted RAFT polymerization, and their application for drug delivery as discussed in the following sections.

## 2.1.1 Microwave-assisted RAFT polymerization

### 2.1.1.1 RAFT polymerization

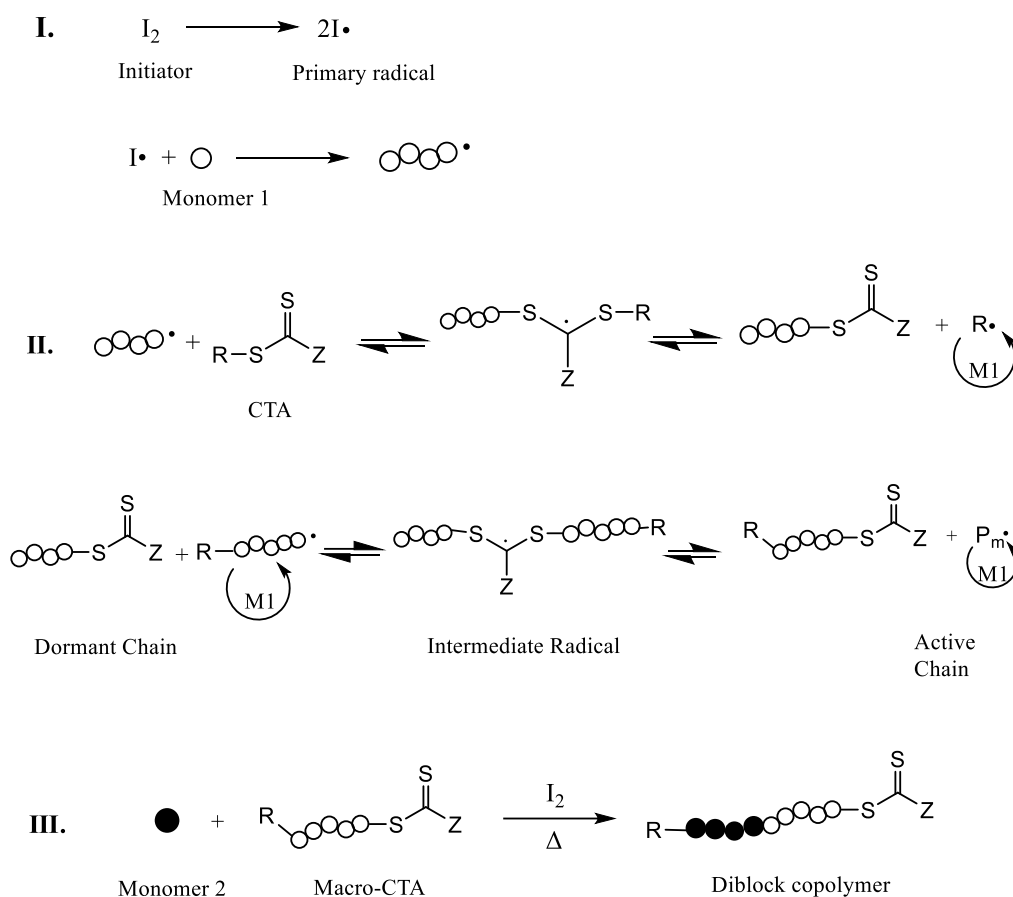
CRP techniques developed in the late 1980s brought about a significant advancement in polymer synthesis, enabling the creation of polymers with well-defined architectures (e.g., multi-block, star, graft, statistical and gradient (co)polymers) and uniform molecular weight distributions,<sup>14–16</sup> which were previously deemed to be unattainable through free radical processes. RAFT polymerization, which was discovered in 1998, is one typical example of CRP techniques, proceeding in a reversible deactivation radical polymerization (RDRP) process.<sup>17</sup> RAFT polymerization is widely regarded as one of the most versatile techniques providing access to functional polymers with precisely controlled molecular weight, narrow polydispersity index (PDI) and defined molecular structures. The benefits of RAFT polymerization include its compatibility with a broad range of functional monomers and reaction media, and its ability to proceed under less stringent reaction conditions.<sup>17–19</sup> For example, RAFT demonstrates good control in the polymerization of vinyl monomers like vinyl acetate and N-vinylpyrrolidone, whereas ATRP and NMP usually provide limited control in such cases. RAFT exhibits versatility in accommodating a wide spectrum of reaction media, including bulk,<sup>20</sup> organic solvents,<sup>21</sup> aqueous solutions,<sup>22</sup> and emulsions<sup>23</sup>. Moreover, it provides a straightforward way to develop end-group-functionalized polymers,<sup>19</sup> facilitating their post-polymerization modifications and selective bonding with biomolecules.

Block copolymers can be readily prepared using RAFT process through sequential polymerization of two monomers, with purification steps carried out prior to each subsequent polymerization. The mechanism is presented in Scheme 2.1. The polymerization begins with the initiation step, where an external source of radicals is required to be introduced to the system

(Scheme 2.1, Step I). While many different sources of initiators have been reported for a RAFT polymerization, such as thermal, photochemical (ultraviolet light,  $\gamma$ -radiation, etc.) and organic peroxide initiators,<sup>17</sup> thermal initiators commonly in the form of azo-based compounds are the most extensively adopted due to their economic accessibility. Degenerative chain transfer in RAFT polymerization is characterized with a chain transfer agent (CTA), also referred to as “RAFT agent”. The CTAs typically contain a thiocarbonylthio moiety ( $ZC(=S)S-$ ) that is transferable and reactive towards radicals, which can facilitate the fragmentation of intermediate RAFT adduct radical (Scheme 2.1, Step II). The functional radical  $R\cdot$  subsequently reacts with monomer to form  $RM\cdot$ , which can reversibly attach to another thiocarbonylthio group. Ultimately, the system reaches an equilibrium between the propagating polymeric radical and the dormant homopolymer. Stopping the polymerization at appropriate conversions reduces the chance of bi-radical termination, thus retaining the “living” thiocarbonylthio chain end. Homopolymers with conserved RAFT end-group can serve as macro-CTAs, to be separated and subsequently chain extended with a second monomer, forming block copolymers.

To achieve precise control over RAFT polymerization, it is of prime significance to select a RAFT agent with proper Z and R group functionality that matches the specific monomer. The R group of the CTA must effectively reinitiate polymerization and readily undergo fragmentation with respect to the propagating radical. The Z group modifies the activity of the thiocarbonyl moiety in terms of radical addition and stabilization of the intermediate RAFT adduct radical. Based on the varying Z groups they possess, RAFT agents can be categorized as either highly active, such as those with  $Z = R$  (dithioesters) or SR (trithiocarbonates), or less active, like those with  $Z = OR$  (xanthates) or NR (dithiocarbamates),<sup>24</sup> concerning their reactivity toward radical addition. The guideline for choosing the Z group and R group with regard to various monomers

have been comprehensively summarized in the literature.<sup>17,25,26</sup> For preparation of well-controlled block copolymers using RAFT polymerization, another key point in addition to RAFT agent selection that needs to be taken into account is the sequence of monomer addition. The homopolymer employed as macro-CTA (Scheme 2.1, Step III) with thiocarbonylthio group should have a higher transfer ability and better leaving ability to allow the growth of the second monomer.<sup>27,28</sup> Overall, excellent control over the molecular weight and PDI of block copolymers through RAFT polymerization can be achieved by making appropriate choices for CTA, initiator, conversion and reaction conditions.



Scheme 2.1. The mechanism of RAFT homopolymerization (I and II) and block copolymerization (III).

### *2.1.1.2 Microwave-assisted synthesis*

Reaction temperature and time are crucial parameters for polymerization process that must be considered carefully. For this purpose, not only conventional heating methods but microwave reactors have also been utilized to investigate and optimize the polymerization conditions. The first report on the application of microwave irradiation for organic synthesis was published by Giguere et al. in 1986.<sup>29</sup> The technical advancements have expanded the use of microwave technology into a wide range of new application areas, including polymer science.<sup>30-32</sup> In this context, different types of polymers have been prepared using microwave-assisted polymer synthesis, including step-growth polymerizations,<sup>33</sup> ring-opening polymerization,<sup>34</sup> and (controlled) radical polymerization techniques.<sup>35</sup> These methods have been well documented in numerous review articles.<sup>36,37</sup> Moreover, a diverse range of monomers, such as styrene, methyl methacrylate, acrylonitrile, acrylamide and vinyl acetate, were polymerized under microwave irradiation with radical polymerizations. These polymerizations were reported to perform in a relatively short period of time using microwave heating while achieving precise control over molecular weight, narrow PDI values and a high end-group fidelity retention.<sup>38,39</sup> Generally, processes performed under microwave heating offer several advantages compared to conventional heating, such as reduced reaction time, increased yields, reduced side reactions as well as improved reproducibility. The main differences in the thermal effect of microwave and conventional heating are summarized and listed in Table 2. 1.

Table 2.1. Different characteristics between microwave irradiation and conventional heating.

<b>Characteristics</b>	<b>Microwave irradiation</b>	<b>Conventional heating</b>
Heat Transfer Mechanism	Dielectric heating	Conductive/convective heating
Heating Uniformity	Often more uniform	May have uneven heating
Speed of Heating	Rapid	Slow
Selective Heating	Selective	Nonselective
Energy Efficiency	More energy-efficient	Less energy-efficient
Reaction Control	Enhanced control	Limited control

Microwave irradiation is electromagnetic irradiation within the frequency range of 0.3 to 300 GHz. The impact of microwave irradiation on chemical reactions results from a combination of both thermal effects (i.e., overheating, hot spots and selective heating) and non-thermal effects.<sup>30,40</sup> In general, microwave irradiation is rapid and volumetric as a consequence of the inverted heat transfer, with the entire material heated uniformly. On the contrary, conventional heating is a slower process that introduces heat from the surface into the sample via conduction and convection. Microwave-enhanced chemistry is based on the ability of microwave radiation to excite polar molecules, either through their dipolar character (dipolar polarization) or ionic conduction. The oscillating electromagnetic field compels the alignment of dipole or ions with the applied electric field, generating heat through molecular rotation, friction, and collisions. The internal heating therefore occurs rapidly due to the direct interaction of the electromagnetic irradiation with the reaction mixture. The amount of heat generated through this process mainly depends on the dielectric properties of the molecules involved, which gives rise to the selective absorption of the radiation as well as heating.<sup>36</sup> Studies also have demonstrated that significant acceleration can be achieved for these reaction components with low absorption capacity by

incorporation of polar additives, such as ionic liquids.<sup>40</sup> The non-thermal effects of microwave irradiation include molecular mobility and diffusion that may increase the possibilities of effective interactions.

### **2.1.2 Self-assembling micelle behaviours**

Owing to the unique dual nature of amphiphilic molecules, they tend to accumulate at the interface of two phases, akin to surfactants. The thermodynamic incompatibility between the hydrophilic (water-attracting) and hydrophobic (water-repelling) regions leads to a spatial organization into high-ordered nanostructures in aqueous media with an array of morphologies such as micelles, vesicles, nanotubes, nanofibers, and lamellae.<sup>41-45</sup> When amphiphilic molecules are introduced to an aqueous environment, they begin to interact with the surrounding solvent molecules. Amphiphilic molecules tend to align themselves by positioning their hydrophilic portions to interact with the aqueous solutions and relocating the hydrophobic blocks away from the water molecules to minimize free energy. This microphase separation is essential to minimize unfavourable interactions between hydrophobic regions of the amphiphiles and water molecules, therefore maximizing stability. As the concentration of amphiphile molecules increases to a certain point in the solution, termed the critical micelle concentration (CMC), individual amphiphilic molecules start to aggregate and self-assembly begins to take place. In most cases, they spontaneously self-assemble into colloidal-sized particles termed micelles, typically exhibiting diameters ranging from 10 to 200 nm. These micelles are characterized by a distinctive core-shell structure in which the central core is composed of the clustered hydrophobic portions of the amphiphilic molecules. From the thermodynamic perspective, micellization is an entropy-driven process that seeks to minimize the free energy of a system by minimizing the hydrophobic-

hydrophilic interface.<sup>46</sup> The entropy gain drives self-assembly as water molecules are released from the structured hydrophilic shell around the aggregated hydrophobic microdomains. The primary forces involved in the self-assembly are noncovalent interactions including hydrophobic effects, hydrogen bonding, van der Waals forces and electrostatic interaction.<sup>47,48</sup>

CRP techniques are valuable tools for synthesizing amphiphilic block copolymers with precise hydrophilic/hydrophobic block ratios. This control over the composition gives a possibility to the design and manipulation of diverse supramolecular architectures. In the scenario of diblock copolymers, depending on the volume fraction of the hydrophilic and hydrophobic blocks, when the solubilizing block predominates, it leads to the aggregation of insoluble blocks aggregates and creation of spherical micelles; In contrast, if the length of the solubilizing block becomes relatively shorter than that of the insoluble block, this can lead to the formation of cylindrical micelles or vesicles.<sup>49-51</sup> The morphology that amphiphilic block copolymer self-assemblies adopts in aqueous solutions can be estimated by the packing parameter,  $P = v / (a_0 l_c)$ , where  $v$  is the effective volume of the hydrophobic chains in the aggregated core,  $a_0$  is the surface area of the head group, and  $l_c$  is the length of the hydrophobic tail.<sup>52-54</sup> As exhibited in Figure 2.1, typically spherical micelles are favored for  $P < 1/3$ , cylindrical micelles when  $1/3 < P < 1/2$ ; vesicles or polymersomes when  $1/2 < P < 1$ ; and a reverse curvature can be obtained when  $P > 1$ . While the packing parameter can be a convenient tool for predicting the shape of nanoassemblies, it does not provide a comprehensive account of the kinetic and thermodynamic factors governing self-assembly processes. The morphology and colloidal properties of amphiphilic block copolymer assemblies can be engineered through various parameters, including the chemical nature of the constituting blocks (i.e., hydrophobicity), hydrophilic/hydrophobic block ratios, block incompatibility, degree of

polymerizations (DPs) of each block, and molecular weight polydispersity.<sup>55-57</sup> Additionally, factors such as external additives, crosslinking of specific block domains, crystallinity within hydrophobic cores and chirality also exert influence on the resulting morphologies of macromolecular assemblies.<sup>58-60</sup>

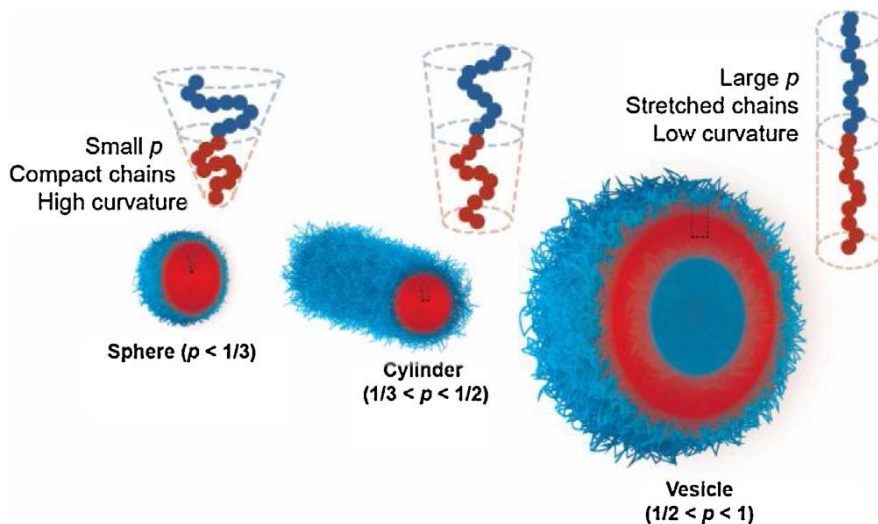


Figure 2.1. The higher-order morphologies formed by block copolymer amphiphiles as predicted by their packing parameter  $P$  in aqueous environment. (Adapted from Varlas et al.<sup>53</sup>)

### 2.1.3 Applications in drug delivery

Polymeric micelles formed by self-assembly of amphiphilic block copolymers have emerged as an ideal platform for the delivery of hydrophobic therapeutics as the hydrophobic core serves as a drug reservoir and thereby improves the solubility of the drug in an aqueous environment. Until now, polymeric micelles have been extensively reported as carriers for anticancer drugs, nucleic acids, proteins, and contrast agents.<sup>61-66</sup> Especially, a large number of clinically approved hydrophobic drugs such as doxorubicin (DOX), paclitaxel (PTX), cisplatin, docetaxel and amphotericin B<sup>67-69</sup> have been successfully solubilized by various polymeric

micellar formulations with significantly increased solubility. For instance, it has been reported that the utilization of poly(ethylene oxide)-*b*-poly(D,L-lactide) (PEO-*b*-PDLLA) micelles resulted in a remarkable 5000-fold increase in the solubility of PTX<sup>70</sup> and up to 12,000-fold increase in the solubility of DOX in aqueous media.<sup>71</sup> The practical utility of polymeric micelles as drug delivery systems have been demonstrated by an increasing number of polymeric micelle formulations, which have progressed to clinical trials in various countries. Table 2.2. displays examples of polymeric micelle-based drugs that have received regulatory approval or undergone clinical evaluation.

Table 2.2. Summary of polymeric micelle-based formulations in clinical trials.

Formulation	Polymer	Drug	Drug loading (%)	Development stage
NK105	PEG–polyaspartate	PTX	23%	phase III <sup>72</sup>
SP1049C	PEG–PPO–PEG	DOX	8.2%	phase III <sup>73</sup>
Genexol-PM	PEG–PLA	PTX	16.7%	phase II <sup>74</sup>
NK012	PEG–polyglutamate	SN-38	20%	phase II <sup>75</sup>
NC-6004	PEG–polyglutamate	Cisplatin	39%	phase II <sup>76</sup>
DTXL-TNP	PLA-PEG	Docetaxel (DTX)	n.a	Phase I <sup>77</sup>
CPC634	m-PEG- <i>b</i> -poly[N-(2-hydroxypropyl) methacrylamide lactate]-DTX	DTX	12%	phase II <sup>78</sup>
NK911	PEG-P(Asp)-DOX	DOX	n.a	Phase I <sup>79</sup>

PEG: poly(ethylene glycol); PPO: poly(propylene oxide); PLA: polylactide

One strong advantage of polymeric micelles as well-suited drug delivery vehicles over others is the chemical flexibility of their structure, which offers an opportunity for the design of drug carriers with versatile functions. That is, polymeric micelles can be customized and tailored

by selecting suitable block copolymers for intended use, like prolonged blood circulation in the bloodstream, controlled drug release, tissue accumulation and penetration, and minimized inherent toxicity.<sup>80,81</sup> For example, incorporating PEG as the hydrophilic shell can increase longevity in blood circulation of micelles as PEG can form a hydrated protective layer on the surface of micelles preventing non-specific interactions with biological components (i.e., phagocytosis by macrophages).<sup>82,83</sup> Besides, adding temperature or pH-responsive polymers which can exhibit specific responses to temperature changes or variations in pH enables site-specific drug delivery or triggers drug release.<sup>84</sup>

Another advantage of polymeric micelles is that their particle size can be easily and precisely tuned by the chemical composition and molecular weight of block polymers rather than the preparation processes. For drug delivery through intravenous injection, it is well-established fact that the ideal carrier size is in the range of *ca.* 10 nm to 200 nm diameter.<sup>85,86</sup> The lower size limit is primarily determined by the need to evade renal excretion. Particles that can easily pass through the kidney's filtration system will be rapidly removed from the bloodstream, resulting in significantly reduced drug-targeting efficiency as the free drugs. Whereas the upper size limit is determined by potential capture by the liver and spleen. Carriers larger than around 400 nm can be easily captured and cleared by the reticuloendothelial systems (RES).<sup>87</sup> Notably, the diameter of polymeric micelles typically falls within the range of 20 nm to 200 nm, making them exceptionally well-suited for drug targeting in terms of their size. In addition, one major breakthrough made by Matsumura and Maeda<sup>88</sup> is the discovery of significant distinctions in the vasculature of cancerous tissues as opposed to normal ones. They demonstrated that the vasculature rapidly forming in solid tumors exhibited increased permeability with “leaky” characteristic and impaired lymphatic

drainage, which consequently facilitates the enhanced accumulation of nanocarrier particles and anticancer drugs around the tumor sites. This phenomenon, termed as the enhanced permeability and retention (EPR) effect, has gained widespread acceptance as a fundamental targeting methodology for achieving "passive" tumor targeting with nano-drug delivery systems. Hence, polymeric micelles can selectively extravasate from the bloodstream into target tumor tissues owing to the EPR effect.

As discussed in Section 2.1.2, polymeric micelles are formed by the aggregate of single amphiphilic chains above CMC. Although polymeric micelles can evade renal excretion and RES capture in the bloodstream and deliver drugs to their target, polymeric micelles need to disassemble into individual polymer molecules, releasing drugs and eventually being excreted by the kidney. CMC is an important indicator of the stability of polymeric micelles under physiological conditions from a practical point of view. If the concentration of amphiphiles in solution is above their CMC, the micelles become thermodynamically stable, preserving their micellar structure. Intact polymeric micelles allow for retention of the encapsulated drugs with prolonged circulation life after administration. Conversely, upon dilution by large volume of blood following injection, micelles with low CMC values will gradually disassemble into unimers leading to the premature release of drugs before reaching the targeted sites. The value of CMC primarily depends on block composition, the types and molecular weight of block copolymers, temperature, pH, and the presence of salt in aqueous media.<sup>89,90</sup> As a general rule, it can be observed that block copolymers with longer hydrophobic blocks tend to exhibit lower CMCs, indicating a higher thermodynamic stability of the micellar structure.

## 2.2 Protein-polymer bioconjugate

Since the FDA granted its approval to the first human recombinant protein drug (insulin) in 1982, many protein-based therapeutics have emerged. Until now, protein drugs constituted more than 30% of the leading 200 drugs in the market. Although proteins represent a crucial category of therapeutics with high target specificity, they face challenges related to rapid clearance from the body and low stability against heat, purification, and various conditions encountered throughout the processes of manufacturing, storage, and transportation.<sup>91</sup> One of the effective approaches to address these limitations involves the conjugation of proteins with polymers. Polymeric particles with customized characteristics and specific surface functionality can be engineered as versatile platforms to serve a variety of purposes. These bioconjugates can yield hybrid materials that combine the stability inherent to polymers with the diversity and functionality of protein biomolecules.<sup>92,93</sup> The most common and successful example is PEG, which has been approved by FDA with more than 17 PEGylated protein drugs in the market to treat a variety of diseases, including chronic hepatitis C, acute lymphatic leukaemia, and rheumatoid arthritis.<sup>94</sup> The advantages of PEGylation include prolonged half-circulation lives in the bloodstream, lowered immunogenicity and enhanced stability of protein therapeutics.<sup>95,96</sup> Despite these advantages, PEG has been reported for its potential immunogenicity and the development of anti-PEG antibodies in some individuals, which eventually lead to reduced drug efficacy and accelerated clearance of PEGylated drugs from the bloodstream.<sup>97</sup> Consequently, there is a growing interest in developing the next generation of protein-polymer bioconjugates with advanced attributes like biocompatibility, biodegradability, the capability to cross biological barriers and stimuli-responsive properties.

The selection of the protein and polymer combination to attain maximum benefits is generally based on various factors such as the specific disease in question, intended applications and protein properties to be improved. More expanded polymer species used for conjugation include PEG analogues like poly(poly(ethylene glycol methyl ether methacrylate)) (p(PEGMA)),<sup>98</sup> poly(N-(2-hydroxypropyl)methacrylamide) (PHPMA),<sup>99</sup> poly(methyl methacrylate) (PMMA),<sup>100</sup> poly(N-isopropylacrylamide) (PNIPAM)).<sup>101</sup> FDA-approved therapeutic proteins (insulin, antibody, hormone, enzyme) are usually chosen for the development of protein-polymer conjugates with a wide range of biomedical applications. Bovine serum albumin (BSA) and lysozyme are also frequently used in different projects with the intention of demonstrating a new concept. Collectively, these hybrid materials exhibit a diverse range of functional attributes that draw from the individual constituents and opening up possibilities for numerous potential applications, including bioimaging, gene and drug delivery, biosensing, bioseparations, and biochips.<sup>102–106</sup>

### **2.2.1 Synthetic approaches**

Attaching one macromolecule to another biomacromolecule always encounters significantly high steric and entropic hindrances. The complexity of conjugation chemistry is further heightened by the desire to use mild reaction conditions to prevent the protein from denaturing and selective chemical reactions to avoid unintended side interactions with non-target amino acids. Today, the main conjugation methods for protein-polymer bioconjugates can be categorized as non-covalent and covalent interactions. Non-covalent conjugation depends on physical interactions driven by relatively weak intermolecular forces, typically involving electrostatic attractions or hydrophobic interactions.<sup>107</sup> While non-covalent approaches offer advantages in terms of easy preparation, they come with the drawback of potentially lower stability and specificity than covalent methods where the protein macromolecules are bonded with

polymers via more stable and reproducible linkages. The approach for the covalent conjugation of proteins to polymers includes “grafting to” and “grafting from” methods.<sup>108–110</sup> Traditionally, prefabricated polymers possessing functional end-groups which are directly conjugated to proteins are referred to as “grafting to” strategy. The polymers are usually synthesized via ATRP or RAFT polymerization techniques and undergo purification before attachment to the biomacromolecule, therefore eliminating the chance of exposure of proteins to harsh chemical reaction conditions. Consequently, the grafting-to method allows compatibility of a wide range of monomers and polymerization conditions. However, it is often subjected to steric hindrance that can lead to reduced conjugation efficiency. Moreover, purification of the resulting bioconjugate from unreacted protein and excessive free polymers can be challenging due to the similar molecular weight or size of these entities. To overcome these problems, “grafting-from” method, as mentioned above, can be used as one alternative to the “grafting-to” technique. It involves *in situ* polymerization process in which polymer chains are initiated and directly grown from initiators or CTAs functionalized with biomacromolecules. This innovative approach was first pioneered by the Maynard group in 2005.<sup>111</sup> In their study, they modified an ATRP initiator with a biotin end-group, which enables the preparation of biotinylated PNIPAM at ambient temperature and ultimately produced thermosensitive streptavidin-PNIPAM conjugates. The grafting-from method offers an effective technique to generate protein-polymer bioconjugates with high conjugation efficiency because of reduced steric limitations. This approach also facilitates convenient purification procedures for isolating the bioconjugate from free polymers. Nevertheless, it necessitates the polymerization conditions (like medium, temperature, pH and monomer types) that are compatible with maintaining the bioactivity of protein biomolecules. It is well-known that CRP techniques have faced challenges in controlling polymerizations conducted in aqueous

conditions at low temperature, making it difficult to achieve a narrow dispersity in the resulting polymer conjugates.

The existence of reactive sites on the protein surface, which are often referred to as "reactive protein handles," are also crucial factors for successful conjugations. These reactive protein handles are functional amino acid residues, such as amine, thiol, carboxylic acid and hydroxy functional groups present at the surface of proteins,<sup>112,113</sup> which can be harnessed to facilitate their coupling with synthesized polymers, initiators and CTAs. As a rule, the conjugation site should be selected and designed away from the active or binding site of proteins, thereby retaining the maximal protein bioactivity. Amines located at the lysine side chains or N-terminus are frequently chosen as targets for protein covalent conjugations. This is achieved through reactions like N-hydroxysuccinimide (NHS) or pentafluorophenyl (PFP) ester chemistry, carbodiimide reactions or amine-aldehyde addition-elimination reactions,<sup>109,114</sup> which have been utilized in the development of many approved PEGylated-protein therapeutics. However, the abundance of lysine on the protein surface often leads to the loss of biological activity of proteins upon non-specific covalent conjugation to polymer particles.<sup>106</sup> Site-specific conjugation involves attaching a polymer to a defined linking point on a protein, affording a well-controlled structure for the protein-polymer conjugate. Cysteine is a popular target for achieving such specific bioconjugation due to its relatively low abundance and high reactivity of thiol groups. For instance, BSA contains only one free cysteine residue (Cys34), which allows for straightforward modification using a variety of reactive groups, including maleimides, disulfides, iodoacetamides, and vinylsulfone groups.<sup>115,116</sup> Other potential targets include phenols present in tyrosine, carboxylic acids found in glutamic acid and aspartic acid, or the C terminus; however, they have

not gained widespread adoption for bioconjugate synthesis due to their lower reactivity or more common occurrence on the protein's surface.

### **2.2.2 Self-assembly of protein-polymer conjugates**

Engineering amphiphilicity into protein-polymer conjugates to link hydrophilic proteins or enzymes with hydrophobic or amphiphilic polymers results in a block copolymer like-giant amphiphiles, which can consequently lead to phase separation and self-organization of high-order structures. While the phase behavior of block copolymers has been extensively studied and well understood, much less attention has been given to the assembly of amphiphilic protein-polymer bioconjugates. In comparison to traditional block copolymers, which are composed of coiled polymer chains, the incorporation of oriented and folded protein building blocks can introduce evident complexities for the self-assembly of protein-polymer conjugates. This is because proteins commonly exhibit heterogeneous surfaces for hydrophobicity, hydrophilicity, and charge distribution. Factors such as protein size and secondary structure composition can significantly influence the resulting self-assembled structures.<sup>117,118</sup> Besides, the physiochemical properties of the polymer building blocks have also been observed to affect the ultimate architectures of self-assembled bioconjugates.<sup>119–121</sup> To date, amphiphilic protein-polymer conjugates have demonstrated the capacity to form a diverse array of morphologies, including micelles, lamellae, cylinders, and gyroids in both bulk and concentrated solutions.<sup>122–125</sup>

Nolte et al.<sup>123</sup> have described protein-containing triblock copolymers, constituted by a synthetic diblock copolymer polystyrene-*b*-PEG (PS<sub>m</sub>-*b*-PEG<sub>113</sub>) and a heme protein, myoglobin (Mb) or horseradish peroxidase (HRP). By adjusting the protein and the polystyrene block length, the HRP- and Mb-containing copolymers self-assembled into vesicles, toroids, rods, octopus-like structures, and lamellae-containing spheres. Several studies have been also carried out by Olsen et

al.<sup>126</sup> on self-assembly behaviours of protein-PNIPAM conjugates. At the beginning, they studied phase behaviour of mCherry-*b*-PNIPAM block copolymers with four different PNIPAM block lengths. In concentrated aqueous solutions, mCherry-PNIPAM conjugates self-assembled into various disordered micellar structures, including nonbirefringent lamellar, lamellar, non-birefringent hexagonal, hexagonally packed cylinders, and perforated lamellar structures. Changes in PNIPAM coil fractions in the conjugates significantly impact the type of ordered phases formed. Their subsequent study has elucidated the impact of protein properties on the phase behavior of protein-polymer bioconjugates in concentrated solutions.<sup>117</sup> Eleven different types of proteins were employed, and the results revealed that protein blocks that are either high molecular weight and have a large percentage of  $\beta$ -sheets or have a molecular weight within the range of 20-36 kDa are likely to form well-ordered protein-PNIPAM block copolymers. These studies demonstrate that the self-assembled architectures of protein-polymer conjugates can be predicted and well controlled by carefully selecting both protein blocks and polymer blocks.

### **2.2.3 Application as drug nanocarriers**

In an ideal scenario, drug delivery systems should be capable of crossing biological barriers and stabilizing therapeutic agents with localized delivery and triggered-drug release while maintaining non-immunogenicity and non-toxicity. Given these stringent criteria, self-assembled protein-polymer conjugates emerge as strong candidates for a versatile platform in delivery systems. Both hydrophobic and hydrophilic therapeutics can be encapsulated within the micelle core or between vesicle and lamellae membranes. Additionally, controls of therapeutic release can be achieved by accommodating a stimuli-responsive polymer, such as PNIPAM, into the bioconjugate's architecture. There are many examples from the literature that highlight the design and preparation of these bioconjugates for drug delivery applications.<sup>127-129</sup> For example, Ge et

al.<sup>130</sup> prepared BSA-PMMA nanoparticles by nanoprecipitation method for the encapsulation of camptothecin (CPT). The encapsulation ratio was determined to be ~ 11 wt% and the encapsulated CPT was released from the nanoparticles over a period of 48 h. Wong et al.<sup>131</sup> reported a protein-polymer bioconjugate PNIPAM-*b*-amilFP497 composed of thermoresponsive polymer (PNIPAM) and a green-fluorescent protein variant (amilFP497). Polymersome structures were formed as observed by confocal microscopy and transmission electron microscopy (TEM) upon increasing the solution temperature to 37 °C. The polymersomes were then loaded with a fluorophore, phycoerythrin 545 (PE545) and an anticancer drug DOX. Due to the differences in their hydrophilicity, hydrophobic PE545 was mainly located inside the membrane, whereas water-soluble DOX salts were encapsulated in both the core and the membrane of the PNIPAM-*b*-amilFP497 polymersomes. A hypoxia-triggered nano-vehicle, referred to as cascaded nanozymogen, was introduced by Li et al.<sup>132</sup> for anti-cancer treatment. This innovative nanostructure was used to co-deliver a hypoxia-activatable pro-protein of RNase and glucose oxidase, using a hypoxia-dissociable polymer to enable effective intracellular protein therapy within cancer cells.

### **2.3 Thermoresponsive polymeric materials in targeted drug delivery**

An effective drug delivery system must meet four key requirements: retention, evasion, targeting, and release.<sup>133</sup> Developing safe and efficient targeted drug delivery systems is of great significance for the overall drug development process. Targeted drug delivery refers to a therapeutic strategy designed to deliver drugs selectively to the desired site of action within the body, thereby minimizing drug toxicity on healthy cells, improving therapeutic efficacy, and reducing side effects.

The easiest way to achieve targeted drug delivery is by direct application of drug formulation to the target site, such as localized transdermal delivery. However, it should be noted that the administration of drugs through the skin is not feasible in most cases and most drugs are intravenously administered to the specific site, e.g., solid tumors. Since 2000s, numerous delivery systems have been developed for targeted drug delivery. Yet, the overall outcomes are not particularly encouraging, given the limited adoption of controlled release formulations in clinical practice. The challenges in achieving targeted drug delivery via intravenous administration arise from numerous obstacles encountered by the delivery vehicle on its journey to the target sites. The first concern is immunogenicity – for a drug delivery system to be effective, it must remain undetected by the immune system, allowing it to circulate in the bloodstream for an adequate time before reaching the intended sites and then extravasate into the tissue of interest. Another critical issue is the stability of the carrier systems. If the drug leaks from the nanocarrier during circulation, most drug-loaded nanoparticles may end up in non-target organs. Therefore, an efficient targeted drug delivery system should ensure the protection of drug payloads during transportation, enabling accumulation, activation, and release exclusively at the intended target site.

Many efforts are invested in the advancement of targeted drug delivery systems, incorporating chemical,<sup>134</sup> physical,<sup>135</sup> and biological<sup>136,137</sup> modifications. Physical targeting achieves localization through external stimuli, such as heat, light, ultrasound, or magnetic fields. Chemical targeting involves modifying the chemical structure of drugs or utilizing pharmacologically inactive prodrugs that are only metabolically activated in the targeted environment. Biological targeting can be realized through various approaches. Drugs or nanocarriers can be functionalized with targeting ligands or antibodies, enabling localized agents to target specific areas through ligand-receptor interactions. Lately, the development of gene

delivery systems and gene-editing technologies offers a targeted approach at the genetic level via introducing therapeutic genes into specific cells.<sup>138,139</sup> Notably, the development of smart biomaterials responsive to specific biological microenvironments (e.g., pH, temperature, redox potentials, etc.) also holds promise as a strategy for achieving targeted drug release. Among others, temperature has been extensively explored as a stimulus for targeted drug delivery. Elevated temperature is internally observed in certain pathological tissues (e.g., tumors), or it can be externally induced by applying external heating sources (e.g., hyperthermia) from a physical perspective.

### **2.3.1 Tumor-targeted drug delivery**

Cancer stands as the most fatal disease affecting humans globally. Projections suggest that by 2040, there will be an estimated 28 million new cases of cancer each year worldwide. In this regard, cancer remains a primary focus of targeted drug delivery research. Cancer cells feature uncontrolled proliferation, resistance to apoptosis and altered cellular energetics. The formidable challenge in treating cancer arises from several factors. To begin with, the tumor microenvironment characterized by irregular tumor vasculature, acidic extracellular pH, and the presence of immune cells, along with cellular-level factors such as over-expression of drug efflux pumps, defective apoptotic machineries, and changes in cellular signaling pathways attributing multidrug resistance (MDR) against therapeutic drugs.<sup>140,141</sup> Secondly, many chemotherapeutic drugs lack desirable physicochemical and pharmacokinetic properties, displaying low solubility and stability, nonspecific nature and high toxicities to both normal and cancer cells. Therefore, targeted therapy emerges as a crucial approach in cancer treatment. Nanosized drug delivery systems have gained considerable attention as a promising strategy for the selective delivery of drugs to cancer cells. These systems can prevent drug degradation, reduce cytotoxicity, and extend

blood circulation time.<sup>142,143</sup> Targeted nano-carrier systems are currently in different stages of development, offering potential advancements in the field of cancer treatment.

The targeting approaches of nanocarrier drug delivery systems can be broadly categorized as passive and active targeting. Passive targeting is primarily dependent on physicochemical properties of nanocarriers and the unique characteristics of tumor physiology. Tumor cells, due to their rapid multiplication, induce the formation of new blood vessels to sustain their proliferation, featuring endothelial gaps that allow nanoparticles up to 500 nm in size to extravasate into the tumor tissue<sup>87</sup> – an effect known as the EPR effect, as discussed in Section 2.1.3. Doxil®, pegylated liposomal doxorubicin, the first FDA-approved nano-drug in 1995, is an example of passively targeted nano-delivery system, inspiring further research into precisely controllable and targeted delivery systems. Passive targeting can also take advantage of the variations between tumor microenvironment and normal tissues, such as pH difference (e.g., low pH in tumor microenvironment), redox systems (e.g., exploiting high level of glutathione in tumor cell), reactive oxygen species (ROS) systems (e.g., an excess amount of H<sub>2</sub>O<sub>2</sub> generated in tumor cell) in the diseased tissues. As a result, stimuli-responsive targeting systems have been extensively investigated, triggered by such stimuli to release the drug exclusively at the target site while sparing normal tissues.<sup>144–148</sup> For instance, tumor cells exhibit variable pH values ranging from 5.6 to 7.0 in different regions, whereas the pH values in blood and normal tissues are typically around 7.4. Xiao et al.<sup>149</sup> reported a pH-sensitive micellar system based on an acetal-linked PEG-*b*-PLA block copolymer and applied to encapsulate an anticancer drug PTX. The results demonstrated that PTX release can be triggered at pH 6.5 and pH 5.5 for both extracellular and intracellular spaces, respectively.

While passive targeting has demonstrated encouraging results, the pursuit of control over precise drug delivery has driven research into active targeting methods that exploit the overexpressed receptors on tumor surfaces. Active targeting of drug carriers to cancer sites involves modifying or coating nanoparticles with targeting moieties, encompassing aptamers, antibodies, peptides and small organic molecules.<sup>136</sup> This modification enhances the affinity of drug-loaded nanocarriers for specific receptors on tumor tissues, facilitating their internalization into tumor cells. The commonly used targeting ligands for conjugation with nanocarriers include transferrin, folate, antibodies, cell surface glycoproteins, etc.<sup>150,151</sup> For instance, peptide sequences featuring the arginine-glycine-aspartic acid (RGD) motif have a strong affinity towards  $\alpha\beta3$  integrins overexpressed by the tumor endothelium. RGD has been studied extensively at the preclinical stage as tumor-targeting ligands for micelles, liposomes, nanoparticles and drug-peptide conjugates.<sup>152–154</sup> It's worth mentioning that the choice of a specific receptor and the physicochemical characteristics of the ligand, including size, shape, hydrophilicity, and stability all play a crucial role in the effectiveness of active targeting.<sup>136</sup>

### **2.3.2 Thermoresponsive polymers**

Polymers that are capable of altering their solubility in response to environmental temperature changes are referred to as thermoresponsive. The temperature at which this change occurs is termed the transition temperature, also known as the critical solution temperature, accompanied by a conformational change in the structure of polymers. There are two main types of thermoresponsive polymers: those with an upper critical solution temperature (UCST) or with a lower critical solution temperature (LCST). Polymers with UCST behavior are insoluble in aqueous solution below their UCST and change to be soluble as temperature increases above it, for example, poly(acrylic acid) and polyacrylamide. The exploration of UCST in aqueous solutions

is less common due to the greater difficulty in achieving this behavior under physiological conditions.<sup>155</sup>

Polymers exhibiting a LCST are completely soluble in aqueous systems below the transition temperature, resulting in a transparent and homogeneous solution. However, above the LCST, phase separation takes place, causing the polymer solution to become cloudy. Consequently, the LCST is also commonly referred to as the cloud points. Below the LCST, the responsive polymer is hydrated and exhibits a random coil conformation due to hydrogen bonding interactions of hydrophilic groups in the polymer (e.g., N-H or C=O) with the surrounding water molecules. Upon heating, hydrogen bonding with water breaks due to the increased water molecular agitation, the polymer-polymer interactions (i.e., intramolecular hydrogen bonding or hydrophobic effect) become predominant, thus leading to the collapse of polymer molecules. With a continued temperature rise, the remaining hydrogen bonds break, and the polymer chains aggregate together forming a hydrophobic globule and eventually separated from the solution. This process is reversible; as the solution undergoes cooling, the hydrophilic characteristics of the responsive polymer can be restored, and the polymer can be miscible with water solutions again. The phase separation behaviour is thermodynamically more favourable as temperature increases.<sup>156</sup> The entropy increase is the main driving force for this process as a result of less ordered water molecules.

The LCST of thermoresponsive polymers can be readily adjusted by incorporating hydrophobic or hydrophilic comonomers through copolymerization. Increasing the overall hydrophilicity of the polymers strengthens their interactions with water molecules, so a higher transition temperature will be needed to disrupt newly formed hydrogen bonds. Conversely, the

addition of hydrophobic groups enhances interactions with hydrophobic species, thereby lowering the LCST. In addition, polymer chain length, molecular weight, concentration and the presence of additives like salt, co-solvents, and surfactants also impact the transition temperature<sup>157</sup> as they can influence hydrogen bonding interactions between polymers and aqueous systems, as well as the electrostatic interactions of polymers in solution. Plenty of thermoresponsive polymers with diverse LCST values have been reported, with Figure 2.2. providing details on the transition temperatures and chemical structures of a selected group in aqueous solution. Notably, poly(N-alkyl (meth)acrylamide)s, particularly homopolymers and copolymers of PNIPAM, have been extensively studied. PNIPAM, with a sharp phase transition around 32 °C which is close to the physiological temperatures, has drawn favorable attention in biomedical applications. However, PNIPAM presents challenges such as concerns about its biocompatibility and resistance to biodegradation under physiological conditions, as it can generate small toxic amide compounds upon hydrolysis. To address these limitations, other thermoresponsive polymers like poly(2-oxazoline), poly(N-vinylcaprolactam) (PNVCL), poly(amino acid)s, and elastin-like polypeptides (ELPs)<sup>158–160</sup> have garnered recent interest in drug delivery applications due to their biodegradability, biocompatibility, and low toxicity. Utilizing diverse forms such as hydrogels, micelles, three-dimensional structures, coatings, and films, thermoresponsive polymers play a crucial role in various biomedical applications, including drug delivery, tissue engineering, wound healing, and gene delivery.<sup>161–164</sup>

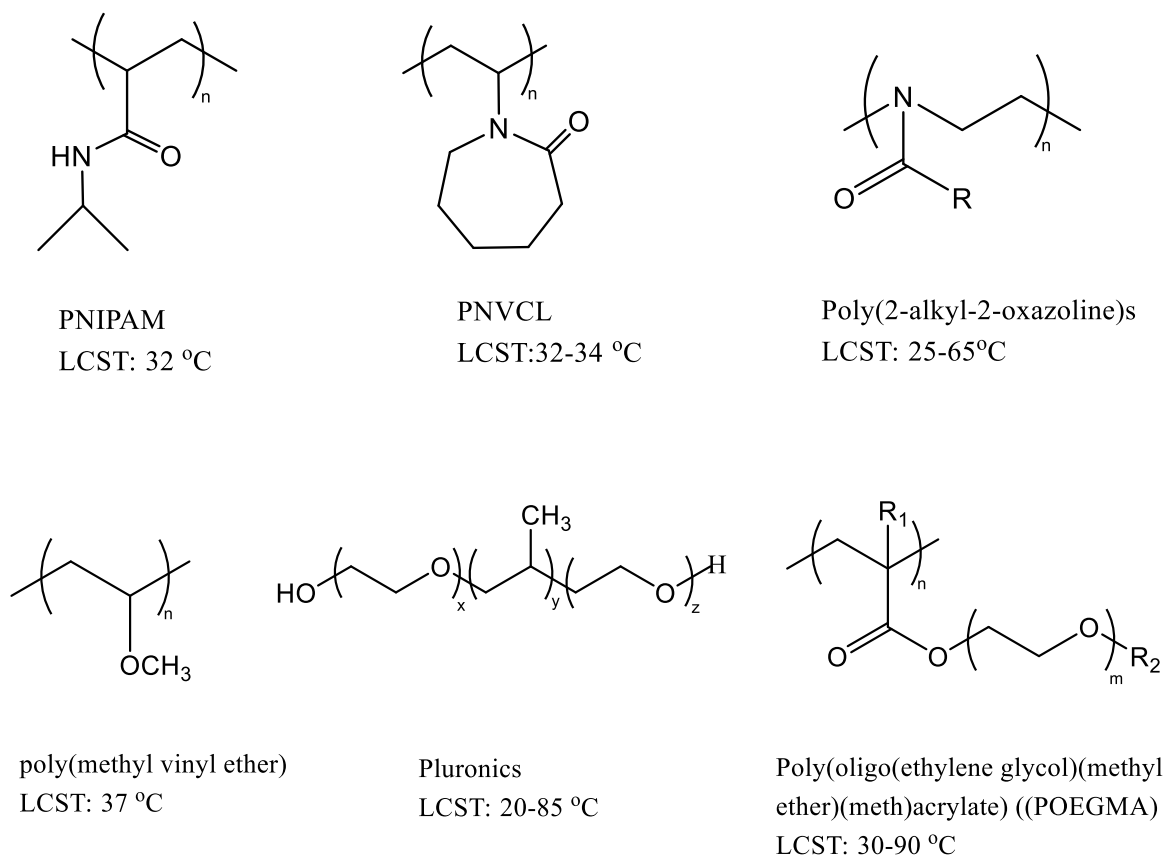


Figure 2.2. Selected polymers with LCST behaviour in aqueous systems.

### 2.3.3 Thermoresponsive micellar drug delivery systems

The integration of temperature-responsive polymers as a pivotal component in micellar drug delivery systems offers notable advantages, including enhanced passive targeting, controlled release and versatility in design. On the one hand, thermoresponsive polymers can serve as a hydrophilic segment, undergoing copolymerization with hydrophobic monomers to produce core-shell amphiphilic (multi-)block copolymer micelles. There are a large number of examples of PNIPAM-based amphiphilic diblock copolymers for delivery of hydrophobic drugs, where the hydrophobic segments involves polystyrene,<sup>165</sup> poly(methyl methacrylate),<sup>166</sup> poly( $\epsilon$ -caprolactone),<sup>167</sup> etc. On the other hand, thermoresponsive polymers can also bond to another

hydrophilic block thus leading to block copolymers that self-assemble into micelles when these polymer solutions are heated above their LCST. Significantly, the LCST of double-hydrophilic block copolymers or multi-block copolymers, incorporating a thermoresponsive segment, can be precisely tuned above body temperature for tumor-targeted drug delivery. Taking advantage of the increased temperature at tumor sites ( $\sim 42$  °C) compared to normal cells (37 °C), temperature-responsive micellar nanocarriers can be programmed and designed to exclusively collapse and disassemble at tumor sites, thus resulting in release of loaded anticancer drugs in response to the elevated temperature around the tumor cells. For example, Liu et al.<sup>168</sup> reported a type of triblock copolymer polymersomes poly(N-vinylcaprolactam)<sub>n</sub>-poly(dimethylsiloxane)<sub>65</sub>-poly(N-vinylcaprolactam)<sub>n</sub> (PNVCL<sub>n</sub>-PDMS<sub>65</sub>-PNVCL<sub>n</sub>) through RAFT polymerization. The permeability of polymersomes loaded with the anticancer drug DOX can be precisely controlled in the temperature range of 37-42°C by regulating the PNVCL length. The increase in the temperature above the LCST of PNVCL would trigger the release of DOX from the polymersomes in an accelerated way. Moreover, thermosensitive polymer-based micellar systems can be synergistically combined with other characteristic biomaterials to create multifunctional delivery systems, offering benefits for tumor-targeting applications.<sup>169,170</sup> A biodegradable dual temperature/pH-responsive drug delivery system composed of mPEG-*b*-poly(N-(2-hydroxypropyl) methacrylamide dilactate)-co-(N-(2-hydroxypropyl) methacrylamide-co-histidine) was established.<sup>171</sup> The result demonstrated the specific release of DOX from the mixed micelles as a result of the slightly acidic environment and body temperature found near tumor sites. By controlling particle size, the carrier could deliver drugs specifically to tumors *in vivo* with restrictive particle extravasation, exhibiting prolonged circulation time and reduced side effects.

Wadajkar et al.<sup>172</sup> developed new magnetic-based core-shell particles consisting of a thermo-responsive shell of poly(N-isopropylacrylamide-acrylamide-allylamine) and a core of poly(lactic-co-glycolic acid) embedded with magnetite nanoparticles. To target melanoma cancer cells, this system was conjugated with Gly-Arg-Gly-Asp-Ser (GRGDS) peptides that specifically bind to the  $\alpha_5\beta_3$  receptors of melanoma cells. The particles exhibited excellent cytocompatibility to normal cells, good potential as imaging probes and efficient uptake by the targeted cancer cells with a rapid release of drugs in response to changes in temperature.

Hence, thermoresponsive micellar structures resulting from the self-assembly of amphiphilic block copolymers hold promise as efficient nanocarriers for drugs. These carriers exhibit controlled and sustained drug release characteristics, attributed to the integration of thermoresponsive polymers, and enhanced tumor-targeting capabilities due to the incorporation of more hydrophilic building blocks.

## 2.4 References

- (1) Smart, T.; Lomas, H.; Massignani, M.; Flores-Merino, M. V.; Perez, L. R.; Battaglia, G. Block Copolymer Nanostructures. *Nano Today* **2008**, *3*, 38–46.
- (2) Price, E.; Guo, Y.; Wang, C.; MOFFITT, M. Block Copolymer Strands with Internal Microphase Separation Structure via Self-Assembly at the Air-Water Interface. *Langmuir* **2009**, *25*, 6398-6406.
- (3) Raffa, P.; Brandenburg, P.; Wever, D. A. Z.; Broekhuis, A. A.; Picchioni, F. Polystyrene-Poly(Sodium Methacrylate) Amphiphilic Block Copolymers by ATRP: Effect of Structure, PH, and Ionic Strength on Rheology of Aqueous Solutions. *Macromolecules* **2013**, *46*, 7106–7111.

- (4) Chaduc, I.; Zhang, W.; Rieger, J.; Lansalot, M.; D'Agosto, F.; Charleux, B. Amphiphilic Block Copolymers from a Direct and One-Pot RAFT Synthesis in Water. *Macromol. Rapid Commun.* **2011**, *32*, 1270–1276.
- (5) Groison, E.; Brusseau, S.; D'Agosto, F.; Magnet, S.; Inoubli, R.; Couvreur, L.; Charleux, B. Well-Defined Amphiphilic Block Copolymer Nanoobjects via Nitroxide-Mediated Emulsion Polymerization. *ACS Macro Lett.* **2012**, *1*, 47–51.
- (6) Xiong, X. B.; Binkhathlan, Z.; Molavi, O.; Lavasanifar, A. Amphiphilic Block Co-Polymers: Preparation and Application in Nanodrug and Gene Delivery. *Acta Biomater.* **2012**, *8*, 2017–2033.
- (7) Cabral, H.; Miyata, K.; Osada, K.; Kataoka, K. Block Copolymer Micelles in Nanomedicine Applications. *Chem. Rev.* **2018**, *118*, 6844–6892.
- (8) Nardin, C.; Widmer, J.; Winterhalter, M.; Meier, W. Amphiphilic Block Copolymer Nanocontainers as Bioreactors. *Eur. Phys. J. E.* **2001**, *4*, 403–410.
- (9) Taubert, A.; Napoli, A.; Meier, W. Self-Assembly of Reactive Amphiphilic Block Copolymers as Mimetics for Biological Membranes. *Curr. Opin. Chem. Biol.* **2004**, *8*, 598–603.
- (10) Saleem, M.; Wang, L.; Yu, H.; Zain-ul-Abdin; Akram, M.; Ullah, R. S. Synthesis of Amphiphilic Block Copolymers Containing Ferrocene–Boronic Acid and Their Micellization, Redox-Responsive Properties and Glucose Sensing. *Colloid Polym. Sci.* **2017**, *295*, 995–1006.
- (11) Kumari, P.; Bera, M. K.; Malik, S.; Kuila, B. K. Amphiphilic and Thermoresponsive Conjugated Block Copolymer with Its Solvent Dependent Optical and Photoluminescence Properties: Toward Sensing Applications. *ACS Appl. Mater. Interfaces* **2015**, *7*, 12348–12354.
- (12) Zeng, J.; Lv, C.; Liu, G.; Zhang, Z.; Dong, Z.; Liu, J. Y.; Wang, Y. A Novel Ion-Imprinted Membrane Induced by Amphiphilic Block Copolymer for Selective Separation of Pt(IV) from Aqueous Solutions. *J. Memb. Sci.* **2019**, *572*, 428–441.

- (13) Lü, J.; Yang, Y.; Gao, J.; Duan, H.; Lü, C. Thermoresponsive Amphiphilic Block Copolymer-Stabilized Gold Nanoparticles: Synthesis and High Catalytic Properties. *Langmuir* **2018**, *34*, 8205–8214.
- (14) Destarac, M. Controlled Radical Polymerization: Industrial Stakes, Obstacles and Achievements. *Macromol. React. Eng.* **2010**, *4*, 165–179.
- (15) Gao, H.; Matyjaszewski, K. Synthesis of Functional Polymers with Controlled Architecture by CRP of Monomers in the Presence of Cross-Linkers: From Stars to Gels. *Prog. Polym. Sci.* **2009**, *34*, 317–350.
- (16) Zhang, H. Controlled/"living" Radical Precipitation Polymerization: A Versatile Polymerization Technique for Advanced Functional Polymers. *Eur. Polym. J.* **2013**, *49*, 579-600.
- (17) Perrier, S. 50th Anniversary Perspective: RAFT Polymerization - A User Guide. *Macromolecules* **2017**, *50*, 7433–7447.
- (18) Moad, G.; Rizzardo, E.; Thang, S. H. RAFT Polymerization and Some of Its Applications. *Chem. Asian J.* **2013**, *8*, 1634–1644.
- (19) Moad, G.; Chong, Y. K.; Postma, A.; Rizzardo, E.; Thang, S. H. Advances in RAFT Polymerization: The Synthesis of Polymers with Defined End-Groups. *Polymer* **2005**, *46*, 8458–8468.
- (20) Altarawneh, I. S.; Srour, M.; Gomes, V. G. RAFT with Bulk and Solution Polymerization: An Approach to Mathematical Modelling and Validation. *Polym. – Plast. Technol. Eng.* **2007**, *46*, 1103–1115.
- (21) Pan, X.; Zhang, F.; Choi, B.; Luo, Y.; Guo, X.; Feng, A.; Thang, S. H. Effect of Solvents on the RAFT Polymerization of N-(2-Hydroxypropyl) Methacrylamide. *Eur. Polym. J.* **2019**, *115*, 166–172.

- (22) Kopeć, M.; Krys, P.; Yuan, R.; Matyjaszewski, K. Aqueous RAFT Polymerization of Acrylonitrile. *Macromolecules* **2016**, *49*, 5877–5883.
- (23) Lansalot, M.; Davis, T. P.; Heuts, J. P. A. RAFT Miniemulsion Polymerization: Influence of the Structure of the RAFT Agent. *Macromolecules* **2002**, *35*, 7582–7591.
- (24) Smith, A. E.; Xu, X.; McCormick, C. L. Stimuli-Responsive Amphiphilic (Co)Polymers via RAFT Polymerization. *Prog. Polym. Sci.* **2010**, *35*, 45–93.
- (25) Keddie, D. J. A Guide to the Synthesis of Block Copolymers Using Reversible-Addition Fragmentation Chain Transfer (RAFT) Polymerization. *Chem. Soc. Rev.* **2014**, *43*, 496–505.
- (26) Hill, M. R.; Carmean, R. N.; Sumerlin, B. S. Expanding the Scope of RAFT Polymerization: Recent Advances and New Horizons. *Macromolecules* **2015**, *48*, 5459–5469.
- (27) Easterling, C. P.; Xia, Y.; Zhao, J.; Fanucci, G. E.; Sumerlin, B. S. Block Copolymer Sequence Inversion through Photoiniferter Polymerization. *ACS Macro Lett.* **2019**, *8*, 1461–1466.
- (28) Vega-Rios, A.; Licea-Claverie, A. Controlled Synthesis of Block Copolymers Containing N-Isopropylacrylamide by RAFT Polymerization. *J. Mex. Chem. Soc.* **2011**, *55*, 21–32.
- (29) Giguere, R. J.; Bray, T. L.; Duncan, S. M.; Majtich, G. Application of Commercial Microwave Ovens to Organic Synthesis. *Tetrahedron Lett.* **1986**, *27*, 4945–4948.
- (30) Hoogenboom, R.; Schubert, U. S. Microwave-Assisted Polymer Synthesis: Recent Developments in a Rapidly Expanding Field of Research. *Macromol. Rapid Commun.* **2007**, *28*, 368–386.
- (31) Kempe, K.; Becer, C. R.; Schubert, U. S. Microwave-Assisted Polymerizations: Recent Status and Future Perspectives. *Macromolecules* **2011**, *44*, 5825–5842.
- (32) Zong, L.; Zhou, S.; Sgriccia, N.; Hawley, M. C.; Kempel, L. C. A Review of Microwave-Assisted Polymer Chemistry (MAPC). *J. Microw. Power Electromag. Energy* **2003**, *38*, 49–74.

- (33) Mallakpour, S.; Zadehnazari, A. Microwave-Assisted Step-Growth Polymerizations (From Polycondensation to C–C Coupling). *Adv. Polym. Sci.* **2016**, *274*, 45–86.
- (34) Singla, P.; Kaur, P.; Mehta, R.; Berek, D.; Upadhyay, S. N. Ring-Opening Polymerization of Lactide Using Microwave and Conventional Heating. *Procedia Chem.* **2012**, *4*, 179–185.
- (35) Brown, S. L.; Rayner, C. M.; Graham, S.; Cooper, A.; Rannard, S.; Perrier, S. Ultra-Fast Microwave Enhanced Reversible Addition-Fragmentation Chain Transfer (RAFT) Polymerization: Monomers to Polymers in Minutes. *Chem. Commun.* **2007**, *21*, 2145–2147.
- (36) Kappe, C. O. Controlled Microwave Heating in Modern Organic Synthesis. *Angew. Chem. Int. Ed.* **2004**, *43*, 6250–6284.
- (37) Dallinger, D.; Kappe, C. O. Microwave-Assisted Synthesis in Water as Solvent. *Chem. Rev.* **2007**, *107*, 2563–2591.
- (38) Ahmadi, R.; Ullah, A. Microwave-Assisted Rapid Synthesis of a Polyether from a Plant Oil Derived Monomer and Its Optimization by Box-Behnken Design. *RSC Adv.* **2017**, *7*, 27946–27959.
- (39) Roy, D.; Ullah, A.; Sumerlin, B. S. Rapid Block Copolymer Synthesis by Microwave-Assisted RAFT Polymerization. *Macromolecules* **2009**, *42*, 7701–7708.
- (40) de la Hoz, A.; Díaz-Ortiz, À.; Moreno, A. Microwaves in Organic Synthesis. Thermal and Non-Thermal Microwave Effects. *Chem. Soc. Rev.* **2005**, *34*, 164–178.
- (41) Jin, L.; Liu, C. H.; Cintron, D.; Luo, Q.; Nieh, M. P.; He, J. Structural Engineering in the Self-Assembly of Amphiphilic Block Copolymers with Reactive Additives: Micelles, Vesicles, and Beyond. *Langmuir* **2021**, *37*, 9865–9872.
- (42) Zhang, J.; Chen, X. F.; Wei, H. B.; Wan, X. H. Tunable Assembly of Amphiphilic Rod-Coil Block Copolymers in Solution. *Chem. Soc. Rev.* **2013**, *42*, 9127–9154.

- (43) Blanz, A.; Madsen, J.; Battaglia, G.; Ryan, A. J.; Armes, S. P. Mechanistic Insights for Block Copolymer Morphologies: How Do Worms Form Vesicles? *J. Am. Chem. Soc.* **2011**, *133*, 16581–16587.
- (44) Holder, S. J.; Sommerdijk, N. A. J. M. New Micellar Morphologies from Amphiphilic Block Copolymers: Disks, Toroids and Bicontinuous Micelles. *Polym. Chem.* **2011**, *2*, 1018–1028.
- (45) Choucair, A.; Eisenberg, A. Control of Amphiphilic Block Copolymer Morphologies Using Solution Conditions. *Eur. Phys. J. E* **2003**, *10*, 37–44.
- (46) Fisicaro, E.; Compari, C.; Duce, E.; Biemmi, M.; Peroni, M.; Braibanti, A. Thermodynamics of Micelle Formation in Water, Hydrophobic Processes and Surfactant Self-Assemblies. *Phys. Chem. Chem. Phys.* **2008**, *10*, 3903–3914.
- (47) Letchford, K.; Burt, H. A Review of the Formation and Classification of Amphiphilic Block Copolymer Nanoparticulate Structures: Micelles, Nanospheres, Nanocapsules and Polymersomes. *Eur. J. Pharm. Biopharm.* **2007**, *65*, 259–269.
- (48) Wang, C.; Wang, Z.; Zhang, X. Amphiphilic Building Blocks for Self-Assembly: From Amphiphiles to Supra-Amphiphiles. *Acc. Chem. Res.* **2012**, *45*, 608–618.
- (49) Krishnan, A.; Roy, S.; Menon, S. Amphiphilic Block Copolymers: From Synthesis Including Living Polymerization Methods to Applications in Drug Delivery. *Eur. Polym. J.* **2022**, *172*, 111224.
- (50) Vazaios, A.; Touris, A.; Echeverria, M.; Zorba, G.; Pitsikalis, M. Micellization Behaviour of Linear and Nonlinear Block Copolymers Based on Poly(n-Hexyl Isocyanate) in Selective Solvents. *Polymers* **2020**, *12*, 1678.
- (51) Karayianni, M.; Pispas, S. Block Copolymer Solution Self-Assembly: Recent Advances, Emerging Trends, and Applications. *J. Polym. Sci.* **2021**, *59*, 1874–1898.

- (52) Blanz, A.; Armes, S. P.; Ryan, A. J. Self-Assembled Block Copolymer Aggregates: From Micelles to Vesicles and Their Biological Applications. *Macromol. Rapid Commun.* **2009**, *30*, 267–277.
- (53) Varlas, S.; Lawrenson, S. B.; Arkinstall, L. A.; O'Reilly, R. K.; Foster, J. C. Self-Assembled Nanostructures from Amphiphilic Block Copolymers Prepared via Ring-Opening Metathesis Polymerization (ROMP). *Prog. Polym. Sci.* **2020**, *107*, 101278.
- (54) Lombardo, D.; Kiselev, M. A.; Magazù, S.; Calandra, P. Amphiphiles Self-Assembly: Basic Concepts and Future Perspectives of Supramolecular Approaches. *Adv. Condens. Matter Phys.* **2015**, *2015*, 151683.
- (55) Yang, P.; Ning, Y.; Neal, T. J.; Jones, E. R.; Parker, B. R.; Armes, S. P. Block Copolymer Microparticles Comprising Inverse Bicontinuous Phases Prepared via Polymerization-Induced Self-Assembly. *Chem. Sci.* **2019**, *10*, 4200–4208.
- (56) Lang, C.; Kumar, M.; Hickey, R. J. Influence of Block Sequence on the Colloidal Self-Assembly of Poly(Norbornene)-Block-Poly(Ethylene Oxide) Amphiphilic Block Polymers Using Rapid Injection Processing. *Polym. Chem.* **2020**, *11*, 375–384.
- (57) Choucair, A.; Eisenberg, A. Control of Amphiphilic Block Copolymer Morphologies Using Solution Conditions. *Eur. Phys. J. E* **2003**, *10*, 37–44.
- (58) Canning, S. L.; Smith, G. N.; Armes, S. P. A Critical Appraisal of RAFT-Mediated Polymerization-Induced Self-Assembly. *Macromolecules* **2016**, *49*, 1985–2001.
- (59) Ellis, C. E.; Garcia-Hernandez, J. D.; Manners, I. Scalable and Uniform Length-Tunable Biodegradable Block Copolymer Nanofibers with a Polycarbonate Core via Living Polymerization-Induced Crystallization-Driven Self-Assembly. *J. Am. Chem. Soc.* **2022**, *144*, 20525–20538.

- (60) Frisch, H.; Tuten, B. T.; Barner-Kowollik, C. Macromolecular Superstructures: A Future Beyond Single Chain Nanoparticles. *Isr. J. Chem.* **2020**, *60*, 86–99.
- (61) Jarak, I.; Pereira-Silva, M.; Santos, A. C.; Veiga, F.; Cabral, H.; Figueiras, A. Multifunctional Polymeric Micelle-Based Nucleic Acid Delivery: Current Advances and Future Perspectives. *Appl. Mater. Today* **2021**, *25*, 101217.
- (62) Piao, C.; Zhuang, C.; Choi, M.; Ha, J.; Lee, M. A RAGE-Antagonist Peptide Potentiates Polymeric Micelle-Mediated Intracellular Delivery of Plasmid DNA for Acute Lung Injury Gene Therapy. *Nanoscale* **2020**, *12*, 13606–13617.
- (63) Li, X.; Li, H.; Liu, G.; Deng, Z.; Wu, S.; Li, P.; Xu, Z.; Xu, H.; Chu, P. K. Magnetite-Loaded Fluorine-Containing Polymeric Micelles for Magnetic Resonance Imaging and Drug Delivery. *Biomaterials* **2012**, *33*, 3013–3024.
- (64) Kedar, U.; Phutane, P.; Shidhaye, S.; Kadam, V. Advances in Polymeric Micelles for Drug Delivery and Tumor Targeting. *Nanomed.: Nanotechnol. Biol. Med.* **2010**, *6*, 714–729.
- (65) Yousefpour Marzbali, M.; Yari Khosroushahi, A. Polymeric Micelles as Mighty Nanocarriers for Cancer Gene Therapy: A Review. *Cancer Chemother. Pharmacol.* **2017**, *79*, 637–649.
- (66) Gao, G. H.; Park, M. J.; Li, Y.; Im, G. H.; Kim, J. H.; Kim, H. N.; Lee, J. W.; Jeon, P.; Bang, O. Y.; Lee, J. H.; Lee, D. S. The Use of PH-Sensitive Positively Charged Polymeric Micelles for Protein Delivery. *Biomaterials* **2012**, *33*, 9157–9164.
- (67) Ma, Y.; Fan, X.; Li, L. PH-Sensitive Polymeric Micelles Formed by Doxorubicin Conjugated Prodrugs for Co-Delivery of Doxorubicin and Paclitaxel. *Carbohydr. Polym.* **2016**, *137*, 19–29.
- (68) Shao, K.; Huang, R.; Li, J.; Han, L.; Ye, L.; Lou, J.; Jiang, C. Angiopep-2 Modified PE-PEG Based Polymeric Micelles for Amphotericin B Delivery Targeted to the Brain. *J. Controlled Release* **2010**, *147*, 118–126.

- (69) Shahin, M.; Safaei-Nikouei, N.; Lavasanifar, A. Polymeric Micelles for PH-Responsive Delivery of Cisplatin. *J Drug Target*. **2014**, *22*, 629–637.
- (70) Leung, S. Y. L.; Jackson, J.; Miyake, H.; Burt, H.; Gleave, M. E. Polymeric Micellar Paclitaxel Phosphorylates Bcl-2 and Induces Apoptotic Regression of Androgen-Independent LNCaP Prostate Tumors. *Prostate* **2000**, *44*, 156–163.
- (71) Pişkin, E.; Kaitian, X.; Denkbaş, E. B.; Küçükyavuz, Z. Novel PDLLA/PEG Copolymer Micelles as Drug Carriers. *J. Biomater. Sci. Polym. Ed.* **1996**, *7*, 359–373.
- (72) Fujiwara, Y.; Mukai, H.; Saeki, T.; Ro, J.; Lin, Y. C.; Nagai, S. E.; Lee, K. S.; Watanabe, J.; Ohtani, S.; Kim, S. B.; Kuroi, K.; Tsugawa, K.; Tokuda, Y.; Iwata, H.; Park, Y. H.; Yang, Y.; Nambu, Y. A Multi-National, Randomised, Open-Label, Parallel, Phase III Non-Inferiority Study Comparing NK105 and Paclitaxel in Metastatic or Recurrent Breast Cancer Patients. *Br. J. Cancer* **2019**, *120*, 475–480.
- (73) Pitto-Barry, A.; Barry, N. P. E. Pluronic® Block-Copolymers in Medicine: From Chemical and Biological Versatility to Rationalisation and Clinical Advances. *Polym. Chem.* **2014**, *5*, 3291–3297.
- (74) Kim, J. Y.; Do, Y. R.; Song, H. S.; Cho, Y. Y.; Ryoo, H. M.; Bae, S. H.; Kim, J. G.; Chae, Y. S.; Kang, B. W.; Baek, J. H.; Kim, M. K.; Lee, K. H.; Park, K. Multicenter Phase II Clinical Trial of Genexol-Pm® with Gemcitabine in Advanced Biliary Tract Cancer. *Anticancer Res.* **2017**, *37*, 1467–1473.
- (75) Hamaguchi, T.; Tsuji, A.; Yamaguchi, K.; Takeda, K.; Uetake, H.; Esaki, T.; Amagai, K.; Sakai, D.; Baba, H.; Kimura, M.; Matsumura, Y.; Tsukamoto, T. A Phase II Study of NK012, a Polymeric Micelle Formulation of SN-38, in Unresectable, Metastatic or Recurrent Colorectal Cancer Patients. *Cancer Chemother. Pharmacol.* **2018**, *82*, 1021–1029.

- (76) Ruxandra Volovat, S.; Ciuleanu, T.-E.; Koralewski, P.; Olson, J. E. G.; Croitoru, A.; Koynov, K.; Stabile, S.; Cerea, G.; Osada, A.; Bobe, I.; Volovat, C. A Multicenter, Single-Arm, Basket Design, Phase II Study of NC-6004 plus Gemcitabine in Patients with Advanced Unresectable Lung, Biliary Tract, or Bladder Cancer. *Oncotarget* **2020**, *11*, 3105-3117.
- (77) Hrkach, J.; Hoff, D. Von; Ali, M. M.; Andrianova, E.; Auer, J.; Campbell, T.; De Witt, D.; Figa, M.; Figueiredo, M.; Horhota, A.; Low, S.; McDonnell, K.; Peeke, E.; Retnarajan, B.; Sabnis, A.; Schnipper, E.; Song, J. J.; Song, Y. H.; Summa, J.; Tompsett, D.; Troiano, G.; Van, T.; Hoven, G.; Wright, J.; Lorusso, P.; Kantoff, P. W.; Bander, N. H.; Sweeney, C.; Farokhzad, O. C.; Langer, R.; Zale, S. Preclinical Development and Clinical Translation of a PSMA-Targeted Docetaxel Nanoparticle with a Differentiated Pharmacological Profile. *Sci. Transl. Med.* **2012**, *4*, 128ra39.
- (78) Boere, I.; Vergote, I.; Hanssen, R.; Jalving, M.; Gennigens, C.; Ottevanger, P.; Van De Wouw, Y. J.; Rijcken, C. J. F.; Mathijssen, R. H. J.; Ledermann, J. CINOVA: A Phase II Study of CPC634 (Nanoparticulate Docetaxel) in Patients with Platinum Resistant Recurrent Ovarian Cancer. *Int. J. Gynecol. Cancer* **2023**, *33*, 1247–1252.
- (79) Matsumura, Y.; Hamaguchi, T.; Ura, T.; Muro, K.; Yamada, Y.; Shimada, Y.; Shirao, K.; Okusaka, T.; Ueno, H.; Ikeda, M.; Watanabe, N. Phase I Clinical Trial and Pharmacokinetic Evaluation of NK911, a Micelle-Encapsulated Doxorubicin. *Br. J. Cancer* **2004**, *91*, 1775–1781.
- (80) Ahmad, Z.; Shah, A.; Siddiq, M.; Kraatz, H. B. Polymeric Micelles as Drug Delivery Vehicles. *RSC Adv.* **2014**, *4*, 17028–17038.
- (81) Gong, J.; Chen, M.; Zheng, Y.; Wang, S.; Wang, Y. Polymeric Micelles Drug Delivery System in Oncology. *J. Controlled Release.* **2012**, *159*, 312–323.
- (82) Kolate, A.; Baradia, D.; Patil, S.; Vhora, I.; Kore, G.; Misra, A. PEG - A Versatile Conjugating Ligand for Drugs and Drug Delivery Systems. *J. Controlled Release.* **2014**, *192*, 67–81.

- (83) D'souza, A. A.; Shegokar, R. Polyethylene Glycol (PEG): A Versatile Polymer for Pharmaceutical Applications. *Expert Opin. Drug Delivery* **2016**, *13*, 1257–1275.
- (84) Hunter, A. C.; Moghimi, S. M. Smart Polymers in Drug Delivery: A Biological Perspective. *Polym. Chem.* **2017**, *8*, 41–51.
- (85) Yokoyama, M. Polymeric Micelles as Drug Carriers: Their Lights and Shadows. *J. Drug Targeting* **2014**, *22*, 576–583.
- (86) Aliabadi, H. M.; Lavasanifar, A. Polymeric Micelles for Drug Delivery. *Expert Opin. Drug Delivery*. **2006**, *3*, 139–162.
- (87) Gullotti, E.; Yeo, Y. Extracellularly Activated Nanocarriers: A New Paradigm of Tumor Targeted Drug Delivery. *Mol. Pharmaceutics*. **2009**, *6*, 1041–1051.
- (88) Matsumura, Y.; Maeda, H. A New Concept for Macromolecular Therapeutics in Cancer Chemotherapy: Mechanism of Tumoritropic Accumulation of Proteins and the Antitumor Agent Smancs. *Cancer Res.* **1986**, *46*, 6387–6392.
- (89) Kulthe, S. S.; Choudhari, Y. M.; Inamdar, N. N.; Mourya, V. Polymeric Micelles: Authoritative Aspects for Drug Delivery. *Des. Monomers Polym.* **2012**, *15*, 465–521.
- (90) Owen, S.; Chan, D.; Shoichet, M. Polymeric Micelle Stability. *Nano Today* **2012**, *7*, 53-65.
- (91) Krause, M. E.; Sahin, E. Chemical and Physical Instabilities in Manufacturing and Storage of Therapeutic Proteins. *Curr. Opin. Biotechnol.* **2019**, *60*, 159–167.
- (92) Liu, X.; Gao, W. Precision Conjugation: An Emerging Tool for Generating Protein–Polymer Conjugates. *Angew. Chem. Int. Ed.* **2021**, *60*, 11024–11035.
- (93) Pelegri-Oday, E. M.; Lin, E. W.; Maynard, H. D. Therapeutic Protein-Polymer Conjugates: Advancing beyond Pegylation. *J. Am. Chem. Soc.* **2014**, *136*, 14323–14332.

- (94) Gupta, V.; Bhavanasi, S.; Quadir, M.; Singh, K.; Ghosh, G.; Vasamreddy, K.; Ghosh, A.; Siahhaan, T. J.; Banerjee, S.; Banerjee, S. K. Protein PEGylation for Cancer Therapy: Bench to Bedside. *J. Cell Commun. Signaling* **2019**, *13*, 319–330.
- (95) Veronese, F. M.; Mero, A. The Impact of PEGylation on Biological Therapies. *Biodrugs* **2008**, *22*, 315–329.
- (96) Mao, L.; Russell, A. J.; Carmali, S. Moving Protein PEGylation from an Art to a Data Science. *Bioconjugate Chem.* **2022**, *33*, 1643–1653.
- (97) Abu Lila, A. S.; Kiwada, H.; Ishida, T. The Accelerated Blood Clearance (ABC) Phenomenon: Clinical Challenge and Approaches to Manage. *J. Controlled Release* **2013**, *172*, 38–47.
- (98) Ryan, S. M.; Wang, X.; Mantovani, G.; Sayers, C. T.; Haddleton, D. M.; Brayden, D. J. Conjugation of Salmon Calcitonin to a Combed-Shaped End Functionalized Poly(Poly(Ethylene Glycol) Methyl Ether Methacrylate) Yields a Bioactive Stable Conjugate. *J. Controlled Release* **2009**, *135*, 51–59.
- (99) Tao, L.; Liu, J.; Davis, T. P. Branched Polymer-Protein Conjugates Made from Mid-Chain-Functional P(HPMA). *Biomacromolecules* **2009**, *10*, 2847–2851.
- (100) Guindani, C.; Feuser, P. E.; Cordeiro, A. P.; de Meneses, A. C.; Possato, J. C.; da Silva Abel, J.; Machado-de-Ávila, R. A.; Sayer, C.; de Araújo, P. H. H. Bovine Serum Albumin Conjugation on Poly(Methyl Methacrylate) Nanoparticles for Targeted Drug Delivery Applications. *J. Drug Deliv. Sci. Technol.* **2020**, *56*, 101490.
- (101) Liu, F.; Cui, Y.; Wang, L.; Wang, H.; Yuan, Y.; Pan, J.; Chen, H.; Yuan, L. Temperature-Responsive Poly(N-Isopropylacrylamide) Modified Gold Nanoparticle-Protein Conjugates for Bioactivity Modulation. *ACS Appl. Mater. Interfaces* **2015**, *7*, 11547–11554.

- (102) Liu, Z.; Chen, N.; Dong, C.; Li, W.; Guo, W.; Wang, H.; Wang, S.; Tan, J.; Tu, Y.; Chang, J. Facile Construction of Near Infrared Fluorescence Nanoprobe with Amphiphilic Protein-Polymer Bioconjugate for Targeted Cell Imaging. *ACS Appl. Mater. Interfaces* **2015**, *7*, 18997–19005.
- (103) Stevens, C. A.; Kaur, K.; Klok, H. A. Self-Assembly of Protein-Polymer Conjugates for Drug Delivery. *Adv. Drug Delivery Rev.* **2021**, *174*, 447–460.
- (104) Paloni, J. M.; Olsen, B. D. Coiled-Coil Domains for Self-Assembly and Sensitivity Enhancement of Protein-Polymer Conjugate Biosensors. *ACS Appl. Polym. Mater.* **2020**, *2*, 1114–1123.
- (105) Taguchi, K.; Lu, H.; Jiang, Y.; Hung, T. T.; Stenzel, M. H. Safety of Nanoparticles Based on Albumin-Polymer Conjugates as a Carrier of Nucleotides for Pancreatic Cancer Therapy. *J. Mater. Chem. B* **2018**, *6*, 6278–6287.
- (106) Zhao, W.; Liu, F.; Chen, Y.; Bai, J.; Gao, W. Synthesis of Well-Defined Protein-Polymer Conjugates for Biomedicine. *Polymer* **2015**, *66*, A1–A10.
- (107) González-Toro, D. C.; Thayumanavan, S. Advances in Polymer and Polymeric Nanostructures for Protein Conjugation. *Eur. Polym. J.* **2013**, *49*, 2906–2918.
- (108) Grover, G. N.; Maynard, H. D. Protein-Polymer Conjugates: Synthetic Approaches by Controlled Radical Polymerizations and Interesting Applications. *Curr. Opin. Chem. Biol.* **2010**, *14*, 818–827.
- (109) Heredia, K. L.; Maynard, H. D. Synthesis of Protein-Polymer Conjugates. *Org. Biomol. Chem.* **2007**, *5*, 45–53.
- (110) Broyer, R. M.; Grover, G. N.; Maynard, H. D. Emerging Synthetic Approaches for Protein-Polymer Conjugations. *Chem. Commun.* **2011**, *47*, 2212–2226.

- (111) Bontempo, D.; Maynard, H. D. Streptavidin as a Macroinitiator for Polymerization: In Situ Protein-Polymer Conjugate Formation Scheme 1. Streptavidin-Initiated Polymerization. *J. Am. Chem. Soc.* **2005**, *127*, 6508–6509.
- (112) Wang, Y.; Wu, C. Site-Specific Conjugation of Polymers to Proteins. *Biomacromolecules* **2018**, *19*, 1804–1825.
- (113) Ko, J. H.; Maynard, H. D. A Guide to Maximizing the Therapeutic Potential of Protein-Polymer Conjugates by Rational Design. *Chem. Soc. Rev.* **2018**, *47*, 8998–9014.
- (114) Ma, C.; Liu, X.; Wu, G.; Zhou, P.; Zhou, Y.; Wang, L.; Huang, X. Efficient Way to Generate Protein-Based Nanoparticles by in-Situ Photoinitiated Polymerization-Induced Self-Assembly. *ACS Macro Lett.* **2017**, *6*, 689–694.
- (115) Jiang, Y.; Lu, H.; Khine, Y. Y.; Dag, A.; Stenzel, M. H. Polyion Complex Micelle Based on Albumin-Polymer Conjugates: Multifunctional Oligonucleotide Transfection Vectors for Anticancer Chemotherapeutics. *Biomacromolecules* **2014**, *15*, 4195–4205.
- (116) Vanparijs, N.; Maji, S.; Louage, B.; Voorhaar, L.; Laplace, D.; Zhang, Q.; Shi, Y.; Hennink, W. E.; Hoogenboom, R.; De Geest, B. G. Polymer-Protein Conjugation via a “grafting to” Approach—a Comparative Study of the Performance of Protein-Reactive RAFT Chain Transfer Agents. *Polym. Chem.* **2015**, *6*, 5602–5614.
- (117) Huang, A.; Paloni, J. M.; Wang, A.; Obermeyer, A. C.; Sureka, H. V.; Yao, H.; Olsen, B. D. Predicting Protein-Polymer Block Copolymer Self-Assembly from Protein Properties. *Biomacromolecules* **2019**, *20*, 3713–3723.
- (118) Lam, C. N.; Yao, H.; Olsen, B. D. The Effect of Protein Electrostatic Interactions on Globular Protein-Polymer Block Copolymer Self-Assembly. *Biomacromolecules* **2016**, *17*, 2820–2829.

- (119) Suguri, T.; Olsen, B. D. Topology Effects on Protein-Polymer Block Copolymer Self-Assembly. *Polym. Chem.* **2019**, *10*, 1751–1761.
- (120) Liu, Z.; Dong, C.; Wang, X.; Wang, H.; Li, W.; Tan, J.; Chang, J. Self-Assembled Biodegradable Protein-Polymer Vesicle as a Tumor-Targeted Nanocarrier. *ACS Appl. Mater. Interfaces* **2014**, *6*, 2393–2400.
- (121) Chang, D.; Lam, C. N.; Tang, S.; Olsen, B. D. Effect of Polymer Chemistry on Globular Protein-Polymer Block Copolymer Self-Assembly. *Polym. Chem.* **2014**, *5*, 4884–4895.
- (122) Vukovic, I.; Voortman, T.; Merino, D.; Portale, G.; Hiekkataipale, P.; Ruokolainen, J.; Brinke, G.; Loos, K. Double Gyroid Network Morphology in Supramolecular Diblock Copolymer Complexes. *Macromolecules* **2012**, *45*, 3503–3512.
- (123) Reynhout, I. C.; Cornelissen, J. J. L. M.; Nolte, R. J. M. Self-Assembled Architectures from Biohybrid Triblock Copolymers. *J. Am. Chem. Soc.* **2007**, *129*, 2327–2332.
- (124) Cao, Q.; He, N.; Wang, Y.; Lu, Z. Self-Assembled Nanostructures from Amphiphilic Globular Protein–Polymer Hybrids. *Polym. Bull.* **2018**, *75*, 2627–2639.
- (125) Liu, X.; Gao, W. In Situ Growth of Self-Assembled Protein-Polymer Nanovesicles for Enhanced Intracellular Protein Delivery. *ACS Appl. Mater. Interfaces* **2017**, *9*, 2023–2028.
- (126) Lam, C. N.; Olsen, B. D. Phase Transitions in Concentrated Solution Self-Assembly of Globular Protein-Polymer Block Copolymers. *Soft Matter* **2013**, *9*, 2393–2402.
- (127) Xia, X. X.; Wang, M.; Lin, Y.; Xu, Q.; Kaplan, D. L. Hydrophobic Drug-Triggered Self-Assembly of Nanoparticles from Silk-Elastin-like Protein Polymers for Drug Delivery. *Biomacromolecules* **2014**, *15*, 908–914.
- (128) Ge, J.; Neofytou, E.; Lei, J.; Beygui, R. E.; Zare, R. N. Protein-Polymer Hybrid Nanoparticles for Drug Delivery. *Small* **2012**, *8*, 3573–3578.

- (129) Welch, R. P.; Lee, H.; Luzuriaga, M. A.; Brohlin, O. R.; Gassensmith, J. J. Protein-Polymer Delivery: Chemistry from the Cold Chain to the Clinic. *Bioconjugate Chem.* **2018**, *29*, 2867–2883.
- (130) Ge, J.; Lei, J.; Zare, R. N. Bovine Serum Albumin-Poly(Methyl Methacrylate) Nanoparticles: An Example of Frustrated Phase Separation. *Nano Lett.* **2011**, *11*, 2551–2554.
- (131) Wong, C. K.; Laos, A. J.; Soeriyadi, A. H.; Wiedenmann, J.; Curmi, P. M. G.; Gooding, J. J.; Marquis, C. P.; Stenzel, M. H.; Thordarson, P. Polymersomes Prepared from Thermoresponsive Fluorescent Protein–Polymer Bioconjugates: Capture of and Report on Drug and Protein Payloads. *Angew. Chem.* **2015**, *127*, 5407–5412.
- (132) Li, X.; Wei, Y.; Wu, Y.; Yin, L. Hypoxia-Induced Pro-Protein Therapy Assisted by a Self-Catalyzed Nanozymogen. *Angew. Chem. Int. Ed.* **2020**, *59*, 22544–22553.
- (133) Mills, J. K.; Needham, D. Targeted Drug Delivery. *Expert Opin. Ther. Pat.* **1999**, *9*, 1499–1513.
- (134) Wang, Z.; Chen, J.; Little, N.; Lu, J. Self-Assembling Prodrug Nanotherapeutics for Synergistic Tumor Targeted Drug Delivery. *Acta Biomater.* **2020**, *111*, 20–28.
- (135) Kauscher, U.; Holme, M. N.; Björnmalm, M.; Stevens, M. M. Physical Stimuli-Responsive Vesicles in Drug Delivery: Beyond Liposomes and Polymersomes. *Adv. Drug Delivery Rev.* **2019**, *138*, 259–275.
- (136) Srinivasarao, M.; Low, P. S. Ligand-Targeted Drug Delivery. *Chem. Rev.* **2017**, *117*, 12133–12164.
- (137) Alley, S. C.; Okeley, N. M.; Senter, P. D. Antibody-Drug Conjugates: Targeted Drug Delivery for Cancer. *Curr. Opin. Chem. Biol.* **2010**, *14*, 529–537.

- (138) Ma, Y.; Mao, G.; Wu, G.; Cui, Z.; Zhang, X. E.; Huang, W. CRISPR-DCas9-Guided and Telomerase-Responsive Nanosystem for Precise Anti-Cancer Drug Delivery. *ACS Appl. Mater. Interfaces* **2021**, *13*, 7890–7896.
- (139) Shim, G.; Kim, D.; Park, G. T.; Jin, H.; Suh, S. K.; Oh, Y. K. Therapeutic Gene Editing: Delivery and Regulatory Perspectives. *Acta Pharmacol. Sin.* **2017**, *38*, 738–753.
- (140) Xue, X.; Liang, X. J. Overcoming Drug Efflux-Based Multidrug Resistance in Cancer with Nanotechnology. *Chin. J. Cancer.* **2012**, *31*, 100–109.
- (141) Emran, T. Bin; Shahriar, A.; Mahmud, A. R.; Rahman, T.; Abir, M. H.; Siddiquee, M. F. R.; Ahmed, H.; Rahman, N.; Nainu, F.; Wahyudin, E.; Mitra, S.; Dhama, K.; Habiballah, M. M.; Haque, S.; Islam, A.; Hassan, M. M. Multidrug Resistance in Cancer: Understanding Molecular Mechanisms, Immunoprevention and Therapeutic Approaches. *Front. Oncol.* **2022**, *12*, 891652.
- (142) Luque-Michel, E.; Imbuluzqueta, E.; Sebastián, V.; Blanco-Prieto, M. J. Clinical Advances of Nanocarrier-Based Cancer Therapy and Diagnostics. *Expert Opin. Drug Delivery.* **2017**, *14*, 75–92.
- (143) Kumari, P.; Ghosh, B.; Biswas, S. Nanocarriers for Cancer-Targeted Drug Delivery. *J. Drug Target.* **2016**, *24*, 179–191.
- (144) Cui, W.; Li, J.; Decher, G. Self-Assembled Smart Nanocarriers for Targeted Drug Delivery. *Adv. Mater.* **2016**, *28*, 1302–1311.
- (145) Kanamala, M.; Wilson, W. R.; Yang, M.; Palmer, B. D.; Wu, Z. Mechanisms and Biomaterials in PH-Responsive Tumour Targeted Drug Delivery: A Review. *Biomaterials* **2016**, *85*, 152–167.
- (146) Raza, A.; Hayat, U.; Rasheed, T.; Bilal, M.; Iqbal, H. M. N. Redox-Responsive Nano-Carriers as Tumor-Targeted Drug Delivery Systems. *Eur. J. Med. Chem.* **2018**, *157*, 705–715.

- (147) Hervault, A.; Dunn, A. E.; Lim, M.; Boyer, C.; Mott, D.; Maenosono, S.; Thanh, N. T. K. Doxorubicin Loaded Dual PH- and Thermo-Responsive Magnetic Nanocarrier for Combined Magnetic Hyperthermia and Targeted Controlled Drug Delivery Applications. *Nanoscale* **2016**, *8*, 12152–12161.
- (148) Du, B.; Jia, S.; Wang, Q.; Ding, X.; Liu, Y.; Yao, H.; Zhou, J. A Self-Targeting, Dual ROS/PH-Responsive Apoferritin Nanocage for Spatiotemporally Controlled Drug Delivery to Breast Cancer. *Biomacromolecules* **2018**, *19*, 1026–1036.
- (149) Xiao, L.; Huang, L.; Moingeon, F.; Gauthier, M.; Yang, G. PH-Responsive Poly(Ethylene Glycol)-Block-Polylactide Micelles for Tumor-Targeted Drug Delivery. *Biomacromolecules* **2017**, *18*, 2711–2722.
- (150) Kwon, I. K.; Lee, S. C.; Han, B.; Park, K. Analysis on the Current Status of Targeted Drug Delivery to Tumors. *J. Controlled Release* **2012**, *164*, 108–114.
- (151) Manzari, M. T.; Shamay, Y.; Kiguchi, H.; Rosen, N.; Scaltriti, M.; Heller, D. A. Targeted Drug Delivery Strategies for Precision Medicines. *Nat. Rev. Mater.* **2021**, *6*, 351–370.
- (152) Chang, C. Y.; Wang, M. C.; Miyagawa, T.; Chen, Z. Y.; Lin, F. H.; Chen, K. H.; Liu, G. S.; Tseng, C. L. Preparation of Arginine–Glycine–Aspartic Acid-Modified Biopolymeric Nanoparticles Containing Epigallocatechin-3-Gallate for Targeting Vascular Endothelial Cells to Inhibit Corneal Neovascularization. *Int. J. Nanomedicine* **2017**, *12*, 279–294.
- (153) Amin, M.; Mansourian, M.; Koning, G. A.; Badiee, A.; Jaafari, M. R.; Ten Hagen, T. L. M. Development of a Novel Cyclic RGD Peptide for Multiple Targeting Approaches of Liposomes to Tumor Region. *J. Controlled Release* **2015**, *220*, 308–315.

- (154) Li, C.; Wang, W.; Xi, Y.; Wang, J.; Chen, J. F.; Yun, J.; Le, Y. Design, Preparation and Characterization of Cyclic RGDfK Peptide Modified Poly(Ethylene Glycol)-Block-Poly(Lactic Acid) Micelle for Targeted Delivery. *Mater. Sci. Eng. C* **2016**, *64*, 303–309.
- (155) Seuring, J.; Agarwal, S. Polymers with Upper Critical Solution Temperature in Aqueous Solution: Unexpected Properties from Known Building Blocks. *ACS Macro Lett.* **2013**, *2*, 597–600.
- (156) Vanparijs, N.; Nuhn, L.; De Geest, B. G. Transiently Thermoresponsive Polymers and Their Applications in Biomedicine. *Chem. Soc. Rev.* **2017**, *46*, 1193–1239.
- (157) Roy, D.; Brooks, W. L. A.; Sumerlin, B. S. New Directions in Thermoresponsive Polymers. *Chem. Soc. Rev.* **2013**, *42*, 7214–7243.
- (158) Weber, C.; Hoogenboom, R.; Schubert, U. S. Temperature Responsive Bio-Compatible Polymers Based on Poly(Ethylene Oxide) and Poly(2-Oxazoline)s. *Prog. Polym. Sci.* **2012**, *37*, 686–714.
- (159) Cortez-Lemus, N. A.; Licea-Claverie, A. Poly(N-Vinylcaprolactam), a Comprehensive Review on a Thermoresponsive Polymer Becoming Popular. *Prog. Polym. Sci.* **2016**, *53*, 1–51.
- (160) Dai, M.; Goudounet, G.; Zhao, H.; Garbay, B.; Garanger, E.; Pecastaings, G.; Schultze, X.; Lecommandoux, S. Thermosensitive Hybrid Elastin-like Polypeptide-Based ABC Triblock Hydrogel. *Macromolecules* **2021**, *54*, 327–340.
- (161) Doberenz, F.; Zeng, K.; Willems, C.; Zhang, K.; Groth, T. Thermoresponsive Polymers and Their Biomedical Application in Tissue Engineering-A Review. *J. Mater. Chem. B* **2020**, *8*, 607–628.

- (162) Ansari, M. J.; Rajendran, R. R.; Mohanto, S.; Agarwal, U.; Panda, K.; Dhotre, K.; Manne, R.; Deepak, A.; Zafar, A.; Yasir, M.; Pramanik, S. Poly(N-Isopropylacrylamide)-Based Hydrogels for Biomedical Applications: A Review of the State-of-the-Art. *Gels* **2022**, *8*, 454.
- (163) Sponchioni, M.; Capasso Palmiero, U.; Moscatelli, D. Thermo-Responsive Polymers: Applications of Smart Materials in Drug Delivery and Tissue Engineering. *Mater. Sci. Eng. C* **2019**, *102*, 589–605.
- (164) Pawar, M. D.; Rathna, G. V. N.; Agrawal, S.; Kuchekar, B. S. Bioactive Thermoresponsive Polyblend Nanofiber Formulations for Wound Healing. *Mater. Sci. Eng. C* **2015**, *48*, 126–137.
- (165) Rahikkala, A.; Aseyev, V.; Tenhu, H.; Kauppinen, E. I.; Raula, J. Thermoresponsive Nanoparticles of Self-Assembled Block Copolymers as Potential Carriers for Drug Delivery and Diagnostics. *Biomacromolecules* **2015**, *16*, 2750–2756.
- (166) Li, Y. Y.; Zhang, X. Z.; Zhu, J. L.; Cheng, H.; Cheng, S. X.; Zhuo, R. X. Self-Assembled, Thermoresponsive Micelles Based on Triblock PMMA-b-PNIPAAm-b-PMMA Copolymer for Drug Delivery. *Nanotechnology* **2007**, *18*, 215605.
- (167) Pourjavadi, A.; Mazaheri Tehrani, Z.; Dastanpour, L. Smart Magnetic Self-Assembled Micelle: An Effective Nanocarrier for Thermo-Triggered Paclitaxel Delivery. *Int. J. Polym. Mater. Polym. Biomaterials* **2019**, *68*, 741–749.
- (168) Liu, F.; Kozlovskaya, V.; Medipelli, S.; Xue, B.; Ahmad, F.; Saeed, M.; Cropek, D.; Kharlampieva, E. Temperature-Sensitive Polymersomes for Controlled Delivery of Anticancer Drugs. *Chem. Mater.* **2015**, *27*, 7945–7956.
- (169) Tabatabaei Rezaei, S. J.; Nabid, M. R.; Niknejad, H.; Entezami, A. A. Multifunctional and Thermoresponsive Unimolecular Micelles for Tumor-Targeted Delivery and Site-Specifically Release of Anticancer Drugs. *Polymer* **2012**, *53*, 3485–3497.

- (170) Shen, B.; Ma, Y.; Yu, S.; Ji, C. Smart Multifunctional Magnetic Nanoparticle-Based Drug Delivery System for Cancer Thermo-Chemotherapy and Intracellular Imaging. *ACS Appl. Mater. Interfaces* **2016**, *8*, 24502–24508.
- (171) Chen, Y. C.; Liao, L. C.; Lu, P. L.; Lo, C. L.; Tsai, H. C.; Huang, C. Y.; Wei, K. C.; Yen, T. C.; Hsiue, G. H. The Accumulation of Dual PH and Temperature Responsive Micelles in Tumors. *Biomaterials* **2012**, *33*, 4576–4588.
- (172) Wadajkar, A. S.; Bhavsar, Z.; Ko, C. Y.; Koppolu, B.; Cui, W.; Tang, L.; Nguyen, K. T. Multifunctional Particles for Melanoma-Targeted Drug Delivery. *Acta Biomater.* **2012**, *8*, 2996–3004.

## **CHAPTER 3. Synthesis and Evaluation of Thermoresponsive Renewable Lipid-based Block Copolymers for Drug Delivery**

### **3.1 Introduction**

Many drug molecules that are currently in the market suffer from short half-life, *in vivo* instability, poor bioavailability and rapid degradation. Since the 1960s, various drug delivery systems, typically polymers including polymeric micelles, liposomes, dendrimers and nanotubes have been developed.<sup>1-6</sup> Their ability to transport therapeutic agents in a targeted and controllable manner is the major goal of modern medicine. Polymeric micelles are nanosized structures formed by self-assembly of amphiphilic block copolymers in aqueous solution. They have two distinct regions with a hydrophilic shell and hydrophobic core that facilitates the solubilisation of poorly soluble pharmaceuticals. There are many advantages of using micelles as drug delivery vehicles over others, such as their ease of preparation, relatively high stability and size advantages enabling passive targeting of tumors through enhanced permeability and retention (EPR) effect.<sup>7-9</sup> Additionally, micelles with versatile functions and characteristics can be easily designed by altering the type and chemical structure of block copolymers. To date, several polymeric micelles as drug delivery vehicles have been authorized or are in clinical trials.<sup>10,11</sup>

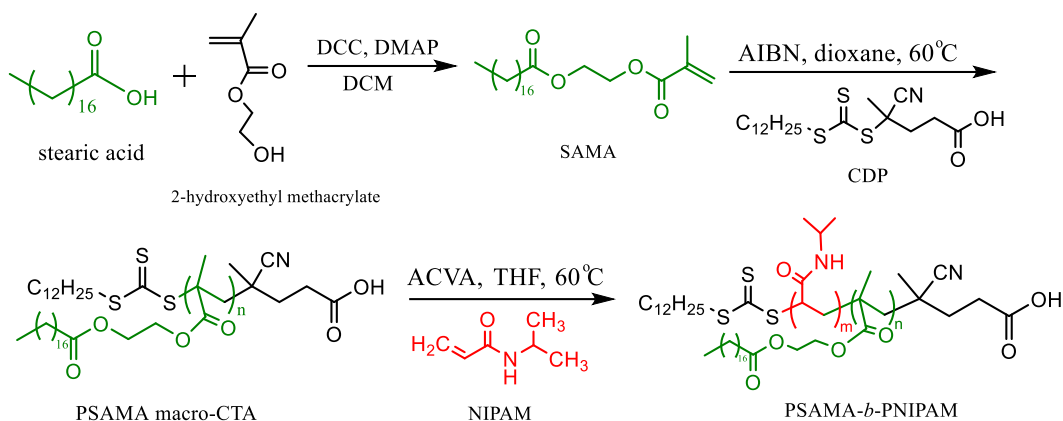
To achieve site-specific drug targeting and on-demand release, research efforts have been devoted to developing advanced drug delivery systems.<sup>12,13</sup> One such example is smart delivery systems, which involve the utilization of stimuli-responsive polymers. These carriers can hold drugs in the course of transport and only release them in response to internal or external stimulus, e.g., heat, pH, enzyme, light and ultrasound, due to a sharp change in their physical properties.<sup>14-18</sup>

Temperature is one of the most extensively investigated stimuli for drug delivery. The drug release from thermoresponsive carriers can be either internally observed in certain pathological tissues (e.g., ~42 °C at tumor sites)<sup>19</sup> or externally achieved by applying an external heating source. Thermoresponsive polymers exhibit a hydrophilic nature below a certain temperature, known as lower critical solution temperature (LCST), but alter to hydrophobic and collapse as temperature increase above their LCST. The LCST values within a desired range can be modulated by introduction of the hydrophobic or hydrophilic co-monomers.<sup>20,21</sup> Poly(N-isopropylacrylamide) (PNIPAM) is the most well-studied thermoresponsive polymer with an LCST around 32 °C in aqueous media, which is close to the physiological temperature of human body. PNIPAM and its copolymers have been extensively exploited for various biomedical applications.<sup>22–24</sup> There are also many examples of PNIPAM-based amphiphilic block copolymers for drug delivery applications, where the hydrophobic segments comprise polystyrene,<sup>25</sup> poly(methyl methacrylate),<sup>26</sup> poly( $\epsilon$ -caprolactone),<sup>27</sup> etc.

Synthesis of block copolymers incorporating biodegradable and biocompatible monomers are highly attractive for micelle preparation due to their potential sustained drug release and low toxicity. In recent years, the use of monomers from renewable feedstocks to replace fossil-based monomers with an aim to promote greener solutions has received special attention. In this regard, fatty acid moieties from renewable plant oils can be considered as great candidates and alternatives to some synthetic hydrophobic monomers due to their good biocompatibility, biodegradability, easy availability and proper hydrophobicity. Up to now, most studies have focused on the application of fatty acid-based polymers into biocomposites, thermoplastics, and elastomers.<sup>28–30</sup> While there are a few examples of fatty acid-based block copolymers using atom transfer radical polymerization (ATRP) or reversible addition-fragmentation chain transfer (RAFT),<sup>31–35</sup> few

attempts have been made in terms of their applications as amphiphilic block copolymers for drug delivery. To the best of the author's knowledge, the microwave-assisted synthesis of thermoresponsive block copolymers from fatty acids and NIPAM and their controlled delivery has not been reported.

In this study, amphiphilic block copolymer containing fatty acid derived polymer poly(2-methacryloyloxy) ethyl stearate (PSAMA) and thermoresponsive polymer PNIPAM was synthesized through RAFT polymerization under microwave irradiation (Scheme 3.1.) and characterized. PSAMA-*b*-PNIPAM block copolymers with narrow polydispersity index (PDI) and well-controlled lengths of different block ratios were prepared and self-assembled in aqueous medium via the combination of co-solvent evaporation and dialysis method. Afterwards, the effect of balance between hydrophilic-hydrophobic interactions on particle size, morphology and critical micelle concentration (CMC) of the polymeric micelles was investigated. Carbamazepine (CBZ), an antiepileptic and anticonvulsant drug, was selected as a hydrophobic model drug to evaluate the drug encapsulation ability of PSAMA-*b*-PNIPAM micelles. Moreover, *in vitro* thermoresponsive drug release behaviour of PSAMA-*b*-PNIPAM micelles was also studied to further explore their potential application as drug carriers.



Scheme 3.1. Synthetic route for amphiphilic block copolymer PSAMA-*b*-PNIPAM via microwave-assisted RAFT polymerization.

## 3.2 Materials and methods

### 3.2.1 Materials

N-isopropylacrylamide (NIPAM, >99%, Sigma, St. Louis, MO, USA) was recrystallized from n-hexane before use. 2, 2'-Azobisisobutyronitrile (AIBN, 98%) and 4,4'-Azobis(4-cyanovaleric acid) (ACVA, ≥98%) were obtained from Sigma (St. Louis, MO, USA) and recrystallized from methanol prior to use. Stearic acid (>98%) was purchased from TCI America (Tokyo, Japan) and used as received. 4-Cyano-4-[(dodecylsulfanylthiocarbonyl)sulfanyl]pentanoic acid (CDP, 97%), dicyclohexylcarbodiimide (DCC, 99%), 4-dimethylaminopyridine (DMAP, 99%), 2-hydroxyethyl methacrylate (HEMA, ≥99%) carbamazepine (CBZ, ≥98%), 1,3,5-trioxane (≥99%), pyrene (98%) and sodium sulphate anhydrous (Na<sub>2</sub>SO<sub>4</sub>, 99%) were purchased from Sigma (St. Louis, MO, USA) and used without any further purification. 1,4-Dioxane (99%, Fisher Scientific, Waltham, MA, USA) and tetrahydrofuran (THF, ≥99%, Sigma, St. Louis, MO, USA) was purified by passing through a short alumina column before use. Chloroform-d (99.8 atom %D), dichloromethane (DCM, ≥99.5%) and ethyl acetate (EtOAc, ≥99.5%) were from Sigma (St. Louis, MO, USA),

while sodium bicarbonate (NaHCO<sub>3</sub>, 99.8%) and sodium chloride (NaCl, 99.9%), diethyl ether (≥99%), methanol (99.8%) and hexane (98.5%) were purchased from Fisher Scientific (Waltham, MA, USA).

### 3.2.2 Synthesis of 2-(methacryloyloxy) ethyl stearate (SAMA)

Fatty acid-based monomer SAMA was synthesized according to the previously reported method<sup>33,36</sup> with slight modification. Typically, stearic acid (52.7 mmol, 15 g) and DMAP (5.27 mmol, 0.6 g) were first dissolved in dry 50 mL DCM and kept in an ice-water bath. The mixture was purged with nitrogen gas while stirring. After 15 min, a solution of DCC (58.0 mmol, 12.0 g) in a minimum volume of DCM was added. HEMA (58.0 mmol, 7.5 g) was subsequently added drop by drop over a period of 20 min. The ice-water bath was then removed, and the reaction mixture stirred for another 24 h at room temperature (25 °C). After the reaction, the mixture was filtered to remove extra reagents. The obtained filtrate was washed with distilled water, saturated NaHCO<sub>3</sub> solution and brine solution in sequence and dried over anhydrous Na<sub>2</sub>SO<sub>4</sub>. The solvent was removed by rotary evaporator at 30 °C and purified using a silica gel column with hexane/EtOAc (95: 5, v/v) as the eluent. The final product with 86% yield (12.9 g) was obtained and its structure was confirmed by <sup>1</sup>H NMR and FTIR.

<sup>1</sup>H NMR (400 MHz, CDCl<sub>3</sub>): δ (ppm) = 6.11 and 5.58 (C=CH<sub>2</sub>, 2H, d), 4.32 (OCH<sub>2</sub>CH<sub>2</sub>O, 4H, t), 2.31 (O=CCH<sub>2</sub>, 2H, t), 1.94 (CH<sub>2</sub>=CCH<sub>3</sub>, 3H, s), 1.61 (O=CCH<sub>2</sub>CH<sub>2</sub>, 2H, m), 1.27 ((-CH<sub>2</sub>)<sub>n</sub>, 28H, m), 0.87 (-CH<sub>2</sub>CH<sub>3</sub>, 3H, t).

### 3.2.3 Synthesis of homopolymers

PSAMA and PNIPAM were synthesized using 4-cyano-4-[[dodecylsulfanylthiocarbonyl]sulfanyl]pentanoic acid (CDP) as the chain transfer agent (CTA) at 60 °C. Molar ratios of [M]: [CTA]: [I] at 25:1:0.2 and 50:1:0.2 were employed for the synthesis of

PSAMA homopolymers with different molecular weights. An example of polymerization of SAMA is described as follows: SAMA monomer (1309 mg, 3.3 mmol), CTA (53.3 mg, 0.13 mol), AIBN (4.3 mg, 0.0264 mmol), and trioxane (80 mg, 0.89 mmol) (internal standard for monomer conversion calculation) were added in a dry glass vial and dissolved in 2.4 mL 1,4-dioxane. The mixture was stirred and purged with nitrogen for 20 min. After that, the vial was placed in the microwave reactor and the reaction was conducted under programmed conditions at 60 °C for a certain time. The reaction was stopped by cooling to room temperature with an ice-water bath and exposing to air. The homopolymer PSAMA was purified by precipitation using 500 mL of methanol for at least three times and dried in a fuming hood at room temperature. In the case of polymerization of NIPAM, the precipitation step was carried out with diethyl ether. The conventional heating methods were performed under the same experimental conditions with an oil bath. The  $M_{n,NMR}$  of PSAMA was calculated from DP values in combination with the molecular weights of RAFT agent by using the equation:  $M_{n,NMR} = DP_{n,PSAMA} \times \text{molecular weight of SAMA} + \text{molecular weight of CTA}$ .

### 3.2.4 Synthesis of PSAMA-*b*-PNIPAM block copolymer

The resulting homopolymers were used as macro-CTA for the synthesis of block copolymer. For this, a typical example when PSAMA was used as the macro-CTA has been described as follows. Into a 10 mL glass vial equipped with a stirrer bar, NIPAM (484.3 mg, 4.28 mmol), PSAMA macro-CTA (67.5 mg, 0.014 mmol), ACVA (0.78 mg, 0.003 mmol), trioxane (40 mg, 0.45 mmol) and 1.6 mL of THF were added. After mixing and deoxygenating with dry nitrogen for 20 min, the reaction was conducted in the microwave for 25 min at 60 °C. The reaction was quenched by cooling the polymer to room temperature and exposing to air. To obtain purified PSAMA-*b*-PNIPAM, the synthesized polymer was precipitated twice in 500 mL of cold hexane

followed by twice in 500 mL of diethyl ether. The final product was dried in a fume hood at ambient temperature prior to characterization with GPC,  $^1\text{H}$  NMR and FTIR. The  $M_n$  value of block copolymer measured by NMR technique was calculated as:  $M_{n,\text{NMR}} = \text{DP}_{n,\text{PNIPAM}} \times \text{molecular weight of NIPAM} + \text{DP}_{n,\text{PSAMA}} \times \text{molecular weight of SAMA} + \text{molecular weight of CTA}$ .

### 3.2.5. Characterization of polymers

Molecular weight and PDI of polymers were determined by gel permeation chromatography (GPC, CA, USA). The GPC instrument consisted of an Agilent 1200 series pump and autosampler, Agilent 1200 series Evaporative Light Scattering Detector and one Phenogel 5  $\mu\text{m}$  500A column ( $300 \times 4.6$  mm), using THF as the eluent at a flow rate of 0.5 mL/min. Samples were prepared in a concentration at 0.5 mg/mL. A series of polystyrene standards were used for calibration of the instrument.  $^1\text{H}$  NMR spectra were recorded on a Varian INOVA spectrometer (CA, USA) operating at 399.79 MHz at 27 °C. All samples were dissolved in deuterated chloroform for the measurements. Purified homopolymers and block copolymers were dried completely and mixed with KBr powder to prepare KBr pellets. FTIR analysis was conducted on IRSprit-L FTIR spectrophotometer (Shimadzu, Kyoto, Japan) with the spectral scanning scope of 400-4000  $\text{cm}^{-1}$ , the number of scans is 40 and resolution is 4  $\text{cm}^{-1}$ . Particle size in aqueous solution was measured by dynamic light scattering (DLS) using Malvern Zetasizer Nano-ZS instrument (MA, USA) equipped with a 4.0 mW He-Ne laser operating at wavelength of 633 nm and scattering angle of 173°. All samples were prepared in a concentration of 0.25  $\text{mg mL}^{-1}$  and measured in triplicate at 25 °C. Fluorescence excitation spectra and UV-vis measurement were performed on a SpectraMax M3 Multi-mode Microplate Reader. TEM analysis was conducted on FEI Morgagni 268 (OR, USA) equipped with Gatan Orius CCD Camera, operating at an acceleration voltage of 80 kV. A drop of polymeric micelles suspension was deposited onto a carbon-coated copper grid

and left for 5 min under ambient conditions. Excess solution was wicked away with filter paper. All samples were negatively stained with phosphotungstic acid (PTA) to improve contrast on the images. A concentration of  $0.25 \text{ mg mL}^{-1}$  was used for the analysis.

### **3.2.6. Determination of critical micelle concentration (CMC)**

The CMC of the block copolymers PSAMA-*b*-PNIPAM was determined by fluorescence measurements using pyrene as a probe. Briefly,  $20 \mu\text{L}$  of pyrene solution at  $3 \times 10^{-4} \text{ M}$  concentration in acetone was added into a series of vials and then acetone was allowed to evaporate. Different concentrations of polymer solution ranging from  $5 \times 10^{-4}$  to  $0.2 \text{ mg/mL}$  were prepared and added to the vials while the final concentration of pyrene in each vial was maintained as  $6 \times 10^{-7} \text{ M}$ . The solutions were kept at room temperature for 24 h before measurements to equilibrate pyrene and micelles. The excitation spectra were recorded from 300 to 350 nm with a fixed emission wavelength at 390 nm. The ratio of fluorescence intensity at two wavelengths 337 nm and 333 nm in the excitation spectra was plotted against the logarithm of block copolymer concentration<sup>37</sup>.

### **3.2.7. Micelle formation**

The micelles of the block copolymer were prepared using the combination of co-solvent evaporation and dialysis method. Briefly, 10 mg of PSAMA-*b*-PNIPAM was dissolved in 5 mL THF and equal amount of distilled water was then added dropwise (ca. 1 droplet per 10 s) to the glass vial under gentle stirring. The prepared solution in the open vial was continued to stir for 6 h and transferred into dialysis tubing (MWCO = 3500 Da). The solution was dialyzed against distilled water overnight to completely remove THF and then lyophilized.

### **3.2.8. Drug loading within micelles**

Carbamazepine (CBZ) was loaded into PSAMA-*b*-PNIPAM micelles using the same method as described above, where 1 mg of CBZ and 10 mg of PSAMA-*b*-PNIPAM was dissolved

in THF at the first step. To calculate drug loading efficiency (DLE) and drug loaded content (DLC), the freeze-dried CBZ-loaded sample was dissolved in THF and the amount of encapsulated drug in polymeric micelles was analyzed by UV-visible spectrophotometer at 287 nm. A linear standard curve between CBZ concentration and UV absorbance at 287 nm was established in advance. The DLE and DLC were calculated according to the following formula<sup>38,39</sup>:

$$\text{DLE (\%)} = \frac{\text{Mass of loaded drug}}{\text{Mass of drug in feed}} \times 100 \quad 3.1$$

$$\text{DLC (\%)} = \frac{\text{Mass of loaded drug}}{\text{Mass of drug-loaded micelle}} \times 100 \quad 3.2$$

### 3.2.9. *In vitro* drug release study

Drug release behavior of CBZ loaded PSAMA-*b*-PNIPAM micelles *in vitro* was studied via dialysis method. A solution of CBZ-loaded polymeric micelles (1 mg/mL) was placed into a dialysis membrane (MWCO = 100-500 Da). This dialysis tube was immersed in a 35 mL physiological buffer (0.01M PBS, pH 7.4) and incubated at 37 °C or 25 °C under gentle stirring. At scheduled time intervals, 2 mL of samples were taken out for measurement and an equal volume of fresh PBS solution was refilled to maintain the sink conditions. The release amount of CBZ was analyzed and monitored by UV-visible spectrophotometer.

## 3.3 Results and discussion

### 3.3.1. Synthesis of block copolymer PSAMA-*b*-PNIPAM

As one of the most versatile controlled radical polymerization (CRP) techniques, RAFT polymerization has been considerably employed for fabrication of block copolymers.<sup>40,41</sup> It provides a convenient route to prepare (co)polymers with predicted compositions, topologies and functionalities.<sup>42,43</sup> As depicted in Scheme 3.1, block copolymer of PSAMA and PNIPAM was

synthesized by sequential monomer addition in two steps. To begin with, homopolymers of PSAMA or PNIPAM using CDP as the RAFT agent were synthesized. The selection of an appropriate thiocarbonylthio moiety of the RAFT agent is the key to successful controlled polymerizations.<sup>44</sup> The CDP was chosen as RAFT agent due to its ability to control polymerization of both SAMA and NIPAM monomers.<sup>33,45</sup> Polymerizations were carried out in 1,4-dioxane at 60 °C and the results are presented in Table 3.1. Both PSAMA and PNIPAM were obtained with different molecular weight and narrow molecular weight distribution.

The sequence of monomer addition has a great effect on the product of RAFT polymerization for the synthesis of block copolymers. In this study, both PSAMA and PNIPAM were employed as the macro-CTA to further copolymerize with the second monomer to produce the block copolymer. However, it was observed that the block copolymer could only be formed when PSAMA was used as the first block (macro-CTA). When starting with a PNIPAM macro-CTA, the final products were found to be the mixture of PSAMA homopolymer and PNIPAM homopolymer. Considering the RAFT mechanism for block copolymerization, the homopolymer (macro-CTA) with thiocarbonylthio group should have a higher transfer ability and better leaving ability to allow the growth of the second monomer<sup>46-48</sup> which was opposite when PNIPAM was used as a macro-CTA therefore block-copolymerization on NIPAM macro-CTA was not successful. Consequently, PSAMA was used as the macro-CTA and PSAMA-*b*-PNIPAM block copolymers with narrow PDI and well-controlled length of different blocks were synthesized.

Table 3.1. Microwave-assisted RAFT polymerization of PSAMA, PNIPAM and PSAMA-*b*-PNIPAM at 60 °C.

Polymer <sup>a</sup>	[M]/[CTA]/[I]	Time (min)	Conv. <sup>b</sup>	M <sub>n</sub> <sup>c</sup> (g/mol)	M <sub>w</sub> /M <sub>n</sub> <sup>c</sup>	M <sub>n,nmr</sub> <sup>b</sup> (g/mol)	Composition <sup>b</sup> SAMA: NIPAM
PSAMA <sub>8</sub>	25:1:0.2	20	28.6%	4730	1.08	3580	100:0
PSAMA <sub>12</sub>	50:1:0.2	20	23.5%	6820	1.10	5160	100:0
PSAMA <sub>21</sub> *	25:1:0.2	300	69.3%	10500	1.09	8610	100:0
PNIPAM <sub>58</sub>	150:1:0.2	30	35.6%	5640	1.06	6960	0:100
PSAMA <sub>8</sub> - <i>b</i> -PNIPAM <sub>49</sub>	100:1:0.2	25	75.6%	9320	1.10	9120	14:86
PSAMA <sub>8</sub> - <i>b</i> -PNIPAM <sub>106</sub>	300:1:0.2	25	62.3%	11430	1.15	15570	7:93
PSAMA <sub>12</sub> - <i>b</i> -PNIPAM <sub>121</sub>	300:1:0.2	25	64.1%	14570	1.18	18860	9:91

<sup>a</sup> The subscripted numbers denote the degree of polymerization of each corresponding block which was determined by <sup>1</sup>H NMR.

<sup>b</sup> Determined by <sup>1</sup>H NMR. <sup>c</sup> Determined by GPC in THF. \*Conventional heating method.

The polymerization reactions were performed under microwave irradiation and conventional heating was also employed for comparison purpose. Table 3.1. shows that when producing PSAMA homopolymers, compared to oil bath heating (300 min), microwave irradiation (20 min) greatly shortened the reaction time, which also provides a rapid and efficient way for synthesis of block polymers using lipid-based monomers and NIPAM. The block copolymers were prepared within 25 min while it usually takes 12-48 h to produce block copolymers with conventional oil bath heating.<sup>40</sup>

### 3.3.2. Characterization of PSAMA-*b*-PNIPAM

The chemical structures of the synthesized monomer SAMA, homopolymer PSAMA and block copolymer PSAMA-*b*-PNIPAM were characterized by  $^1\text{H}$  NMR spectroscopy. The assigning of various proton signals marked with different letters are displayed in Figure 3.1. In the  $^1\text{H}$  NMR spectrum of monomer SAMA, the proton peaks labeled as *h* and *i* were attributed to vinyl proton signals. Monomer conversion was calculated by comparing the integration of these vinyl protons before and after polymerization using 1,3,5-trioxane as an internal standard ( $\delta = 5.10$  ppm). The signals at 2.39-2.62 ppm found in the spectrum of PSAMA homopolymer corresponded to HOOC-CH<sub>2</sub>-CH<sub>2</sub>-C(CN)(CH<sub>3</sub>)- moiety in RAFT agent.<sup>49</sup> The degree of polymerization (DP) of PSAMA macro-CTA by end-group analysis was determined, based on the integral ratio of the repeating chain protons at 4.12-4.37 ppm, derived from the side chain -O-CH<sub>2</sub>-CH<sub>2</sub>-O-, to methylene protons H<sub>a</sub> in the CTA agent (at 2.39-2.62 ppm). The NMR spectrum of PSAMA-*b*-PNIPAM proved the presence of all characteristic peaks from each block. In order to determine the molar ratio of PSAMA to PNIPAM in the block copolymers, the integrated peak area at 4.12-4.37 ppm from PSAMA segment was compared with that of methine proton (*H<sub>j</sub>* at 3.88-4.10 ppm) from PNIPAM polymer backbone.

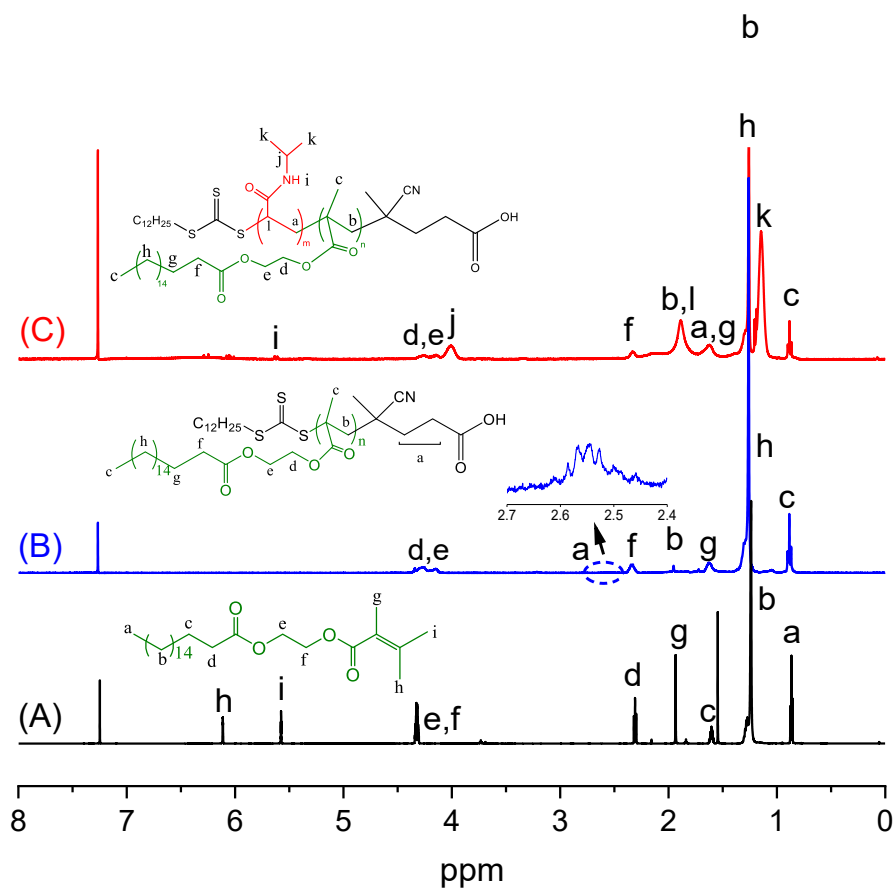


Figure 3.1.  $^1\text{H}$  NMR spectrum of (A) SAMA, (B) PSAMA and (C) PSAMA-*b*-PNIPAM.

Starting with PSAMA<sub>8</sub> and PSAMA<sub>12</sub> as macro-CTA, three PSAMA-*b*-PNIPAM block copolymers with variable block lengths using different molar ratios of monomer to macro-CTA were synthesized, at a fixed ratio of  $[\text{macro-CTA}]/[\text{AIBN}] = 0.2$ . The GPC spectra of homopolymers and block copolymers are shown in Figure 3.2. GPC curves of PSAMA-*b*-PNIPAM moved towards the higher molecular weight region in contrast to PSAMA macro-CTA while maintaining low PDI ( $< 1.2$ ). The GPC peaks were all unimodal and symmetric without any bimolecular termination products or unreacted macro-CTA. Therefore, GPC results further confirmed the successful chain extension of PSAMA macro-CTA and block copolymerization. The molecular weights measured by GPC matched reasonably well with  $M_{n,\text{NMR}}$  based on DP, in spite of some discrepancy with the theoretical molecular weights calculated on the basis of

monomer conversion by NMR. Note that the molecular weights measured by GPC are relative values with respect to polystyrene standards.

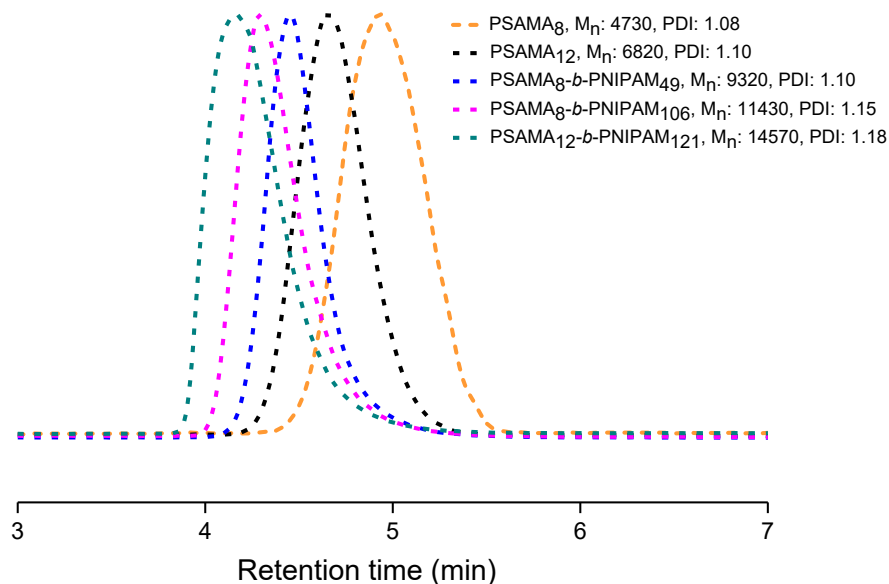


Figure 3.2. GPC traces of block copolymer PSAMA-*b*-PNIPAM and its PSAMA macro-CTA.

The structural differences of monomer, homopolymers and block copolymer were also studied by FTIR. As illustrated in Figure 3.3, in the IR spectrum of SAMA monomer, the peak for C=C was observed at  $1645\text{ cm}^{-1}$ . The peaks at  $1724\text{ cm}^{-1}$  and  $1742\text{ cm}^{-1}$  corresponded to the two ester carbonyl groups stretching. It was found that after polymerization C=C double bond peak disappeared and there was a broad C=O peak at  $1735\text{ cm}^{-1}$  in the spectrum of PSAMA. In the spectrum of PSAMA-*b*-PNIPAM, all characteristic absorption peaks can be observed associated with both blocks. For example, it is including stretching vibration of ester carbonyl group in PSAMA at  $1735\text{ cm}^{-1}$  and secondary amide C=O stretching at  $1652\text{ cm}^{-1}$ , amide N-H bending at  $1541\text{ cm}^{-1}$  as well as N-H stretching at  $3200\text{-}3400\text{ cm}^{-1}$  which belong to PNIPAM. In conclusion, FTIR spectra also supported the successful preparation of block copolymer.

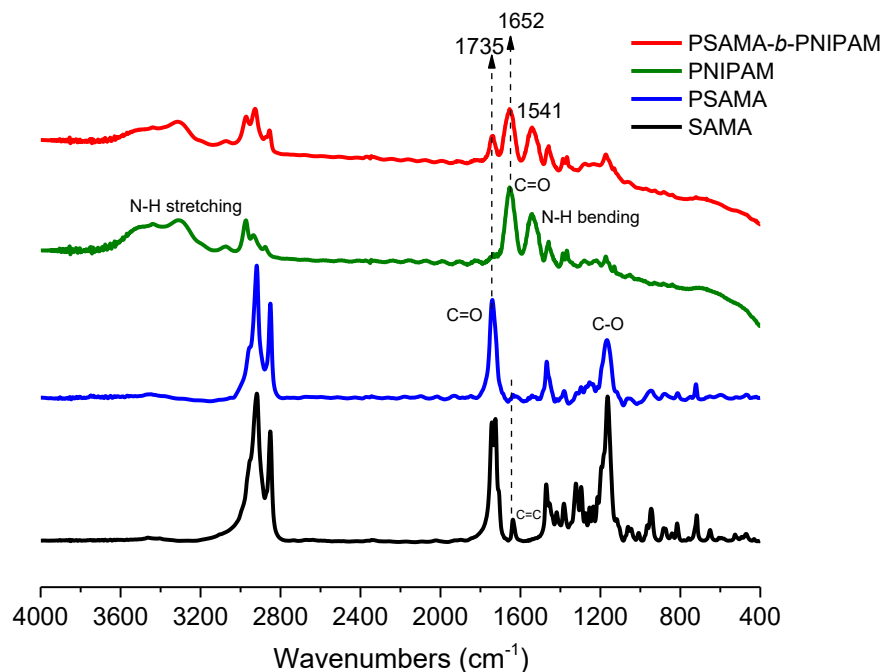


Figure 3.3. FTIR spectrum of SAMA, PSAMA, PNIPAM and PSAMA-*b*-PNIPAM.

### 3.3.3. Self-assembly study of PSAMA-*b*-PNIPAM

Amphiphilic block copolymers can spontaneously form various higher order structures in aqueous solutions with a size range of 10-200 nm. Their shapes are typically discovered as spherical when the length of a hydrophilic segment outnumbered that of a hydrophobic one,<sup>50,51</sup> whereas other structures including rods, vesicles and cylinders are also reported on block copolymers with a very long hydrophobic block.<sup>52-54</sup> For the designed amphiphilic block copolymer PSAMA-*b*-PNIPAM, fatty acid based hydrophobic block PSAMA is the core and the thermoresponsive hydrophilic block PNIPAM is the shell of the micelle.

To study the self-assembly behavior of PSAMA-*b*-PNIPAM, the hydrodynamic diameter ( $D_h$ ) of block copolymer micelles was determined by DLS at 25 °C (Figure 3.4.). Their average  $D_h$  values were measured as 27, 28 and 31 nm for PSAMA<sub>8</sub>-*b*-PNIPAM<sub>49</sub>, PSAMA<sub>8</sub>-*b*-PNIPAM<sub>106</sub>

and PSAMA<sub>12</sub>-*b*-PNIPAM<sub>121</sub>, respectively. The size of nano-assemblies was increased with the increasing PSAMA block length and molecular weight of the block copolymer, which proves that micellar size can be well tuned by adjusting molecular characteristics of both blocks. In drug delivery through the bloodstream, the size and shape of nanocarriers play a crucial part in their biodistribution, circulation time and cellular uptake. A range of 10-100 nm diameter was reported to be the most ideal because this size carrier can efficiently avoid clearance by the kidney and recognition by the reticuloendothelial system (RES), resulting in longer circulation time.<sup>55,56</sup> More importantly, these carriers can selectively extravasate from the leaky vasculature around tumor sites based on EPR effect and accumulate at the target sites.<sup>57</sup>

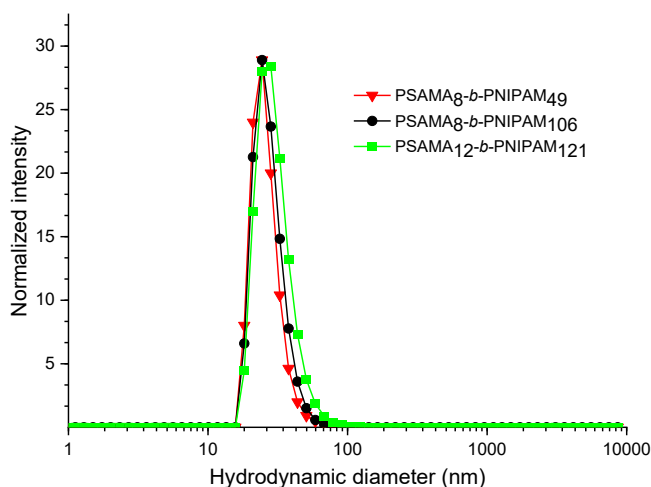


Figure 3.4. DLS distributions for PSAMA-*b*-PNIPAM in aqueous solution at 25 °C.

The morphology of self-assembled block copolymer particles was further explored by TEM. As displayed in Figure 3.5, all the PSAMA-*b*-PNIPAM copolymers with different block ratios self-assembled into spherical core-shell micelles. From TEM images, the micellar sizes were observed approximately in the range of 10-40 nm. It is noteworthy that unlike individual well-dispersed spheres formed by PSAMA<sub>8</sub>-*b*-PNIPAM<sub>106</sub> (Figure 3.5a), the micelles prepared by

PSAMA<sub>12</sub>-*b*-PNIPAM<sub>121</sub> showed some aggregation behaviour (Figure 3.5b). This may be as a result of the longer hydrophobic content, the lipophilic tail of stearic acid being less mobile and incompactly packed during the micelle formation leading to their interactions with hydrophobic chains from other micelles. Moreover, it is interesting to notice that when the micelle solution was heated at 50 °C, PSAMA-*b*-PNIPAM micelles rapidly agglomerated and precipitated in aqueous solution (Figure 3.5c). This proved the thermoresponsive nature of the synthesized micelles, suggesting that PNIPAM has transitioned from hydrophilic to hydrophobic.

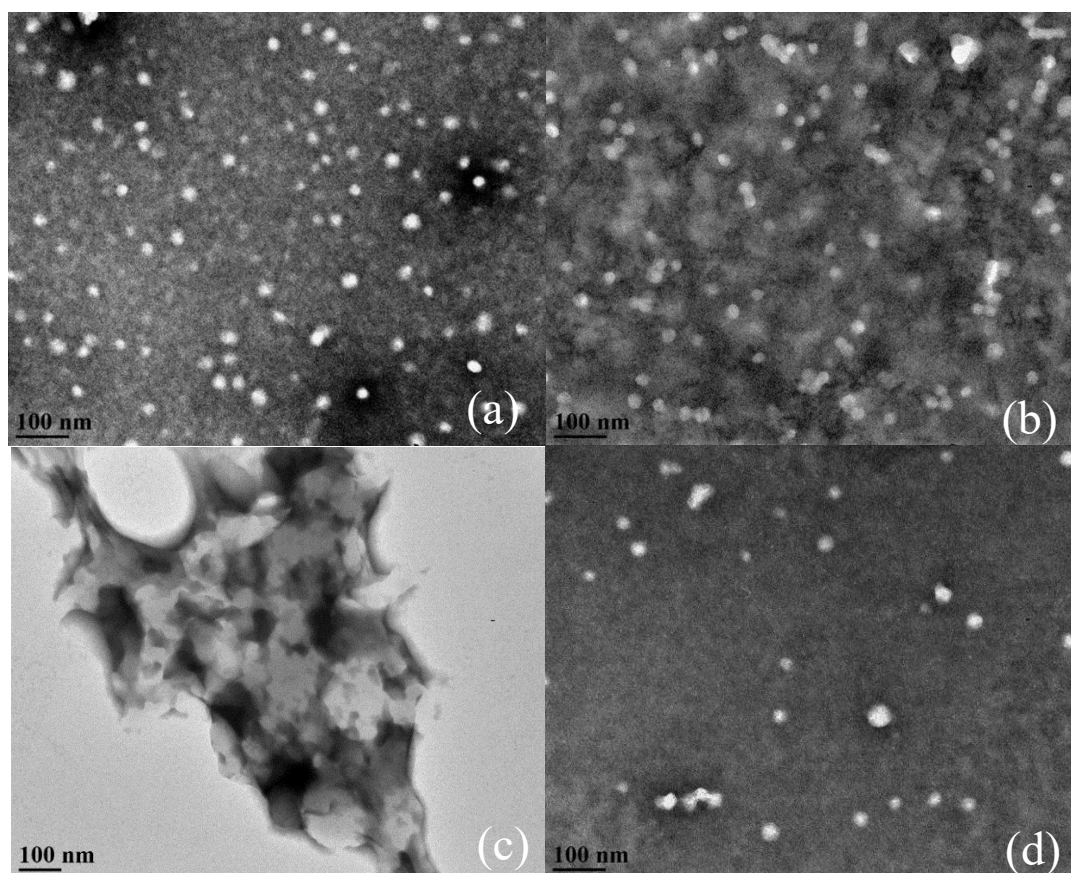


Figure 3.5. TEM images of (a) PSAMA<sub>8</sub>-*b*-PNIPAM<sub>106</sub>; (b) PSAMA<sub>12</sub>-*b*-PNIPAM<sub>121</sub>; (c) PSAMA<sub>8</sub>-*b*-PNIPAM<sub>106</sub> micelle solution heated at 50 °C; (d) CBZ-loaded PSAMA<sub>8</sub>-*b*-PNIPAM<sub>106</sub>.

### 3.3.4. CMC determination

Amphiphilic molecules begin to aggregate and self-assemble as their concentration reaches the threshold concentration called CMC. CMC is a significant indication of polymeric micelles' stability in light of their application as targeted drug carriers.<sup>58</sup> Upon injection into bloodstream, micelles are diluted by large volume of blood and those with high CMC value may disassemble into unimers, leading to premature release of encapsulated drugs. In the present study, CMC was determined by fluorescence technique using pyrene as the probe. Pyrene is a hydrophobic fluorescent probe with strong sensitivity to surrounding microenvironment. During micelle formation, pyrene preferably transfers from polar solution to a hydrophobic core within micelles, causing a red shift in excitation spectrum maximum of pyrene from 333 nm to 337 nm. Hence, the ratio of fluorescence intensity at two wavelengths 337 nm and 333 nm ( $I_{337}/I_{333}$ ) were plotted against the logarithm of PSAMA-*b*-PNIPAM concentration for measuring CMC values.

As shown in Figure 3.6. below a certain concentration,  $I_{337}/I_{333}$  values remained relatively steady. Above this concentration, there was a sharp increase of  $I_{337}/I_{333}$  values, implying the incorporation of pyrene into the micelle hydrophobic core. The intersection point of the two straight lines through plots of  $I_{337}/I_{333}$  ratios versus the block copolymer concentration was referred to as CMC. In this study, the CMC values of PSAMA<sub>8</sub>-*b*-PNIPAM<sub>49</sub>, PSAMA<sub>8</sub>-*b*-PNIPAM<sub>106</sub> and PSAMA<sub>12</sub>-*b*-PNIPAM<sub>121</sub> were measured as 0.0036, 0.0119 and 0.0058 mg/mL, respectively. Their CMC values decreased with the increasing PSAMA ratios in the block copolymer chains. The obvious dependence of CMC values on the length of hydrophilic/hydrophobic segment can be explained as: increased hydrophobicity strengthens the interactions between hydrophobic chains thus enhances aggregation tendency for amphiphiles to form micelles and thereby lowers the CMC. This trend is in accordance with previous reports.<sup>49,59</sup>

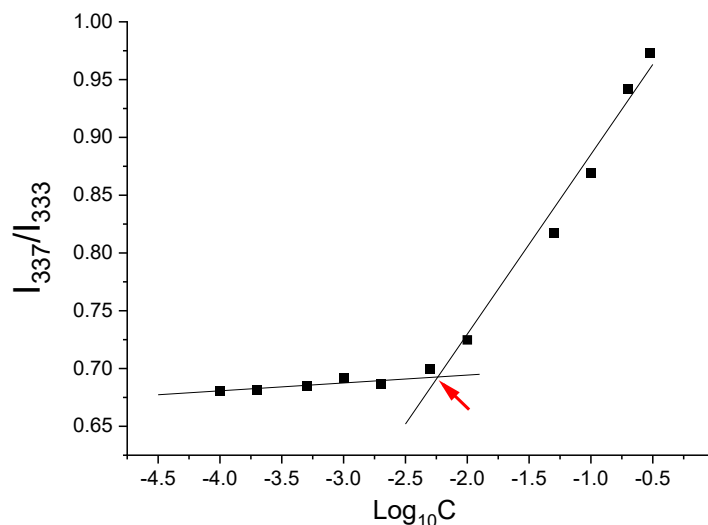


Figure 3.6. Plots of the intensity ratio  $I_{337}/I_{333}$  of pyrene excitation spectra versus logarithm of concentration for PSAMA<sub>12</sub>-*b*-PNIPAM<sub>121</sub>.

### 3.3.5. Drug loading and release behavior of block copolymer PSAMA-*b*-PNIPAM

Carbamazepine (CBZ), a lipophilic drug to treat epilepsy and nerve pain, was used as a model drug to investigate the drug loading efficiency and *in vitro* release performance of PSAMA-*b*-PNIPAM micelles. The CBZ-loaded polymeric micelle was also studied by TEM. TEM image (Figure 3.5d) showed that the drug-loaded PSAMA-*b*-PNIPAM micelles maintained their spherical morphology as expected but their size was approximately 42 nm which was slightly larger than that of the blank micelles. To explore the impact of hydrophilic and hydrophobic chain length on drug loading efficiency, several PSAMA-*b*-PNIPAM were prepared with different block lengths and their DLE and DLC are listed in Table 3.2. Among these block copolymers, the maximum drug loading efficiency and drug loading content of 31.6% and 2.9% were observed for PSAMA<sub>8</sub>-*b*-PNIPAM<sub>49</sub>. The length and structure of core-forming segment play a significant role in drug loading efficiency as hydrophobic drugs are physically entrapped into a hydrophobic core via hydrophobic interaction. Therefore, generally greater volume of core-forming polymer can

contribute to higher encapsulation efficiency. However, in the case of this study, the reason that PSAMA<sub>8-*b*</sub>-PNIPAM<sub>49</sub> exhibits the highest drug loading capacity may be associated with the balance between hydrophilic and hydrophobic blocks in aqueous medium. Combined with results observed by TEM for PSAMA<sub>12-*b*</sub>-PNIPAM<sub>121</sub>, the partial aggregation behaviour of micelles may also impede the drug loading into the micellar core. Especially, it is important to note that the process conditions for CBZ encapsulation were not optimized to maximize DLE and DLC, but primarily to demonstrate the capability of these micelles as drug carriers. Factors affecting the drug loading efficiency of polymeric micelles include polymer-drug ratio, molecular weight of the block copolymer, polymer-drug compatibility and encapsulation methods.<sup>60</sup>

Table 3.2. Drug loading characteristics of CBZ-loaded micelles.

	DLE (%)	DLC (%)
PSAMA <sub>8-<i>b</i></sub> -PNIPAM <sub>49</sub>	31.6	2.9
PSAMA <sub>8-<i>b</i></sub> -PNIPAM <sub>106</sub>	24.4	2.2
PSAMA <sub>12-<i>b</i></sub> -PNIPAM <sub>121</sub>	22.2	2.0

The drug release behaviours of CBZ-loaded PSAMA-*b*-PNIPAM micelle formulations were investigated in simulated physiological conditions (0.01M PBS, pH 7.4). Different temperatures (25 °C and 37 °C) were applied to evaluate the thermo-sensitivity of PSAMA-*b*-PNIPAM micelles. As presented in Figure 3.7, the CBZ release amount and rate at 37 °C was far more dramatic than that at 25 °C, demonstrating an obvious temperature-triggered response. The percentage of the CBZ released from PSAMA<sub>8-*b*</sub>-PNIPAM<sub>106</sub> was about 20% and 65% within 36 h, and 35% and 92% within 72 h at 25 and 37 °C, respectively. Considering the LCST of the block copolymer was measured within the range of 30-32 °C (refer to Figure S3.1.), the accelerated drug

release at 37 °C is due to the phase transition behaviour of block copolymer above its LCST. This leads to collapse and shrinkage of block copolymer micelles, and consequently causes the drug to diffuse out more quickly. Relatively, the drug release rate at 25 °C may mainly depend on the micellar dissociation and polymer degradation.

The *in vitro* release of free CBZ was also conducted for comparison. The data showed that as for free CBZ release at 37 °C, approximately 90% of CBZ was released into the medium in the first 2 h, and it took about 3 h in total for its complete release. The release behavior of CBZ loaded in copolymer micelles was quite different under the same conditions. A typical two-phase release profile was found with a relatively rapid release phase during initial period owing to the release of CBZ which was located at the interface of the shell (PNIPAM segment) and the core (PSAMA segment), followed by a sustained and slow release up to 84 h at body temperature. No significant difference of release pattern was observed among the three drug-loaded PSAMA-*b*-PNIPAM micelles, and they all showed good control for CBZ release at 37 °C.

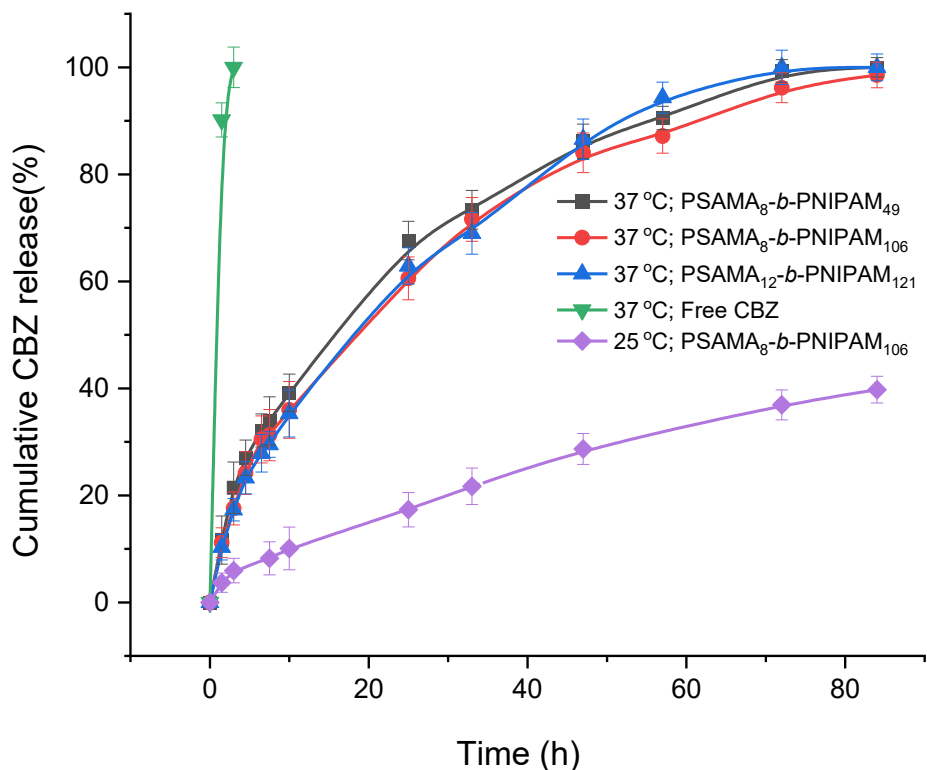


Figure 3.7. Release profiles *in vitro* of free CBZ and CBZ drug-loaded micelles in PBS (pH 7.4) at 37 °C and 25 °C.

### 3.4 Conclusions

In summary, temperature-responsive amphiphilic block copolymer PSAMA-*b*-PNIPAM comprising of stearic acid-based methacrylate polymer and PNIPAM by RAFT polymerization have been synthesized under microwave irradiation. Well-controlled block copolymers with variable block length were prepared by controlling the feeding ratio of monomers to macro-CTA. These amphiphilic block copolymers could spontaneously be assembled into spherical micelles with an average size range of ~30 nm. The balance between hydrophobic and hydrophilic segment had an impact on morphology, CMC and drug encapsulation performance of PSAMA-*b*-PNIPAM micelles. When increasing the block lengths of stearic acid segment, the CMC values decreased due to the stronger hydrophobic interaction, whereas micelles showed some aggregation attributed

to long hydrophobic tail of fatty acid and thus leading to lower encapsulation efficiency. Approximately 31.6% of CBZ can be loaded into PSAMA-*b*-PNIPAM micelles when the mass ratio of micelles to drug was fixed at 10:1. Improvement of drug loading efficiency can be implemented by optimization of self-assembly conditions and polymer-to-drug ratios in future studies. Complete release of drug from PSAMA-*b*-PNIPAM micelles with a sustained release behaviour was observed at 37 °C. Overall, these results suggest that these block copolymers can be potentially used for controlled delivery of drugs. These finding indicate an opportunity to explore utilization of renewable materials as replacements of non-renewable materials for smart delivery systems.

### 3.5 References

- (1) Alavi, M.; Karimi, N.; Safaei, M. Application of Various Types of Liposomes in Drug Delivery Systems. *Adv. Pharm. Bull.* **2017**, *7*, 3–9.
- (2) Kesharwani, P.; Jain, K.; Jain, N. K. Dendrimer as Nanocarrier for Drug Delivery. *Prog. Polym. Sci.* **2014**, *39*, 268–307.
- (3) Huang, H.; Yuan, Q.; Shah, J. S.; Misra, R. D. K. A New Family of Folate-Decorated and Carbon Nanotube-Mediated Drug Delivery System: Synthesis and Drug Delivery Response. *Adv. Drug Delivery Rev.* **2011**, *63*, 1332–1339.
- (4) Din, F. U.; Aman, W.; Ullah, I.; Qureshi, O. S.; Mustapha, O.; Shafique, S.; Zeb, A. Effective Use of Nanocarriers as Drug Delivery Systems for the Treatment of Selected Tumors. *Int. J. Nanomed.* **2017**, *12*, 7291–7309.
- (5) Peer, D.; KarP, J. M.; Hong, S.; faroKHzaD, oMiD C.; Margalit, riMona; Langer, Robert. Nanocarriers as an Emerging Platform for Cancer Therapy. *Nat. Nanotechnol.* **2007**, *2*, 751–760.

- (6) Miyata, K.; Christie, R. J.; Kataoka, K. Polymeric Micelles for Nano-Scale Drug Delivery. *React. Funct. Polym.* **2011**, *71*, 227–234.
- (7) Kulthe, S. S.; Choudhari, Y. M.; Inamdar, N. N.; Mourya, V. Polymeric Micelles: Authoritative Aspects for Drug Delivery. *Des. Monomers Polym.* **2012**, *15*, 465–521.
- (8) Kedar, U.; Phutane, P.; Shidhaye, S.; Kadam, V. Advances in Polymeric Micelles for Drug Delivery and Tumor Targeting. *Nanomed.: Nanotechnol. Biol. Med.* **2010**, *6*, 714–729.
- (9) Torchilin, V. Tumor Delivery of Macromolecular Drugs Based on the EPR Effect. *Adv. Drug Delivery Rev.* **2011**, *63*, 131–135.
- (10) Hwang, D.; Ramsey, J. D.; Kabanov, A. v. Polymeric Micelles for the Delivery of Poorly Soluble Drugs: From Nanoformulation to Clinical Approval. *Adv. Drug Delivery Rev.* **2020**, *156*, 80–118.
- (11) Lu, Y.; Park, K. Polymeric Micelles and Alternative Nanosized Delivery Vehicles for Poorly Soluble Drugs. *Int. J. Pharm.* **2013**, *453*, 198–214.
- (12) Zhang, Y.; Chan, H. F.; Leong, K. W. Advanced Materials and Processing for Drug Delivery: The Past and the Future. *Adv. Drug Delivery Rev.* **2013**, *65*, 104–120.
- (13) Kim, S.; Kim, J. H.; Jeon, O.; Kwon, I. C.; Park, K. Engineered Polymers for Advanced Drug Delivery. *Eur. J. Pharm. Biopharm.* **2009**, *71*, 420–430.
- (14) Shahriari, M.; Zahiri, M.; Abnous, K.; Taghdisi, S. M.; Ramezani, M.; Alibolandi, M. Enzyme Responsive Drug Delivery Systems in Cancer Treatment. *J. Controlled Release* **2019**, *308*, 172–189.
- (15) Popat, A.; Liu, J.; Lu, G. Q.; Qiao, S. Z. A PH-Responsive Drug Delivery System Based on Chitosan Coated Mesoporous Silica Nanoparticles. *J. Mater. Chem.* **2012**, *22*, 11173–11178.

- (16) Zhang, L.; Guo, R.; Yang, M.; Jiang, X.; Liu, B. Thermo and PH Dual-Responsive Nanoparticles for Anti-Cancer Drug Delivery. *Adv. Mater.* **2007**, *19*, 2988–2992.
- (17) Mura, S.; Nicolas, J.; Couvreur, P. Stimuli-Responsive Nanocarriers for Drug Delivery. *Nat. Mater.* **2013**, *12*, 991–1003.
- (18) Raza, A.; Rasheed, T.; Nabeel, F.; Hayat, U.; Bilal, M.; Iqbal, H. M. N. Endogenous and Exogenous Stimuli-Responsive Drug Delivery Systems for Programmed Site-Specific Release. *Molecules* **2019**, *24*, 1117.
- (19) Liu, M.; Du, H.; Zhang, W.; Zhai, G. Internal Stimuli-Responsive Nanocarriers for Drug Delivery: Design Strategies and Applications. *Mater. Sci. Eng. C* **2017**, *71*, 1267-1280.
- (20) Lue, S. J.; Chen, C. H.; Shih, C. M. Tuning of Lower Critical Solution Temperature (LCST) of Poly(N-Isopropylacrylamide-Co-Acrylic Acid) Hydrogels. *J. Macromol. Sci., Part B: Phys.* **2011**, *50*, 563–579.
- (21) Dalgakiran, E.; Tatlipinar, H. The Role of Hydrophobic Hydration in the LCST Behaviour of PEOGMA300 by All-Atom Molecular Dynamics Simulations. *Phys. Chem. Chem. Phys.* **2018**, *20*, 15389–15399.
- (22) Zhao, X. Q.; Wang, T. X.; Liu, W.; Wang, C. D.; Wang, D.; Shang, T.; Shen, L. H.; Ren, L. Multifunctional Au@IPN-PNIPAAm Nanogels for Cancer Cell Imaging and Combined Chemo-Photothermal Treatment. *J. Mater. Chem.* **2011**, *21*, 7240–7247.
- (23) Moran, M. T.; Carroll, W. M.; Selezneva, I.; Gorelov, A.; Rochev, Y. Cell Growth and Detachment from Protein-Coated PNIPAAm-Based Copolymers. *J. Biomed. Mater. Res., Part A* **2007**, *81*, 870–876.
- (24) Lanzalaco, S.; Armelin, E. Poly(N-Isopropylacrylamide) and Copolymers: A Review on Recent Progresses in Biomedical Applications. *Gels* **2017**, *3*, 36.

- (25) Qian, S.; Liu, R.; Han, G.; Shi, K.; Zhang, W. Star Amphiphilic Block Copolymers: Synthesis: Via Polymerization-Induced Self-Assembly and Crosslinking within Nanoparticles, and Solution and Interfacial Properties. *Polym. Chem.* **2020**, *11*, 2532–2541.
- (26) Li, Y. Y.; Zhang, X. Z.; Zhu, J. L.; Cheng, H.; Cheng, S. X.; Zhuo, R. X. Self-Assembled, Thermoresponsive Micelles Based on Triblock PMMA-*b*-PNIPAAm-*b*-PMMA Copolymer for Drug Delivery. *Nanotechnology* **2007**, *18*, 215605.
- (27) Chang, C.; Wei, H.; Quan, C. Y.; Li, Y. Y.; Liu, J.; Wang, Z. C.; Cheng, S. X.; Zhang, X. Z.; Zhuo, R. X. Fabrication of Thermosensitive PCL-PNIPAAm-PCL Triblock Copolymeric Micelles for Drug Delivery. *J. Polym. Sci., Part A: Polym. Chem.* **2008**, *46*, 3048–3057.
- (28) Wang, S.; Vajjala Kesava, S.; Gomez, E. D.; Robertson, M. L. Sustainable Thermoplastic Elastomers Derived from Fatty Acids. *Macromolecules* **2013**, *46*, 7202–7212.
- (29) Maisonneuve, L.; Lebarbé, T.; Grau, E.; Cramail, H. Structure-Properties Relationship of Fatty Acid-Based Thermoplastics as Synthetic Polymer Mimics. *Polym. Chem.* **2013**, *4*, 5472–5517.
- (30) Zhang, J.; Zhang, C.; Madbouly, S. A. In Situ Polymerization of Bio-Based Thermosetting Polyurethane/Graphene Oxide Nanocomposites. *J. Appl. Polym. Sci.* **2015**, *132*, 41751.
- (31) György, C.; Hunter, S. J.; Girou, C.; Derry, M. J.; Armes, S. P. Synthesis of Poly(Stearyl Methacrylate)-Poly(2-Hydroxypropyl Methacrylate) Diblock Copolymer Nanoparticles: Via RAFT Dispersion Polymerization of 2-Hydroxypropyl Methacrylate in Mineral Oil. *Polym. Chem.* **2020**, *11*, 4579–4590.
- (32) Obeng, M.; Milani, A. H.; Musa, M. S.; Cui, Z.; Fielding, L. A.; Farrand, L.; Goulding, M.; Saunders, B. R. Self-Assembly of Poly(Lauryl Methacrylate)-*b*-Poly(Benzyl Methacrylate) Nano-

Objects Synthesised by ATRP and Their Temperature-Responsive Dispersion Properties. *Soft Matter* **2017**, *13*, 2228–2238.

(33) Maiti, B.; De, P. RAFT Polymerization of Fatty Acid Containing Monomers: Controlled Synthesis of Polymers from Renewable Resources. *RSC Adv.* **2013**, *3*, 24983–24990.

(34) Jena, S. S.; Roy, S. G.; Azmeera, V.; De, P. Solvent-Dependent Self-Assembly Behaviour of Block Copolymers Having Side-Chain Amino Acid and Fatty Acid Block Segments. *React. Funct. Polym.* **2016**, *99*, 26–34.

(35) Zhao, X.; Shan, G. PSMA-*b*-PNIPAM Copolymer Micelles with Both a Hydrophobic Segment and a Hydrophilic Terminal Group: Synthesis, Micelle Formation, and Characterization. *Colloid Polym. Sci.* **2019**, *297*, 1353–1363.

(36) Arshad, M.; Pradhan, R. A.; Ullah, A. Synthesis of Lipid-Based Amphiphilic Block Copolymer and Its Evaluation as Nano Drug Carrier. *Mater. Sci. Eng. C* **2017**, *76*, 217–223.

(37) Chang, L.; Liu, J.; Zhang, J.; Deng, L.; Dong, A. PH-Sensitive Nanoparticles Prepared from Amphiphilic and Biodegradable Methoxy Poly(Ethylene Glycol)-Block-(Polycaprolactone-Graft-Poly(Methacrylic Acid)) for Oral Drug Delivery. *Polym. Chem.* **2013**, *4*, 1430–1438.

(38) Zhang, S.; Arshad, M.; Ullah, A. Drug Encapsulation and Release Behavior of Telechelic Nanoparticles. *Nanotechnology* **2015**, *26*, 415703.

(39) Huh, K. M.; Lee, S. C.; Cho, Y. W.; Lee, J.; Jeong, J. H.; Park, K. Hydrotropic Polymer Micelle System for Delivery of Paclitaxel. *J. Controlled Release* **2005**, *101*, 59–68.

(40) Gao, C.; Wu, J.; Zhou, H.; Qu, Y.; Li, B.; Zhang, W. Self-Assembled Blends of AB/BAB Block Copolymers Prepared through Dispersion RAFT Polymerization. *Macromolecules* **2016**, *49*, 4490–4500.

- (41) York, A. W.; Kirkland, S. E.; McCormick, C. L. Advances in the Synthesis of Amphiphilic Block Copolymers via RAFT Polymerization: Stimuli-Responsive Drug and Gene Delivery. *Adv. Drug Delivery Rev.* **2008**, *60*, 1018-1036.
- (42) Wan, W. M.; Hong, C. Y.; Pan, C. Y. One-Pot Synthesis of Nanomaterials via RAFT Polymerization Induced Self-Assembly and Morphology Transition. *Chem. Commun.* **2009**, *39*, 5883–5885.
- (43) Craig, A. F.; Clark, E. E.; Sahu, I. D.; Zhang, R.; Frantz, N. D.; Al-Abdul-Wahid, M. S.; Dabney-Smith, C.; Konkolewicz, D.; Lorigan, G. A. Tuning the Size of Styrene-Maleic Acid Copolymer-Lipid Nanoparticles (SMALPs) Using RAFT Polymerization for Biophysical Studies. *Biochim. Biophys. Acta, Biomembr.* **2016**, *1858*, 2931–2939.
- (44) Perrier, S. 50th Anniversary Perspective: RAFT Polymerization-A User Guide. *Macromolecules* **2017**, *50*, 7433–7447.
- (45) Uemukai, T.; Hioki, T.; Ishifune, M. Thermoresponsive and Redox Behaviors of Poly(N - Isopropylacrylamide)-Based Block Copolymers Having TEMPO Groups as Their Side Chains. *Int. J. Polym. Sci.* **2013**, *2013*, 196145.
- (46) Vega-Rios, A.; Licea-Claverie, A. Controlled Synthesis of Block Copolymers Containing N-Isopropylacrylamide by RAFT Polymerization. *J. Mex. Chem. Soc.* **2011**, *55*, 21–32.
- (47) Sumerlin, B. S.; Lowe, A. B.; Thomas, D. B.; Convertine, A. J.; Donovan, M. S.; McCormick, C. L. Aqueous Solution Properties of PH-Responsive AB Diblock Acrylamido-Styrenic Copolymers Synthesized via Aqueous Reversible Addition-Fragmentation Chain Transfer. *J. Polym. Sci., Part A: Polym. Chem.* **2004**, *42*, 1724–1734.
- (48) Rizzardo, E.; Chen, M.; Chong, B.; Moad, G.; Skidmore, M.; Thang, S. H. RAFT Polymerization: Adding to the Picture. *Macromol. Symp.* **2007**, *248*, 104–116.

- (49) Maiti, B.; Maiti, S.; De, P. Self-Assembly of Well-Defined Fatty Acid Based Amphiphilic Thermoresponsive Random Copolymers. *RSC Adv.* **2016**, *6*, 19322–19330.
- (50) Zhai, S.; Ma, Y.; Chen, Y.; Li, D.; Cao, J.; Liu, Y.; Cai, M.; Xie, X.; Chen, Y.; Luo, X. Synthesis of an Amphiphilic Block Copolymer Containing Zwitterionic Sulfobetaine as a Novel PH-Sensitive Drug Carrier. *Polym. Chem.* **2014**, *5*, 1285–1297.
- (51) Kakde, D.; Taresco, V.; Bansal, K. K.; Magennis, E. P.; Howdle, S. M.; Mantovani, G.; Irvine, D. J.; Alexander, C. Amphiphilic Block Copolymers from a Renewable  $\epsilon$ -Decalactone Monomer: Prediction and Characterization of Micellar Core Effects on Drug Encapsulation and Release. *J. Mater. Chem. B* **2016**, *4*, 7119–7129.
- (52) Schmelz, J.; Schedl, A. E.; Steinlein, C.; Manners, I.; Schmalz, H. Length Control and Block-Type Architectures in Worm-like Micelles with Polyethylene Cores. *J. Am. Chem. Soc.* **2012**, *134*, 14217–14225.
- (53) Lei, L.; Gohy, J. F.; Willet, N.; Zhang, J. X.; Varshney, S.; Jérôme, R. Tuning of the Morphology of Core-Shell-Corona Micelles in Water. I. Transition from Sphere to Cylinder. *Macromolecules* **2004**, *37*, 1089–1094.
- (54) Ott, C.; Hoogenboom, R.; Hoepfener, S.; Wouters, D.; Gohy, J. F.; Schubert, U. S. Tuning the Morphologies of Amphiphilic Metallo-Supramolecular Triblock Terpolymers: From Spherical Micelles to Switchable Vesicles. *Soft Matter* **2009**, *5*, 84–91.
- (55) Yokoyama, M. Polymeric Micelles as Drug Carriers: Their Lights and Shadows. *J. Drug Target.* **2014**, *22*, 576–583.
- (56) Ghezzi, M.; Pescina, S.; Padula, C.; Santi, P.; del Favero, E.; Cantù, L.; Nicoli, S. Polymeric Micelles in Drug Delivery: An Insight of the Techniques for Their Characterization and Assessment in Biorelevant Conditions. *J. Controlled Release* **2021**, *332*, 312–336.

- (57) Miyata, K.; Christie, R. J.; Kataoka, K. Polymeric Micelles for Nano-Scale Drug Delivery. *React. Funct. Polym.* **2011**, *71*, 227–234.
- (58) Owen, S. C.; Chan, D. P. Y.; Shoichet, M. S. Polymeric Micelle Stability. *Nano Today* **2012**, *7*, 53–65.
- (59) Wu, Q.; Yi, J.; Yin, Z.; Wang, S.; Yang, Q.; Wu, S.; Song, X.; Zhang, G. Synthesis and Self-Assembly of New Amphiphilic Thermosensitive Poly(N-Vinylcaprolactam)/Poly( $\epsilon$ -Caprolactone) Block Copolymers via the Combination of Ring-Opening Polymerization and Click Chemistry. *J. Polym. Res.* **2013**, *20*, 262.
- (60) Aliabadi, H. M.; Lavasanifar, A. Polymeric Micelles for Drug Delivery. *Expert Opin. Drug Delivery* **2006**, *3*, 139–162.

# **CHAPTER 4. Tunable Self-assembly of Lipid-based Block Polymeric Micelles with Temperature-sensitive Poly(vinylcaprolactam) Shell for Effective Anticancer Drug Delivery**

## **4.1 Introduction**

Amphiphilic polymers (i.e., block or graft copolymers) possess distinct hydrophilic and hydrophobic domains, enabling the spontaneous formation of nanosized micellar structures in the aqueous environment. These polymers have attracted significant interest as potent drug delivery platforms due to their peculiar characteristics. Notably, they feature a hydrophobic core that facilitates the solubilization of poorly soluble therapeutics, coupled with a hydrophilic shell that ensures compatibility and stability of micelles in an aqueous surrounding environment. Additionally, their tunable size allows preferential accumulation at compromised tissue sites, such as tumors, leveraging the enhanced permeability and retention (EPR) effect.<sup>1-3</sup> Over the past recent decades, in order to advance nanomedicines for humans, an array of functional block copolymers have been proposed to develop micelle-based delivery systems tailored for clinical use.<sup>4</sup> Biodegradability and biocompatibility are two critical factors in designing polymeric micelles for safe and efficient drug delivery. The incorporation of biodegradable materials as drug nanocarriers offer a number of advantages, including prolonged circulation time, sustained release, improved therapeutic efficacy, reduced toxicity, and *in vivo* degradability.<sup>3</sup>

Lipids, as naturally occurring biomolecules, have broad applications in the pharmaceutical industry.<sup>5,6</sup> Most drug delivery systems approved by FDA rely on liposome or lipid-based formulations, in particular, lipid nanoparticles have been successfully utilized for transporting

mRNA-based vaccines against SARS-CoV-2. Conjugates of phospholipids with hydrophilic polymers (PEG or polyvinylpyrrolidone (PVP)) have also been reported for their capacity to load sparingly soluble drugs.<sup>7,8</sup> However, their efficiency to encapsulate drugs is restricted by the limited space within the hydrophobic core due to the two relatively short fatty acid acyls. In the meantime, with the growing concern over environmental and health-related issues, the scientific community has put forth various polymers such as polyesters and polyurethanes that are developed from vegetable oils through step growth polymerization or oxypolymerization for different industrial applications.<sup>9-11</sup> One of the primary constituents in vegetable oils is fatty acids which are mostly saturated and perform as chain terminators in the polymerization process. Only a few attempts have been made on fatty acid-based polymers through radical polymerization by modifying carboxylic acid functional groups on the fatty acid structure.<sup>12</sup> Lately, the advancement of controlled radical polymerization (CRP) techniques has enabled the preparation of various well-defined fatty acid-based (meth)acrylate block copolymers via reversible addition-fragmentation chain transfer (RAFT) or atom transfer radical polymerization (ATRP).<sup>13-16</sup> Despite these developments, the majority of studies on fatty acid-based polymers have been directed toward their applications as coating, elastomer, or adhesives,<sup>17-19</sup> with little attention given to their potential biomedical applications as amphiphilic block copolymers for drug delivery. Fatty acid residues are anticipated to offer a robust capability for drug encapsulation as hydrophobic core-forming materials for the fabrication of controlled block copolymer micelles, along with favorable attributes such as biocompatibility and biodegradability. Furthermore, the use of monomers derived from renewable feedstocks to substitute fossil-based monomers holds the potential to advance green and sustainable approaches within drug delivery systems.

Thermo-sensitive polymers have become a focus of interest as an important component in nanocarrier design ascribing to their temperature-sensitive nature, which enables selective transportation, controlled release and limited off-targeted accumulation of drugs.<sup>20</sup> These polymers are usually in hydrophilic state below the lower critical solution temperature (LCST), exhibiting a reversible transition to hydrophobic state as the temperature rises above their LCST. Poly(N-isopropylacrylamide) (PNIPAM) is one of the most extensively explored thermo-responsive polymers. Nevertheless, it is worth noting that the backbone of PNIPAM is not subject to biodegradation under physiological conditions since they can produce small toxic amide compounds upon hydrolysis, thus hindering their potential applicability in biomedical field.<sup>21</sup> In contrast, Poly(N-vinylcaprolactam) (PNVCL), another temperature-responsive non-ionic polymer, possesses excellent biocompatibility, nontoxicity, solubility and stability against hydrolysis, making it well-suited for various biomedical applications.<sup>22</sup> Additionally, PNVCL exhibiting aggregation-induced emission (AIE) characteristics has recently emerged as a promising fluorescent polymeric thermometer for the early detection of diseases.<sup>23</sup> Unlike the sharp phase transition of PNIPAM at the LCST, PNVCL undergoes a continuous coil-globule transition within the temperature range of 36 to 50 °C,<sup>24</sup> dependent on the polymer concentration and molecular weight. However, the popularity of PNVCL faces a limitation attributed to the challenge of achieving controlled polymerization of NVCL. Until recently, a few CRP techniques have been applied to produce a variety of PNVCL-based block copolymers, including ATRP, RAFT and ring-opening polymerization.<sup>25-28</sup> There has been increased interest in developing PNVCL-based drug delivery systems over the past years, and the main types include hydrogels, micro/nanogels and micro/nanoparticles.<sup>24,29-31</sup> Notably, the synthesis of PNVCL and fatty acid-based amphiphilic block copolymers for controlled drug delivery has not been reported.

Herein, we present the synthesis and characterization of innovative thermo-responsive amphiphilic block copolymers, namely poly(vinyl stearate)-*b*-PNVCL (PVS-*b*-PNVCL) and poly(vinyl laurate)-*b*-PNVCL (PVL-*b*-PNVCL) showcasing significant potential for drug delivery applications. PVS-*b*-PNVCL and PVL-*b*-PNVCL block copolymers with well-controlled different block lengths were prepared through RAFT polymerization under microwave irradiation (Scheme 1). The resulting micellar structures, formed through self-assembly in aqueous solution, were characterized in terms of their critical micelle concentration (CMC), particle size and morphology. Nile Red-loaded micelles were prepared to test their micellar stability in biological conditions. Afterwards, thermo-sensitivity and drug encapsulation/release behaviour of PVS-*b*-PNVCL micelles were evaluated using doxorubicin (DOX) as a model anticancer drug. Moreover, their effectiveness as an anticancer drug delivery system was examined via cell viability and cellular uptake studies using both the cancerous HeLa cell line and human embryonic kidney (HEK) 293T cell line. This investigation underscores the potential to further explore the utilization of renewable materials with good biocompatibility and biodegradability as replacements of synthetic materials for smart drug delivery nanoplateforms.

## **4.2 Materials and methods**

### **4.2.1 Materials**

*N*-Vinylcaprolactam (NVCL, 98%, Sigma, St. Louis, MO, USA) was recrystallized from *n*-hexane before use. Vinyl stearate (95%) and vinyl laurate ( $\geq 99\%$ ) were purchased from Sigma (St. Louis, MO, USA) and recrystallized from acetone before use. 2,2'-Azobisisobutyronitrile (AIBN, 98%, Sigma, St. Louis, MO, USA) was recrystallized from methanol prior to use. Doxorubicin hydrochloride (99%), potassium ethyl xanthogenate (96%), methyl 2-

bromopropionate (98%), 1,3,5-trioxane ( $\geq 99\%$ ), pyrene (98%) and 4',6-diamidino-2-phenylindole dihydrochloride (DAPI,  $\geq 98\%$ ) were purchased from Sigma (St. Louis, MO, USA) and used without any further purification. Fetal bovine serum (FBS) and Nile Red (99%) was purchased from Fisher Scientific (Waltham, MA, USA) and used as received. 1,4-Dioxane (99%, Fisher scientific, Waltham, MA, USA) and tetrahydrofuran (THF,  $\geq 99\%$ , Sigma, St. Louis, MO, USA) was purified by passing through a short alumina column before use. All other chemicals were of reagent grade and used as received.

#### 4.2.2 Synthesis of O-ethyl-S-(1-methoxycarbonyl) ethyldithiocarbonate (XA1)

The RAFT agent was prepared according to the previously reported method with minor modifications.<sup>32</sup> Briefly, 2.24 mL of methyl 2-bromopropionate was dissolved in 40 mL of methanol and the kept in an ice bath. Potassium ethyl xanthogenate (3.66 g, 22.8 mmol) was then slowly added and the reaction mixture was stirred for 24 h at room temperature (25 °C). After the reaction, the white KBr precipitate was filtered, and the filtrate was extracted with diethyl ether. The organic layer was collected, washed three times with water and dried over anhydrous Na<sub>2</sub>SO<sub>4</sub>. A yellow liquid was obtained after the organic solvent evaporation.

<sup>1</sup>H NMR (400 MHz, CDCl<sub>3</sub>):  $\delta$  (ppm) = 4.63 (q, 2H, -OCH<sub>2</sub>CH<sub>3</sub>), 4.38 (q, 1H, -CHCH<sub>3</sub>), 3.75 (s, 3H, -CH<sub>3</sub>), 1.57 (d, 3H, -CHCH<sub>3</sub>), 1.41 (t, 3H, -CH<sub>2</sub>CH<sub>3</sub>).

#### 4.2.3 Synthesis of PVS and PVL macro-CTA

PVS and PVL homopolymers were synthesized using O-ethyl-S-(1-methoxycarbonyl) ethyldithiocarbonate as the chain transfer agent (CTA) at 60 °C under microwave irradiation. An example of polymerization of VS is described as follows: VS monomer (1242 mg, 4 mmol), CTA (11.2 mg, 0.04 mmol), AIBN (1.3 mg, 0.008 mmol), and trioxane (80 mg, 0.89 mmol) were dissolved in 1.8 mL of 1,4-dioxane. The solution was stirred and purged with nitrogen for 20 min

and then irradiated in the microwave reactor at 60 °C for a certain time. Monomer conversion was determined by <sup>1</sup>H NMR with trioxane as the internal reference. The reaction was quenched by cooling to room temperature with an ice-water bath. The polymers were precipitated in methanol for three times (from acetone solution), filtered and dried in a vacuum oven at room temperature.

#### **4.2.4 Synthesis of PVS-*b*-PNVCL and PVL-*b*-PNVCL block copolymers**

The block copolymers PVS-*b*-PNVCL and PVL-*b*-PNVCL were subsequently synthesized by RAFT polymerization with PVS and PVL homopolymers as macro-CTA respectively. Various molar ratios of [M] to [CTA] were utilized to produce block copolymers with distinct block ratios. For instance, for preparation of the PVS-*b*-PNVCL, NVCL (556.8 mg, 4 mmol), PVS (141.1 mg, 0.02 mmol), AIBN (0.66 mg, 0.004 mmol), trioxane (40 mg, 0.45 mmol) and 0.8 mL of THF were added into a 10 mL microwave vial equipped with a stirrer bar. After mixing and purging with dry nitrogen for 20 min, the vial was placed into the microwave instrument's cavity and the polymerization reaction was conducted under programmed conditions at 60 °C for 28 min. The polymerization was terminated by rapidly cooling to room temperature with an ice bath and exposing the mixture to air. The block copolymers were purified by precipitation from cold diethyl ether for three times. The final product was filtered, collected, and dried in a vacuum oven at room temperature.

#### **4.2.5 Characterization of the block copolymer**

<sup>1</sup>H NMR spectra were acquired on a Varian INOVA spectrometer (CA, USA) operating at 400 MHz. All samples were dissolved in CDCl<sub>3</sub> and analyzed at 25 °C. Gel permeation chromatography (GPC, CA, USA) instrument was equipped with an Agilent 1200 series pump and autosampler, Agilent 1200 series Evaporative Light Scattering Detector, and one Phenogel 5 μm 500A column (300 × 4.6 mm). THF was employed as the eluent at a flow rate of 0.5 mL/min. A

series of monodisperse polystyrene standards were used for the instrument calibration. FTIR analysis was conducted on IRSprit-L FTIR spectrophotometer (Shimadzu, Kyoto, Japan) using KBr pellet method.

#### **4.2.6 Preparation and characterization of micelles**

The block copolymer micelles were prepared by solvent switch method. Briefly, 10 mg of block copolymer was dissolved in 5 mL of THF/DMSO (7/3, v/v). Then, 7 mL distilled water was subsequently added dropwise to the solution under stirring. The prepared solution was stirred for additional 8 h without capping at room temperature. The suspension was transferred into a dialysis membrane (MWCO = 3500 Da) and dialyzed against distilled water overnight. The micelles were obtained after lyophilisation.

Particle size and size distribution of block copolymer micelles in aqueous solution were analyzed by dynamic light scattering (DLS) using Malvern Zetasizer Nano-ZS instrument (MA, USA) equipped with a 4.0 mW He-Ne laser ( $\lambda = 633$  nm) at a scattering angle of  $173^\circ$ . All measurements were performed in triplicates at 25 °C or 37 °C. Fluorescence excitation spectra were obtained on a SpectraMax M3 Multi-mode Microplate Reader (CA, USA). Optical transmittance was recorded on OPTIZEN POP UV-Vis Spectrophotometer (Daejeon, South Korea). TEM analysis was conducted on JEOL JEM-2100 (Tokyo, Japan) operating at an acceleration voltage of 200 kV. Briefly, 5  $\mu$ L of polymeric micelle suspension was deposited onto a carbon film supported copper grid that has previously been glow discharged using Cressington 208 Carbon Coater. After leaving in air for 5 min, excess solution was blotted with a strip of filter paper. All samples were negatively stained with 2% uranyl acetate and allowed to sit for 1 min. The excess staining solution was gently blotted away, and the grid was dried under ambient conditions.

#### 4.2.7 Determination of critical micelle concentration (CMC)

The CMC measurements were carried out using pyrene as a fluorescence probe. A 20  $\mu\text{L}$  of pyrene solution ( $3 \times 10^{-4}$  M in acetone) was added into different vials and then the acetone was allowed to evaporate. A series of polymer aqueous solutions with concentrations ranging from 0.1 to 200 mg/L were prepared separately and added to the vials while the final concentration of pyrene in each vial was kept constant at  $6 \times 10^{-7}$  M. After equilibration at room temperature for 24 h, the excitation spectra were recorded from 300 to 350 nm at a fixed emission wavelength of 390 nm. The CMC values were then determined based on the change of fluorescence intensity ratio at 337 nm and 333 nm with the varying block copolymer concentration.

#### 4.2.8 DOX encapsulation and *in vitro* release studies

##### 4.2.8.1 Preparation of DOX-loaded micelles

DOX·HCl was first dissolved in DMSO and reacted with 3 equiv of triethylamine for 3 h. The neutralized DOX solution (500  $\mu\text{L}$ ) was added to 5 mL of PVS-*b*-PNVCL or PVL-*b*-PNVCL solution in THF/DMSO (7/3, v/v) and stirred for 30 min at room temperature. Afterwards, 7 mL of distilled water was added dropwise to the DOX polymer solution under stirring. After stirring for another 8 h, the mixture was subjected to dialysis as described above to obtain DOX-loaded block copolymer micelles. For drug quantification, freeze-dried DOX-loaded micelles were dissolved in DMSO and the amount of encapsulated DOX in polymeric micelles was analyzed by UV spectrophotometer at 485 nm. A standard curve of free DOX as control was established in advance. The drug loading efficiency (DLE) and drug loading content (DLC) were calculated according to the following equations:

$$\text{DLE (\%)} = \frac{\text{Weight of loaded drug}}{\text{Weight of drug in feed}} \times 100 \quad 4.1$$

$$\text{DLC (\%)} = \frac{\text{Weight of loaded drug}}{\text{Weight of drug-loaded micelle}} \times 100 \quad 4.2$$

#### 4.2.8.2 Temperature-triggered release of DOX

The drug release profile of DOX-loaded block copolymer micelles was studied at 37 °C or 25 °C in a buffer solution (0.01M PBS, pH 7.4) via dialysis diffusion method. A solution of DOX-loaded polymeric micelles at a concentration of 1 mg/mL was placed into a dialysis membrane (MWCO = 3500 Da). The dialysis bag was immersed into a beaker containing 35 mL of physiological buffer and incubated under gentle stirring. Then 2 mL of each dialysate was taken out from the release medium for analysis at predetermined time intervals and replenished with an equal volume of fresh PBS solution to maintain the sink conditions. The release amount of DOX was monitored and measured by a UV-vis spectrophotometer. The release studies were performed in triplicates and each data point was expressed as mean ± SD.

#### 4.2.9 Serum stability of the micelles

The block copolymer (10 mg) was first dissolved in 1.5 mL of THF and then mixed with 0.2 mL of a stock solution of Nile Red (NR) in THF (5.0 mg/mL). The deionized water (5 mL) was added dropwise to the THF solution under vigorous agitation. After stirring for 5 h, the mixture was transferred to dialysis tubing (MWCO = 3500 Da) and dialyzed against deionized water for 18 h. The micelle solution was finally filtered through a syringe filter (0.45 µm pore size). The resulting NR-loaded PVS-*b*-PNVCL micelles were incubated in PBS supplemented with 10% FBS or only PBS solution. The stability of micelles loaded with NR was analyzed over a period of 72

h at room temperature. Their emission spectra were recorded at specified time intervals with a fixed excitation wavelength at 570 nm.

#### **4.2.10 Cell experiments**

##### *4.2.10.1 Cell culture*

Human embryonic kidney 293T (HEK 293T) cells and human cervical cancer cells HeLa were cultured in Dulbecco's modified Eagle medium (DMEM) containing 10% fetal bovine serum (FBS) and 100 µg/mL penicillin/streptomycin at 37 °C in a humidified atmosphere with 5% CO<sub>2</sub>.

##### *4.2.10.2 Cell viability assay*

The *in vitro* cytotoxicity of blank micelles and DOX-loaded micelles was assessed by 3-(4,5-dimethylthiazol-2-yl)-5-(3-carboxymethoxyphenyl)-2-(4-sulfophenyl)-2*H*-tetrazolium (MTS) assay. HEK 293T cells and HeLa cells were seeded into 96-well plates at a density of  $5 \times 10^4$  cells/well and incubated overnight at 37 °C. The DMEM medium with serum was then replaced by tested samples (PVS-*b*-PNVCL micelles, DOX-loaded micelles and free DOX) at concentrations of 0-200 µg/mL. The cells without any treatment were used as control and supplemented with equal volume of fresh medium. The cells were subsequently incubated for 24 and 48 h. The culture medium was replaced with 100 µL of fresh DMEM, followed by the addition of 20 µL of MTS Reagent (Abcam, Waltham, USA) and further incubated for 2 h. The absorbance was measured at 490 nm using a Synergy H1 microplate reader (Biotek, SB, USA) to analyze the cell viability profile. All statistical analyses were performed using GraphPad Prism software version 8.0 for Windows (GraphPad Software, San Diego, CA, USA).

##### *4.2.10.3 Cellular uptake assay*

HeLa cells were seeded ( $12 \times 10^5$  cells/well) on a 12-well plate with a glass coverslip and incubated at 37 °C under 5% CO<sub>2</sub> for 24 h. The medium was replaced with DOX-loaded micelle

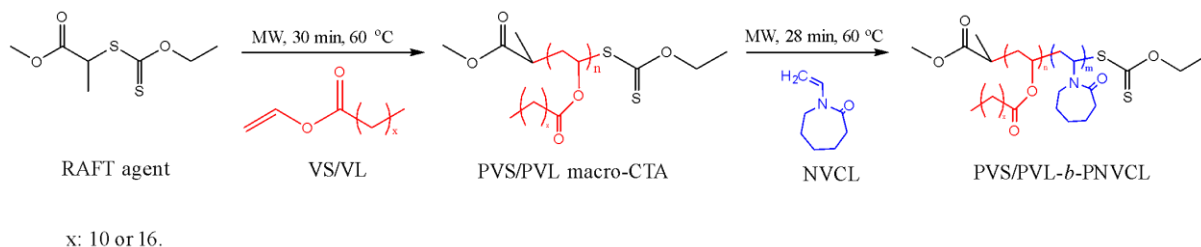
solutions at a final DOX concentration of 10 µg/mL. Free DOX with the same concentration was also studied as a comparison. After 4 h or 24 h of incubation, cells were washed with 1× phosphate-buffered saline (PBS) for three times and then fixed with 4% paraformaldehyde for 20 min at room temperature. Afterwards, the cells were washed three times with PBS and stained with DAPI for 10 min and kept in PBS. The cells treated with fluorescent dye were observed and imaged using a confocal laser scanning microscope (Leica TCS SP5 Confocal, NC, USA). DOX was excited using a 470 nm laser and collected in the red channel. DAPI was excited using a 358 nm laser and collected in the blue channel.

### 4.3 Results and Discussion

While there are few studies reported on the copolymerization of fatty acids with acrylamide monomers such as *N*-isopropylacrylamide (NIPAM) (Chapter 3) and *N,N*-dimethylacrylamide (DMA),<sup>33</sup> there has been significantly less attention paid to *N*-vinylcaprolactam. Preliminary studies were performed to investigate if a controlled block copolymer of PNVCL and lipids (different type of fatty acids) can be prepared. During initial trials, the effect of the sequence of monomer addition on the block copolymerization was explored. Surprisingly, the block copolymers were exclusively successfully prepared when PVS or PVL was used as the first block. The effects of fatty acid type and fatty acid block chain length on the subsequent micellization was investigated. The homopolymers (macro-CTAs) of PVS and PVL were subsequently extended by copolymerization with NVCL to provide accelerated access to block copolymers and to study their self-assembly, drug encapsulation and release behaviours, serum stability, cellular compatibility and uptakes.

### 4.3.1 Synthesis and characterization of PVS-*b*-PNVCL and PVL-*b*-PNVCL

The block copolymers of PVS-*b*-PNVCL and PVL-*b*-PNVCL were synthesized under microwave irradiation (Scheme 4.1.). To begin with, PVS and PVL homopolymers were obtained by RAFT polymerization using XA1 as the chain transfer agent after 30 min of reaction. The number-average molecular weight ( $M_n$ ) and dispersity index ( $\mathcal{D}$ ) of PVS and PVL were determined by GPC (Figure S4.1, in Appendix B). Synthesis of the block copolymers with variable block lengths was subsequently performed with PVS or PVL as the micro-RAFT agent at 60 °C for 28 min, using different molar ratios of monomer to macro-CTA. The selection of a proper RAFT agent and the order of monomer addition are both crucial factors for the synthesis of block copolymers, especially for less activated monomers like NVCL. PNVCL homopolymer was synthesized and then block copolymerized with lipid monomers, but the attempts were unsuccessful. In reverse, the homopolymerizations of lipids (VS & VL) were carried out and then blocked with PNVCL. Following this, lipid block with PNVCL was able to be extended. It was noted that PNVCL homopolymer (macro-CTA) cannot reinitiate the copolymerization of VS and VL. A plausible explanation for this could be that PNVCL intermediates with thiocarbonylthio group are highly stable and have poor leaving ability to allow the growth of the second monomer.<sup>34</sup>



Scheme 4.1. Illustration of the synthetic route for block copolymer PVS/PVL-*b*-PNVCL via RAFT polymerization under microwave irradiation.

The chemical structures of purified homopolymers and block copolymers were confirmed with  $^1\text{H}$  NMR spectroscopy and FTIR. The identification of all proton signals labeled with different letters is illustrated in Figure 4.1. The  $^1\text{H}$  NMR spectra of PVS and PVS-*b*-PNVCL show successful chain extension of PVS on account of the presence of all characteristic peaks from each block. New signals referring to PNVCL at 1.41-1.76 ppm ( $\text{CH}_2$  of caprolactam ring and backbone), 2.31-2.50 ppm ( $\text{COCH}_2$ ), 3.10-3.31 ppm ( $\text{NCH}_2$ ) and 4.40 ppm ( $\text{NCH}$ ) were observed. All typical absorption peaks of both the fatty acid-based block and PNVCL block are visible in the FTIR spectrum of the block copolymer (Figure S4.2, Appendix B). The peak at  $1738\text{ cm}^{-1}$  corresponding to ester carbonyl group demonstrated the existence of the PVS segment. In comparison with the IR spectrum of PVS homopolymer, new peaks which belong to PNVCL side chains appeared after block copolymerization, including an intense peak at  $1640\text{ cm}^{-1}$  originating from the characteristic  $\text{C}=\text{O}$  stretching vibration in amide and an absorption peak at  $1483\text{ cm}^{-1}$  attributed to  $\text{C}-\text{N}$  stretching vibration. In conclusion, FTIR results also supported the formation of block copolymers.

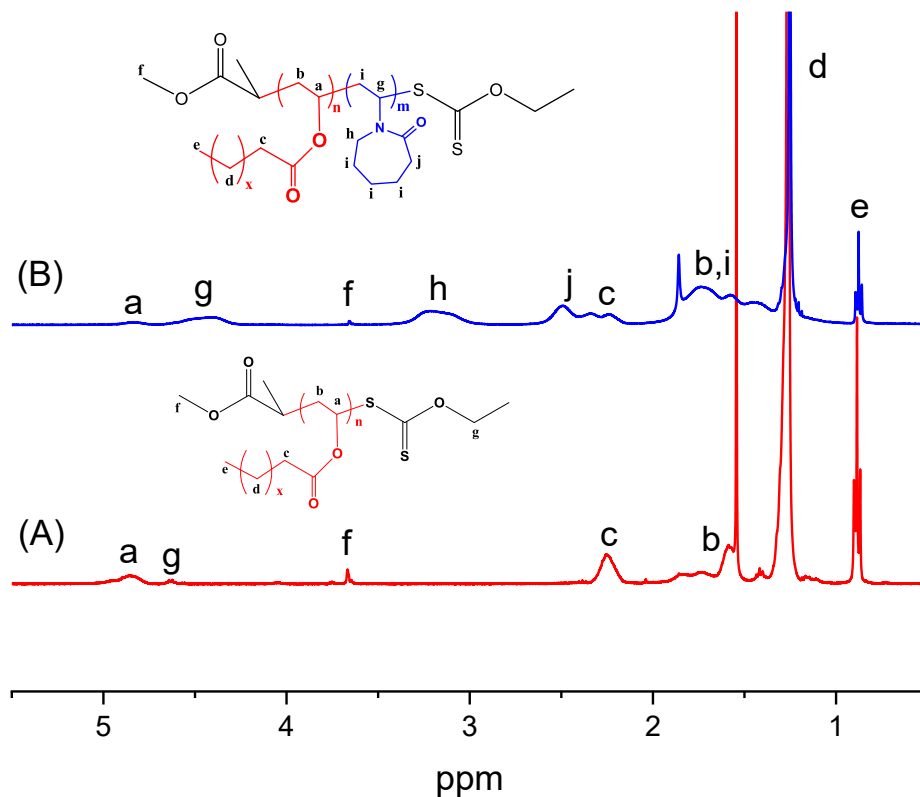


Figure 4.1.  $^1\text{H}$  NMR spectrum of (A) PVS and (B) PVS-*b*-PNVCL.

Although PVS-*b*-PNVCL has good solubility in THF solution, its molecular weight and  $\bar{M}_w$  were hardly determined by gel permeation chromatography (GPC) using THF as an eluent. Similar results have previously been reported and ascribed to some affinity of PNVCL to the stationary phase.<sup>35,36</sup> In this study, molecular weight and block composition of block copolymers were calculated by  $^1\text{H}$  NMR analysis and the results are summarized in Table 4.1. The degree of polymerization (DP) of PVS macro-RAFT agent was determined based on the integral ratio of the repeating chain protons  $H_e$  at 0.86-0.91 ppm, derived from methyl end group  $-\text{CH}_3$  in the side chain, to methyl protons of the xanthate moiety  $H_f$  in the RAFT agent (at 3.7 ppm). In order to determine the molar ratio of PVS to PNVCL in the block copolymers, the integrated peak area at

0.86-0.91 ppm from PVS fraction was compared with that of methylene proton  $H_h$  (at 3.10-3.31 ppm) from PNVCL side chain. The  $M_{n,NMR}$  of PVS and PVS-*b*-PNVCL were then calculated from DP values, namely repeating units of each block. The theoretical molecular weight was estimated based on monomer conversion by comparing the integration difference of vinyl protons of VS or NVCL before and after polymerization with 1,3,5-trioxane as an internal standard ( $\delta = 5.10$  ppm). The  $M_{n,theo}$  values were generally close to the corresponding  $M_{n,NMR}$  estimated from degrees of polymerization. The occasional deviation may be attributed to sampling process in the monomer conversion determination<sup>37</sup> which is employed in measuring the theoretical molecular weight. Besides, it was reported that the loss of sensitivity of NMR spectroscopy at high molecular weights (> 25 kDa) and impurities can result in the variability of molecular weights determined by NMR techniques.<sup>38</sup>

Table 4.1. Microwave-assisted RAFT polymerization of homopolymers and block copolymers at 60 °C.

Polymer <sup>a</sup>	[M]/[CTA]/[I]	Time (min)	Conv. <sup>b</sup> (%)	M <sub>n,theo</sub> <sup>c</sup> (kg/mol)	M <sub>n,nmr</sub> <sup>d</sup> (kg/mol)	Composition <sup>b</sup> VS/VL: NVCL
PVS <sub>9</sub>	100:1:0.2	30	12.0	4.0	3.1	100:0
PVS <sub>18</sub>	120:1:0.2	30	16.3	6.4	5.9	100:0
PVL <sub>16</sub>	100:1:0.2	30	17.9	4.3	3.9	100:0
PVL <sub>27</sub>	120:1:0.2	30	22.1	6.3	6.4	100:0
PVS <sub>9</sub> - <i>b</i> -PNVCL <sub>18</sub>	100:1:0.2	28	24.2	7.4	5.6	34:66
PVS <sub>18</sub> - <i>b</i> -PNVCL <sub>35</sub>	200:1:0.2	28	22.9	12.7	10.7	34:66
PVS <sub>18</sub> - <i>b</i> -PNVCL <sub>72</sub>	300:1:0.2	28	26.3	17.3	15.9	20:80
PVS <sub>18</sub> - <i>b</i> -PNVCL <sub>95</sub>	400:1:0.2	28	26.1	20.9	19.1	16:84
PVL <sub>16</sub> - <i>b</i> -PNVCL <sub>54</sub>	150:1:0.2	28	28.3	10.3	11.4	23:77
PVL <sub>27</sub> - <i>b</i> -PNVCL <sub>153</sub>	300:1:0.2	28	38.1	22.2	27.7	15:85

a. The subscripted numbers denote the degree of polymerization.

b. Determined by <sup>1</sup>H NMR.

c. Calculated by <sup>1</sup>H NMR.  $M_{n,theo} = [\text{monomer}]/[\text{CTA}] \times \text{molecular weight of monomer} \times \text{monomer conversion} + \text{molecular weight of (macro)CTA}$ .

d. Calculated by <sup>1</sup>H NMR.  $M_{n,nmr} = DP_n \times \text{molecular weight of the monomer} + \text{molecular weight of (macro)CTA}$ .

### 4.3.2 Self-assembly behaviour of block copolymers

A solvent switch method was employed to induce the self-assembly of the amphiphilic block copolymers PVS-*b*-PNVCL and PVL-*b*-PNVCL into micelles in aqueous medium. Their micellization behaviour was first characterized by measuring their CMC with pyrene as the fluorescent probe. Pyrene is known to preferentially transfer from polar surrounding into

hydrophobic microdomain (e.g., core of micelles), accompanied by a red shift in its excitation spectrum maximum from 333 nm to 337 nm. Therefore, the ratio of fluorescence intensities at 337 nm and 333 nm ( $I_{337}/I_{333}$ ) was plotted against the logarithm of different block copolymer concentrations for determining their CMC values (Figure 4.2.). The CMC values were calculated to be in the range of 1.10 to 3.11 mg/L for the series of PVS-*b*-PNVCL and PVL-*b*-PNVCL as summarized in Table 4.2. At a constant hydrophobic block length, the CMC values of PVS-*b*-PNVCL decreased with an increase in PVS ratios in the block copolymer chains. This could possibly be the result of increased hydrophobicity leading to enhancement in the interactions between hydrophobic chains thus resulting in stronger aggregation tendency for the amphiphiles to form micelles.<sup>39</sup> For the case of PVL-*b*-PNVCL, it should be noted that CMC is influenced by various factors, such as the molecular weight and dispersity index of the block copolymer, specific chemical structure of different blocks, and the appropriate balance between the hydrophilic and hydrophobic segments.<sup>39,40</sup> The CMC values observed in these fatty acid-based block copolymers were significantly lower than those of micelles prepared from PEG-lipid conjugates ( $\sim 10^{-5}$  M),<sup>8</sup> representing their higher stability against extreme dilution upon injection into bloodstream.

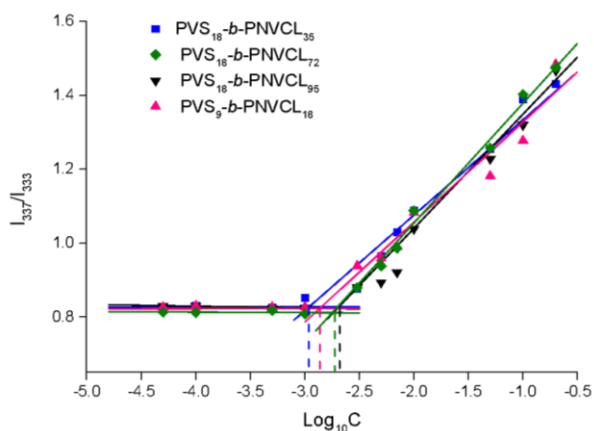


Figure 4.2. Plots of the intensity ratio  $I_{337}/I_{333}$  of pyrene excitation spectra versus logarithm of concentration of PVS-*b*-PNVCL.

Table 4.2. Characteristics of blank and DOX-loaded polymeric micelles.

Polymers	DOX-free micelles				DOX-loaded micelles			
	diameter (nm)	PDI	CMC (mg/L)	Polymer/DOX	diameter (nm)	PDI	DLE (%)	DLC (%)
PVS <sub>9</sub> - <i>b</i> -PNVCL <sub>18</sub>	80.5±4.0	0.160±0.004	1.80	10:1	97.1±2.8	0.194±0.008	42.9	3.9
PVS <sub>18</sub> - <i>b</i> -PNVCL <sub>35</sub>	110.5±0.5	0.178±0.005	1.10	10:1	120.7±1.5	0.060±0.008	59.7	5.4
				10:2	129.5±0.8	0.065±0.009	62.6	10.4
PVS <sub>18</sub> - <i>b</i> -PNVCL <sub>72</sub>	72.4±0.6	0.090±0.009	1.41	10:1	84.4±2.0	0.172±0.005	55.0	5.0
PVS <sub>18</sub> - <i>b</i> -PNVCL <sub>95</sub>	74.7±0.9	0.126±0.006	1.97	10:1	91.7±3.5	0.168±0.005	52.6	4.8
PVL <sub>16</sub> - <i>b</i> -PNVCL <sub>54</sub>	144.7±5.8	0.313±0.033	3.11	10:1	159.9±5.2	0.217±0.016	50.8	4.6
				10:2	151.9±2.6	0.226±0.001	44.9	7.5
PVL <sub>35</sub> - <i>b</i> -PNVCL <sub>153</sub>	129.8±0.8	0.299±0.001	1.75	10:1	142.5±12.3	0.307±0.028	37.0	3.4

The as-prepared polymeric micelles were also studied by both DLS and TEM for their size and morphology. DLS results showed that all PVS-*b*-PNVCL micelles exhibit unimodal size distribution and detailed data have been recorded in Table 4.2. By adjusting the PNVCL chain length and molecular weight of PVS-*b*-PNVCL, the particle sizes of micelles can be tuned into the range of 72.4-110.5 nm. As shown in Table 4.2, as the PNVCL content increased from 66 to 84 mol % in the block copolymers, the average diameter of the micelles reduced from 110.5 to 74.7 nm and exhibited a more uniform particle size distribution (PDI) with the same PVS block length. This result is consistent with previous findings<sup>24,41,42</sup> suggesting that an increase in the hydrophilic corona steric repulsion resulting from longer hydrophilic chains contributes to a decreased size of self-assembled particles. The morphologies of high-order structures formed by self-assembly of PVS-*b*-PNVCL in aqueous solution were visualized by TEM. As illustrated in Figure 4.3, exclusively spherical micelles were observed when the hydrophilic block PNVCL reached over 72 repeating units whereas coexistence of worm-like and spherical structures were found for PVS<sub>18</sub>-*b*-PNVCL<sub>35</sub>. This observation demonstrates the dimension and morphology of these self-assembled nanostructures can be well tuned by adjusting the length and ratios of each block. The results presented by TEM are in good agreement with the data from DLS regarding the micellar size. It is interesting to notice that the particle sizes of micelles made from PVL-*b*-PNVL were larger and presented a relatively broad size distribution compared to PVS-*b*-PNVCL, which was also confirmed by TEM results (Figure S4.3, Appendix B). Variations observed in micellar size and size distribution of block copolymers based on PVS and PVL can be partly attributed to the differences in block lengths. Furthermore, this impact can be elucidated by the presence of different fatty acids with varying carbon chain lengths. Longer fatty acid chains can pack more densely and tightly within the micelle core during self-assembly because of the increased

hydrophobic interactions and intermolecular van der Waals interactions, whereas shorter fatty acid chains may result in less efficient and looser packing, which can lead to larger micelles and a broader range of particle size. In addition, shorter fatty acid chains usually exhibit higher chain mobility compared to longer chains within the hydrophobic core, resulting in more dynamic and flexible self-assembled structures with broader size distribution.

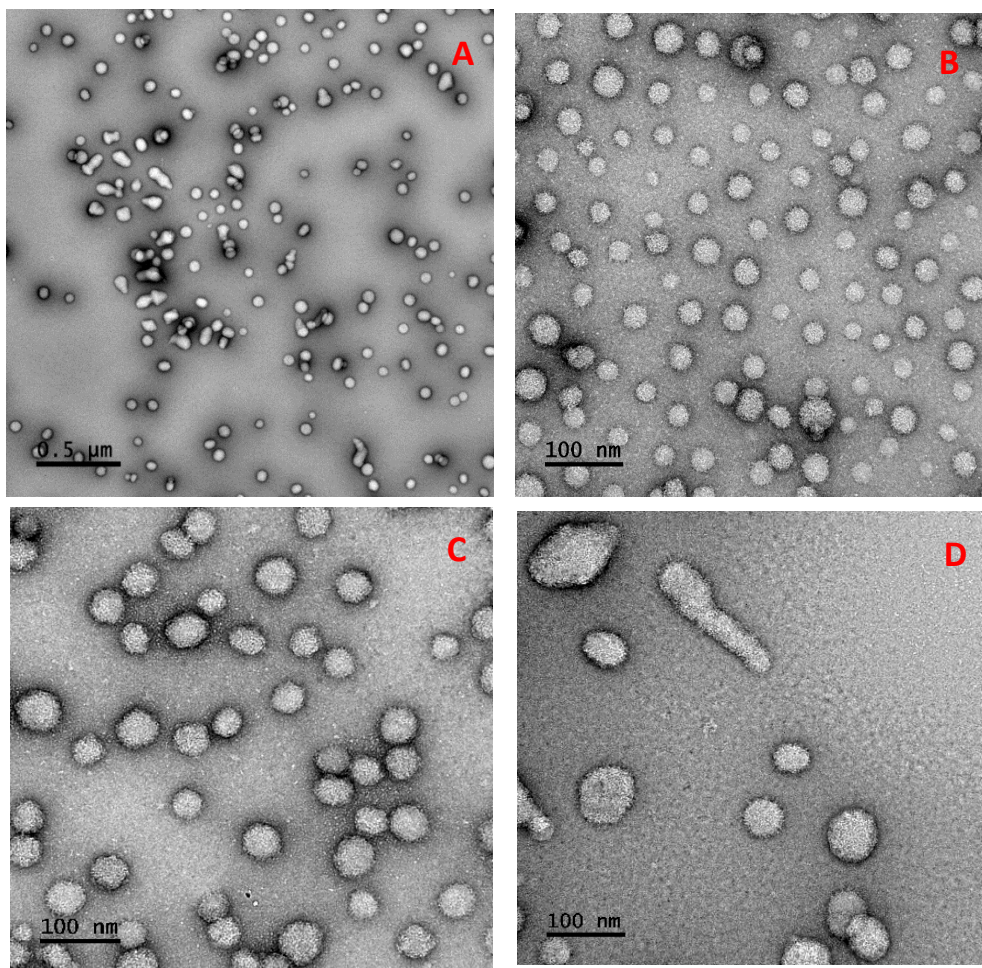


Figure 4.3. TEM images of self-assemblies formed by (A) PVS<sub>18</sub>-*b*-PNVCL<sub>35</sub>; (B) PVS<sub>18</sub>-*b*-PNVCL<sub>72</sub>; (C) PVS<sub>18</sub>-*b*-PNVCL<sub>95</sub>; (D) worm-like structures of PVS<sub>18</sub>-*b*-PNVCL<sub>35</sub>.

To further exploit PVS-*b*-PNVCL as a potential drug delivery vehicle, the particle size of PVS<sub>18</sub>-*b*-PNVCL<sub>35</sub> with different concentrations at 37 °C was investigated. It can be seen from Figure 4.4, the micellar size increased by 4.1 nm with the PVS<sub>18</sub>-*b*-PNVCL<sub>35</sub> concentration increased from 0.25 mg/mL to 1 mg/mL at 25 °C. As the temperature increased from 25 °C to 37 °C, the average diameter of micelles with 0.5 mg/mL dropped from 111.2 ± 5.9 (PDI: 0.175) to 96.2 ± 1.6 (PDI: 0.151) and those with 1 mg/mL decreased from 114.6 ± 0.7 (PDI: 0.198) to 96.3 ± 1.8 (PDI: 0.150). An obvious temperature-triggered response was noted as moderate decreases in micellar size with the elevated environmental temperature. The micelles became even reasonably stable without any aggregation. This phenomenon could be due to the fact that PNVCL at temperatures above their LCST becomes less soluble in water which increases the tendency for these amphiphiles to aggregate together, leading to slight compression in micellar sizes. Similar findings were also reported for the PNIPAM-based block copolymers.<sup>43-45</sup> Overall, the micellar size of PVS-*b*-PNVCL is less than 100 nm at the physiological temperature, which is reported to be an ideal size for drug carriers.<sup>46</sup> This size carrier enables not only efficient avoidance of elimination by the kidney and recognition by the reticuloendothelial system (RES), but also selective extravasation from the leaky vasculature and accumulation at the tumor sites based on the EPR effect.<sup>47</sup>

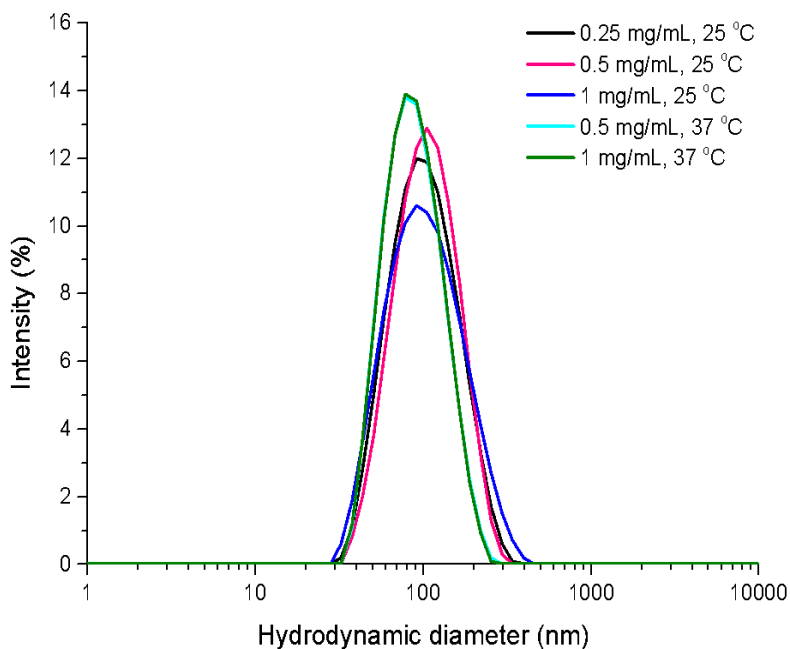


Figure 4.4. DLS distributions for PVS<sub>18</sub>-*b*-PNVCL<sub>35</sub> in aqueous solution at 25 °C and 37 °C.

#### 4.3.3 Drug encapsulation and *in vitro* temperature-triggered release of PVS/PVL-*b*-PNVCL

PVS/PVL-*b*-PNVCL micelles were tested as a potential drug delivery vector since the very long hydrophobic aliphatic chain of fatty acid moiety is assumed to be able to incorporate hydrophobic molecules through hydrophobic interactions. DOX was used as a hydrophobic anticancer drug model. The size and the morphology of the DOX-loaded micelles were also characterized by DLS and TEM analysis. As presented in Table 4.2, it was found that the sizes of all the micelles increased 10-20 nm after loading DOX while maintaining their narrow size distribution. It is noteworthy that PDI of PVS<sub>18</sub>-*b*-PNVCL<sub>35</sub> decreased from 0.178 to 0.06 after encapsulation of drugs, indicating the formation of monodisperse micelles. TEM results further confirmed that DOX-loaded PVS<sub>18</sub>-*b*-PNVCL<sub>35</sub> micelles exclusively had a spherical morphology (Figure 4.5). The incorporation of DOX induced rod-to-sphere morphological transitions

contributing to more uniform size distribution and shape. This could be because the hydrophobic drugs have stabilized the micelle through the increased hydrophobic interactions between encapsulated drug and micelle core,<sup>48,49</sup> which can impede the micelles forming aggregates in aqueous solution.<sup>50</sup>

DOX was loaded into the PVS/PVL-*b*-PNVCL micelles at the feed ratio of polymer to drug at 10:1 or 10:2 (w/w), with theoretical DLC calculated to be 9.0% or 16.7%, respectively. The DLE and DLC of PVS/PVL-*b*-PNVCL micelles prepared with different block lengths are listed in Table 4.2. The DLE of all micelles was in the range of 37.0-62.6%, corresponding to DLC of 3.4-10.4%. Among these block copolymers, the maximum encapsulation efficiency was observed for PVS<sub>18</sub>-*b*-PNVL<sub>35</sub>. Therefore, it was selected as the example for the following serum stability and cellular studies. To ensure an effective drug dose and therapeutic function, a significant amount of carrier materials is often required. However, this can lead to concerns about systemic toxicity and place an additional burden on body for degradation and excretion of these carriers. Drug delivery systems with high DLC can minimize the need for excessive excipients, facilitate tunable dosing in pharmaceutical formulation, diminish side effects and enhance therapeutic efficacy. Factors affecting the drug loading efficiency of polymeric micelles include block length of core-forming segment, hydrophilic-hydrophobic balance and molecular weight of the block copolymer, polymer-drug compatibility, encapsulation methods, etc.

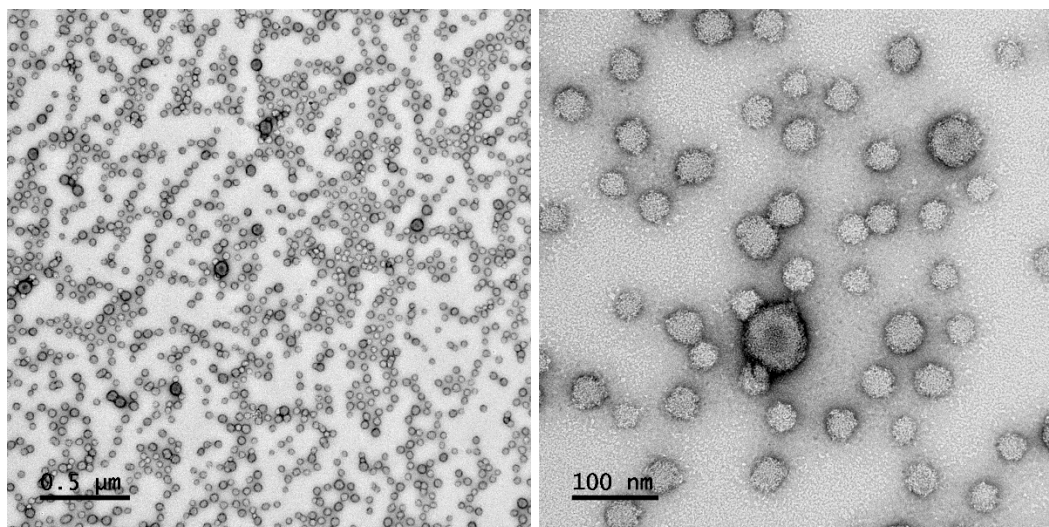


Figure 4.5. TEM images of DOX-loaded PVS<sub>18</sub>-*b*-PNVCL<sub>35</sub>.

The drug release behaviours of DOX-loaded PVS-*b*-PNVCL micelle formulations were investigated in simulated physiological conditions (0.01M PBS, pH 7.4) at different temperatures (25 °C and 37 °C). DOX release profiles from different polymeric micelles are depicted in Figure 4.6. and the release of free DOX was conducted for comparison. The polymeric micelles showed obvious temperature-triggered DOX release behavior as the temperature increased from 25 °C to 37 °C. The percentage of the DOX released from PVS<sub>18</sub>-*b*-PNVCL<sub>35</sub> was 46% and 69% within 24 h, 53% and 90% within 72 h at 25 and 37 °C, respectively. The accelerated drug release at higher temperatures was attributed to the disassembly of the micelles caused by the hydrophilic/hydrophobic transition behaviour of PNVCL segment above the LCST of PVS-*b*-PNVCL (~ 33 °C, Figure S4.4, Appendix B).

It was shown that DOX release from PVS-*b*-PNVCL micelles proceeded in a controlled manner at 37 °C, which is distinct from the release profile of free DOX (DOX•HCl) under the same conditions. The data showed that free DOX release was very rapid in the first two hours

(64.2%) and about 90% of the drug was released into the medium in 10 h. Whereas for both DOX-loaded PVS-*b*-PNCL micelles, a typical two-phase DOX release pattern was found. A relatively rapid release of DOX during the first 24 h due to the diffusion of DOX which was located at the surface or interface of the shell (PNVCL segment) and the core (PVS segment), and a sustained and slow release up to 72 h was followed. Moreover, the release of DOX from PVS<sub>18</sub>-*b*-PNVCL<sub>95</sub> was retarded in comparison with that from PVS<sub>18</sub>-*b*-PNVCL<sub>35</sub> micelles, which was 78% within 72 h. Overall; the controllable drug release of PVS-*b*-PNVCL micelles is in favor of their application as drug nanocarriers.

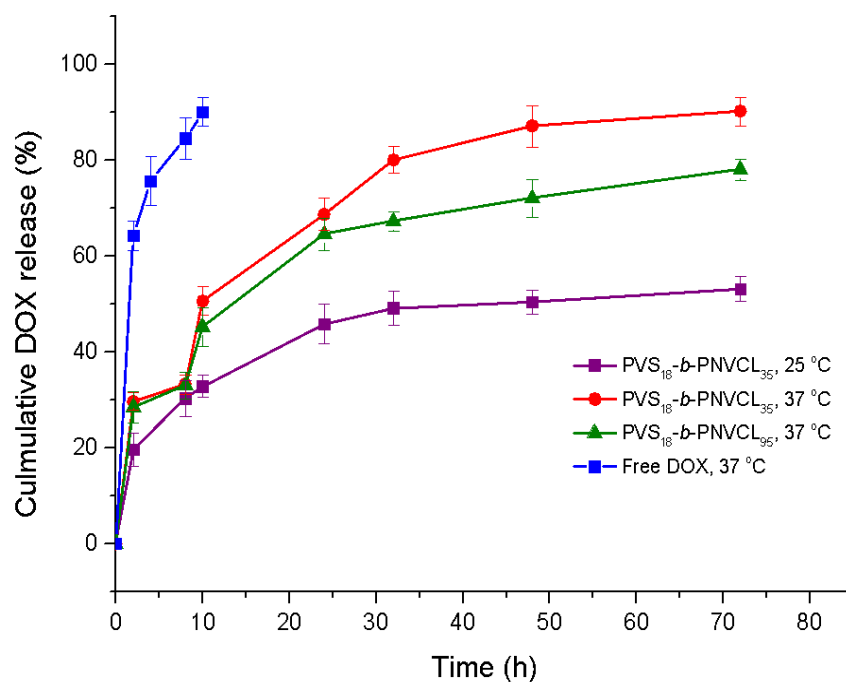


Figure 4.6. Release profiles *in vitro* of free DOX and DOX-loaded micelles in PBS (pH 7.4) at 37 °C and 25 °C.

#### 4.3.4 Stability of PVS-*b*-PNCL in the presence of serum proteins

Upon intravenous injection and circulation in blood, self-assembled micelles are easily subjected to plasma protein absorption, consequently leading to micellar disassembly. To investigate the stability of PVS-*b*-PNCL micelles in the biological environment, NR-loaded micelles were incubated in PBS and FBS (10 vol% in PBS). Their fluorescence emission spectra were measured over a period of 72 h. NR is a hydrophobic fluorescent probe that can only show strong fluorescence in hydrophobic environments.<sup>51,52</sup> Upon demicellization, the aqueous environment would cause a significant reduction in the emission intensity of NR. It can be seen from Figure 4.7, the fluorescence intensity of NR decreased to a small extent, but a majority of the micelles were stable in 10% FBS during a 72-h period. Meanwhile, NR-loaded micelles were found to have excellent micelle stability in the PBS, since the fluorescence intensity of NR was almost the same for up to 15 days (Figure S4.5, Appendix B). These results suggested that PVS<sub>18</sub>-*b*-PNCL<sub>35</sub> micelles were not destabilized by serum proteins and could safely protect the cargo in the core.

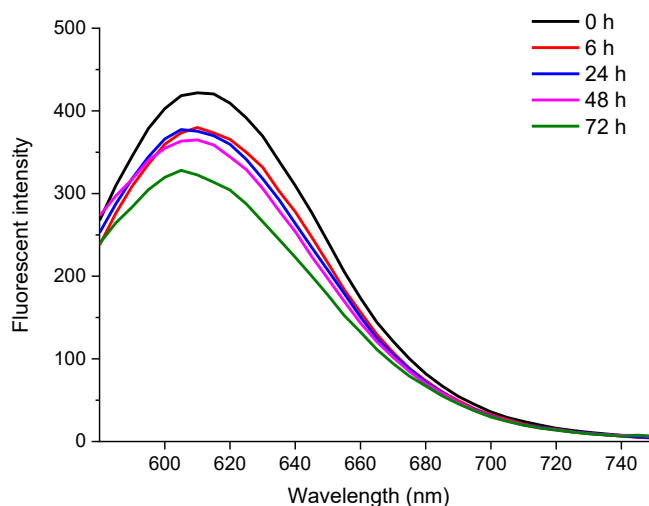


Figure 4.7. Fluorescence emission spectra (excitation at 570 nm) of NR-loaded PVS<sub>18</sub>-*b*-PNVCL<sub>35</sub> micelles incubated with 10% FBS.

#### 4.3.5 *In vitro* cytotoxicity of PVS-*b*-PNVCL

To evaluate the suitability of the micellar system for drug delivery, the biocompatibility of the block copolymer micelles was assessed by MTS assays on both cancerous (HeLa) and normal (HEK 293T) cell lines. Cells were incubated with different concentrations of PVS<sub>18</sub>-*b*-PNVCL<sub>35</sub> and their viability was evaluated after 24 and 48 h. As shown in Figure 4.8A and B, the block copolymer micelles (up to 200 µg/mL) showed high biocompatibility in both cell lines with more than 90% of cell viability after 48 h of incubation. These results demonstrated that PVS-*b*-PNVCL micelles were highly biocompatible and could be suitable for biomedical applications.

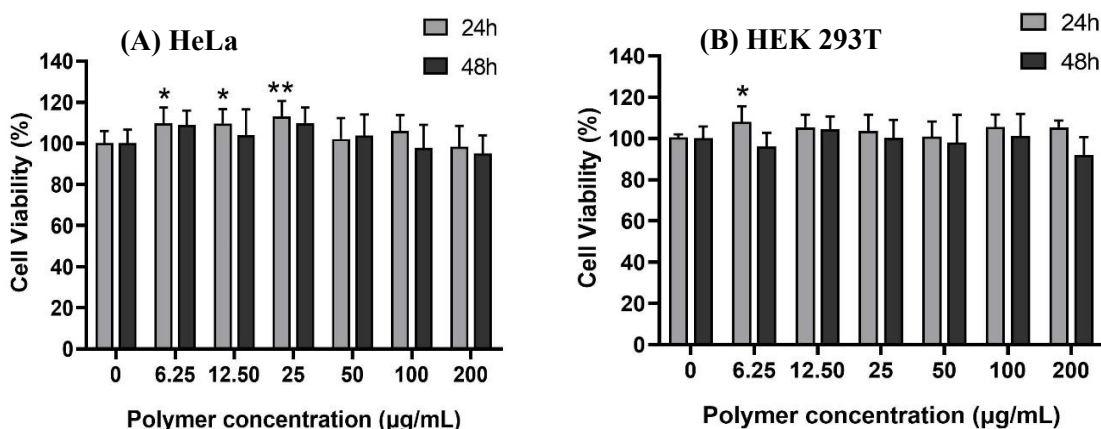


Figure 4.8. Cell viability results for (A) HeLa and (B) HEK 293T cells treated with different concentrations of PVS<sub>18</sub>-*b*-PNVCL<sub>35</sub>. Experiments were carried out three times independently and data are presented as mean  $\pm$  SD. \* $p < 0.05$ ; \*\* $p < 0.01$ , comparing with polymer concentration at 0 µg/mL.

The cytotoxicity of DOX-loaded micelles and free DOX with concentrations ranging from 0.625 to 20 µg/mL was tested in HeLa cells and HEK 293T cells. Figure 4.9A and B displayed the cell viability of HeLa cells incubated with free DOX and DOX-loaded PVS<sub>18</sub>-*b*-PNVCL<sub>35</sub> micelles for 24 or 48 h. As shown in Figure 4.9A, free DOX showed slightly higher toxicity than loaded DOX at the equivalent dose after 24 h treatment, but the difference was not statistically significant.

The IC<sub>50</sub> value (a concentration of 50% cell killing) of free DOX and DOX-loaded micelles were estimated to be 2.5 and 5 µg/mL, respectively. When incubated for 48 h, DOX-loaded micelles killed more than 80% of HeLa cells at higher concentrations (>5 µg/mL) which showed similar efficiency as free Dox. The slower cell-killing rate of DOX-loaded micelles was possibly related to the sustained release of DOX from micelles and different cellular uptake pathways for free drugs and micelles. The toxic effects of loaded and free DOX were also evaluated in HEK 293T. As illustrated in Figure S4.6. (Appendix B), the DOX-loaded micelles showed lower cytotoxicity than that of free DOX.

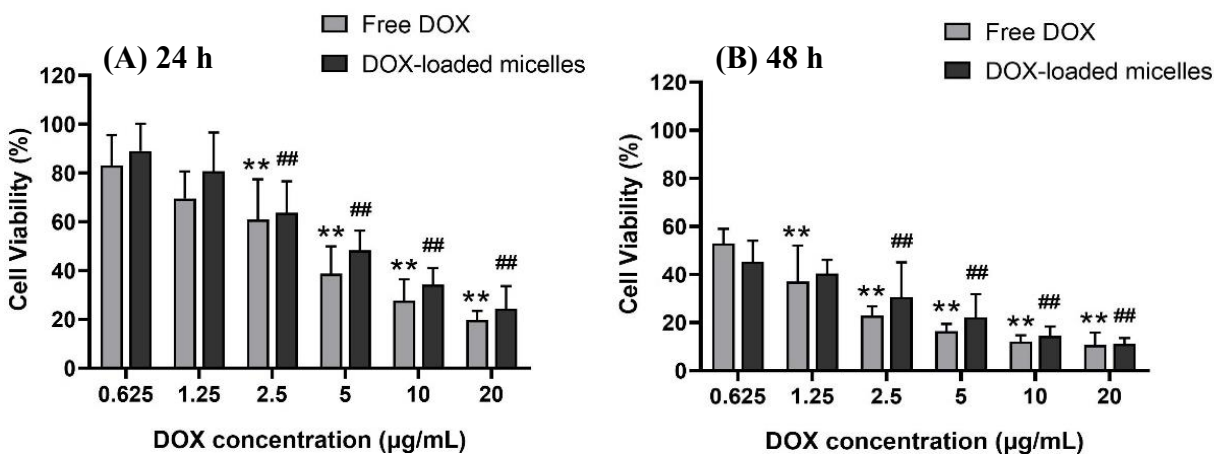


Figure 4.9. Effect of DOX-loaded PVS<sub>18</sub>-*b*-PNVCL<sub>35</sub> micelles on HeLa cell viability. HeLa cells were incubated with free DOX as control and DOX-loaded micelles for 24 h (A) or 48 h (B). Data were presented as mean ± SD and obtained from three independent experiments. \*\**p*<0.01, comparing with DOX concentration at 0.625 µg/mL (Free Dox group); ##*p*<0.01, comparing with DOX concentration at 0.625 µg/mL (DOX-loaded micelles group).

#### 4.3.6 *In vitro* uptake of PVS-*b*-PNVCL in cellular models

The cellular uptake and intracellular distribution of the DOX-loaded micelles were examined under confocal laser scanning microscope (CLSM). Free DOX and DOX-loaded micelles prepared with PVS<sub>18</sub>-*b*-PNVCL<sub>35</sub> were incubated with HeLa cells for 4 and 24 h. As shown in Figure 4.10, after 4 h of incubation, red fluorescence color of DOX was detected in the

cytoplasm for both free DOX and DOX-loaded micelles. DOX-loaded micelles were found to exhibit more intense DOX-fluorescence than free DOX. As the incubation time was prolonged to 24 h, the intracellular distribution of the encapsulated DOX was distinct from that of free DOX. The red DOX signal appeared to be throughout the whole cell including both the cytoplasm and nucleus for DOX-loaded micelle, while with free DOX it was primarily observed in cell nuclei. Higher-magnification images (1000×) can be seen in Figure S4.7 (Appendix B). Notably, DOX is a small molecule that can be transported rapidly into cells via passive diffusion. Upon arrival at the nucleus, DOX can induce cell death by intercalating with DNA and preventing DNA replication.<sup>53</sup> However, different from free drugs, drugs encapsulated into polymers with larger particle sizes were reported to enter the cells through endocytosis.<sup>54,55</sup> As a result, the delayed cellular uptake of DOX loaded into micelles might be because drugs first needed to be released from the micelles into the cytoplasm and then delivered to cell nuclei. These results correspond well with their time-dependent cell-killing properties as observed in cell viability assay and further prove the successful delivery and uptake of loaded drugs.

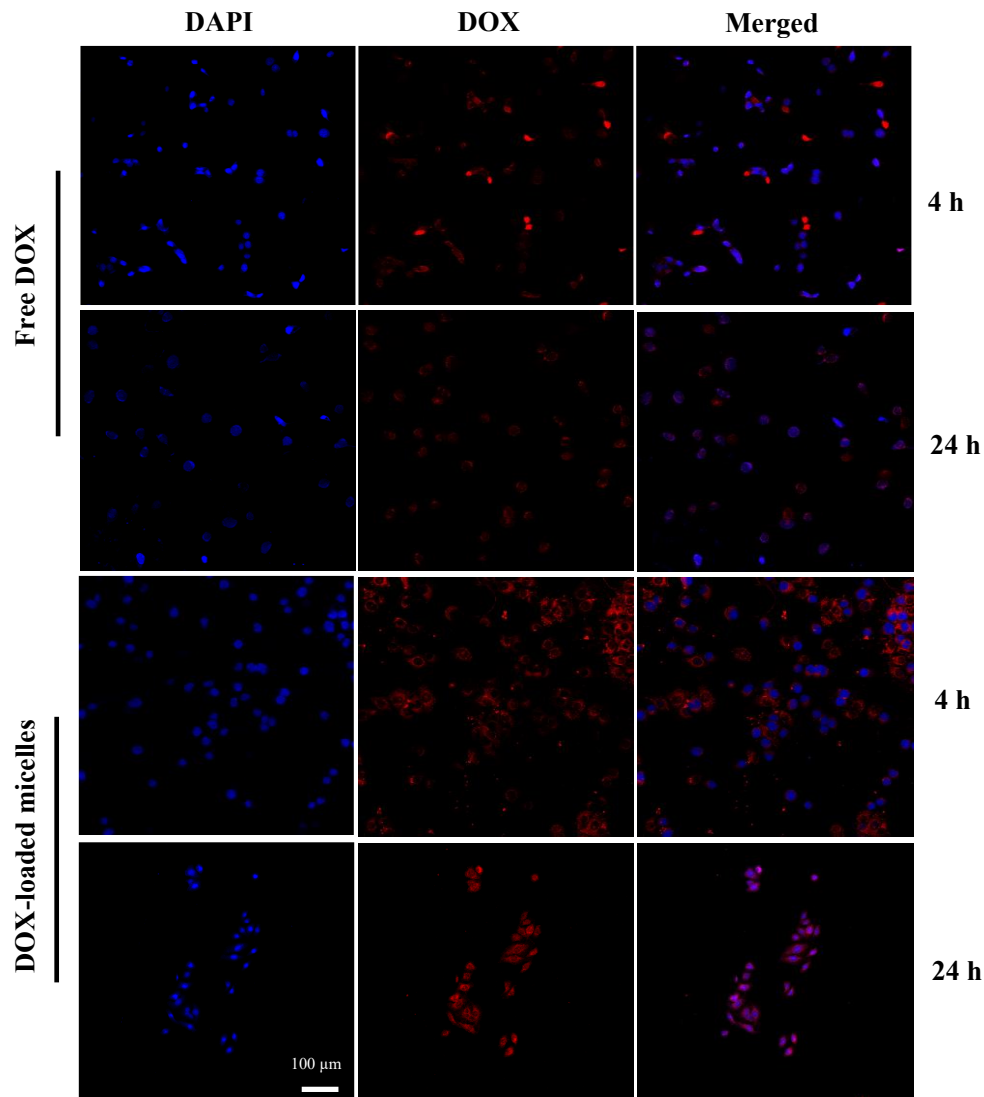


Figure 4.10. CLSM images ( $400\times$ ) of HeLa cells treated with DOX encapsulated into PVS<sub>18</sub>-*b*-PNVCL<sub>35</sub> micelles and free DOX for 4 h or 24 h.

#### 4.4 Conclusions

In summary, we successfully synthesized block copolymers, PVS/PVL-*b*-PNVCL, containing fatty acid-based polymer (PVS/PVL) and thermo-responsive polymer (PNVCL) through microwave-assisted RAFT polymerization. In aqueous medium, these block copolymers demonstrated the ability to self-assemble into micellar structures. Their CMC, particle size, and

morphology were influenced by the ratio of hydrophilic/hydrophobic segments in block copolymers. For PVS-*b*-NVCL, an increase in the hydrophilic block length (more than 72 repeating units), led to the formation of smaller, spherical micelles (~80 nm) with a more uniform particle size distribution and relatively higher CMC values. Conversely, both worm-like and spherical structures were exhibited by PVS<sub>18</sub>-*b*-PNVCL<sub>35</sub> with an average size of 111 nm and displayed low CMC values of 1.10 mg/L. The particle size reduction at elevated temperatures was attributed to the compactness of PNVCL block. It is also noteworthy that both block length and the choice of different chain lengths of fatty acids as the hydrophobic block in block copolymers can influence micellar size during self-assembly. Micelles from PVL-*b*-PNVL have larger particle sizes (130-145 nm) with a relatively broad size distribution. Efficient loading of the anticancer drug DOX into the micellar core was achieved, with a DLC of up to 10.4%. The DOX-loaded micelles exhibited temperature-triggered drug release, reaching a cumulative release of 80% after 72 h. These block copolymer micelles demonstrated excellent biocompatibility and serum stability, making them promising for biomedical applications. DOX-loaded micelles were able to be internalized and accumulated into the cells and showed a high cytotoxic effect against HeLa cells. Thus, the biocompatible polymeric micelles developed in this study hold potential as smart delivery vehicles in biomedical applications.

#### **4.5 References**

(1) Ghezzi, M.; Pescina, S.; Padula, C.; Santi, P.; Del Favero, E.; Cantù, L.; Nicoli, S. Polymeric Micelles in Drug Delivery: An Insight of the Techniques for Their Characterization and Assessment in Biorelevant Conditions. *J. Controlled Release* **2021**, *332*, 312–336.

- (2) Biswas, S.; Kumari, P.; Lakhani, P. M.; Ghosh, B. Recent Advances in Polymeric Micelles for Anti-Cancer Drug Delivery. *Eur. J. Pharm. Sci.* **2016**, *83*, 184–202.
- (3) Deng, C.; Jiang, Y.; Cheng, R.; Meng, F.; Zhong, Z. Biodegradable Polymeric Micelles for Targeted and Controlled Anticancer Drug Delivery: Promises, Progress and Prospects. *Nano Today* **2012**, *7*, 467–480.
- (4) Hwang, D.; Ramsey, J. D.; Kabanov, A. V. Polymeric Micelles for the Delivery of Poorly Soluble Drugs: From Nanoformulation to Clinical Approval. *Adv. Drug Delivery Rev.* **2020**, *156*, 80–118.
- (5) Fattahi, N.; Shahbazi, M. A.; Maleki, A.; Hamidi, M.; Ramazani, A.; Santos, H. A. Emerging Insights on Drug Delivery by Fatty Acid Mediated Synthesis of Lipophilic Prodrugs as Novel Nanomedicines. *J. Controlled Release* **2020**, *326*, 556–598.
- (6) Siepmann, J.; Faham, A.; Clas, S. D.; Boyd, B. J.; Jannin, V.; Bernkop-Schnürch, A.; Zhao, H.; Lecommandoux, S.; Evans, J. C.; Allen, C.; Merkel, O. M.; Costabile, G.; Alexander, M. R.; Wildman, R. D.; Roberts, C. J.; Leroux, J. C. Lipids and Polymers in Pharmaceutical Technology: Lifelong Companions. *Int. J. Pharm.* **2019**, *558*, 128–142.
- (7) Joshy, K. S.; Snigdha, S.; Anne, G.; Nandakumar, K.; Laly, A., P.; Sabu, T. Poly (Vinyl Pyrrolidone)-Lipid Based Hybrid Nanoparticles for Anti Viral Drug Delivery. *Chem. Phys. Lipids* **2018**, *210*, 82–89.
- (8) Gill, K. K.; Kaddoumi, A.; Nazzal, S. PEG-Lipid Micelles as Drug Carriers: Physiochemical Attributes, Formulation Principles and Biological Implication. *J. Drug Target.* **2015**, *23*, 222–231.
- (9) Kaikade, D. S.; Sabnis, A. S. Polyurethane Foams from Vegetable Oil-Based Polyols: A Review. *Polym. Bull.* **2023**, *80*, 2239–2261.

- (10) Lebarbé, T.; Grau, E.; Gadenne, B.; Alfos, C.; Cramail, H. Synthesis of Fatty Acid-Based Polyesters and Their Blends with Poly(l-Lactide) as a Way to Tailor PLLA Toughness. *ACS Sustainable Chem. Eng.* **2015**, *3*, 283–292.
- (11) Zhang, C.; Madbouly, S. A.; Kessler, M. R. Biobased Polyurethanes Prepared from Different Vegetable Oils. *ACS Appl. Mater. Interfaces* **2015**, *7*, 1226–1233.
- (12) Lomège, J.; Lapinte, V.; Negrell, C.; Robin, J. J.; Caillol, S. Fatty Acid-Based Radically Polymerizable Monomers: From Novel Poly(Meth)Acrylates to Cutting-Edge Properties. *Biomacromolecules* **2019**, *20*, 4–26.
- (13) Obeng, M.; Milani, A. H.; Musa, M. S.; Cui, Z.; Fielding, L. A.; Farrand, L.; Goulding, M.; Saunders, B. R. Self-Assembly of Poly(Lauryl Methacrylate)-b-Poly(Benzyl Methacrylate) Nano-Objects Synthesised by ATRP and Their Temperature-Responsive Dispersion Properties. *Soft Matter* **2017**, *13*, 2228–2238.
- (14) György, C.; Hunter, S. J.; Girou, C.; Derry, M. J.; Armes, S. P. Synthesis of Poly(Stearyl Methacrylate)-Poly(2-Hydroxypropyl Methacrylate) Diblock Copolymer Nanoparticles: Via RAFT Dispersion Polymerization of 2-Hydroxypropyl Methacrylate in Mineral Oil. *Polym. Chem.* **2020**, *11*, 4579–4590.
- (15) Maiti, B.; De, P. RAFT Polymerization of Fatty Acid Containing Monomers: Controlled Synthesis of Polymers from Renewable Resources. *RSC Adv.* **2013**, *3*, 24983–24990.
- (16) Dutertre, F.; Pennarun, P. Y.; Colombani, O.; Nicol, E. Straightforward Synthesis of Poly(Lauryl Acrylate)-b-Poly(Stearyl Acrylate) Diblock Copolymers by ATRP. *Eur. Polym. J.* **2011**, *47*, 343–351.
- (17) Wang, S.; Vajjala Kesava, S.; Gomez, E. D.; Robertson, M. L. Sustainable Thermoplastic Elastomers Derived from Fatty Acids. *Macromolecules* **2013**, *46*, 7202–7212.

- (18) Singh, A. P.; Gunasekaran, G.; Suryanarayana, C.; Balaji Naik, R. Fatty Acid Based Waterborne Air Drying Epoxy Ester Resin for Coating Applications. *Prog. Org. Coat.* **2015**, *87*, 95–105.
- (19) Li, A.; Li, K. Pressure-Sensitive Adhesives Based on Soybean Fatty Acids. *RSC Adv.* **2014**, *4*, 21521–21530.
- (20) Bordat, A.; Boissenot, T.; Nicolas, J.; Tsapis, N. Thermoresponsive Polymer Nanocarriers for Biomedical Applications. *Adv. Drug Deliv Rev.* **2019**, *138*, 167–192.
- (21) Cortez-Lemus, N. A.; Licea-Claverie, A. Poly(N-Vinylcaprolactam), a Comprehensive Review on a Thermoresponsive Polymer Becoming Popular. *Prog. Polym. Sci.* **2016**, *53*, 1–51.
- (22) Vihola H, Laukkanen A, Valtola L, Tenhu H, Hirvonen J. Cytotoxicity of thermosensitive polymers poly(N-isopropylacrylamide), poly(N-vinylcaprolactam) and amphiphilically modified poly(N-vinylcaprolactam). *Biomaterials* **2005**, *26*, 3055-3064.
- (23) Saha, B.; Ruidas, B.; Mete, S.; Mukhopadhyay, C.; Bauri, K.; De, P. AIE-active Non-conjugated Poly(N-vinylcaprolactam) as a Fluorescent Thermometer for Intracellular Temperature Imaging. *Chem. Sci.* **2020**, *11*, 141- 147.
- (24) Kozlovskaya, V.; Liu, F.; Yang, Y.; Ingle, K.; Qian, S.; Halade, G. V.; Urban, V. S.; Kharlampieva, E. Temperature-Responsive Polymersomes of Poly(3-Methyl-N-Vinylcaprolactam)-Block-Poly(N-Vinylpyrrolidone) to Decrease Doxorubicin-Induced Cardiotoxicity. *Biomacromolecules* **2019**, *20*, 3989–4000.
- (25) Singh, P.; Srivastava, A.; Kumar, R. Synthesis and Characterization of Nano Micelles of Poly(N-Acrylamidohexanoic Acid)-*b*-Poly(N-Vinylcaprolactam) via RAFT Process: Solubilizing and Releasing of Hydrophobic Molecules. *Polymer* **2015**, *57*, 51–61.

- (26) Góis, J. R.; Serra, A. C.; Coelho, J. F. J. Synthesis and Characterization of New Temperature-Responsive Nanocarriers Based on POEOMA-*b*-PNVCL Prepared Using a Combination of ATRP, RAFT and CuAAC. *Eur. Polym. J.* **2016**, *81*, 224–238.
- (27) Kermagoret, A.; Fustin, C. A.; Bourguignon, M.; Detrembleur, C.; Jérôme, C.; Debuigne, A. One-Pot Controlled Synthesis of Double Thermoresponsive N-Vinylcaprolactam-Based Copolymers with Tunable LCSTs. *Polym. Chem.* **2013**, *4*, 2575–2583.
- (28) Wu, Q.; Yi, J.; Wang, S.; Liu, D.; Song, X.; Zhang, G. Synthesis and Self-Assembly of New Amphiphilic Thermosensitive Poly(N-Vinylcaprolactam)/Poly(d,l-Lactide) Block Copolymers via the Combination of Ring-Opening Polymerization and Click Chemistry. *Polym. Bull.* **2015**, *72*, 1449–1466.
- (29) Kozlovskaya, V.; Kharlampieva, E. Self-Assemblies of Thermoresponsive Poly(N-Vinylcaprolactam) Polymers for Applications in Biomedical Field. *ACS Appl. Polym. Mater.* **2020**, *2*, 26–39.
- (30) Etchenausia, L.; Villar-Alvarez, E.; Forcada, J.; Save, M.; Taboada, P. Evaluation of Cationic Core-Shell Thermoresponsive Poly(N-Vinylcaprolactam)-Based Microgels as Potential Drug Delivery Nanocarriers. *Mater. Sci. Eng., C* **2019**, *104*, 109871.
- (31) Madhusudana Rao, K.; Mallikarjuna, B.; Krishna Rao, K. S. V.; Siraj, S.; Chowdoji Rao, K.; Subha, M. C. S. Novel Thermo/PH Sensitive Nanogels Composed from Poly(N-Vinylcaprolactam) for Controlled Release of an Anticancer Drug. *Colloids Surf., B* **2013**, *102*, 891–897.
- (32) Góis, J. R.; Popov, A. V.; Guliashvili, T.; Serra, A. C.; Coelho, J. F. J. Synthesis of Functionalized Poly(Vinyl Acetate) Mediated by Alkyne-Terminated RAFT Agents. *RSC Adv.* **2015**, *5*, 91225–91234.

- (33) Arshad, M.; Pradhan, R. A.; Ullah, A. Synthesis of Lipid-Based Amphiphilic Block Copolymer and Its Evaluation as Nano Drug Carrier. *Mater. Sci. Eng. C* **2017**, *76*, 217–223.
- (34) Rizzardo, E.; Chen, M.; Chong, B.; Moad, G.; Skidmore, M.; Thang, S.H. RAFT Polymerization: Adding to the Picture. *Macromolecules* **2007**, *248*, 104–116.
- (35) Wan, D.; Zhou, Q.; Pu, H.; Yang, G. Controlled Radical Polymerization of N-Vinylcaprolactam Mediated by Xanthate or Dithiocarbamate. *Polym. Sci., Part A: Polym. Chem.* **2008**, *46*, 3756–3765.
- (36) Beija, M.; Marty, J. D.; Destarac, M. Thermoresponsive Poly(N-Vinyl Caprolactam)-Coated Gold Nanoparticles: Sharp Reversible Response and Easy Tunability. *Chem. Commun.* **2011**, *47*, 2826–2828.
- (37) Li, F.; Zhou, F.; Romano, D.; Rastogi, S. Synthesis and Characterization of Well-Defined High-Molecular-Weight PDLA-*b*-PLLA and PDLA-*b*-PLLA-*b*-PDLA Stereo-Block Copolymers. *Macromolecules* **2023**, *56*, 1995–2008.
- (38) Izunobi, J. U.; Higginbotham, C. L. Polymer Molecular Weight Analysis by <sup>1</sup>H NMR Spectroscopy. *J. Chem. Educ.* **2011**, *88*, 1098–1104.
- (39) Sandoval, R. W.; Williams, D. E.; Kim, J.; Roth, C. B.; Torkelson, J. M. Critical Micelle Concentrations of Block and Gradient Copolymers in Homopolymer: Effects of Sequence Distribution, Composition, and Molecular Weight. *J. Polym. Sci. B: Polym. Phys.* **2008**, *46*, 2672–2682.
- (40) Migliore, N.; Picchioni, F.; Raffa, P. The Effect of Macromolecular Structure on the Rheology and Surface Properties of Amphiphilic Random Polystyrene-*R*-Poly(Meth)Acrylate Copolymers Prepared by RDRP. *Soft Matter* **2020**, *16*, 2836–2846.

- (41) Yang, Y.; Alford, A.; Kozlovskaya, V.; Zhao, S.; Joshi, H.; Kim, E.; Qian, S.; Urban, V.; Cropek, D.; Aksimentiev, A.; Kharlampieva, E. Effect of Temperature and Hydrophilic Ratio on the Structure of Poly(N-Vinylcaprolactam)- Block-Poly(Dimethylsiloxane)- Block-Poly(N-Vinylcaprolactam) Polymersomes. *ACS Appl. Polym. Mater.* **2019**, *1*, 722–736.
- (42) Liang, X.; Kozlovskaya, V.; Cox, C. P.; Wang, Y.; Saeed, M.; Kharlampieva, E. Synthesis and Self-Assembly of Thermosensitive Double-Hydrophilic Poly(N-Vinylcaprolactam)-*b*-Poly(N-Vinyl-2-Pyrrolidone) Diblock Copolymers. *J. Polym. Sci., Part A: Polym. Chem.* **2014**, *52*, 2725–2737.
- (43) Du, B.; Mei, A.; Yang, Y.; Zhang, Q.; Wang, Q.; Xu, J.; Fan, Z. Synthesis and Micelle Behavior of (PNIPAm-PtBA-PNIPAm)<sub>m</sub> Amphiphilic Multiblock Copolymer. *Polymer* **2010**, *51*, 3493–3502.
- (44) Luo, Y. L.; Yang, X. L.; Xu, F.; Chen, Y. S.; Zhang, B. Thermosensitive PNIPAM-*b*-HTPB Block Copolymer Micelles: Molecular Architectures and Camptothecin Drug Release. *Colloids Surf., B* **2014**, *114*, 150–157.
- (45) Wan, X.; Liu, T.; Liu, S. Synthesis of Amphiphilic Tadpole-Shaped Linear-Cyclic Diblock Copolymers via Ring-Opening Polymerization Directly Initiating from Cyclic Precursors and Their Application as Drug Nanocarriers. *Biomacromolecules* **2011**, *12*, 1146–1154.
- (46) Yokoyama, M. Polymeric Micelles as Drug Carriers: Their Lights and Shadows. *J Drug Targeting* **2014**, *22*, 576–583.
- (47) Ghezzi, M.; Pescina, S.; Padula, C.; Santi, P.; Del Favero, E.; Cantù, L.; Nicoli, S. Polymeric Micelles in Drug Delivery: An Insight of the Techniques for Their Characterization and Assessment in Biorelevant Conditions. *J. Controlled Release* **2021**, *332*, 312–336.

- (48) Owen, S. C.; Chan, D. P. Y.; Shoichet, M. S. Polymeric Micelle Stability. *Nano Today* **2012**, *7*, 53–65.
- (49) Lee, J.; Cho, E. C.; Cho, K. Incorporation and Release Behavior of Hydrophobic Drug in Functionalized Poly(D,L-Lactide)-Block-Poly(Ethylene Oxide) Micelles. *J. Controlled Release* **2004**, *94*, 323–335.
- (50) Wang, J.; Li, Y.; Dong, X.; Wang, Y.; Chong, X.; Yu, T.; Zhang, F.; Chen, D.; Zhang, L.; Gao, J.; Yang, C.; Han, J.; Li, W. A Micelle Self-Assembled from Doxorubicin-Arabinoside Conjugates with PH-Cleavable Bond for Synergistic Antitumor Therapy. *Nanoscale Res. Lett.* **2017**, *12*, 73.
- (51) Park, J.; Moon, M.; Seo, M.; Choi, H.; Kim, S. Y. Well-Defined Star-Shaped Rod-Coil Diblock Copolymers as a New Class of Unimolecular Micelles: Encapsulation of Guests and Thermoresponsive Phase Transition. *Macromolecules* **2010**, *43*, 8304–8313.
- (52) Rainbolt, E. A.; Miller, J. B.; Washington, K. E.; Senevirathne, S. A.; Biewer, M. C.; Siegwart, D. J.; Stefan, M. C. Fine-Tuning Thermoresponsive Functional Poly( $\epsilon$ -Caprolactone)s to Enhance Micelle Stability and Drug Loading. *J. Mater. Chem. B* **2015**, *3*, 1779–1787.
- (53) Rivankar, S. An Overview of Doxorubicin Formulations in Cancer Therapy. *Journal of Cancer Research and Therapeutics. J. Cancer Res. Ther.* **2014**, *10*, 853–858.
- (54) Mosquera, J.; García, I.; Liz-Marzán, L. M. Cellular Uptake of Nanoparticles versus Small Molecules: A Matter of Size. *Acc. Chem. Res.* **2018**, *51*, 2305–2313.
- (55) Bej, R.; Achazi, K.; Haag, R.; Ghosh, S. Polymersome Formation by Amphiphilic Polyglycerol- b-Polydisulfide- b-Polyglycerol and Glutathione-Triggered Intracellular Drug Delivery. *Biomacromolecules* **2020**, *21*, 3353–3363.

## **CHAPTER 5. Polymersomes Prepared from Lipid-based Protein-polymer Conjugate with Temperature-sensitivity for Targeted Drug Delivery**

### **5.1 Introduction**

Compartmentalization is a fundamental trait exhibited by cells and organelles, facilitating the execution of various cellular functions in an organized and controlled manner. To bridge the gap between biology, chemistry, and engineering, efforts to replicate structures and functions of natural compartments have been made from a variety of fields, including medicine, biotechnology, energy, and materials science.<sup>1-5</sup> Notably, protein-polymer conjugates, a burgeoning category of artificial cell-like architectures<sup>6-8</sup>, have emerged showcasing synthetic structures combined with biological entities enabling them to operate as supramolecular polymer assemblies. Within the realm of hybrid materials, protein-polymer conjugates uniquely integrate the tunable chemical properties of polymers with diverse biological characteristics of protein biomolecules. This integration often results in enhanced stabilities, improved pharmacokinetics, prolonged in vivo circulation half-life, and additional functionalities for the resulting conjugates<sup>9</sup>. Consequently, these conjugates find robust applications in diverse fields, including drug/gene delivery<sup>10-12</sup>, nanoreactors<sup>13,14</sup>, artificial cells<sup>15</sup>, biosensing<sup>16</sup>, tissue engineering<sup>17</sup>, and more. An exemplary case illustrating the success of this approach is the utilization of PEGylated proteins, which have been approved by US Food and Drug Administration and demonstrated remarkable clinical efficacy in treating various diseases.<sup>18</sup>

In recent years, diverse polymer species have been exploited to couple with proteins, expanding their applicability<sup>19,20</sup>, particularly emphasizing the hydrophilic and stimuli-responsive

polymers. Poly(N-isopropylacrylamide) (PNIPAM), as one of the most well-studied thermoresponsive polymers, has undergone thorough exploitation in its conjugation with proteins, employing both “grafting to” or “grafting from” approaches.<sup>21–23</sup> Protein-PNIPAM conjugates have demonstrated considerable potential across various domains such as drug delivery, diagnostic, enzyme immobilization and biocatalysis.<sup>24–26</sup> However, it is crucial to highlight that the PNIPAM backbone is not subject to biodegradation under physiological conditions as they can potentially produce small toxic amide compounds upon hydrolysis.<sup>27</sup> In contrast, Poly(N-vinylcaprolactam) (PNVCL) is an alternative temperature-responsive non-ionic polymer with excellent biocompatibility, nontoxicity, and resistance to hydrolysis, rendering it suitable for a broad spectrum of biomedical applications.<sup>28</sup> More significantly, PNVCL, featuring aggregation-induced emission (AIE) characteristics, has been recently reported as a promising fluorescent polymeric thermometer for the early detection of diseases.<sup>29</sup> Unlike the sharp phase transition observed in PNIPAM at the Lower Critical Solution Temperature (LCST) of approximately 32 °C, PNVCL undergoes a continuous coil-globule transition within the temperature range of 36 to 50 °C. This transition is influenced by the factors such as polymer concentration and molecular weight. An inherent challenge associated with the widespread adoption of PNVCL arises from the challenge of polymerizing NVCL in a controlled fashion. While the formation of self-assembled compartments by giant amphiphiles of protein-polymer conjugates holds promise for presenting additional attractive functionalities, the conjugation of proteins with hydrophobic polymers is acknowledged to be challenging due to the restricted choice of solvent. With the focus on the design of nanosized self-assembled proteinosomes, we have introduced amphiphilic block copolymers as a fundamental building block for constructing the complex system without affecting protein activities. Lipids, essential and biocompatible components of cell membranes, are

considered ideal candidates for investigations of cell-mimicking systems in biological and nanomedicine fields. During the last few years, advancements in controlled radical polymerization (CRP) methods have facilitated the synthesis of well-defined various fatty acid-based block copolymers. This has been made possible through reversible addition-fragmentation chain transfer (RAFT) or atom transfer radical polymerization (ATRP) techniques.<sup>30-32</sup> The fatty acid residues, known for their favorable biocompatibility and biodegradability, are expected to serve as a robust hydrophobic segment for the fabrication of diverse polymer assemblies, owing to their long saturated/unsaturated carbon chains. However, despite their potential, relatively limited attention has been given towards exploring their biomedical applications as amphiphilic block copolymers.

In this study, we describe the synthesis of novel functional thermo-sensitive protein-polymer bioconjugate amphiphiles comprising bovine serum albumin (BSA) and poly(vinyl stearate)-*b*-PNVCL (PVS-*b*-PNVCL). BSA was selected for its abundance, safety, and multifunctionality,<sup>33</sup> with a specific on its only free cysteine-34 residues, frequently targeted for site-specific conjugations. The selection of the conjugation site and the conjugation method was deemed pivotal to preventing the protein's bioactivity post-modifications.<sup>34</sup> In this context, to fabricate a structurally defined polymer bioconjugate with protein, a "grafting to" approach, which involves the coupling of a functional group on the polymer to reactive amino acids presented on protein surfaces, was employed. The "grafting to" approach offers a distinct advantage by eliminating the potential exposure of proteins to denaturing conditions (non-polar solvent, temperature, etc.) during the polymerization process, in contrast to "grafting from" method. The findings offer encouragement for further exploration of their diverse applications, ranging from delivery systems, nanoreactors, bioimaging tools, or as essential instruments for gaining insights into biological mechanisms in the future.

## 5.2 Materials and methods

### 5.2.1 Materials

*N*-Vinylcaprolactam (NVCL, 98%, Sigma, St. Louis, MO, USA) underwent recrystallization from *n*-hexane prior to utilization. Vinyl stearate (95%, Sigma, St. Louis, MO, USA) was recrystallized from acetone prior to use. 4,4'-Azobis(4-cyanovaleric acid) (ACVA,  $\geq 98\%$ , Sigma, St. Louis, MO, USA) was recrystallized from methanol before use. Bovine serum albumin (BSA,  $>96\%$ , Sigma, St. Louis, MO, USA), potassium ethyl xanthogenate (96%, Sigma, St. Louis, MO, USA), 2-bromopropionic acid ( $>98\%$ , TCI America, Tokyo, Japan), 2,2'-dithiodipyridine (98%, Acros Organics, Geel, Belgium), 3-mercapto-1-propanol ( $>97\%$ , Thermo Scientific, Waltham, MA, USA), 1,3,5-trioxane ( $\geq 99\%$ , Sigma, St. Louis, MO, USA), Doxorubicin hydrochloride (99%, Sigma, St. Louis, MO, USA), tris(2-carboxyethyl)phosphine hydrochloride (TCEP, 98%, Thermo Scientific, Waltham, MA, USA), 5,5'-dithiobis-(2-nitrobenzoic acid) (Ellman's reagent,  $\geq 98\%$ , Sigma, St. Louis, MO, USA), Dithiothreitol (DTT, 97%, Sigma, St. Louis, MO, USA), and 4',6-diamidino-2-phenylindole dihydrochloride (DAPI,  $\geq 98\%$ , Sigma, St. Louis, MO, USA) were used without any further purification. Tetrahydrofuran (THF,  $\geq 99\%$ , Sigma, St. Louis, MO, USA) was purified by passing through a short alumina column before use. All other chemicals were of reagent grade and used as received.

### 5.2.2 Synthesis of S-2-(3-(pyridin-2-yl)disulfanyl)propyl propanoate-O-ethyl xanthate (X2)

The methods for synthesis of 3-(2-pyridinyl)disulfanylpropanol and S-(2-propionic acid)-O-ethyl xanthate (X1) were provided in supplementary materials (Appendix C). 3-(2-pyridinyl)disulfanylpropanol (300 mg, 1.49 mmol) and S-(2-propionic acid)-O-ethyl xanthate (345.6 mg, 1.79 mmol) were dissolved in 25 mL of dry dichloromethane (DCM) and placed in an

ice-water bath. Subsequently, EDC (342.8 mg, 1.79 mmol) and DMAP (122.2 mg, 0.15 mmol) were added sequentially. The reaction was allowed to proceed at room temperature with constant stirring for 16 h. After the reaction completion, the crude product was concentrated and subjected to purification through silica gel column chromatography, using hexane/EtOAc (2: 1, v/v) as the eluent. The final product (422 mg, 75%) was obtained as a yellow oil.

### 5.2.3 Synthesis of PVS and PVS-*b*-PNVCL with PDS functionality

PDS end-functionalized PVS and PVS-*b*-PNVCL were synthesized via microwave-assisted reversible addition-fragmentation chain transfer (RAFT) polymerization. PVS homopolymer was initially synthesized using the as-prepared X2 as the chain transfer agent (CTA). In a typical example, VS monomer (1117.8 mg, 3.6 mmol), X2 (4.5 mg, 0.012 mmol), ACVA (0.67 mg, 0.0024 mmol), and trioxane (50 mg, 0.56 mmol) were dissolved in 1.7 mL of THF. The mixture was purged with nitrogen for 25 min and placed in the microwave reactor under irradiation at 70 °C for 30 min. The reaction was terminated by cooling to room temperature with an ice-water bath. <sup>1</sup>H NMR spectroscopy was conducted to determine monomer conversion with trioxane employed as the internal standard. The obtained product was dissolved in acetone and precipitated in methanol for three times. The precipitate was then filtered, collected and dried in a vacuum oven for 24 h. The purified pyridyl disulfide terminated PVS was subsequently used as macro-CTA to further block copolymerize with NVCL in THF, using ACVA as initiator at a NVCL: Macro-CTA: ACVA ratio of 400:1:0.2. The polymerization reaction was conducted under programmed conditions for 30 min with microwave heating at 70 °C. Purification of PVS-*b*-PNVCL block copolymer was achieved through three successive precipitations in cold diethyl ether. After drying under vacuum, the white solid product was obtained. The pyridyl disulfide functionality of the

block copolymers was determined with DTT-induced reduction method according to previous reports.<sup>35,36</sup>

#### **5.2.4 Reduction of bovine serum albumin (BSA) and determination of free thiols using Ellman's assay**

BSA was reduced with TCEP according to previously reported procedure.<sup>37</sup> The free thiols present on BSA was quantified via Ellman's assay<sup>36</sup>. Briefly, Ellman's reagent solution was firstly prepared by dissolving 4 mg of 5,5'-dithio-bis-(2-nitrobenzoic acid) (DTNB) in 1 ml of 0.1 M phosphate buffer (pH = 8.0, containing 1mM EDTA). Subsequently, 4 mg of samples to be analyzed was added to 2.5 mL of the buffer solution, followed by the addition of 50  $\mu$ L of Ellman's reagent. The solution was mixed thoroughly and incubated for 25 min at ambient temperature. The absorbance of the mixture at 412 nm was analyzed by a UV/vis spectrophotometer. The thiol concentration was calculated according to the Beer-Lambert's law. (The molar extinction coefficient of 2-nitro-5-thiobenzoic acid was considered as 14,150  $M^{-1}cm^{-1}$  at 412 nm)

#### **5.2.5 Conjugation of the reduced BSA to polymers**

The reduced BSA (14.2 mg, 0.2  $\mu$ mol) was dissolved in 4 mL of bicarbonate buffer (0.1 M, pH 8.2) and a solution of PVS-*b*-PNVCL (25.4 mg, 2  $\mu$ mol, molecular weight determined from <sup>1</sup>H NMR) in 2 mL of DMSO was added dropwise (ca. 1 droplet per 10 s) to the BSA solution under stirring. The mixture was continued to stir for 25 h at room temperature (25 °C) and then subjected to centrifugation at 20 °C (3080  $\times$  g, 15 min) to remove un-reacted polymers. The supernatant was transferred into a dialysis membrane (MWCO = 25 000 Da) and dialyzed against water for 24 h, lyophilized, and analyzed by MALDI-TOF and DLS.

### 5.2.6 Thermally induced precipitation

Free BSA can be removed from the BSA-polymer conjugates through thermally induced precipitation, by taking advantage of the phase transition behaviour of PNVCL segment at LCST. After dialysis and lyophilization, a solution containing the conjugate in DI water at a concentration of 30 mg/mL was heated at 40 °C for 15 min, followed by centrifugation at  $37632 \times g$  at 37 °C for 2 min. The supernatant was carefully discarded, and the precipitate was redissolved in DI water. The above process was repeated to ensure complete removal of unconjugated BSA. Afterwards, the precipitate was collected and lyophilized to obtain the purified BSA-PVS-*b*-PNVCL bioconjugates.

### 5.2.7 LCST determination of the bioconjugates

The LCST behaviour of BSA-PVS-*b*-PNVCL (1 mg/mL in DI water) was studied with turbidimetry measurements using a UV/vis spectrophotometer at 500 nm. The sample solution was heated from 25 to 50 °C at a rate of ca. 0.2 °C/min with 5 min equilibration time at each increment. LCST value is defined as the temperature at which there is a 50% transmittance decrease.

### 5.2.8 Preparation of DOX-loaded BSA-polymer nanoparticles

To prepare the drug-loaded nanoconjugates, DOX·HCl was first neutralized with 3 equiv. of triethylamine for 3 h. The neutralized DOX was dissolved in the 2 mL of DMSO and added dropwise to 4 mL of buffer solution containing 10 mg of BSA-PVS-*b*-PNVCL. After gentle stirring for 4 h, the suspension was dialyzed against distilled water overnight with a dialysis membrane (MWCO = 3500 Da). The powder of DOX-incorporated nanoparticles was obtained after freeze drying. To measure the drug loading efficiency of the nanoconjugates, DOX-loaded

conjugates were dissolved in DMSO, and the amount of encapsulated DOX was determined by UV spectrophotometer at 485 nm by comparing to the calibration curve.

### 5.2.9 Characterization

**Spectroscopy:**  $^1\text{H}$  NMR spectra were acquired on a Bruker AvanceNeo spectrometer (MA, USA) operating at 500 MHz with deuterated  $\text{CDCl}_3$  as the solvent. Attenuated Total Reflectance Fourier Transform Infrared Spectroscopic (ATR-FTIR) spectra of PVS and PVS-*b*-PNVCL were obtained between 400 and 4000  $\text{cm}^{-1}$  on Bruker Alpha FTIR spectrophotometer (Bruker Optics, Leipzig, Germany) equipped with single-bounce diamond ATR crystal. For each sample, 16 scans were performed at room temperature. UV/vis transmittance measurements were recorded by SpectraMax M3 Multi-mode Microplate Reader (CA, USA).

**Dynamic Light Scattering (DLS):** Particle size and size distribution (PDI) of BSA-PVS-*b*-PNVCL in aqueous solutions were measured at different temperatures (25 °C, 37 °C or 42 °C) by DLS as described in Section 4.2.6 (Chapter 4).

**Transmission Electron Microscopy (TEM):** TEM analysis was conducted on JEOL JEM-2100, following the procedures outlined in Section 4.2.6 (Chapter 4).

**Matrix-assisted Laser Desorption/Ionization Time-of-Flight (MALDI-TOF):** MALDI mass spectra were collected on a Bruker ultrafleXtreme MALDI-TOF/TOF spectrometer (Bruker, Bremen, Germany). Linear positive mode was used. Sinapinic acid (10 mg/mL in acetonitrile and water (1/1, v/v) with 0.1% tetrafluoroacetic acid) was used as the matrix for BSA-polymer bioconjugate. Sample solution (2 mg/mL) was prepared by dissolving the bioconjugates in acetonitrile and water (1/1, v/v) with 0.1% trifluoroacetic acid. Matrix and sample solutions were mixed at 1:1, 1  $\mu\text{L}$  of this mixture was spotted on the sample plate, and the spots were air-dried

before analysis. 2-[(2E)-3-(4-tert-butylphenyl)-2-methylprop-2-enylidene]malononitrile (DCTB) (10 mg/mL in dichloromethane) was employed as the matrix for PVS-*b*-PNVCL block copolymer.

**Sodium dodecyl sulfate polyacrylamide gel electrophoresis (SDS-PAGE):** The SDS-PAGE was performed using a Bio-Rad PowerPac 300 Electrophoresis system with 10% Mini-PROTEAN® TGX™ Precast Protein Gels (Bio-Rad, CA, USA) at 150 V voltage and 400 mA current for 55 min. For non-reducing conditions, samples were mixed with 2× Laemmli Sample Buffer (Bio-Rad) in a ratio of 1:1. For reducing conditions, 5% freshly made β-mercaptoethanol was added and the samples were heated at 95 °C for 5 min. The gel was stained using Coomassie Blue for visualization of protein bands.

#### 5.2.10 *In vitro* cell viability assay

The MTS assay was used to evaluate the *in vitro* cytotoxicity of BSA-PVS-*b*-PNVCL conjugates and DOX-loaded conjugates. Human embryonic kidney 293T (HEK 293T) cells and human cervical cancer cell line HeLa were seeded into 96-well plates ( $1 \times 10^4$  cells per well) and cultured in Dulbecco's modified Eagle medium (DMEM, supplemented with 10% fetal bovine serum (FBS) and 1% penicillin/streptomycin) in a humidified atmosphere with 5% CO<sub>2</sub> at 37 °C overnight. The DMEM medium with FBS was then replaced by various concentrations of bioconjugates with or without DOX. Untreated cells were used as the control and added with an equal volume of fresh medium. The cells were incubated for 24, 48 or 72 h, and the culture medium was replaced with 100 μL of fresh DMEM. Subsequently, 20 μL of MTS Reagent (Abcam, Waltham, USA) was added and incubated for another 1 h. The absorbance was recorded at 490 nm using a Synergy H1 microplate reader (Biotek, SB, USA) to assess the cell viability profile. All statistical analyses were performed using GraphPad Prism software version 8.0 for Windows (GraphPad Software, San Diego, CA, USA).

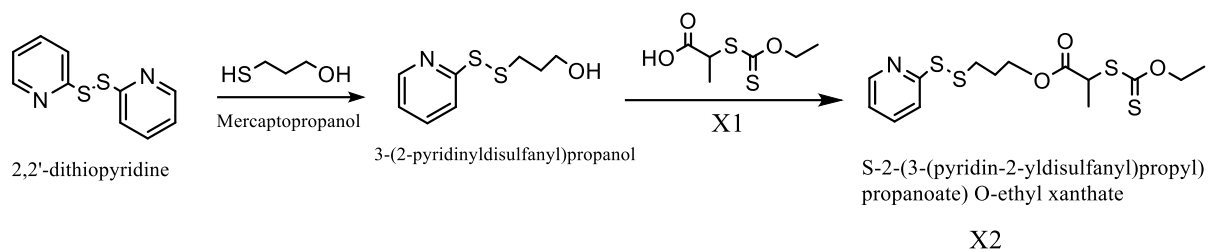
### 5.2.11 Cellular uptake assay

HeLa cells were seeded at a density of  $2 \times 10^5$  cells/well on a 12-well plate with a glass coverslip and cultured for 24 h. The medium was replaced with DOX-loaded conjugate and free DOX solutions, respectively, at a DOX concentration of 10  $\mu\text{g/mL}$ . After incubation for different time intervals, cells were washed for three times with  $1 \times$  phosphate buffered saline (PBS) and then fixed with 4% paraformaldehyde for 20 min at room temperature (25 °C). After fixation, the cells were subject to another triple washing with PBS, followed by staining with DAPI for 10 min and preservation in PBS. Cells treated with fluorescent dye were observed under a laser scanning confocal microscope system (Leica TCS SP5 Confocal, NC, USA). DOX was excited using a 470 nm laser and captured in the red channel, while DAPI was excited using a 358 nm laser and collected in the blue channel.

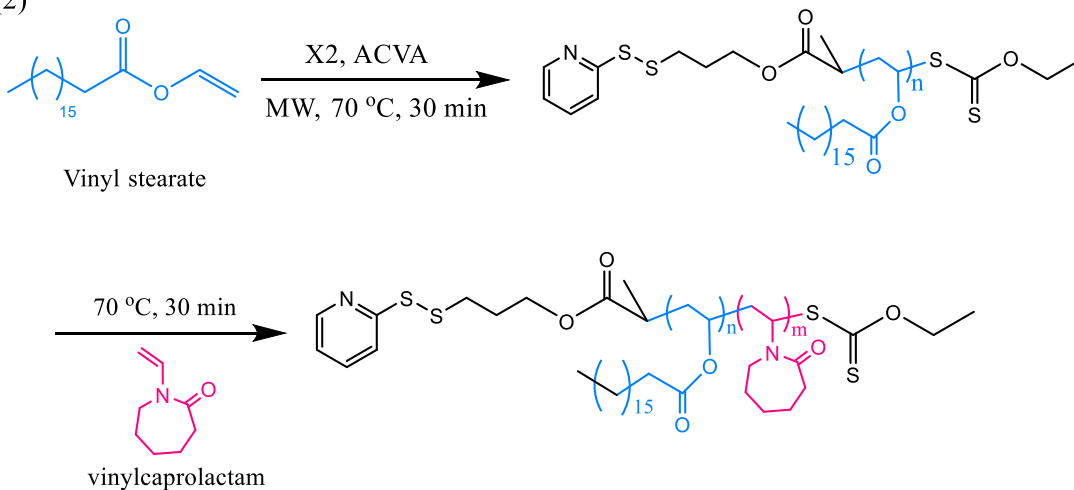
## 5.3 Results and discussion

The strategy of the preparation of the BSA-PVS-*b*-PNVCL bioconjugate is illustrated in Scheme 5.1. In this study, we designed a PVS-*b*-PNVCL block copolymer with a PDS end group through consecutive microwave-assisted reversible addition fragmentation chain transfer (RAFT) polymerization. Subsequently, the block copolymer was conjugated with the free thiols on protein BSA via a reversible disulfide bond. The resulting BSA-PVS-*b*-PNVCL conjugates were allowed to self-assemble in aqueous solution via dialysis method and characterized in terms of particle size and morphology. Comprehensive studies, including thermoresponsive properties, drug encapsulation, biocompatibility assessments, in vitro cytotoxicity assays, and cellular uptake investigations were carried out afterwards.

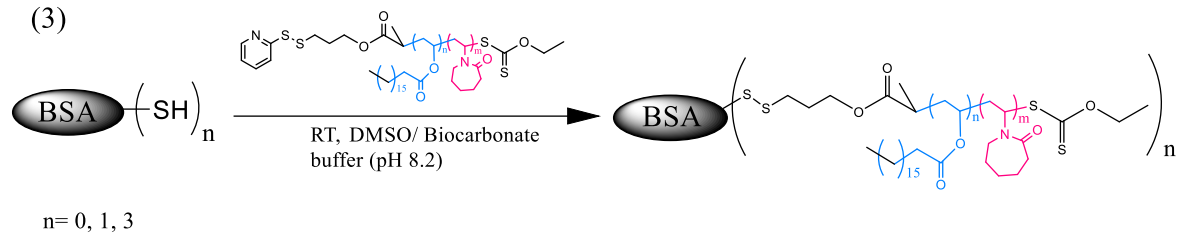
(1)



(2)



(3)



Scheme 5.1. Synthetic route for BSA-PVS-*b*-PNVCL bioconjugate.

### 5.3.1 Preparation of pyridyl disulfide functional homopolymers and block copolymers

For the successful attachment of a polymer to proteins, a crucial requirement is high fidelity of reactive end group for conjugation. Controlled radical polymerization techniques offer a convenient route for fabricating polymers with precisely controlled molecular weight, chain length, narrow polydispersity, and site-specific functionality.<sup>38</sup> Specifically, RAFT polymerization, has proven capable of producing diverse architectures compatible with varying monomers, providing a straightforward platform for molecular engineering of polymer bioconjugates via functional chain transfer agents (CTA).<sup>39</sup>

Among the frequently employed sites for preparing site-specific polymer bioconjugations is the free thiol on cysteine residues. While several thiol-reactive groups like maleimides, vinyl sulfones, and alkynes have been explored<sup>37,40</sup>, the pyridyl disulfide group remains attractive due to its rapid exchange reaction with thiols. Moreover, the reversible disulfide linkage formed between the polymer and biomolecule can be cleaved in a reductive cellular environment such as elevated levels of glutathione found in diseased tissues<sup>41</sup>, allowing the release of the therapeutic biomolecules.

In this study, a pyridyl disulfide terminated xanthate-based CTA was designed and characterized using <sup>1</sup>H NMR. (Figure S5.1, Appendix C). The choice of a suitable RAFT agent is crucial for successful synthesis of block copolymers, especially for less activated monomers like NVCL. A Xanthate-type RAFT agent was selected due to its reported effectiveness in controlling the radical polymerization of nonconjugated N-vinyl monomers through RAFT and macromolecular design via the interchange of xanthates (MADIX) process.<sup>42</sup> The RAFT agent (X2) was used for the polymerization of vinyl stearate resulting in a hydrophobic homopolymer with a pyridyl disulfide end group. The polymerization, conducted under microwave irradiation at

a [VS]: [PDS-CTA]: [ACVA] ratio of 300: 1: 0.2 in THF at 70 °C, achieved the monomer conversion of 90% after 30 min. The conversion was determined by comparing the integration of vinyl protons of the monomer (VS) with an internal standard, 1,3,5-trioxane ( $\delta = 5.10$  ppm). This analysis was conducted before and after polymerization process. The resultant PVS homopolymer served as the macro-CTA, extending with NVCL to produce the block copolymer PDS bearing PVS-*b*-PNVCL at 70 °C. The chemical structures of PVS and PVS-*b*-PNVCL were identified and confirmed by ATR-FTIR (Figure S5.2, Appendix C) and  $^1\text{H-NMR}$  spectroscopy (Figure 5.1.). In the  $^1\text{H-NMR}$  spectra, characteristic peaks for PVS included those at 0.86-0.91 ppm ( $\text{CH}_3$  end group) and 4.86 ppm ( $-\text{CH-O}$ ), as illustrated in Figure 5.1. Signals referring to PNVCL at 1.41-1.76 ppm ( $\text{CH}_2$  of caprolactam ring and backbone), 2.31-2.50 ppm ( $\text{COCH}_2$ ), 3.10-3.31 ppm ( $\text{NCH}_2$ ) and 4.40 ppm ( $\text{NCH}$ ) were also present. Notably, signals at 7.0-8.5 ppm from phenyl protons on the pyridine group were observed for both PVS and PVS-*b*-PNVCL, indicating the successful retention of the PDS functional end-group after block copolymerization. The PDS functionality was determined as 82% for PVS by comparing the integration of the proton ortho to the pyridyl nitrogen ( $\text{H}_a$ ) with the methylene protons adjacent to the disulfide ( $\text{H}_c$ ).<sup>36</sup> Due to the complexity of integration for  $\text{H}_c$  in the block copolymer, the functionality of the PDS end group in PVS-*b*-PNVCL was analyzed by treating with powerful reducing agent dithiothreitol (DTT). The result revealed that 78% of the block copolymer chains was retained the activated end group. The molecular weights of homopolymer and block copolymer were analyzed by  $^1\text{H NMR}$  and the result are summarized in Table 5.1.

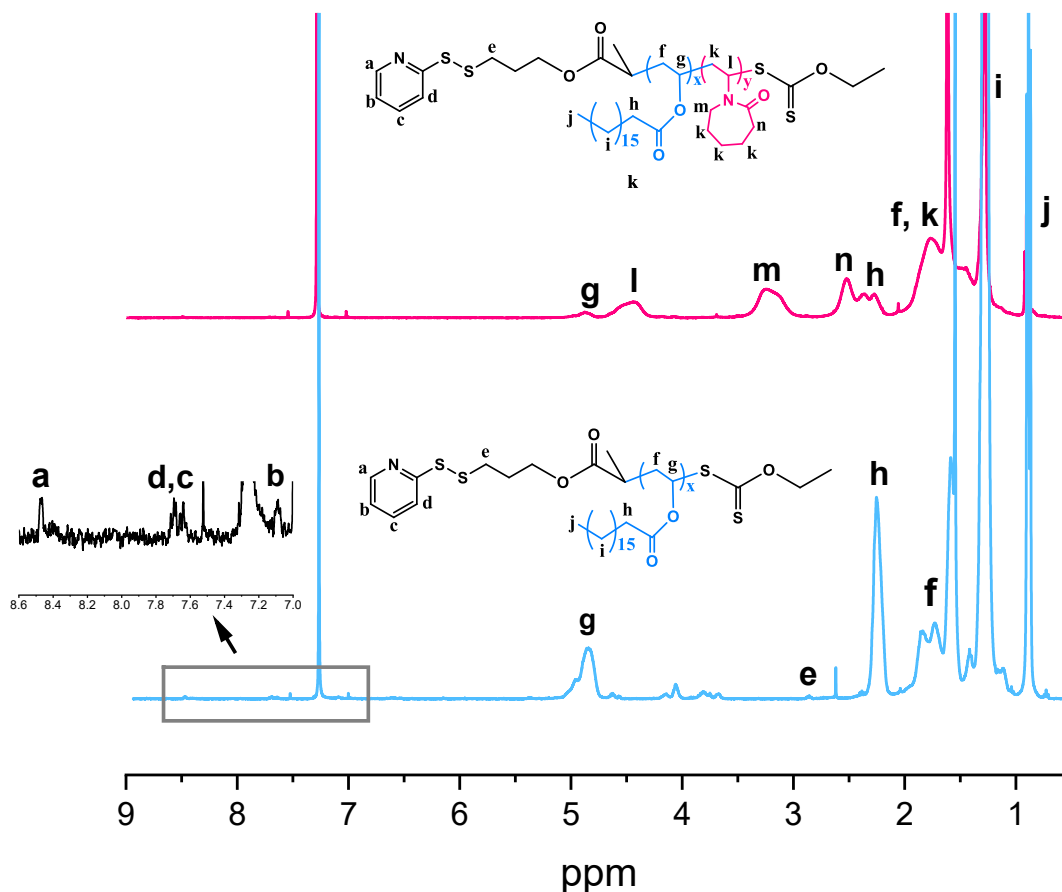


Figure 5.1.  $^1\text{H}$  NMR spectrum of PVS and PVS-*b*-PNVCL

Table 5.1. Microwave-assisted RAFT polymerization of PVS and PVS-*b*-PNVCL at 70 °C.

Polymer <sup>a</sup>	[M]/[CTA]/[I]	Time (min)	Conv. <sup>b</sup> (%)	$M_{n,theo}^c$ (g/mol)	$M_{n,nmr}^d$ (g/mol)	PDS end group retention (%)
PVS <sub>15</sub>	300:1:0.2	30	6.4	6339	5035	84
PVS <sub>15</sub> - <i>b</i> -PNVCL <sub>55</sub>	400:1:0.2	30	23.6	19478	12690	78

a. The subscripted numbers denote degree of polymerization (DP). The DP of PVS homopolymer was determined based on the integral ratio of H<sub>j</sub> at 0.86-0.91 ppm to methyl protons of the xanthate moiety at 3.7 ppm. The DP of PNVCCL was measured by comparing the integrated peak area at 0.86-0.91 ppm from PVS fraction with that of methylene proton H<sub>m</sub> (at 3.10-3.31 ppm) from PNVCCL side chain.

b. Determined by  $^1\text{H}$  NMR.

c. Calculated by  $^1\text{H}$  NMR.  $M_{n,theo} = [\text{monomer}]/[\text{CTA}] \times \text{molecular weight of monomer} \times \text{monomer conversion} + \text{molecular weight of CTA}$

d. Calculated by  $^1\text{H}$  NMR.  $M_{n,nmr} = \text{DP}_n \times \text{molecular weight of monomer} + \text{molecular weight of CTA}$

### 5.3.2 Preparation and characterization of BSA-PVS-*b*-PNVCL bioconjugates

In the literature, it has been reported that only about 50% of the sulfhydryl groups on BSA are accessible for polymer conjugation considering partial oxidation at Cys-34. To enhance the availability of free thiols for subsequent coupling reactions, BSA was first reduced using tris-(2-carboxyethyl) phosphine hydrochloride (TCEP). Ellman's assay revealed a notable increase in the average percentage of free thiols on BSA from approximately 31% to 183% after reduction. This suggests the cleavage of one disulfide bond within BSA, providing at least one thiol group per BSA molecule for subsequent bioconjugation. The BSA-PVS-*b*-PNVCL conjugates were then prepared through thiol-disulfide exchange reaction between PDS-PVS-*b*-PNVCL and reduced BSA in DMSO/bicarbonate buffer mixed solution. Following a 24-h incubation, the mixture was subjected to centrifugation and dialysis before being analyzed by MALDI-TOF. As shown in Figure 5.2A, the reduced BSA exhibited a molecular weight of ~66 kDa and  $m/z = \sim 33$  kDa for the doubly charged BSA. The MALDI-TOF spectrum of the conjugate sample (Figure 5.2B) confirmed successful conjugation of PVS-*b*-PNVCL with BSA, evidenced by peaks at  $m/z = \sim 67$  kDa for unreacted BSA, ~71 kDa for singly charged conjugates, and ~36 kDa for doubly charged conjugates. This suggests that the molecular weight of PVS-*b*-PNVCL attached to BSA was around 4 kDa, consistent with the block copolymer's molecular weight measured by MALDI-TOF (Figure S5.3, Appendix C). In addition, the results implied that the majority of PVS-*b*-PNVCL block copolymers likely conjugated with BSA in a one-to-one reaction. However, a discrepancy between the molecular weight of the block copolymer measured by MALDI-TOF and NMR was observed. This difference can be attributed to the challenges in MALDI-TOF for copolymer analysis, including different ionization regimes for each monomer and loss of sensitivity as

polymer mass increases.<sup>43,44</sup> Despite signal intensity limitations in reflecting the actual quantities of polymer-protein conjugates compared to free protein, the free BSA was detected in the product. To address this, thermally induced precipitation method<sup>21</sup> was employed to separate unreacted BSA from the conjugates, leveraging the temperature-sensitive properties of PNVCL segments. Subsequently, Ellman's assay of the purified conjugates indicated reduced reduction in free thiol content to 48% after the block copolymer was covalently linked to BSA.

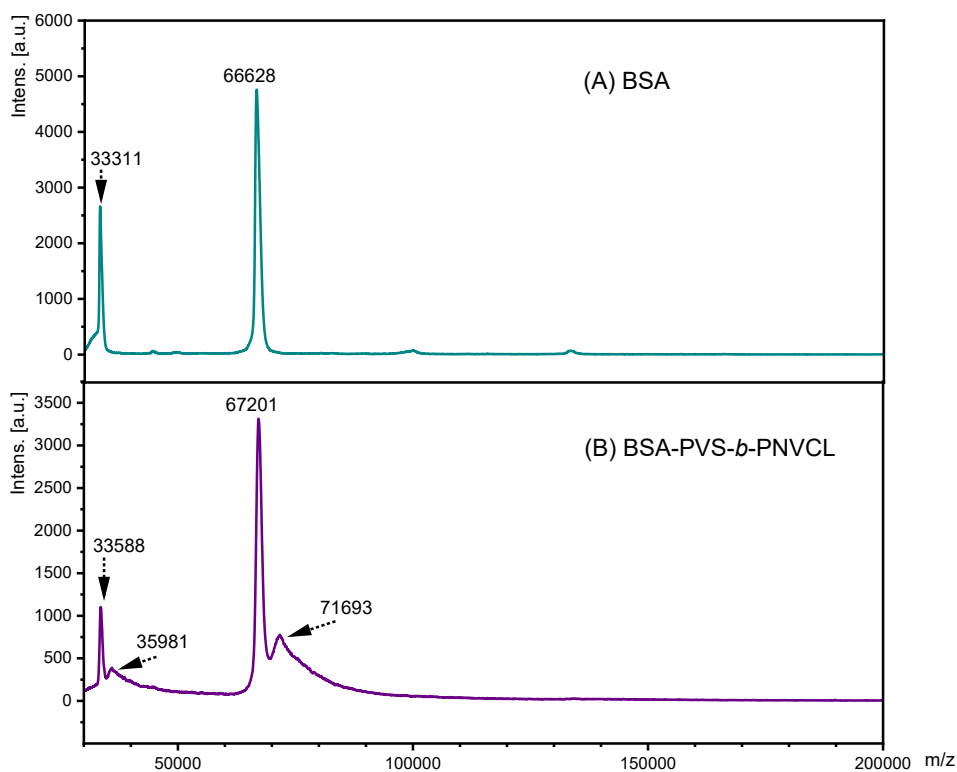


Figure 5.2. MALDI-TOF spectrum of (A) BSA and (B) BSA-polymer conjugate.

The conjugation of PVS-*b*-PNVCL and BSA was further confirmed through SDS-PAGE. To ascertain whether the block copolymer was coupled to BSA via a disulfide linkage, we conducted the analysis under both reductive and non-reductive conditions. As presented in Figure

5.3, a typical elongated band of the purified bioconjugate appeared at the top of the gel (lane 5 and 6) under non-reductive condition. This elongation can be attributed to the amphiphilicity of BSA-PVS-*b*-PNVCL conjugates impeding their movement within the gel. Conversely, under reductive conditions, the disulfide bond between the polymer and protein was cleaved, resulting in the disappearance of conjugate bands and subsequent detection of BSA (lane 8 and 9). This observation underscores the reduction-responsive property of the bioconjugate.

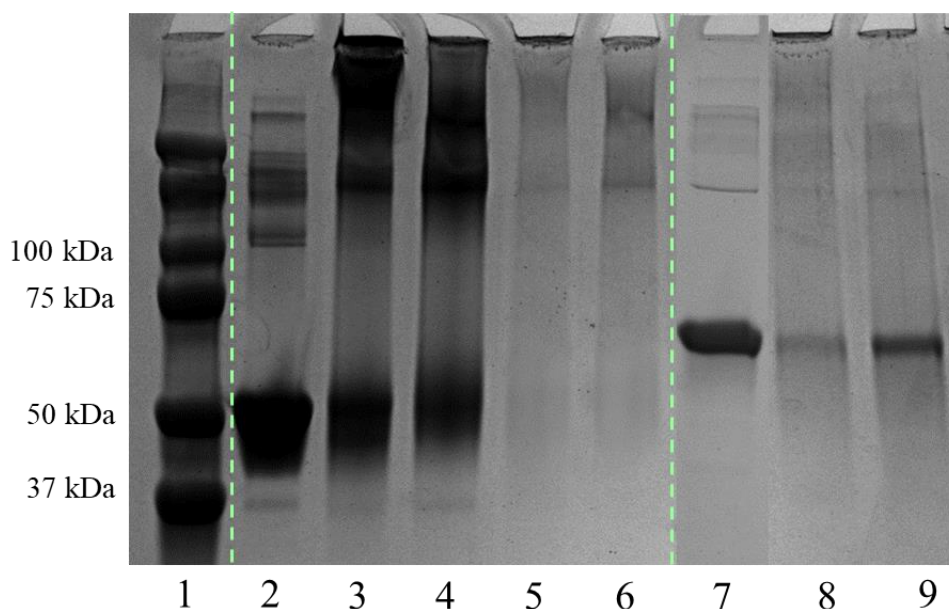


Figure 5.3. SDS-PAGE electropherogram of BSA and bioconjugates. Lanes 1-6: non-reducing conditions and Lanes 7-8: reducing conditions. Lane 1: Protein marker; Lane 2,7: BSA; Lane 3: BSA-PVS-*b*-PNVCL 1 after dialysis; Lane 4: BSA-PVS-*b*-PNVCL 2 after dialysis; Lane 5,8: Thermally precipitated BSA-PVS-*b*-PNVCL 1; Lane 6,9: Thermally precipitated BSA-PVS-*b*-PNVCL 2.

### 5.3.3 Self-assembly behaviour of BSA-PVS-*b*-PNVCL bioconjugates

The giant amphiphilic protein-polymer conjugates exhibit spontaneous self-assembly, wherein the micellization of the BSA-PVS-*b*-PNVCL conjugate occurs during dialysis against water. The hydrodynamic diameter and size distribution of the purified BSA-PVS-*b*-PNVCL nanoparticles were assessed using DLS. As depicted in Figure 5.4, the self-assembled nanostructures demonstrated an average diameter of 200 nm with a PDI of 0.3. By using thermally induced precipitation method, free BSA particles (7 nm) was completely removed from the conjugates. The morphology of the self-assembled aggregates was further examined via TEM, as depicted in Figure 5.5. The TEM results revealed that the nanoparticles self-assembled into vesicles with a spherical morphology. The particle size obtained from TEM closely aligned with DLS measurements, acknowledging that the nanoparticles were in dehydrated state during TEM observation.

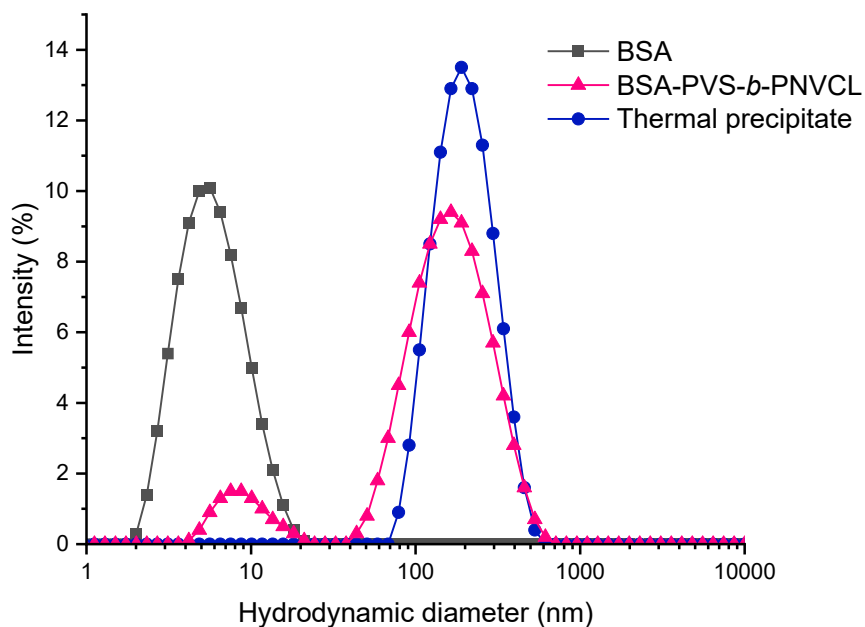


Figure 5.4. DLS distributions of BSA and BSA-PVS-*b*-PNVCL in aqueous solution at 25 °C.

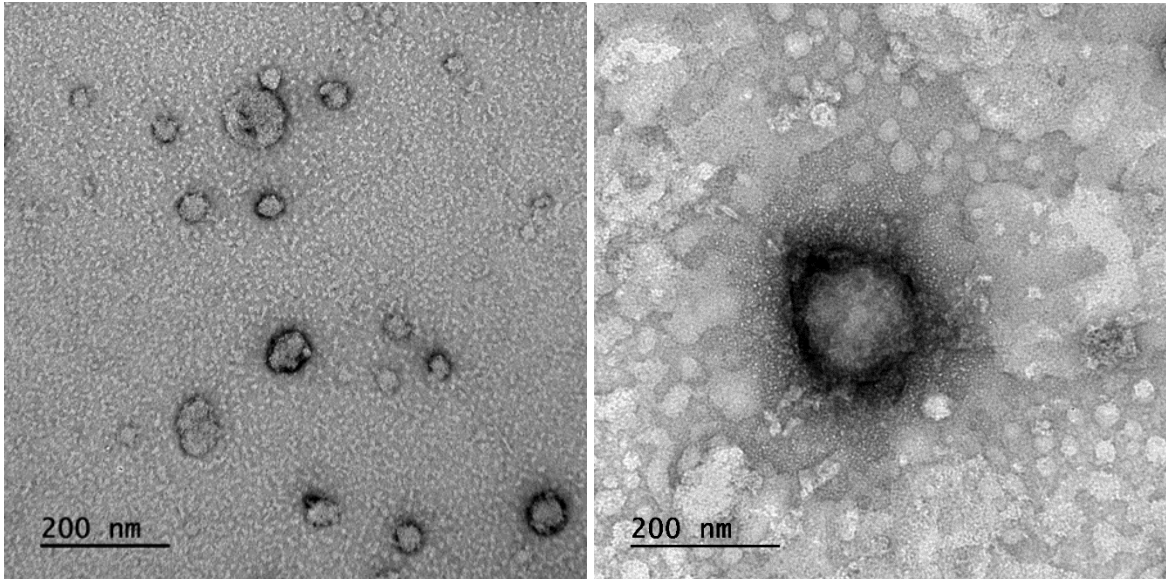


Figure 5.5. TEM images of purified BSA-PVS-*b*-PNVCL self-assemblies

#### 5.3.4 Thermoreponsiveness of bioconjugates

PNVCL is a temperature-responsive polymer that exhibits phase transition behavior in aqueous solutions, responding to changes in temperature. Above its lower critical solution temperature (LCST), PNVCL undergoes dehydration due to disruption of hydrogen bonding with water molecules upon heating. This results in the dominance of intermolecular hydrophobic interactions.<sup>45</sup> The LCST values within a desired range can be easily tuned by incorporation of hydrophobic or hydrophilic comonomers.<sup>46</sup> The LCST behaviour of BSA-PVS-*b*-PNVCL conjugates was explored by measurement of UV/vis transmittance at 500 nm as a function of temperature, with PNVCL as a comparison. The LCST was defined as the temperature at which there was a 50% decrease of the maximum transmittance. As illustrated in Figure 5.6, BSA-PVS-*b*-PNVCL conjugates exhibited higher LCST values (approximately 39.5 °C) compared to PNVCL (36.5 °C) while maintaining an equal polymer chain length. The increased hydrophilicity of the

macromolecules after BSA attachment contributed to the elevated transition temperature of the bioconjugate. Materials with an LCST above body temperature hold special significance in achieving targeted drug delivery, as they can selectively release drug at tumor sites due to local temperature around  $\sim 40\text{-}42\text{ }^{\circ}\text{C}$  or drug can be released using hyperthermia approach.

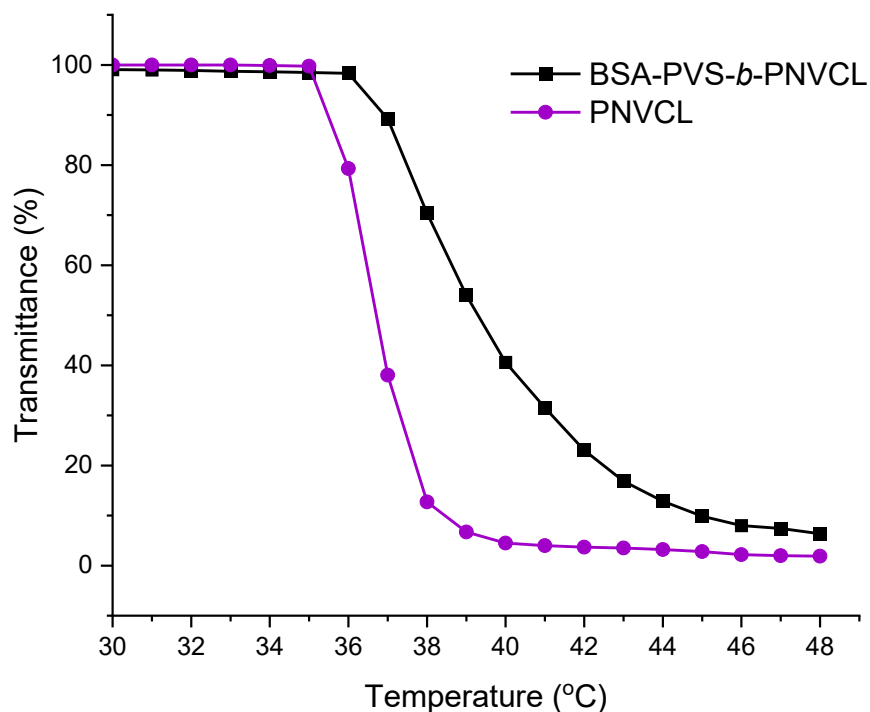


Figure 5.6. Plot of relative absorbance at 500 nm of PNVCL and BSA-PVS-*b*-PNVCL bioconjugate in aqueous solution as a function of temperature.

The change in the hydrodynamic diameter ( $D_h$ ) of BSA-PVS-*b*-PNVCL conjugates at different temperatures was monitored using DLS measurements (Figure 5.7.). At temperatures below the LCST ( $25\text{ }^{\circ}\text{C}$ ), PNVCL segment remained in hydrophilic nature and the conjugate self-assembled into nanoparticles with an average diameter of 210 nm. Upon reaching  $37\text{ }^{\circ}\text{C}$ , the PNVCL segment exhibited a partial transition from hydrophilic to hydrophobic, initiating aggregation, evident from the increased  $D_h$  measuring 492 nm. Subsequent elevation of the

temperature to 42 °C prompted the small-sized aggregates to coalesce into larger particles during phase transition due to the further dehydration from PNVCL fraction. Consequently, their particle size increased significantly to 912 nm above LCST.

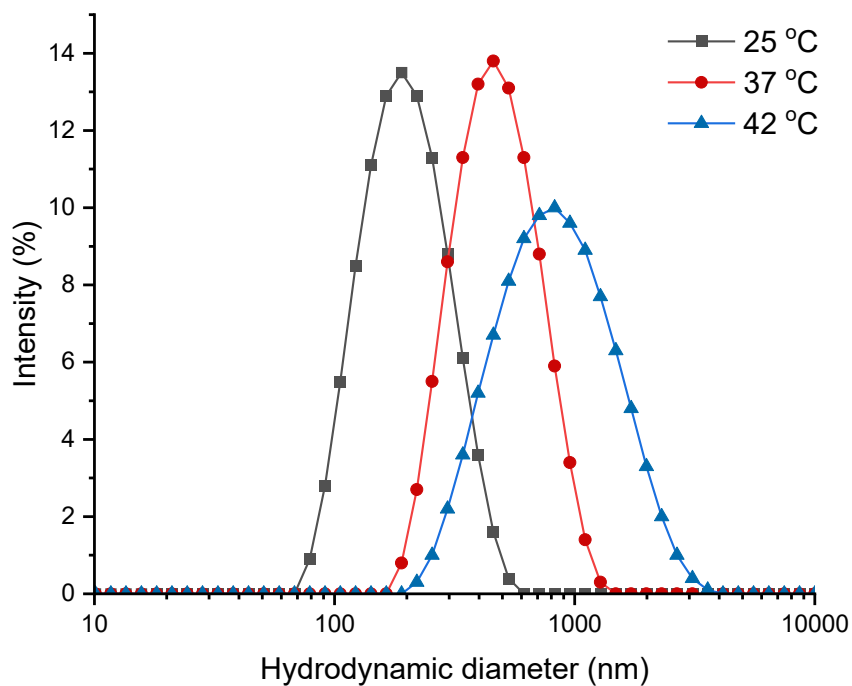


Figure 5.7. DLS distributions of BSA-PVS-*b*-PNVCL in aqueous solution at different temperatures

### 5.3.5 Drug-loaded protein-polymer bioconjugates

DOX was selected as a model for a hydrophobic anticancer drug and was encapsulated within BSA-PVS-*b*-PNVCL polymersomes using the dialysis method. The BSA-PVS-*b*-PNVCL conjugate demonstrated notably high DOX loading contents (DLC). Specifically, it reached 11.9% at a bioconjugate: drug ratio of 5:1 (w/w) and 25.6% at a bioconjugate: drug ratio of 5:2, as determined by UV/vis spectrometry. The size and morphology of the DOX-loaded BSA-PVS-*b*-PNVCL nanoparticles were also characterized through DLS and TEM analysis. As shown in Table

5.2, compared to self-assembled blank bioconjugates, the nanostructures exhibited reduced sizes ranging from 106 to 124 nm after DOX loading, with a more uniform size distribution. The TEM image (Figure 5.8.) of the DOX-loaded BSA-PVS-*b*-PNVCL nanoassemblies depicted a well-defined spherical morphology with particle sizes below 100 nm. Considering these results collectively, a plausible assumption is that the initially formed vesicles underwent a transformation into smaller spheres after the loading hydrophobic drugs. Various factors, including intramolecular interactions of drug hydrophobic components, changes in the thermodynamic stability of the system, etc., could contribute to this phenomenon. Notably, prior instances of drug-induced morphology transitions, such as shift from a worm to a polymersome have been documented in the literature.<sup>47,48</sup>

Table 5.2. Characteristics of DOX-loaded bioconjugates

DOX-loaded bioconjugates				
Conjugate/DOX	diameter (nm)	PDI	DLE (%)	DLC (%)
5:1	106.3	0.244	71.7	11.9
5:2	124.5	0.204	89.6	25.6

\*Drug loading efficiency (DLE) (%) = Mass of drug incorporated/Mass of drug fed × 100

Drug loading content (DLC) (%) = Mass of drug incorporated/Mass of drug-loaded bioconjugates × 100

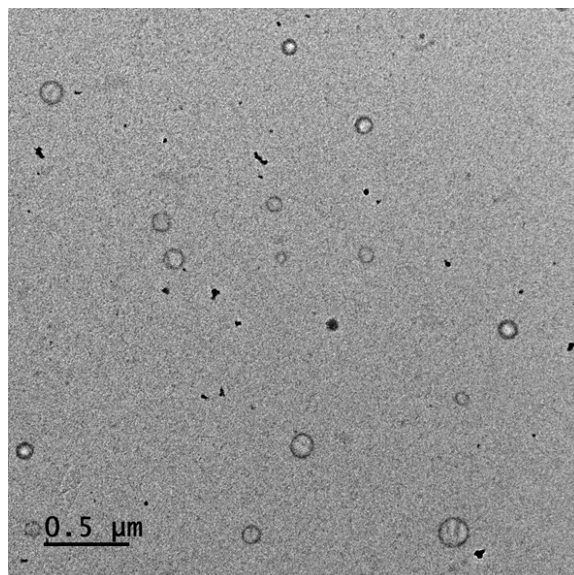


Figure 5.8. TEM images of DOX-loaded BSA-PVS-*b*-PNVCL bioconjugates.

### 5.3.6 *In vitro* cytotoxicity of BSA-PVS-*b*-PNVCL conjugate

To access the biocompatibility of BSA-PVS-*b*-PNVCL conjugate, we performed cytotoxicity evaluations using MTS assays on two cell lines: HeLa cells and HEK 293T cells. Figure 5.9. illustrates cell viability at various concentrations of the conjugates after 24, 48 and 72 h of incubation. Remarkably, no discernible cytotoxic effects were observed for the BSA-PVS-*b*-PNVCL bioconjugates, even at concentrations up to 500 μg/mL, on both tumor cells (HeLa) and normal cells (HEK 293T). The viability of both cell lines exceeded 90% after 72 h of incubation, underscoring the exceptional biocompatibility of BSA-PVS-*b*-PNVCL bioconjugates.

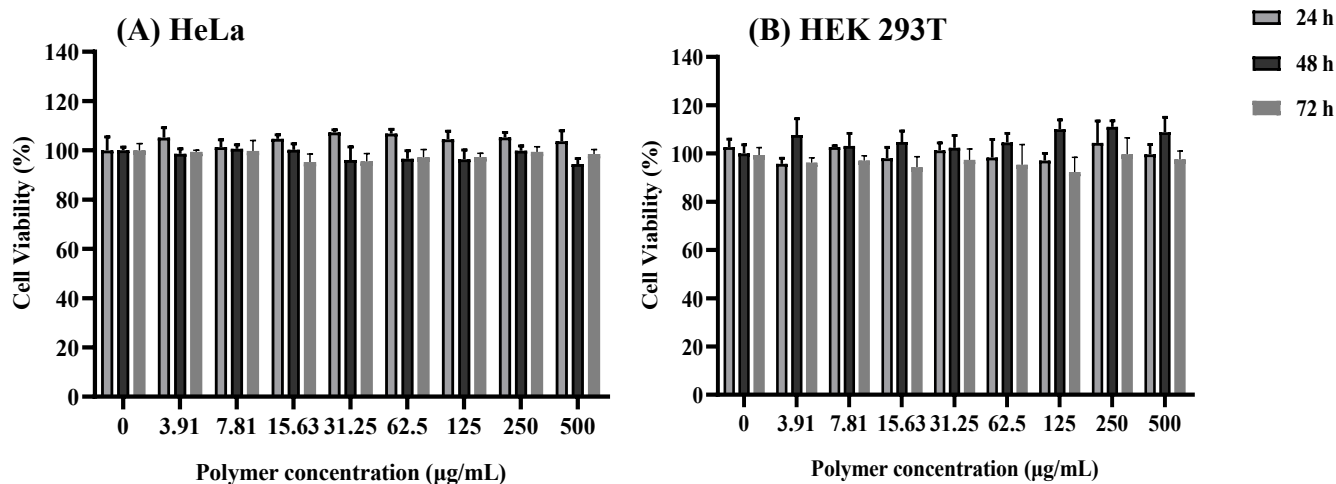


Figure 5.9. *In vitro* cytotoxicity of BSA-PVS-*b*-PNVCL conjugate with (A) HeLa and (B) HEK 293T cells after incubation for 24, 48, 72 h. Experiments were carried out three times independently and data are presented as mean  $\pm$  SD.

The *in vitro* anticancer efficacy of DOX-loaded nanoconjugates was assessed using HeLa cells, with free DOX employed for comparative analysis across a range of equivalent DOX concentrations spanning from 0.31 to 40  $\mu\text{g/mL}$ . As illustrated in Figure 5.10A, a 24 h exposure revealed a 50% survival of HeLa cells at a DOX concentration of 5  $\mu\text{g/mL}$  (equivalent to the conjugate concentration of 19.5  $\mu\text{g/mL}$ ) when treated with DOX-loaded conjugates. In contrast, the concentration required for 50% cell death with free DOX was estimated as 1  $\mu\text{g/mL}$ . Extending the incubation period to 48 h (Figure 5.10B), DOX-loaded BSA-PVS-*b*-PNVCL conjugates demonstrated an impressive cell killing performance, exceeding 80% at DOX concentrations of 2.5  $\mu\text{g/mL}$ . Interestingly, this exhibited a comparable cell-killing efficiency to free Dox when the DOX concentration reached above 5  $\mu\text{g/mL}$ , highlighting a clear dose-dependent and time-dependent cytotoxic effect. The slower cell-killing rate observed with loaded DOX, compared to free DOX, can be attributed to gradual release of DOX from the conjugates at 37  $^{\circ}\text{C}$ , coupled with distinct cellular uptake mechanisms for free drugs and polymersomes. Despite these findings, it is imperative to acknowledge the inherent challenges associated with free drugs in practical *in vivo*

applications, such as rapid clearance, low solubility, and high toxicity. The results indicated that BSA-PVS-*b*-PNVCL conjugates hold promise as a potential anti-cancer drug delivery system, offering both drug protection and enhanced therapeutic efficacy.

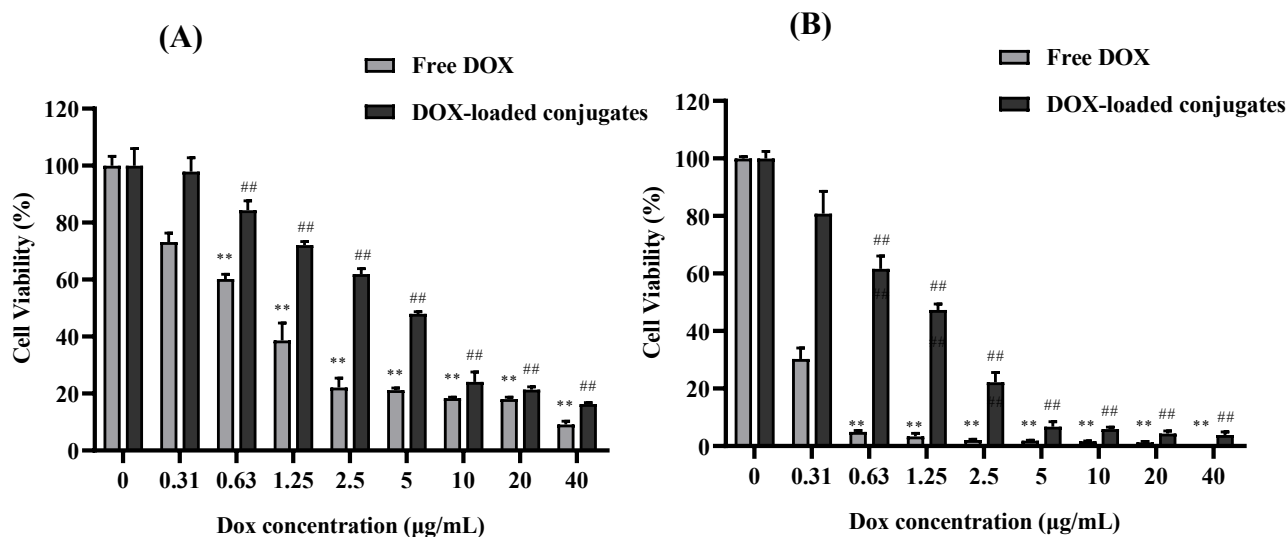


Figure 5.10. Cell viability of HeLa cells after incubation with DOX-loaded BSA-PVS-*b*-PNVCL conjugates for 24 h (A) or 48 h (B). Free DOX was used as a control. Data were presented as mean  $\pm$  SD. \*\* $p < 0.01$ , comparing with DOX concentration at 0.31  $\mu\text{g/mL}$  (Free Dox group); ## $p < 0.01$ , comparing with DOX concentration at 0.31  $\mu\text{g/mL}$  (DOX-loaded conjugates group).

### 5.3.7 *In vitro* uptake of bioconjugates in cellular models

The cellular uptake and intracellular localization of the DOX-loaded BSA-PVS-*b*-PNVCL conjugates were observed using a confocal laser scanning microscope (CLSM). The DAPI was employed to stain cell nuclei in blue, while the inherent red fluorescence of DOX facilitated its visualization. As shown in Figure 5.11, both the free DOX and DOX-loaded protein-polymer conjugates penetrated the cell membrane and were internalized by HeLa cells after a 4 h incubation period. Notably, free DOX localized in cell nuclei, whereas DOX-loaded conjugates were predominantly detected in the cytoplasm. With an extended incubation period from 24 to 48 h, the

encapsulated DOX within the conjugates underwent a transition in distribution. Initially dispersed throughout the entire cell, including both the cytoplasm and nucleus, DOX eventually exclusively localized in cell nuclei. It is important to highlight that due to its small molecular size, DOX can rapidly enter cells through passive diffusion. Once in the nucleus, DOX exerts its antitumor effects by disrupting DNA structures through intercalation, inducing DNA strand breakages, and causing cell damage.<sup>49</sup> In contrast to free drugs, studies have indicated that drug-incorporated nanoparticles enter cells through the endocytosis process.<sup>50,51</sup> Consequently, after internalization into cells, DOX may initially be released from the conjugates into the cytoplasm before being transported to the cell nuclei. These findings offer an explanation for the time-dependent cell-killing characteristics observed in the cell viability assay, providing further confirmation of the effective delivery and uptake of DOX.

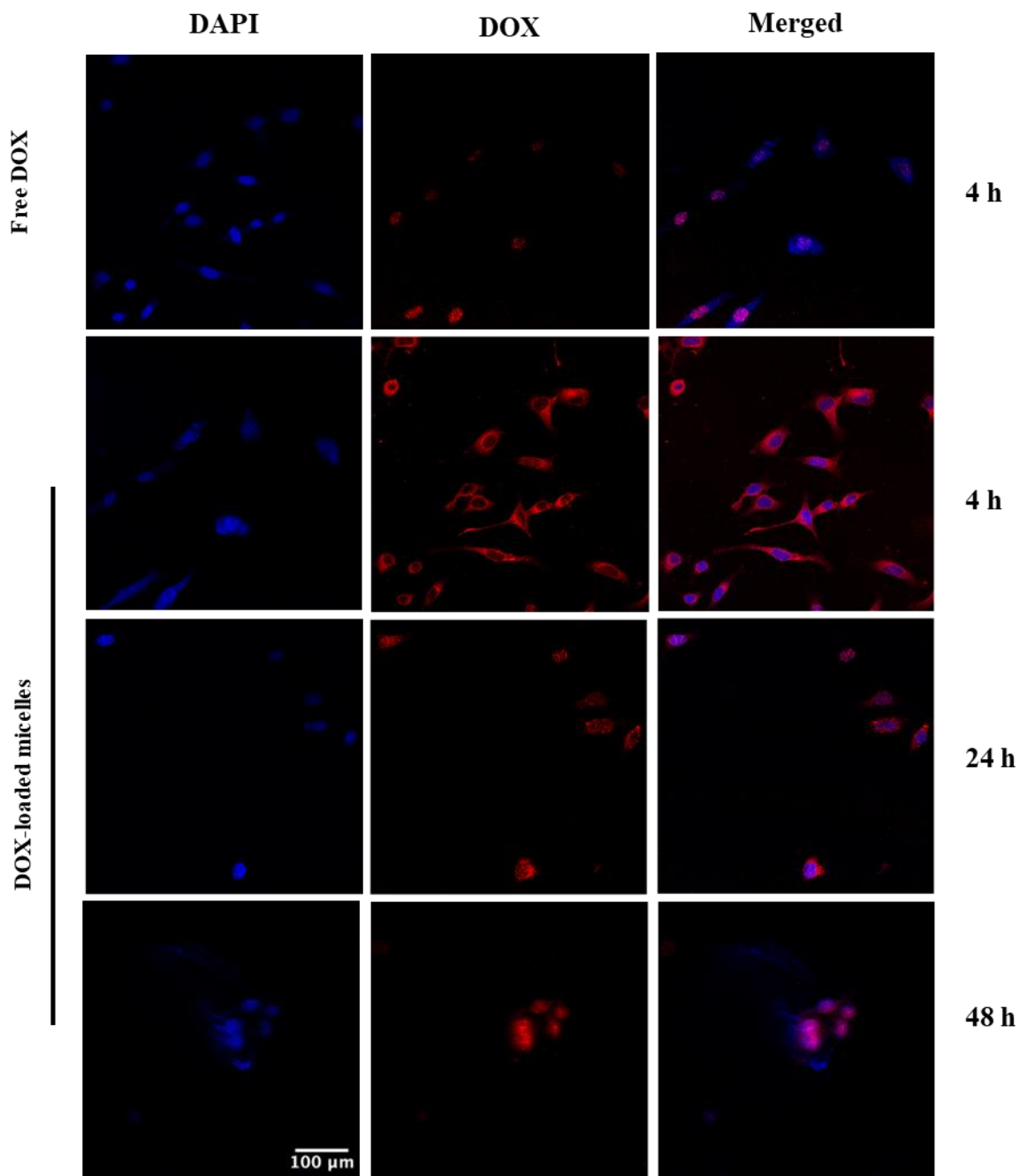


Figure 5.11. CLSM images of free DOX and DOX-loaded BSA-PVS-*b*-PNVCL conjugates in HeLa cells at different incubation times.

## 5.4 Conclusions

In this study, we have adopted a facile approach to fabricate temperature-responsive protein-polymer bioconjugates comprising lipid-based amphiphilic block copolymers and hydrophilic protein BSA. The building blocks were covalently linked through the exchange reactions involving the pyridyl disulfide groups on the RAFT agent and the free thiols on BSA. The resulting bioconjugates exhibited a well-defined structure, excellent biocompatibility, and low cytotoxicity. The loading of DOX into the nanoconjugates achieved a high capacity of 25.6%, displaying effective *in vitro* antitumor activity and efficient cellular uptake. These characteristics collectively underscore the promising potential of these bioconjugates as an anti-cancer drug nanocarriers. Furthermore, the tumor-targeting capability of the protein-based polymersome was significantly improved by incorporating thermoresponsive PNVCL and hydrophilic BSA into the hybrid building blocks. As the bioconjugates displayed phase transition behaviour at around 40 °C slightly higher than body temperature, triggering the rapid drug release exclusively at the tumor sites. We envision that these biocompatible BSA-PVS-*b*-PNVCL nanoconjugates could present a promising strategy for practical cancer treatment, contributing to the diversification of smart protein-polymer hybrid species, particularly as alternatives to PNIPAM-based systems.

## 5.5 References

- (1) Gaur, D.; Dubey, N. C.; Tripathi, B. P. Biocatalytic Self-Assembled Synthetic Vesicles and Coacervates: From Single Compartment to Artificial Cells. *Adv. Colloid Interface Sci.* **2022**, *299*, 102566.
- (2) Buddingh', B. C.; Van Hest, J. C. M. Artificial Cells: Synthetic Compartments with Life-like Functionality and Adaptivity. *Acc. Chem. Res.* **2017**, *50*, 769–777.
- (3) Li, J.; Jamieson, W. D.; Dimitriou, P.; Xu, W.; Rohde, P.; Martinac, B.; Baker, M.; Drinkwater, B. W.; Castell, O. K.; Barrow, D. A. Building Programmable Multicompartment Artificial Cells Incorporating Remotely Activated Protein Channels Using Microfluidics and Acoustic Levitation. *Nat. Commun.* **2022**, *13*, 4125.
- (4) Lu, A. X.; Oh, H.; Terrell, J. L.; Bentley, W. E.; Raghavan, S. R. A New Design for an Artificial Cell: Polymer Microcapsules with Addressable Inner Compartments That Can Harbor Biomolecules, Colloids or Microbial Species. *Chem. Sci.* **2017**, *8*, 6893–6903.
- (5) Guindani, C.; da Silva, L. C.; Cao, S.; Ivanov, T.; Landfester, K. Synthetic Cells: From Simple Bio-Inspired Modules to Sophisticated Integrated Systems. *Angew. Chem. Int. Ed.* **2022**, *61*, e202110855.
- (6) Wang, L.; Wen, P.; Liu, X.; Zhou, Y.; Li, M.; Huang, Y.; Geng, L.; Mann, S.; Huang, X. Single-Step Fabrication of Multi-Compartmentalized Biphasic Proteinosomes. *Chem. Commun.* **2017**, *53*, 8537–8540.
- (7) Charan, H.; Glebe, U.; Anand, D.; Kinzel, J.; Zhu, L.; Bocola, M.; Garakani, T. M.; Schwaneberg, U.; Böker, A. Nano-Thin Walled Micro-Compartments from Transmembrane Protein-Polymer Conjugates. *Soft Matter* **2017**, *13*, 2866–2875.

- (8) Zhao, H.; Ibarboure, E.; Ibrahimova, V.; Xiao, Y.; Garanger, E.; Lecommandoux, S. Spatiotemporal Dynamic Assembly/Disassembly of Organelle-Mimics Based on Intrinsically Disordered Protein-Polymer Conjugates. *Adv. Sci.* **2021**, *8*, 2102508.
- (9) Zhao, W.; Liu, F.; Chen, Y.; Bai, J.; Gao, W. Synthesis of Well-Defined Protein-Polymer Conjugates for Biomedicine. *Polymer* **2015**, *66*, A1–A10.
- (10) Liu, Z.; Dong, C.; Wang, X.; Wang, H.; Li, W.; Tan, J.; Chang, J. Self-Assembled Biodegradable Protein-Polymer Vesicle as a Tumor-Targeted Nanocarrier. *ACS Appl. Mater. Interfaces* **2014**, *6*, 2393–2400.
- (11) Gustafson, J. A.; Ghandehari, H. Silk-Elastinlike Protein Polymers for Matrix-Mediated Cancer Gene Therapy. *Adv. Drug Delivery Rev.* **2010**, *62*, 1509–1523.
- (12) Jiang, Y.; Lu, H.; Dag, A.; Hart-Smith, G.; Stenzel, M. H. Albumin-Polymer Conjugate Nanoparticles and Their Interactions with Prostate Cancer Cells in 2D and 3D Culture: Comparison between PMMA and PCL. *J Mater. Chem. B* **2016**, *4*, 2017–2027.
- (13) Palivan, C. G.; Fischer-Onaca, O.; Delcea, M.; Ite, F.; Meier, W. Protein-Polymer Nanoreactors for Medical Applications. *Chem. Soc. Rev.* **2012**, *41*, 2800–2823.
- (14) Li, X.; Cao, Y.; Luo, K.; Sun, Y.; Xiong, J.; Wang, L.; Liu, Z.; Li, J.; Ma, J.; Ge, J.; Xiao, H.; Zare, R. N. Highly Active Enzyme–Metal Nanohybrids Synthesized in Protein–Polymer Conjugates. *Nat. Catal.* **2019**, *2*, 718–725.
- (15) Huang, X.; Li, M.; Green, D. C.; Williams, D. S.; Patil, A. J.; Mann, S. Interfacial Assembly of Protein-Polymer Nano-Conjugates into Stimulus-Responsive Biomimetic Protocells. *Nat. Commun.* **2013**, *4*, 2239.
- (16) Paloni, J. M.; Dong, X. H.; Olsen, B. D. Protein-Polymer Block Copolymer Thin Films for Highly Sensitive Detection of Small Proteins in Biological Fluids. *ACS Sens.* **2019**, *4*, 2869–2878.

- (17) Gonen-Wadmany, M.; Oss-Ronen, L.; Seliktar, D. Protein-Polymer Conjugates for Forming Photopolymerizable Biomimetic Hydrogels for Tissue Engineering. *Biomaterials* **2007**, *28*, 3876–3886.
- (18) Alconcel, S. N. S.; Baas, A. S.; Maynard, H. D. FDA-Approved Poly(Ethylene Glycol)-Protein Conjugate Drugs. *Polym. Chem.* **2011**, *2*, 1442–1448.
- (19) Cobo, I.; Li, M.; Sumerlin, B. S.; Perrier, S. Smart Hybrid Materials by Conjugation of Responsive Polymers to Biomacromolecules. *Nat. Mater.* **2015**, *14*, 143–149.
- (20) Qi, Y.; Chilkoti, A. Protein-Polymer Conjugation-Moving beyond PEGylation. *Curr. Opin. Chem. Biol.* **2015**, *28*, 181–193.
- (21) De, P.; Li, M.; Gondi, S. R.; Sumerlin, B. S. Temperature-Regulated Activity of Responsive Polymer-Protein Conjugates Prepared by Grafting-from via RAFT Polymerization. *J. Am. Chem. Soc.* **2008**, *130*, 11288–11289.
- (22) Trzebicka, B.; Szweda, R.; Kosowski, D.; Szweda, D.; Otulakowski, Ł.; Haladjova, E.; Dworak, A. Thermoresponsive Polymer-Peptide/Protein Conjugates. *Prog. Polym. Sci.* **2017**, *68*, 35–76.
- (23) Li, M.; De Priyadarsi; Gondi, S. R.; Sumerlin, B. S. Responsive Polymer-Protein Bioconjugates Prepared by RAFT Polymerization and Copper-Catalyzed Azide-Alkyne Click Chemistry. *Macromol. Rapid Commun.* **2008**, *29*, 1172–1176.
- (24) Hoffman, J. M.; Stayton, P. S.; Hoffman, A. S.; Lai, J. J. Stimuli-Responsive Reagent System for Enabling Microfluidic Immunoassays with Biomarker Purification and Enrichment. *Bioconjugate Chem.* **2015**, *26*, 29–38.

- (25) Liu, F.; Cui, Y.; Wang, L.; Wang, H.; Yuan, Y.; Pan, J.; Chen, H.; Yuan, L. Temperature-Responsive Poly(N -Isopropylacrylamide) Modified Gold Nanoparticle-Protein Conjugates for Bioactivity Modulation. *ACS Appl. Mater. Interfaces* **2015**, *7*, 11547–11554.
- (26) Huang, X.; Patil, A. J.; Li, M.; Mann, S. Design and Construction of Higher-Order Structure and Function in Proteinosome-Based Protocells. *J. Am. Chem. Soc.* **2014**, *136*, 9225–9234.
- (27) Cortez-Lemus, N. A.; Licea-Claverie, A. Poly(N-Vinylcaprolactam), a Comprehensive Review on a Thermoresponsive Polymer Becoming Popular. *Prog. Polym. Sci.* **2016**, *53*, 1–51.
- (28) Liu, J.; Debuigne, A.; Detrembleur, C.; Jérôme, C. Poly(N-Vinylcaprolactam): A Thermoresponsive Macromolecule with Promising Future in Biomedical Field. *Adv. Healthc. Mater.* **2014**, *3*, 1941–1968.
- (29) Saha, B.; Ruidas, B.; Mete, S.; Mukhopadhyay, C. Das; Bauri, K.; De, P. AIE-Active Non-Conjugated Poly(N-Vinylcaprolactam) as a Fluorescent Thermometer for Intracellular Temperature Imaging. *Chem. Sci.* **2020**, *11*, 141–147.
- (30) Sajjad, H.; Tolman, W. B.; Reineke, T. M. Block Copolymer Pressure-Sensitive Adhesives Derived from Fatty Acids and Triacetic Acid Lactone. *ACS Appl. Polym. Mater.* **2020**, *2*, 2719–2728.
- (31) Maiti, B.; De, P. RAFT Polymerization of Fatty Acid Containing Monomers: Controlled Synthesis of Polymers from Renewable Resources. *RSC Adv.* **2013**, *3*, 24983–24990.
- (32) Yu, J.; Lu, C.; Wang, C.; Wang, J.; Fan, Y.; Chu, F. Sustainable Thermoplastic Elastomers Derived from Cellulose, Fatty Acid and Furfural via ATRP and Click Chemistry. *Carbohydr. Polym.* **2017**, *176*, 83–90.
- (33) Jiang, Y.; Stenzel, M. Drug Delivery Vehicles Based on Albumin–Polymer Conjugates. *Macromol. Biosci.* **2016**, *16*, 791–802.

- (34) Boyer, C.; Huang, X.; Whittaker, M. R.; Bulmus, V.; Davis, T. P. An Overview of Protein-Polymer Particles. *Soft Matter* **2011**, *7*, 1599–1614.
- (35) Boz, R. K.; Aydin, D.; Kocak, S.; Golba, B.; Sanyal, R.; Sanyal, A. Redox-Responsive Hydrogels for Tunable and “On-Demand” Release of Biomacromolecules. *Bioconjugate Chem.* **2022**, *33*, 839–847.
- (36) Bontempo, D.; Heredia, K. L.; Fish, B. A.; Maynard, H. D. Cysteine-Reactive Polymers Synthesized by Atom Transfer Radical Polymerization for Conjugation to Proteins. *J. Am. Chem. Soc.* **2004**, *126*, 15372–15373.
- (37) Heredia, K. L.; Bontempo, D.; Ly, T.; Byers, J. T.; Halstenberg, S.; Maynard, H. D. In Situ Preparation of Protein - “Smart” Polymer Conjugates with Retention of Bioactivity. *J. Am. Chem. Soc.* **2005**, *127*, 16955–16960.
- (38) Matyjaszewski, K.; Spanswick, J. Controlled/living Radical Polymerization. *Mater. Today* **2005**, *8*, 26-33
- (39) Bulmus, V. RAFT Polymerization Mediated Bioconjugation Strategies. *Polym. Chem.* **2011**, *2*, 1463–1472.
- (40) Stenzel, M. H. Bioconjugation Using Thiols: Old Chemistry Rediscovered to Connect Polymers with Nature’s Building Blocks. *ACS Macro Lett.* **2013**, *2*, 14–18.
- (41) Altinbasak, I.; Arslan, M.; Sanyal, R.; Sanyal, A. Pyridyl Disulfide-Based Thiol-Disulfide Exchange Reaction: Shaping the Design of Redox-Responsive Polymeric Materials. *Polym. Chem.* **2020**, *11*, 7603–7624.
- (42) Nakabayashi, K.; Mori, H. Recent Progress in Controlled Radical Polymerization of N-Vinyl Monomers. *Eur. Polym. J.* **2013**, *49*, 2808–2838.

- (43) Giordanengo, R.; Viel, S.; Hidalgo, M.; Allard-Breton, B.; Thévand, A.; Charles, L. Analytical Strategy for the Molecular Weight Determination of Random Copolymers of Poly(Methyl Methacrylate) and Poly(Methacrylic Acid). *J. Am. Soc. Mass Spectrom.* **2010**, *21*, 1075–1085.
- (44) Town, J. S.; Jones, G. R.; Haddleton, D. M. MALDI-LID-ToF/ToF Analysis of Statistical and Diblock Polyacrylate Copolymers. *Polym. Chem.* **2018**, *9*, 4631–4641.
- (45) Roy, D.; Brooks, W. L. A.; Sumerlin, B. S. New Directions in Thermoresponsive Polymers. *Chem. Soc. Rev.* **2013**, *42*, 7214–7243.
- (46) Dalgakiran, E.; Tatlipinar, H. The Role of Hydrophobic Hydration in the LCST Behaviour of PEOGMA300 by All-Atom Molecular Dynamics Simulations. *Phys. Chem. Chem. Phys.* **2018**, *20*, 15389–15399.
- (47) Cao, C.; Chen, F.; Garvey, C. J.; Stenzel, M. H. Drug-Directed Morphology Changes in Polymerization-Induced Self-Assembly (PISA) Influence the Biological Behavior of Nanoparticles. *ACS Appl. Mater. Interfaces* **2020**, *12*, 30221–30233.
- (48) Cao, C.; Zhao, J.; Chen, F.; Lu, M.; Khine, Y. Y.; Macmillan, A.; Garvey, C. J.; Stenzel, M. H. Drug-Induced Morphology Transition of Self-Assembled Glycopolymers: Insight into the Drug-Polymer Interaction. *Chem. Mater.* **2018**, *30*, 5227–5236.
- (49) Taymaz-Nikerel, H.; Karabekmez, M. E.; Eraslan, S.; Kırdar, B. Doxorubicin Induces an Extensive Transcriptional and Metabolic Rewiring in Yeast Cells. *Sci. Rep.* **2018**, *8*, 13672.
- (50) Zhou, P.; Wu, S.; Hegazy, M.; Li, H.; Xu, X.; Lu, H.; Huang, X. Engineered Borate Ester Conjugated Protein-Polymer Nanoconjugates for PH-Responsive Drug Delivery. *Mater. Sci. Eng. C* **2019**, *104*, 109914.
- (51) Liu, X.; Gao, W. In Situ Growth of Self-Assembled Protein-Polymer Nanovesicles for Enhanced Intracellular Protein Delivery. *ACS Appl. Mater. Interfaces* **2017**, *9*, 2023–2028.

## CHAPTER 6. General Discussion and Future Directions

### 6.1 General conclusions

Nanocarriers have been recognized as an effective platform for improving drug solubilization, altering drug biodistribution, and prolonging their half-life in the bloodstream. Achieving controlled drug release and targeting a drug to a specific site remain the overall goal and challenge of modern drug delivery technologies. Encouraged by the growing number of FDA-approval nanomedicines, drug delivery innovations that utilize diverse functional materials and combine different technologies are underway.

This PhD thesis research aimed to synthesize and investigate thermoresponsive renewable lipid-based block copolymers, along with their bioconjugates with proteins, as effective anti-cancer drug delivery vehicles. The thesis consists of one chapter as a literature review and three chapters with experimental data. The key findings and overall conclusions are summarized below.

In Chapter Three, a stearic acid-based methacrylate polymer (PSAMA) was synthesized by microwave-assisted RAFT polymerization at 60 °C for 20 min, and it was further used as a macro-CTA to block copolymerize with NIPAM to produce the thermoresponsive amphiphilic block copolymer PSAMA-*b*-PNIPAM within 25 min. It has been proven that microwave irradiation considerably shortened the reaction time. Besides, these amphiphilic block copolymers could spontaneously be assembled into spherical micelles with an average size range of ~30 nm via the combination of co-solvent evaporation and dialysis method. The balance between hydrophobic and hydrophilic segments had an impact on the morphology and critical micelle concentration (CMC) of PSAMA-*b*-PNIPAM micelles. When increasing the block lengths of the

stearic acid segment, the CMC values decreased due to the stronger hydrophobic interaction, whereas micelles showed some aggregation attributed to the long hydrophobic tail of fatty acid. To demonstrate the proof-of-concept, carbamazepine (CBZ) was selected as a hydrophobic model drug to evaluate the performance of these micelles as nanocarriers. The results indicated 31.6% of CBZ was effectively loaded into PSAMA-*b*-PNIPAM micelles. The drug release showed an obvious temperature-triggered response at body temperature, with a sustained and slow release lasting up to 84 h. These results demonstrated the feasibility of utilizing renewable fatty-acid based polymers as hydrophobic core-forming materials for drug encapsulation. By incorporating the thermoresponsive polymer PNIPAM, these smart nanocarriers presented controlled and sustained drug release characteristics.

To investigate the impact of fatty acid type on self-assembly and drug encapsulation, two distinct fatty acid-based polymers, poly(vinyl stearate) (PVS) and poly(vinyl laurate) (PVL), were prepared as the hydrophobic segments for the polymeric micelles, as discussed in Chapter Four. Given the significance of biocompatibility and biodegradability in practical biological applications, another thermoresponsive polymer, poly(N-vinylcaprolactam) (PNVCL), was employed as the hydrophilic shell. Upon varying fatty acid type and hydrophilic/hydrophobic block lengths, the self-assembly behaviour of the block copolymer (PVS/PVL-*b*-PNVCL) proved to be highly tunable in terms of their morphology and particle size. For PVS-*b*-NVCL, with an increase of hydrophilic block length, they tend to form spherical micelles with smaller particle sizes, more uniform particle size distribution and relatively higher CMC values, whereas both worm-like and spherical structures were found for PVS<sub>18</sub>-*b*-PNVCL<sub>35</sub> with an average size of 111 nm and low CMC values of 1.10 mg/L. Notably, micelles made from PVL-*b*-PNVCL exhibited exclusively

spherical morphology and larger particle sizes with a relatively broad size distribution. This could be attributed to the less efficient and looser packing or higher chain mobility of shorter fatty acid chains. PVS-*b*-NVCL polymeric micelles demonstrated high drug loading capacity of the anticancer drug DOX, good serum stability, controlled drug release, favorable biocompatibility, and efficient *in vitro* uptake. In this study, a safe, efficient and tunable lipid-based micellar system was developed for smart drug delivery and potential cancer treatments.

Chapter Five describes a protein-polymer bioconjugate containing bovine serum albumin (BSA) and lipid-based thermoresponsive amphiphilic block copolymer (PVS-*b*-PNVCL). The resultant bioconjugates exhibited a well-defined structure, satisfactory biocompatibility, and low cytotoxicity. In an aqueous environment, the amphiphilic BSA-polymer conjugates can self-assemble into the vesicular compartments with a particle size of approximately 200 nm. DOX was successfully encapsulated into the conjugates with a high loading capacity of 25.6%, demonstrating effective *in vitro* antitumor activity and efficient cellular uptake. These attributes all suggested their promising potential as an anti-cancer drug nanocarrier. Additionally, the lower critical solution temperature (LCST) of the bioconjugates was tuned to around 40 °C due to the incorporation of hydrophilic BSA, which enables their targeted drug delivery to tumors. These smart protein-polymer conjugates with multifunctionalities are far more promising than most traditional drug delivery vehicles, particularly in the field of anti-cancer therapy.

In conclusion, this work successfully prepared lipid-based amphiphilic block copolymers and protein-polymer bioconjugates, each exhibiting thermoresponsive properties. These materials can spontaneously self-assemble into high-order structures with different morphologies in aqueous medium. Notably, they offer potential as effective drug nanocarriers, featured with a high drug

loading capacity due to the large core volume facilitated by hydrophobic fatty acid-based polymers, controlled and sustained drug release characteristics attributed to the incorporation of thermoresponsive polymers, and enhanced tumor-targeting capability due to the attachment with proteins. This study suggests an opportunity to further explore the utilization of renewable materials as hydrophobic building blocks with good biocompatibility and biodegradability as replacements of synthetic materials to advance green and sustainable approaches within smart drug delivery systems and holds promising implications for future advancements in cancer therapies.

## **6.2 Recommendations for future research**

To better address current gaps in the drug delivery field, the recommended future investigations and studies from different perspectives are listed as follows:

(a) Considering that organic solvents and chemicals have been employed in this study, to improve the safety profile of drug formulations, organic trace analysis should be carried out to identify any residual amounts of organic compounds through NMR or chromatography techniques.

(b) The biodegradability of these polymeric micelles, and their protein-based bioconjugates should be investigated to meet the requirements of drug delivery applications.

(c) The pharmacokinetics and pharmacodynamics of drug nanocarriers developed in this study should be assessed with *in vivo* animal models, which is an essential step for the translation of laboratory products to preclinical applications.

(d) The thermoresponsive lipid-based block copolymers can be further functionalized with advanced materials for the integration of efficient and targeted drug delivery. For example, these block copolymers can be extended with a hydrophilic monomer (e.g. PEG) to produce the triblock copolymers with increased LCSTs above body temperature. Alternatively, they can conjugate with

ligands or molecules that can actively attach to the surface of certain target tissues for achieving active-targeting strategies.

(e) The bioactivity of BSA should be determined after conjugation with block copolymers.

(f) In addition to small-molecule drugs, new generations of therapeutics, such as proteins, peptides and antibodies, are playing an increasingly important role. The encapsulation capability of BSA-PVS-*b*-PNVCL for these macromolecules should be explored.

(g) Other biomedical applications of these amphiphilic block copolymer and protein conjugates can be further explored. This includes investigating their potential utilization as adjuvants, or in bioimaging and bioreactors, etc.

(h) Modern advanced techniques such as machine learning or computational modelling can be applied to improve the performance of the prepared nanocarriers for drug delivery by predicting the potential interactions between drugs and specific targets within the body, drug pharmacokinetic profile, optimal drug delivery system formulations *in vivo*.

## BIBLIOGRAPHY

- Abu Lila, A. S.; Kiwada, H.; Ishida, T. The Accelerated Blood Clearance (ABC) Phenomenon: Clinical Challenge and Approaches to Manage. *J. Controlled Release* **2013**, *172*, 38–47.
- Ahmad, Z.; Shah, A.; Siddiq, M.; Kraatz, H. B. Polymeric Micelles as Drug Delivery Vehicles. *RSC Adv.* **2014**, *4*, 17028–17038.
- Ahmadi, R.; Ullah, A. Microwave-Assisted Rapid Synthesis of a Polyether from a Plant Oil Derived Monomer and Its Optimization by Box-Behnken Design. *RSC Adv.* **2017**, *7*, 27946–27959.
- Alavi, M.; Karimi, N.; Safaei, M. Application of Various Types of Liposomes in Drug Delivery Systems. *Adv. Pharm. Bull.* **2017**, *7*, 3–9.
- Alconcel, S. N. S.; Baas, A. S.; Maynard, H. D. FDA-Approved Poly(Ethylene Glycol)-Protein Conjugate Drugs. *Polym. Chem.* **2011**, *2*, 1442–1448.
- Aliabadi, H. M.; Lavasanifar, A. Polymeric Micelles for Drug Delivery. *Expert Opin. Drug Delivery.* **2006**, *3*, 139–162.
- Alley, S. C.; Okeley, N. M.; Senter, P. D. Antibody-Drug Conjugates: Targeted Drug Delivery for Cancer. *Curr. Opin. Chem. Biol.* **2010**, *14*, 529–537.
- Altarawneh, I. S.; Srour, M.; Gomes, V. G. RAFT with Bulk and Solution Polymerization: An Approach to Mathematical Modelling and Validation. *Polym. – Plast. Technol. Eng.* **2007**, *46*, 1103–1115.
- Altinbasak, I.; Arslan, M.; Sanyal, R.; Sanyal, A. Pyridyl Disulfide-Based Thiol-Disulfide Exchange Reaction: Shaping the Design of Redox-Responsive Polymeric Materials. *Polym. Chem.* **2020**, *11*, 7603–7624.

- Amin, M.; Mansourian, M.; Koning, G. A.; Badiiee, A.; Jaafari, M. R.; Ten Hagen, T. L. M. Development of a Novel Cyclic RGD Peptide for Multiple Targeting Approaches of Liposomes to Tumor Region. *J. Controlled Release* **2015**, *220*, 308–315.
- Ansari, M. J.; Rajendran, R. R.; Mohanto, S.; Agarwal, U.; Panda, K.; Dhotre, K.; Manne, R.; Deepak, A.; Zafar, A.; Yasir, M.; Pramanik, S. Poly(N-Isopropylacrylamide)-Based Hydrogels for Biomedical Applications: A Review of the State-of-the-Art. *Gels* **2022**, *8*, 454.
- Arshad, M.; Pradhan, R. A.; Ullah, A. Synthesis of Lipid-Based Amphiphilic Block Copolymer and Its Evaluation as Nano Drug Carrier. *Mater. Sci. Eng. C* **2017**, *76*, 217–223.
- Barth, R. F.; Adams, D. M.; Soloway, A. H.; Alam, F.; Darbyl, M. V. Starburst Dendrimer-Monoclonal Antibody Immunoconjugates: Evaluation as a Potential Delivery System for Neutron Capture Therapy. *Bioconjugate Chem.* **1994**, *5*, 58–68.
- Beija, M.; Marty, J. D.; Destarac, M. Thermoresponsive Poly(N-Vinyl Caprolactam)-Coated Gold Nanoparticles: Sharp Reversible Response and Easy Tunability. *Chem. Commun.* **2011**, *47*, 2826–2828.
- Bej, R.; Achazi, K.; Haag, R.; Ghosh, S. Polymersome Formation by Amphiphilic Polyglycerol-*b*-Polydisulfide-*b*-Polyglycerol and Glutathione-Triggered Intracellular Drug Delivery. *Biomacromolecules* **2020**, *21*, 3353–3363.
- Biswas, S.; Kumari, P.; Lakhani, P. M.; Ghosh, B. Recent Advances in Polymeric Micelles for Anti-Cancer Drug Delivery. *Eur. J. Pharm. Sci.* **2016**, *83*, 184–202.
- Blanazs, A.; Armes, S. P.; Ryan, A. J. Self-Assembled Block Copolymer Aggregates: From Micelles to Vesicles and Their Biological Applications. *Macromol. Rapid Commun.* **2009**, *30*, 267–277.

- Blanazs, A.; Madsen, J.; Battaglia, G.; Ryan, A. J.; Armes, S. P. Mechanistic Insights for Block Copolymer Morphologies: How Do Worms Form Vesicles? *J. Am. Chem. Soc.* **2011**, *133*, 16581–16587.
- Boere, I.; Vergote, I.; Hanssen, R.; Jalving, M.; Gennigens, C.; Ottevanger, P.; Van De Wouw, Y. J.; Rijcken, C. J. F.; Mathijssen, R. H. J.; Ledermann, J. CINOVA: A Phase II Study of CPC634 (Nanoparticulate Docetaxel) in Patients with Platinum Resistant Recurrent Ovarian Cancer. *Int. J. Gynecol. Cancer* **2023**, *33*, 1247–1252.
- Bonetti, R.; Parker, W. O. Insights into Polymerization of Vegetable Oil: Oligomerization of Oleic Acid. *JAACS*. **2019**, *96*, 1181–1184.
- Bontempo, D.; Heredia, K. L.; Fish, B. A.; Maynard, H. D. Cysteine-Reactive Polymers Synthesized by Atom Transfer Radical Polymerization for Conjugation to Proteins. *J. Am. Chem. Soc.* **2004**, *126*, 15372–15373.
- Bontempo, D.; Maynard, H. D. Streptavidin as a Macroinitiator for Polymerization: In Situ Protein-Polymer Conjugate Formation Scheme 1. Streptavidin-Initiated Polymerization. *J. Am. Chem. Soc.* **2005**, *127*, 6508–6509.
- Bordat, A.; Boissenot, T.; Nicolas, J.; Tsapis, N. Thermoresponsive Polymer Nanocarriers for Biomedical Applications. *Adv. Drug Deliv Rev.* **2019**, *138*, 167–192.
- Boyer, C.; Huang, X.; Whittaker, M. R.; Bulmus, V.; Davis, T. P. An Overview of Protein-Polymer Particles. *Soft Matter* **2011**, *7*, 1599–1614.
- Boz, R. K.; Aydin, D.; Kocak, S.; Golba, B.; Sanyal, R.; Sanyal, A. Redox-Responsive Hydrogels for Tunable and “On-Demand” Release of Biomacromolecules. *Bioconjugate Chem.* **2022**, *33*, 839–847.

- Brannon-Peppas, L. Recent Advances on the Use of Biodegradable Microparticles and Nanoparticles in Controlled Drug Delivery. *Int. J. Pharm.* **1995**, *116*, 1–9.
- Brown, S. L.; Rayner, C. M.; Graham, S.; Cooper, A.; Rannard, S.; Perrier, S. Ultra-Fast Microwave Enhanced Reversible Addition-Fragmentation Chain Transfer (RAFT) Polymerization: Monomers to Polymers in Minutes. *Chem. Commun.* **2007**, *21*, 2145–2147.
- Broyer, R. M.; Grover, G. N.; Maynard, H. D. Emerging Synthetic Approaches for Protein-Polymer Conjugations. *Chem. Commun.* **2011**, *47*, 2212–2226.
- Buddingh', B. C.; Van Hest, J. C. M. Artificial Cells: Synthetic Compartments with Life-like Functionality and Adaptivity. *Acc. Chem. Res.* **2017**, *50*, 769–777.
- Bulmus, V. RAFT Polymerization Mediated Bioconjugation Strategies. *Polym. Chem.* **2011**, *2*, 1463–1472.
- Cabral, H.; Miyata, K.; Osada, K.; Kataoka, K. Block Copolymer Micelles in Nanomedicine Applications. *Chem. Rev.* **2018**, *118*, 6844–6892.
- Canning, S. L.; Smith, G. N.; Armes, S. P. A Critical Appraisal of RAFT-Mediated Polymerization-Induced Self-Assembly. *Macromolecules* **2016**, *49*, 1985–2001.
- Cao, C.; Chen, F.; Garvey, C. J.; Stenzel, M. H. Drug-Directed Morphology Changes in Polymerization-Induced Self-Assembly (PISA) Influence the Biological Behavior of Nanoparticles. *ACS Appl. Mater. Interfaces* **2020**, *12*, 30221–30233.
- Cao, C.; Zhao, J.; Chen, F.; Lu, M.; Khine, Y. Y.; Macmillan, A.; Garvey, C. J.; Stenzel, M. H. Drug-Induced Morphology Transition of Self-Assembled Glycopolymers: Insight into the Drug-Polymer Interaction. *Chem. Mater.* **2018**, *30*, 5227–5236.
- Cao, Q.; He, N.; Wang, Y.; Lu, Z. Self-Assembled Nanostructures from Amphiphilic Globular Protein–Polymer Hybrids. *Polym. Bull.* **2018**, *75*, 2627–2639.

- Chaduc, I.; Zhang, W.; Rieger, J.; Lansalot, M.; D'Agosto, F.; Charleux, B. Amphiphilic Block Copolymers from a Direct and One-Pot RAFT Synthesis in Water. *Macromol. Rapid Commun.* **2011**, *32*, 1270–1276.
- Chang, C. Y.; Wang, M. C.; Miyagawa, T.; Chen, Z. Y.; Lin, F. H.; Chen, K. H.; Liu, G. S.; Tseng, C. L. Preparation of Arginine–Glycine–Aspartic Acid-Modified Biopolymeric Nanoparticles Containing Epigallocatechin-3-Gallate for Targeting Vascular Endothelial Cells to Inhibit Corneal Neovascularization. *Int. J. Nanomedicine* **2017**, *12*, 279–294.
- Chang, C.; Wei, H.; Quan, C. Y.; Li, Y. Y.; Liu, J.; Wang, Z. C.; Cheng, S. X.; Zhang, X. Z.; Zhuo, R. X. Fabrication of Thermosensitive PCL-PNIPAAm-PCL Triblock Copolymeric Micelles for Drug Delivery. *J. Polym. Sci., Part A: Polym. Chem.* **2008**, *46*, 3048–3057.
- Chang, D.; Lam, C. N.; Tang, S.; Olsen, B. D. Effect of Polymer Chemistry on Globular Protein-Polymer Block Copolymer Self-Assembly. *Polym. Chem.* **2014**, *5*, 4884–4895.
- Chang, L.; Liu, J.; Zhang, J.; Deng, L.; Dong, A. PH-Sensitive Nanoparticles Prepared from Amphiphilic and Biodegradable Methoxy Poly(Ethylene Glycol)-Block-(Polycaprolactone-Graft-Poly(Methacrylic Acid)) for Oral Drug Delivery. *Polym. Chem.* **2013**, *4*, 1430–1438.
- Charan, H.; Glebe, U.; Anand, D.; Kinzel, J.; Zhu, L.; Bocola, M.; Garakani, T. M.; Schwaneberg, U.; Böker, A. Nano-Thin Walled Micro-Compartments from Transmembrane Protein-Polymer Conjugates. *Soft Matter* **2017**, *13*, 2866–2875.
- Chen, Y. C.; Liao, L. C.; Lu, P. L.; Lo, C. L.; Tsai, H. C.; Huang, C. Y.; Wei, K. C.; Yen, T. C.; Hsiue, G. H. The Accumulation of Dual PH and Temperature Responsive Micelles in Tumors. *Biomaterials* **2012**, *33*, 4576–4588.

- Choucair, A.; Eisenberg, A. Control of Amphiphilic Block Copolymer Morphologies Using Solution Conditions. *Eur. Phys. J. E* **2003**, *10*, 37–44.
- Cobo, I.; Li, M.; Sumerlin, B. S.; Perrier, S. Smart Hybrid Materials by Conjugation of Responsive Polymers to Biomacromolecules. *Nat. Mater.* **2015**, *14*, 143–149.
- Cortez-Lemus, N. A.; Licea-Claverie, A. Poly(N-Vinylcaprolactam), a Comprehensive Review on a Thermoresponsive Polymer Becoming Popular. *Prog. Polym. Sci.* **2016**, *53*, 1–51.
- Cortez-Lemus, N. A.; Licea-Claverie, A. Poly(N-Vinylcaprolactam), a Comprehensive Review on a Thermoresponsive Polymer Becoming Popular. *Prog. Polym. Sci.* **2016**, *53*, 1–51.
- Craig, A. F.; Clark, E. E.; Sahu, I. D.; Zhang, R.; Frantz, N. D.; Al-Abdul-Wahid, M. S.; Dabney-Smith, C.; Konkolewicz, D.; Lorigan, G. A. Tuning the Size of Styrene-Maleic Acid Copolymer-Lipid Nanoparticles (SMALPs) Using RAFT Polymerization for Biophysical Studies. *Biochim. Biophys. Acta, Biomembr.* **2016**, *1858*, 2931–2939.
- Cui, W.; Li, J.; Decher, G. Self-Assembled Smart Nanocarriers for Targeted Drug Delivery. *Adv. Mater.* **2016**, *28*, 1302–1311.
- D'souza, A. A.; Shegokar, R. Polyethylene Glycol (PEG): A Versatile Polymer for Pharmaceutical Applications. *Expert Opin. Drug Delivery* **2016**, *13*, 1257–1275.
- Dai, M.; Goudounet, G.; Zhao, H.; Garbay, B.; Garanger, E.; Pecastaings, G.; Schultze, X.; Lecommandoux, S. Thermosensitive Hybrid Elastin-like Polypeptide-Based ABC Triblock Hydrogel. *Macromolecules* **2021**, *54*, 327–340.
- Dalgakiran, E.; Tatlipinar, H. The Role of Hydrophobic Hydration in the LCST Behaviour of POEGMA300 by All-Atom Molecular Dynamics Simulations. *Phys. Chem. Chem. Phys.* **2018**, *20*, 15389–15399.

- Dallinger, D.; Kappe, C. O. Microwave-Assisted Synthesis in Water as Solvent. *Chem. Rev.* **2007**, *107*, 2563–2591.
- de la Hoz, A.; Díaz-Ortiz, À.; Moreno, A. Microwaves in Organic Synthesis. Thermal and Non-Thermal Microwave Effects. *Chem. Soc. Rev.* **2005**, *34*, 164–178.
- De, P.; Li, M.; Gondi, S. R.; Sumerlin, B. S. Temperature-Regulated Activity of Responsive Polymer-Protein Conjugates Prepared by Grafting-from via RAFT Polymerization. *J. Am. Chem. Soc.* **2008**, *130*, 11288–11289.
- Deng, C.; Jiang, Y.; Cheng, R.; Meng, F.; Zhong, Z. Biodegradable Polymeric Micelles for Targeted and Controlled Anticancer Drug Delivery: Promises, Progress and Prospects. *Nano Today* **2012**, *7*, 467–480.
- Destarac, M. Controlled Radical Polymerization: Industrial Stakes, Obstacles and Achievements. *Macromol. React. Eng.* **2010**, *4*, 165–179.
- Din, F. U.; Aman, W.; Ullah, I.; Qureshi, O. S.; Mustapha, O.; Shafique, S.; Zeb, A. Effective Use of Nanocarriers as Drug Delivery Systems for the Treatment of Selected Tumors. *Int. J. Nanomed.* **2017**, *12*, 7291–7309.
- Doberenz, F.; Zeng, K.; Willems, C.; Zhang, K.; Groth, T. Thermoresponsive Polymers and Their Biomedical Application in Tissue Engineering-A Review. *J. Mater. Chem. B* **2020**, *8*, 607–628.
- Du, B.; Jia, S.; Wang, Q.; Ding, X.; Liu, Y.; Yao, H.; Zhou, J. A Self-Targeting, Dual ROS/PH-Responsive Apoferritin Nanocage for Spatiotemporally Controlled Drug Delivery to Breast Cancer. *Biomacromolecules* **2018**, *19*, 1026–1036.

- Du, B.; Mei, A.; Yang, Y.; Zhang, Q.; Wang, Q.; Xu, J.; Fan, Z. Synthesis and Micelle Behavior of (PNIPAm-PtBA-PNIPAm)<sub>m</sub> Amphiphilic Multiblock Copolymer. *Polymer* **2010**, *51*, 3493–3502.
- Dutertre, F.; Pennarun, P. Y.; Colombani, O.; Nicol, E. Straightforward Synthesis of Poly(Lauryl Acrylate)-b-Poly(Stearyl Acrylate) Diblock Copolymers by ATRP. *Eur. Polym. J.* **2011**, *47*, 343–351.
- Easterling, C. P.; Xia, Y.; Zhao, J.; Fanucci, G. E.; Sumerlin, B. S. Block Copolymer Sequence Inversion through Photoiniferter Polymerization. *ACS Macro Lett.* **2019**, *8*, 1461–1466.
- Ellis, C. E.; Garcia-Hernandez, J. D.; Manners, I. Scalable and Uniform Length-Tunable Biodegradable Block Copolymer Nanofibers with a Polycarbonate Core via Living Polymerization-Induced Crystallization-Driven Self-Assembly. *J. Am. Chem. Soc.* **2022**, *144*, 20525–20538.
- Emran, T. Bin; Shahriar, A.; Mahmud, A. R.; Rahman, T.; Abir, M. H.; Siddiquee, M. F. R.; Ahmed, H.; Rahman, N.; Nainu, F.; Wahyudin, E.; Mitra, S.; Dhama, K.; Habiballah, M. M.; Haque, S.; Islam, A.; Hassan, M. M. Multidrug Resistance in Cancer: Understanding Molecular Mechanisms, Immunoprevention and Therapeutic Approaches. *Front. Oncol.* **2022**, *12*, 891652.
- Englert, C.; Brendel, J. C.; Majdanski, T. C.; Yildirim, T.; Schubert, S.; Gottschaldt, M.; Windhab, N.; Schubert, U. S. Pharmapolymers in the 21st Century: Synthetic Polymers in Drug Delivery Applications. *Prog. Polym. Sci.* **2018**, *87*, 107–164.
- Etchenausia, L.; Villar-Alvarez, E.; Forcada, J.; Save, M.; Taboada, P. Evaluation of Cationic Core-Shell Thermoresponsive Poly(N-Vinylcaprolactam)-Based Microgels as Potential Drug Delivery Nanocarriers. *Mater. Sci. Eng. C* **2019**, *104*, 109871.

- Ezike, T. C.; Okpala, U. S.; Onoja, U. L.; Nwike, C. P.; Ezeako, E. C.; Okpara, O. J.; Okoroafor, C. C.; Eze, S. C.; Kalu, O. L.; Odoh, E. C.; Nwadike, U. G.; Ogbodo, J. O.; Umeh, B. U.; Ossai, E. C.; Nwanguma, B. C. Advances in Drug Delivery Systems, Challenges and Future Directions. *Heliyon* **2023**, *9*, e17488.
- Fattahi, N.; Shahbazi, M. A.; Maleki, A.; Hamidi, M.; Ramazani, A.; Santos, H. A. Emerging Insights on Drug Delivery by Fatty Acid Mediated Synthesis of Lipophilic Prodrugs as Novel Nanomedicines. *J. Controlled Release* **2020**, *326*, 556–598.
- Fisicaro, E.; Compari, C.; Duce, E.; Biemmi, M.; Peroni, M.; Braibanti, A. Thermodynamics of Micelle Formation in Water, Hydrophobic Processes and Surfactant Self-Assemblies. *Phys. Chem. Chem. Phys.* **2008**, *10*, 3903–3914.
- Frisch, H.; Tuten, B. T.; Barner-Kowollik, C. Macromolecular Superstructures: A Future Beyond Single Chain Nanoparticles. *Isr. J. Chem.* **2020**, *60*, 86–99.
- Fujiwara, Y.; Mukai, H.; Saeki, T.; Ro, J.; Lin, Y. C.; Nagai, S. E.; Lee, K. S.; Watanabe, J.; Ohtani, S.; Kim, S. B.; Kuroi, K.; Tsugawa, K.; Tokuda, Y.; Iwata, H.; Park, Y. H.; Yang, Y.; Nambu, Y. A Multi-National, Randomised, Open-Label, Parallel, Phase III Non-Inferiority Study Comparing NK105 and Paclitaxel in Metastatic or Recurrent Breast Cancer Patients. *Br. J. Cancer* **2019**, *120*, 475–480.
- Gaglieri, C.; Alarcon, R. T.; de Moura, A.; Bannach, G. Vegetable Oils as Monomeric and Polymeric Materials: A Graphical Review. *Curr. Res. Green Sustainable Chem.* **2022**, *5*, 100343.
- Gao, C.; Wu, J.; Zhou, H.; Qu, Y.; Li, B.; Zhang, W. Self-Assembled Blends of AB/BAB Block Copolymers Prepared through Dispersion RAFT Polymerization. *Macromolecules* **2016**, *49*, 4490–4500.

- Gao, G. H.; Park, M. J.; Li, Y.; Im, G. H.; Kim, J. H.; Kim, H. N.; Lee, J. W.; Jeon, P.; Bang, O. Y.; Lee, J. H.; Lee, D. S. The Use of PH-Sensitive Positively Charged Polymeric Micelles for Protein Delivery. *Biomaterials* **2012**, *33*, 9157–9164.
- Gao, H.; Matyjaszewski, K. Synthesis of Functional Polymers with Controlled Architecture by CRP of Monomers in the Presence of Cross-Linkers: From Stars to Gels. *Prog. Polym. Sci.* **2009**, *34*, 317–350.
- Gaur, D.; Dubey, N. C.; Tripathi, B. P. Biocatalytic Self-Assembled Synthetic Vesicles and Coacervates: From Single Compartment to Artificial Cells. *Adv. Colloid Interface Sci.* **2022**, *299*, 102566.
- Ge, J.; Lei, J.; Zare, R. N. Bovine Serum Albumin - Poly(Methyl Methacrylate) Nanoparticles: An Example of Frustrated Phase Separation. *Nano Lett.* **2011**, *11*, 2551–2554.
- Ge, J.; Neofytou, E.; Lei, J.; Beygui, R. E.; Zare, R. N. Protein-Polymer Hybrid Nanoparticles for Drug Delivery. *Small* **2012**, *8*, 3573–3578.
- Ghadiri, M. R. Self-Assembled Nanoscale Tubular Ensembles. *Adv. Mater.* **1995**, *7*, 675–677.
- Ghezzi, M.; Pescina, S.; Padula, C.; Santi, P.; Del Favero, E.; Cantù, L.; Nicoli, S. Polymeric Micelles in Drug Delivery: An Insight of the Techniques for Their Characterization and Assessment in Biorelevant Conditions. *J. Controlled Release* **2021**, *332*, 312–336.
- Giguere, R. J.; Bray, T. L.; Duncan, S. M.; Majetich, G. Application of Commercial Microwave Ovens to Organic Synthesis. *Tetrahedron Lett.* **1986**, *27*, 4945–4948.
- Gill, K. K.; Kaddoumi, A.; Nazzal, S. PEG-Lipid Micelles as Drug Carriers: Physiochemical Attributes, Formulation Principles and Biological Implication. *J. Drug Target.* **2015**, *23*, 222–231.

- Giordanengo, R.; Viel, S.; Hidalgo, M.; Allard-Breton, B.; Thévand, A.; Charles, L. Analytical Strategy for the Molecular Weight Determination of Random Copolymers of Poly(Methyl Methacrylate) and Poly(Methacrylic Acid). *J. Am. Soc. Mass Spectrom.* **2010**, *21*, 1075–1085.
- Góis, J. R.; Popov, A. V.; Guliashvili, T.; Serra, A. C.; Coelho, J. F. J. Synthesis of Functionalized Poly(Vinyl Acetate) Mediated by Alkyne-Terminated RAFT Agents. *RSC Adv.* **2015**, *5*, 91225–91234.
- Góis, J. R.; Serra, A. C.; Coelho, J. F. J. Synthesis and Characterization of New Temperature-Responsive Nanocarriers Based on POEOMA-b-PNVCL Prepared Using a Combination of ATRP, RAFT and CuAAC. *Eur. Polym. J.* **2016**, *81*, 224–238.
- Gonen-Wadmany, M.; Oss-Ronen, L.; Seliktar, D. Protein-Polymer Conjugates for Forming Photopolymerizable Biomimetic Hydrogels for Tissue Engineering. *Biomaterials* **2007**, *28*, 3876–3886.
- Gong, J.; Chen, M.; Zheng, Y.; Wang, S.; Wang, Y. Polymeric Micelles Drug Delivery System in Oncology. *J. Controlled Release.* **2012**, *159*, 312–323.
- González-Toro, D. C.; Thayumanavan, S. Advances in Polymer and Polymeric Nanostructures for Protein Conjugation. *Eur. Polym. J.* **2013**, *49*, 2906–2918.
- Graham, N. B.; Mcneiu, M. E. Hydrogels for Controlled Drug Delivery. *Biomaterials* **1984**, *5*, 27–36.
- Gregoriadis, G.; Ryman, B. E. Liposomes as Carriers of Enzymes or Drugs: A New Approach to the Treatment of Storage Diseases. *Biochem. J.* **1971**, *124*, 58.

- Groison, E.; Brusseau, S.; D'Agosto, F.; Magnet, S.; Inoubli, R.; Couvreur, L.; Charleux, B. Well-Defined Amphiphilic Block Copolymer Nanoobjects via Nitroxide-Mediated Emulsion Polymerization. *ACS Macro Lett.* **2012**, *1*, 47–51.
- Grover, G. N.; Maynard, H. D. Protein-Polymer Conjugates: Synthetic Approaches by Controlled Radical Polymerizations and Interesting Applications. *Curr. Opin. Chem. Biol.* **2010**, *14*, 818–827.
- Grund, S.; Bauer, M.; Fischer, D. Polymers in Drug Delivery-State of the Art and Future Trends. *Adv. Eng. Mater.* **2011**, *13*, 61–87.
- Guindani, C.; da Silva, L. C.; Cao, S.; Ivanov, T.; Landfester, K. Synthetic Cells: From Simple Bio-Inspired Modules to Sophisticated Integrated Systems. *Angew. Chem. Int. Ed.* **2022**, *61*, e202110855.
- Guindani, C.; Feuser, P. E.; Cordeiro, A. P.; de Meneses, A. C.; Possato, J. C.; da Silva Abel, J.; Machado-de-Ávila, R. A.; Sayer, C.; de Araújo, P. H. H. Bovine Serum Albumin Conjugation on Poly(Methyl Methacrylate) Nanoparticles for Targeted Drug Delivery Applications. *J. Drug Deliv. Sci. Technol.* **2020**, *56*, 101490.
- Gullotti, E.; Yeo, Y. Extracellularly Activated Nanocarriers: A New Paradigm of Tumor Targeted Drug Delivery. *Mol. Pharmaceutics.* **2009**, *6*, 1041–1051.
- Gupta, V.; Bhavanasi, S.; Quadir, M.; Singh, K.; Ghosh, G.; Vasamreddy, K.; Ghosh, A.; Siahhan, T. J.; Banerjee, S.; Banerjee, S. K. Protein PEGylation for Cancer Therapy: Bench to Bedside. *J. Cell Commun. Signaling* **2019**, *13*, 319–330.
- Gustafson, J. A.; Ghandehari, H. Silk-Elastinlike Protein Polymers for Matrix-Mediated Cancer Gene Therapy. *Adv. Drug Delivery Rev.* **2010**, *62*, 1509–1523.

- György, C.; Hunter, S. J.; Girou, C.; Derry, M. J.; Armes, S. P. Synthesis of Poly(Stearyl Methacrylate)-Poly(2-Hydroxypropyl Methacrylate) Diblock Copolymer Nanoparticles: Via RAFT Dispersion Polymerization of 2-Hydroxypropyl Methacrylate in Mineral Oil. *Polym. Chem.* **2020**, *11*, 4579–4590.
- Hamaguchi, T.; Tsuji, A.; Yamaguchi, K.; Takeda, K.; Uetake, H.; Esaki, T.; Amagai, K.; Sakai, D.; Baba, H.; Kimura, M.; Matsumura, Y.; Tsukamoto, T. A Phase II Study of NK012, a Polymeric Micelle Formulation of SN-38, in Unresectable, Metastatic or Recurrent Colorectal Cancer Patients. *Cancer Chemother. Pharmacol.* **2018**, *82*, 1021–1029.
- Heredia, K. L.; Bontempo, D.; Ly, T.; Byers, J. T.; Halstenberg, S.; Maynard, H. D. In Situ Preparation of Protein - “Smart” Polymer Conjugates with Retention of Bioactivity. *J. Am. Chem. Soc.* **2005**, *127*, 16955–16960.
- Heredia, K. L.; Maynard, H. D. Synthesis of Protein-Polymer Conjugates. *Org. Biomol. Chem.* **2007**, *5*, 45–53.
- Hervault, A.; Dunn, A. E.; Lim, M.; Boyer, C.; Mott, D.; Maenosono, S.; Thanh, N. T. K. Doxorubicin Loaded Dual PH- and Thermo-Responsive Magnetic Nanocarrier for Combined Magnetic Hyperthermia and Targeted Controlled Drug Delivery Applications. *Nanoscale* **2016**, *8*, 12152–12161.
- Hill, M. R.; Carmean, R. N.; Sumerlin, B. S. Expanding the Scope of RAFT Polymerization: Recent Advances and New Horizons. *Macromolecules* **2015**, *48*, 5459–5469.
- Hoffman, J. M.; Stayton, P. S.; Hoffman, A. S.; Lai, J. J. Stimuli-Responsive Reagent System for Enabling Microfluidic Immunoassays with Biomarker Purification and Enrichment. *Bioconjugate Chem.* **2015**, *26*, 29–38.

- Holder, S. J.; Sommerdijk, N. A. J. M. New Micellar Morphologies from Amphiphilic Block Copolymers: Disks, Toroids and Bicontinuous Micelles. *Polym. Chem.* **2011**, *2*, 1018–1028.
- Hoogenboom, R.; Schubert, U. S. Microwave-Assisted Polymer Synthesis: Recent Developments in a Rapidly Expanding Field of Research. *Macromol. Rapid Commun.* **2007**, *28*, 368–386.
- Hrkach, J.; Hoff, D. Von; Ali, M. M.; Andrianova, E.; Auer, J.; Campbell, T.; De Witt, D.; Figa, M.; Figueiredo, M.; Horhota, A.; Low, S.; McDonnell, K.; Peeke, E.; Retnarajan, B.; Sabnis, A.; Schnipper, E.; Song, J. J.; Song, Y. H.; Summa, J.; Tompsett, D.; Troiano, G.; Van, T.; Hoven, G.; Wright, J.; Lorusso, P.; Kantoff, P. W.; Bander, N. H.; Sweeney, C.; Farokhzad, O. C.; Langer, R.; Zale, S. Preclinical Development and Clinical Translation of a PSMA-Targeted Docetaxel Nanoparticle with a Differentiated Pharmacological Profile. *Sci. Transl. Med.* **2012**, *4*, 128ra39.
- Huang, A.; Paloni, J. M.; Wang, A.; Obermeyer, A. C.; Sureka, H. V.; Yao, H.; Olsen, B. D. Predicting Protein-Polymer Block Copolymer Self-Assembly from Protein Properties. *Biomacromolecules* **2019**, *20*, 3713–3723.
- Huang, H.; Yuan, Q.; Shah, J. S.; Misra, R. D. K. A New Family of Folate-Decorated and Carbon Nanotube-Mediated Drug Delivery System: Synthesis and Drug Delivery Response. *Adv. Drug Delivery Rev.* **2011**, *63*, 1332–1339.
- Huang, X.; Li, M.; Green, D. C.; Williams, D. S.; Patil, A. J.; Mann, S. Interfacial Assembly of Protein-Polymer Nano-Conjugates into Stimulus-Responsive Biomimetic Protocells. *Nat. Commun.* **2013**, *4*, 2239.
- Huang, X.; Patil, A. J.; Li, M.; Mann, S. Design and Construction of Higher-Order Structure and Function in Proteinosome-Based Protocells. *J. Am. Chem. Soc.* **2014**, *136*, 9225–9234.

- Huh, K. M.; Lee, S. C.; Cho, Y. W.; Lee, J.; Jeong, J. H.; Park, K. Hydrotropic Polymer Micelle System for Delivery of Paclitaxel. *J. Controlled Release* **2005**, *101*, 59–68.
- Hunter, A. C.; Moghimi, S. M. Smart Polymers in Drug Delivery: A Biological Perspective. *Polym. Chem.* **2017**, *8*, 41–51.
- Hwang, D.; Ramsey, J. D.; Kabanov, A. V. Polymeric Micelles for the Delivery of Poorly Soluble Drugs: From Nanoformulation to Clinical Approval. *Adv. Drug Delivery Rev.* **2020**, *156*, 80–118.
- Izunobi, J. U.; Higginbotham, C. L. Polymer Molecular Weight Analysis by <sup>1</sup>H NMR Spectroscopy. *J. Chem. Educ.* **2011**, *88*, 1098–1104.
- Jarak, I.; Pereira-Silva, M.; Santos, A. C.; Veiga, F.; Cabral, H.; Figueiras, A. Multifunctional Polymeric Micelle-Based Nucleic Acid Delivery: Current Advances and Future Perspectives. *Appl. Mater. Today* **2021**, *25*, 101217.
- Jena, S. S.; Roy, S. G.; Azmeera, V.; De, P. Solvent-Dependent Self-Assembly Behaviour of Block Copolymers Having Side-Chain Amino Acid and Fatty Acid Block Segments. *React. Funct. Polym.* **2016**, *99*, 26–34.
- Jiang, Y.; Lu, H.; Dag, A.; Hart-Smith, G.; Stenzel, M. H. Albumin-Polymer Conjugate Nanoparticles and Their Interactions with Prostate Cancer Cells in 2D and 3D Culture: Comparison between PMMA and PCL. *J Mater. Chem. B* **2016**, *4*, 2017–2027.
- Jiang, Y.; Lu, H.; Khine, Y. Y.; Dag, A.; Stenzel, M. H. Polyion Complex Micelle Based on Albumin-Polymer Conjugates: Multifunctional Oligonucleotide Transfection Vectors for Anticancer Chemotherapeutics. *Biomacromolecules* **2014**, *15*, 4195–4205.
- Jiang, Y.; Stenzel, M. Drug Delivery Vehicles Based on Albumin–Polymer Conjugates. *Macromol. Biosci.* **2016**, *16*, 791–802.

- Jin, L.; Liu, C. H.; Cintron, D.; Luo, Q.; Nieh, M. P.; He, J. Structural Engineering in the Self-Assembly of Amphiphilic Block Copolymers with Reactive Additives: Micelles, Vesicles, and Beyond. *Langmuir* **2021**, *37*, 9865–9872.
- Joshy, K. S.; Snigdha, S.; Anne, G.; Nandakumar, K.; Laly. A., P.; Sabu, T. Poly (Vinyl Pyrrolidone)-Lipid Based Hybrid Nanoparticles for Anti Viral Drug Delivery. *Chem. Phys. Lipids* **2018**, *210*, 82–89.
- Kaikade, D. S.; Sabnis, A. S. Polyurethane Foams from Vegetable Oil-Based Polyols: A Review. *Polym. Bull.* **2023**, *80*, 2239–2261.
- Kakde, D.; Taresco, V.; Bansal, K. K.; Magennis, E. P.; Howdle, S. M.; Mantovani, G.; Irvine, D. J.; Alexander, C. Amphiphilic Block Copolymers from a Renewable  $\epsilon$ -Decalactone Monomer: Prediction and Characterization of Micellar Core Effects on Drug Encapsulation and Release. *J. Mater. Chem. B* **2016**, *4*, 7119–7129.
- Kanamala, M.; Wilson, W. R.; Yang, M.; Palmer, B. D.; Wu, Z. Mechanisms and Biomaterials in PH-Responsive Tumour Targeted Drug Delivery: A Review. *Biomaterials* **2016**, *85*, 152–167.
- Kaneda, Y. Virosomes: Evolution of the Liposome as a Targeted Drug Delivery System. *Adv. Drug Delivery Rev.* **2000**, *43*, 197–205.
- Kappe, C. O. Controlled Microwave Heating in Modern Organic Synthesis. *Angew. Chem. Int. Ed.* **2004**, *43*, 6250–6284.
- Karayianni, M.; Pispas, S. Block Copolymer Solution Self-Assembly: Recent Advances, Emerging Trends, and Applications. *J. Polym. Sci.* **2021**, *59*, 1874–1898.
- Kataoka, K.; Kwon, G. S.; Yokoyama, M.; Okano, T.; Sakurai, Y. Block Copolymer Micelles as Vehicles for Drug Delivery. *J. Controlled Release* **1993**, *24*, 119–132.

- Kauscher, U.; Holme, M. N.; Björnmalm, M.; Stevens, M. M. Physical Stimuli-Responsive Vesicles in Drug Delivery: Beyond Liposomes and Polymersomes. *Adv. Drug Delivery Rev.* **2019**, *138*, 259–275.
- Kedar, U.; Phutane, P.; Shidhaye, S.; Kadam, V. Advances in Polymeric Micelles for Drug Delivery and Tumor Targeting. *Nanomed.: Nanotechnol. Biol. Med.* **2010**, *6*, 714–729.
- Keddie, D. J. A Guide to the Synthesis of Block Copolymers Using Reversible-Addition Fragmentation Chain Transfer (RAFT) Polymerization. *Chem. Soc. Rev.* **2014**, *43*, 496–505.
- Kempe, K.; Becer, C. R.; Schubert, U. S. Microwave-Assisted Polymerizations: Recent Status and Future Perspectives. *Macromolecules* **2011**, *44*, 5825–5842.
- Kermagoret, A.; Fustin, C. A.; Bourguignon, M.; Detrembleur, C.; Jérôme, C.; Debuigne, A. One-Pot Controlled Synthesis of Double Thermoresponsive N-Vinylcaprolactam-Based Copolymers with Tunable LCSTs. *Polym. Chem.* **2013**, *4*, 2575–2583.
- Kesharwani, P.; Jain, K.; Jain, N. K. Dendrimer as Nanocarrier for Drug Delivery. *Prog. Polym. Sci.* **2014**, *39*, 268–307.
- Kim, J. Y.; Do, Y. R.; Song, H. S.; Cho, Y. Y.; Ryoo, H. M.; Bae, S. H.; Kim, J. G.; Chae, Y. S.; Kang, B. W.; Baek, J. H.; Kim, M. K.; Lee, K. H.; Park, K. Multicenter Phase II Clinical Trial of Genexol-Pm® with Gemcitabine in Advanced Biliary Tract Cancer. *Anticancer Res.* **2017**, *37*, 1467–1473.
- Kim, S.; Kim, J. H.; Jeon, O.; Kwon, I. C.; Park, K. Engineered Polymers for Advanced Drug Delivery. *Eur. J. Pharm. Biopharm.* **2009**, *71*, 420–430.
- Ko, J. H.; Maynard, H. D. A Guide to Maximizing the Therapeutic Potential of Protein-Polymer Conjugates by Rational Design. *Chem. Soc. Rev.* **2018**, *47*, 8998–9014.

- Kolate, A.; Baradia, D.; Patil, S.; Vhora, I.; Kore, G.; Misra, A. PEG - A Versatile Conjugating Ligand for Drugs and Drug Delivery Systems. *J. Controlled Release*. **2014**, *192*, 67–81.
- Kopeć, M.; Krys, P.; Yuan, R.; Matyjaszewski, K. Aqueous RAFT Polymerization of Acrylonitrile. *Macromolecules* **2016**, *49*, 5877–5883.
- Kozlovskaya, V.; Kharlampieva, E. Self-Assemblies of Thermoresponsive Poly(N-Vinylcaprolactam) Polymers for Applications in Biomedical Field. *ACS Appl. Polym. Mater.* **2020**, *2*, 26–39.
- Kozlovskaya, V.; Liu, F.; Yang, Y.; Ingle, K.; Qian, S.; Halade, G. V.; Urban, V. S.; Kharlampieva, E. Temperature-Responsive Polymersomes of Poly(3-Methyl-N-Vinylcaprolactam)-Block-Poly(N-Vinylpyrrolidone) to Decrease Doxorubicin-Induced Cardiotoxicity. *Biomacromolecules* **2019**, *20*, 3989–4000.
- Krause, M. E.; Sahin, E. Chemical and Physical Instabilities in Manufacturing and Storage of Therapeutic Proteins. *Curr. Opin. Biotechnol.* **2019**, *60*, 159–167.
- Krishnan, A.; Roy, S.; Menon, S. Amphiphilic Block Copolymers: From Synthesis Including Living Polymerization Methods to Applications in Drug Delivery. *Eur. Polym. J.* **2022**, *172*, 111224.
- Kulthe, S. S.; Choudhari, Y. M.; Inamdar, N. N.; Mourya, V. Polymeric Micelles: Authoritative Aspects for Drug Delivery. *Des. Monomers Polym.* **2012**, *15*, 465–521.
- Kumari, P.; Bera, M. K.; Malik, S.; Kuila, B. K. Amphiphilic and Thermoresponsive Conjugated Block Copolymer with Its Solvent Dependent Optical and Photoluminescence Properties: Toward Sensing Applications. *ACS Appl. Mater. Interfaces* **2015**, *7*, 12348–12354.
- Kumari, P.; Ghosh, B.; Biswas, S. Nanocarriers for Cancer-Targeted Drug Delivery. *J. Drug Targeting*. **2016**, *24*, 179–191.

- Kwon, I. K.; Lee, S. C.; Han, B.; Park, K. Analysis on the Current Status of Targeted Drug Delivery to Tumors. *J. Controlled Release* **2012**, *164*, 108–114.
- Lam, C. N.; Olsen, B. D. Phase Transitions in Concentrated Solution Self-Assembly of Globular Protein-Polymer Block Copolymers. *Soft Matter* **2013**, *9*, 2393–2402.
- Lam, C. N.; Yao, H.; Olsen, B. D. The Effect of Protein Electrostatic Interactions on Globular Protein-Polymer Block Copolymer Self-Assembly. *Biomacromolecules* **2016**, *17*, 2820–2829.
- Lang, C.; Kumar, M.; Hickey, R. J. Influence of Block Sequence on the Colloidal Self-Assembly of Poly(Norbornene)-Block-Poly(Ethylene Oxide) Amphiphilic Block Polymers Using Rapid Injection Processing. *Polym. Chem.* **2020**, *11*, 375–384.
- Lansalot, M.; Davis, T. P.; Heuts, J. P. A. RAFT Miniemulsion Polymerization: Influence of the Structure of the RAFT Agent. *Macromolecules* **2002**, *35*, 7582–7591.
- Lanzalaco, S.; Armelin, E. Poly(N-Isopropylacrylamide) and Copolymers: A Review on Recent Progresses in Biomedical Applications. *Gels* **2017**, *3*, 36.
- Lebarbé, T.; Grau, E.; Gadenne, B.; Alfos, C.; Cramail, H. Synthesis of Fatty Acid-Based Polyesters and Their Blends with Poly(l-Lactide) as a Way to Tailor PLLA Toughness. *ACS Sustainable Chem. Eng.* **2015**, *3*, 283–292.
- Lee, J.; Cho, E. C.; Cho, K. Incorporation and Release Behavior of Hydrophobic Drug in Functionalized Poly(D,L-Lactide)-Block-Poly(Ethylene Oxide) Micelles. *J. Controlled Release* **2004**, *94*, 323–335.
- Lei, L.; Gohy, J. F.; Willet, N.; Zhang, J. X.; Varshney, S.; Jérôme, R. Tuning of the Morphology of Core-Shell-Corona Micelles in Water. I. Transition from Sphere to Cylinder. *Macromolecules* **2004**, *37*, 1089–1094.

- Leong, K. W.; Langer, R. Polymeric Controlled Drug Delivery. *Adv. Drug Delivery Rev.* **1987**, *1*, 199–233.
- Letchford, K.; Burt, H. A Review of the Formation and Classification of Amphiphilic Block Copolymer Nanoparticulate Structures: Micelles, Nanospheres, Nanocapsules and Polymersomes. *Eur. J. Pharm. Biopharm.* **2007**, *65*, 259–269.
- Leung, S. Y. L.; Jackson, J.; Miyake, H.; Burt, H.; Gleave, M. E. Polymeric Micellar Paclitaxel Phosphorylates Bcl-2 and Induces Apoptotic Regression of Androgen-Independent LNCaP Prostate Tumors. *Prostate* **2000**, *44*, 156–163.
- Li, A.; Li, K. Pressure-Sensitive Adhesives Based on Soybean Fatty Acids. *RSC Adv.* **2014**, *4*, 21521–21530.
- Li, C.; Wang, W.; Xi, Y.; Wang, J.; Chen, J. F.; Yun, J.; Le, Y. Design, Preparation and Characterization of Cyclic RGDfK Peptide Modified Poly(Ethylene Glycol)-Block-Poly(Lactic Acid) Micelle for Targeted Delivery. *Mater. Sci. Eng. C* **2016**, *64*, 303–309.
- Li, F.; Zhou, F.; Romano, D.; Rastogi, S. Synthesis and Characterization of Well-Defined High-Molecular-Weight PDLA-*b*-PLLA and PDLA-*b*-PLLA-*b*-PDLA Stereo-Block Copolymers. *Macromolecules* **2023**, *56*, 1995–2008.
- Li, J.; Jamieson, W. D.; Dimitriou, P.; Xu, W.; Rohde, P.; Martinac, B.; Baker, M.; Drinkwater, B. W.; Castell, O. K.; Barrow, D. A. Building Programmable Multicompartment Artificial Cells Incorporating Remotely Activated Protein Channels Using Microfluidics and Acoustic Levitation. *Nat. Commun.* **2022**, *13*, 4125.
- Li, M.; De Priyadarsi; Gondi, S. R.; Sumerlin, B. S. Responsive Polymer-Protein Bioconjugates Prepared by RAFT Polymerization and Copper-Catalyzed Azide-Alkyne Click Chemistry. *Macromol. Rapid Commun.* **2008**, *29*, 1172–1176.

- Li, X.; Cao, Y.; Luo, K.; Sun, Y.; Xiong, J.; Wang, L.; Liu, Z.; Li, J.; Ma, J.; Ge, J.; Xiao, H.; Zare, R. N. Highly Active Enzyme–Metal Nanohybrids Synthesized in Protein–Polymer Conjugates. *Nat. Catal.* **2019**, *2*, 718–725.
- Li, X.; Li, H.; Liu, G.; Deng, Z.; Wu, S.; Li, P.; Xu, Z.; Xu, H.; Chu, P. K. Magnetite-Loaded Fluorine-Containing Polymeric Micelles for Magnetic Resonance Imaging and Drug Delivery. *Biomaterials* **2012**, *33*, 3013–3024.
- Li, X.; Wei, Y.; Wu, Y.; Yin, L. Hypoxia-Induced Pro-Protein Therapy Assisted by a Self-Catalyzed Nanozymogen. *Angew. Chem. Int. Ed.* **2020**, *59*, 22544–22553.
- Li, Y. Y.; Zhang, X. Z.; Zhu, J. L.; Cheng, H.; Cheng, S. X.; Zhuo, R. X. Self-Assembled, Thermoresponsive Micelles Based on Triblock PMMA-*b*-PNIPAAm-*b*-PMMA Copolymer for Drug Delivery. *Nanotechnology* **2007**, *18*, 215605.
- Li, Y.; Xiao, K.; Luo, J.; Lee, J.; Pan, S.; Lam, K. S. A Novel Size-Tunable Nanocarrier System for Targeted Anticancer Drug Delivery. *J. Controlled Release* **2010**, *144*, 314–323.
- Liang, X.; Kozlovskaya, V.; Cox, C. P.; Wang, Y.; Saeed, M.; Kharlampieva, E. Synthesis and Self-Assembly of Thermosensitive Double-Hydrophilic Poly(N-Vinylcaprolactam)-*b*-Poly(N-Vinyl-2-Pyrrolidone) Diblock Copolymers. *J. Polym. Sci., Part A: Polym. Chem.* **2014**, *52*, 2725–2737.
- Liu, F.; Cui, Y.; Wang, L.; Wang, H.; Yuan, Y.; Pan, J.; Chen, H.; Yuan, L. Temperature-Responsive Poly(N-Isopropylacrylamide) Modified Gold Nanoparticle-Protein Conjugates for Bioactivity Modulation. *ACS Appl. Mater. Interfaces* **2015**, *7*, 11547–11554.
- Liu, F.; Kozlovskaya, V.; Medipelli, S.; Xue, B.; Ahmad, F.; Saeed, M.; Cropek, D.; Kharlampieva, E. Temperature-Sensitive Polymersomes for Controlled Delivery of Anticancer Drugs. *Chem. Mater.* **2015**, *27*, 7945–7956.

- Liu, J.; Debuigne, A.; Detrembleur, C.; Jérôme, C. Poly(N-Vinylcaprolactam): A Thermoresponsive Macromolecule with Promising Future in Biomedical Field. *Adv. Healthc. Mater.* **2014**, *3*, 1941–1968.
- Liu, M.; Du, H.; Zhang, W.; Zhai, G. Internal Stimuli-Responsive Nanocarriers for Drug Delivery: Design Strategies and Applications. *Mater. Sci. Eng. C* **2017**, *71*, 1267-1280.
- Liu, X.; Gao, W. In Situ Growth of Self-Assembled Protein-Polymer Nanovesicles for Enhanced Intracellular Protein Delivery. *ACS Appl. Mater. Interfaces* **2017**, *9*, 2023–2028.
- Liu, X.; Gao, W. Precision Conjugation: An Emerging Tool for Generating Protein–Polymer Conjugates. *Angew. Chem. Int. Ed.* **2021**, *60*, 11024–11035.
- Liu, Z.; Chen, N.; Dong, C.; Li, W.; Guo, W.; Wang, H.; Wang, S.; Tan, J.; Tu, Y.; Chang, J. Facile Construction of Near Infrared Fluorescence Nanoprobe with Amphiphilic Protein-Polymer Bioconjugate for Targeted Cell Imaging. *ACS Appl. Mater. Interfaces* **2015**, *7*, 18997–19005.
- Liu, Z.; Dong, C.; Wang, X.; Wang, H.; Li, W.; Tan, J.; Chang, J. Self-Assembled Biodegradable Protein-Polymer Vesicle as a Tumor-Targeted Nanocarrier. *ACS Appl. Mater. Interfaces* **2014**, *6*, 2393–2400.
- Lombardo, D.; Kiselev, M. A.; Magazù, S.; Calandra, P. Amphiphiles Self-Assembly: Basic Concepts and Future Perspectives of Supramolecular Approaches. *Adv. Condens. Matter Phys.* **2015**, *2015*, 151683.
- Lomège, J.; Lapinte, V.; Negrell, C.; Robin, J. J.; Caillol, S. Fatty Acid-Based Radically Polymerizable Monomers: From Novel Poly(Meth)Acrylates to Cutting-Edge Properties. *Biomacromolecules* **2019**, *20*, 4–26.

- Lu, A. X.; Oh, H.; Terrell, J. L.; Bentley, W. E.; Raghavan, S. R. A New Design for an Artificial Cell: Polymer Microcapsules with Addressable Inner Compartments That Can Harbor Biomolecules, Colloids or Microbial Species. *Chem. Sci.* **2017**, *8*, 6893–6903.
- Lü, J.; Yang, Y.; Gao, J.; Duan, H.; Lü, C. Thermoresponsive Amphiphilic Block Copolymer-Stabilized Gold Nanoparticles: Synthesis and High Catalytic Properties. *Langmuir* **2018**, *34*, 8205–8214.
- Lu, Y.; Park, K. Polymeric Micelles and Alternative Nanosized Delivery Vehicles for Poorly Soluble Drugs. *Int. J. Pharm.* **2013**, *453*, 198–214.
- Lue, S. J.; Chen, C. H.; Shih, C. M. Tuning of Lower Critical Solution Temperature (LCST) of Poly(N-Isopropylacrylamide-Co-Acrylic Acid) Hydrogels. *J. Macromol. Sci., Part B: Phys.* **2011**, *50*, 563–579.
- Luo, Y. L.; Yang, X. L.; Xu, F.; Chen, Y. S.; Zhang, B. Thermosensitive PNIPAM-b-HTPB Block Copolymer Micelles: Molecular Architectures and Camptothecin Drug Release. *Colloids Surf., B* **2014**, *114*, 150–157.
- Luque-Michel, E.; Imbuluzqueta, E.; Sebastián, V.; Blanco-Prieto, M. J. Clinical Advances of Nanocarrier-Based Cancer Therapy and Diagnostics. *Expert Opin. Drug Delivery.* **2017**, *14*, 75–92.
- Ma, C.; Liu, X.; Wu, G.; Zhou, P.; Zhou, Y.; Wang, L.; Huang, X. Efficient Way to Generate Protein-Based Nanoparticles by in-Situ Photoinitiated Polymerization-Induced Self-Assembly. *ACS Macro Lett.* **2017**, *6*, 689–694.
- Ma, Y.; Fan, X.; Li, L. PH-Sensitive Polymeric Micelles Formed by Doxorubicin Conjugated Prodrugs for Co-Delivery of Doxorubicin and Paclitaxel. *Carbohydr. Polym.* **2016**, *137*, 19–29.

- Ma, Y.; Mao, G.; Wu, G.; Cui, Z.; Zhang, X. E.; Huang, W. CRISPR-DCas9-Guided and Telomerase-Responsive Nanosystem for Precise Anti-Cancer Drug Delivery. *ACS Appl. Mater. Interfaces* **2021**, *13*, 7890–7896.
- Madhusudana Rao, K.; Mallikarjuna, B.; Krishna Rao, K. S. V.; Siraj, S.; Chowdoji Rao, K.; Subha, M. C. S. Novel Thermo/PH Sensitive Nanogels Composed from Poly(N-Vinylcaprolactam) for Controlled Release of an Anticancer Drug. *Colloids Surf., B* **2013**, *102*, 891–897.
- Maisonneuve, L.; Lebarbé, T.; Grau, E.; Cramail, H. Structure-Properties Relationship of Fatty Acid-Based Thermoplastics as Synthetic Polymer Mimics. *Polym. Chem.* **2013**, *4*, 5472–5517.
- Maiti, B.; De, P. RAFT Polymerization of Fatty Acid Containing Monomers: Controlled Synthesis of Polymers from Renewable Resources. *RSC Adv.* **2013**, *3*, 24983–24990.
- Maiti, B.; Kumar, S.; De Priyadarsi. Controlled RAFT Synthesis of Side-Chain Oleic Acid Containing Polymers and Their Post-Polymerization Functionalization. *RSC Adv.* **2014**, *4*, 56415–56423.
- Maiti, B.; Maiti, S.; De, P. Self-Assembly of Well-Defined Fatty Acid Based Amphiphilic Thermoresponsive Random Copolymers. *RSC Adv.* **2016**, *6*, 19322–19330.
- Mallakpour, S.; Zadehnazari, A. Microwave-Assisted Step-Growth Polymerizations (From Polycondensation to C–C Coupling). *Adv. Polym. Sci.* **2016**, *274*, 45–86.
- Manzari, M. T.; Shamy, Y.; Kiguchi, H.; Rosen, N.; Scaltriti, M.; Heller, D. A. Targeted Drug Delivery Strategies for Precision Medicines. *Nat. Rev. Mater.* **2021**, *6*, 351–370.
- Mao, L.; Russell, A. J.; Carmali, S. Moving Protein PEGylation from an Art to a Data Science. *Bioconjugate Chem.* **2022**, *33*, 1643–1653.

- Matsumura, Y.; Hamaguchi, T.; Ura, T.; Muro, K.; Yamada, Y.; Shimada, Y.; Shirao, K.; Okusaka, T.; Ueno, H.; Ikeda, M.; Watanabe, N. Phase I Clinical Trial and Pharmacokinetic Evaluation of NK911, a Micelle-Encapsulated Doxorubicin. *Br. J. Cancer* **2004**, *91*, 1775–1781.
- Matsumura, Y.; Maeda, H. A New Concept for Macromolecular Therapeutics in Cancer Chemotherapy: Mechanism of Tumoritropic Accumulation of Proteins and the Antitumor Agent Smancs. *Cancer Res.* **1986**, *46*, 6387–6392.
- Matyjaszewski, K.; Spanswick, J. Controlled/living Radical Polymerization. *Mater. Today* **2005**, *8*, 26-33
- Mehnert, W.; Mäder, K. Solid Lipid Nanoparticles: Production, Characterization and Applications. *Adv. Drug Delivery Rev.* **2012**, *64*, 83–101.
- Migliore, N.; Picchioni, F.; Raffa, P. The Effect of Macromolecular Structure on the Rheology and Surface Properties of Amphiphilic Random Polystyrene-R-Poly(Meth)Acrylate Copolymers Prepared by RDRP. *Soft Matter* **2020**, *16*, 2836–2846.
- Mills, J. K.; Needham, D. Targeted Drug Delivery. *Expert Opin. Ther. Pat.* **1999**, *9*, 1499–1513.
- Miyata, K.; Christie, R. J.; Kataoka, K. Polymeric Micelles for Nano-Scale Drug Delivery. *React. Funct. Polym.* **2011**, *71*, 227–234.
- Moad, G.; Chong, Y. K.; Postma, A.; Rizzardo, E.; Thang, S. H. Advances in RAFT Polymerization: The Synthesis of Polymers with Defined End-Groups. *Polymer* **2005**, *46*, 8458–8468.
- Moad, G.; Rizzardo, E.; Thang, S. H. RAFT Polymerization and Some of Its Applications. *Chem. Asian J.* **2013**, *8*, 1634–1644.

- Moran, M. T.; Carroll, W. M.; Selezneva, I.; Gorelov, A.; Rochev, Y. Cell Growth and Detachment from Protein-Coated PNIPAAm-Based Copolymers. *J. Biomed. Mater. Res., Part A* **2007**, *81*, 870–876.
- Mosquera, J.; García, I.; Liz-Marzán, L. M. Cellular Uptake of Nanoparticles versus Small Molecules: A Matter of Size. *Acc. Chem. Res.* **2018**, *51*, 2305–2313.
- Mura, S.; Nicolas, J.; Couvreur, P. Stimuli-Responsive Nanocarriers for Drug Delivery. *Nat. Mater.* **2013**, *12*, 991–1003.
- Nakabayashi, K.; Mori, H. Recent Progress in Controlled Radical Polymerization of N-Vinyl Monomers. *Eur. Polym. J.* **2013**, *49*, 2808–2838.
- Nardin, C.; Widmer, J.; Winterhalter, M.; Meier, W. Amphiphilic Block Copolymer Nanocontainers as Bioreactors. *Eur. Phys. J. E.* **2001**, *4*, 403–410.
- Obeng, M.; Milani, A. H.; Musa, M. S.; Cui, Z.; Fielding, L. A.; Farrand, L.; Goulding, M.; Saunders, B. R. Self-Assembly of Poly(Lauryl Methacrylate)-b-Poly(Benzyl Methacrylate) Nano-Objects Synthesised by ATRP and Their Temperature-Responsive Dispersion Properties. *Soft Matter* **2017**, *13*, 2228–2238.
- Ott, C.; Hoogenboom, R.; Hoepfener, S.; Wouters, D.; Gohy, J. F.; Schubert, U. S. Tuning the Morphologies of Amphiphilic Metallo-Supramolecular Triblock Terpolymers: From Spherical Micelles to Switchable Vesicles. *Soft Matter* **2009**, *5*, 84–91.
- Owen, S. C.; Chan, D. P. Y.; Shoichet, M. S. Polymeric Micelle Stability. *Nano Today* **2012**, *7*, 53–65.
- Palivan, C. G.; Fischer-Onaca, O.; Delcea, M.; Iteț, F.; Meier, W. Protein-Polymer Nanoreactors for Medical Applications. *Chem. Soc. Rev.* **2012**, *41*, 2800–2823.

- Paloni, J. M.; Dong, X. H.; Olsen, B. D. Protein-Polymer Block Copolymer Thin Films for Highly Sensitive Detection of Small Proteins in Biological Fluids. *ACS Sens.* **2019**, *4*, 2869–2878.
- Paloni, J. M.; Olsen, B. D. Coiled-Coil Domains for Self-Assembly and Sensitivity Enhancement of Protein-Polymer Conjugate Biosensors. *ACS Appl. Polym. Mater.* **2020**, *2*, 1114–1123.
- Pan, X.; Zhang, F.; Choi, B.; Luo, Y.; Guo, X.; Feng, A.; Thang, S. H. Effect of Solvents on the RAFT Polymerization of N-(2-Hydroxypropyl) Methacrylamide. *Eur. Polym. J.* **2019**, *115*, 166–172.
- Park, H.; Otte, A.; Park, K. Evolution of Drug Delivery Systems: From 1950 to 2020 and beyond. *J. Controlled Release* **2022**, *342*, 53–65.
- Park, J.; Moon, M.; Seo, M.; Choi, H.; Kim, S. Y. Well-Defined Star-Shaped Rod-Coil Diblock Copolymers as a New Class of Unimolecular Micelles: Encapsulation of Guests and Thermoresponsive Phase Transition. *Macromolecules* **2010**, *43*, 8304–8313.
- Park, K. Controlled Drug Delivery Systems: Past Forward and Future Back. *J. Controlled Release* **2014**, *190*, 3–8.
- Pawar, M. D.; Rathna, G. V. N.; Agrawal, S.; Kuchekar, B. S. Bioactive Thermoresponsive Polyblend Nanofiber Formulations for Wound Healing. *Mater. Sci. Eng. C* **2015**, *48*, 126–137.
- Peer, D.; KarP, J. M.; Hong, S.; faroKHzaD, oMiD C.; Margalit, riMona; Langer, Robert. Nanocarriers as an Emerging Platform for Cancer Therapy. *Nat. Nanotechnol.* **2007**, *2*, 751–760.
- Pelegri-Oday, E. M.; Lin, E. W.; Maynard, H. D. Therapeutic Protein-Polymer Conjugates: Advancing beyond Pegylation. *J. Am. Chem. Soc.* **2014**, *136*, 14323–14332.

- Perrier, S. 50th Anniversary Perspective: RAFT Polymerization - A User Guide. *Macromolecules* **2017**, *50*, 7433–7447.
- Piao, C.; Zhuang, C.; Choi, M.; Ha, J.; Lee, M. A RAGE-Antagonist Peptide Potentiates Polymeric Micelle-Mediated Intracellular Delivery of Plasmid DNA for Acute Lung Injury Gene Therapy. *Nanoscale* **2020**, *12*, 13606–13617.
- Pişkin, E.; Kaitian, X.; Denkbaş, E. B.; Küçükyavuz, Z. Novel PDLLA/PEG Copolymer Micelles as Drug Carriers. *J. Biomater. Sci. Polym. Ed.* **1996**, *7*, 359–373.
- Pitto-Barry, A.; Barry, N. P. E. Pluronic® Block-Copolymers in Medicine: From Chemical and Biological Versatility to Rationalisation and Clinical Advances. *Polym. Chem.* **2014**, *5*, 3291–3297.
- Popat, A.; Liu, J.; Lu, G. Q.; Qiao, S. Z. A PH-Responsive Drug Delivery System Based on Chitosan Coated Mesoporous Silica Nanoparticles. *J. Mater. Chem.* **2012**, *22*, 11173–11178.
- Pourjavadi, A.; Mazaheri Tehrani, Z.; Dastanpour, L. Smart Magnetic Self-Assembled Micelle: An Effective Nanocarrier for Thermo-Triggered Paclitaxel Delivery. *Int. J. Polym. Mater. Polym. Biomater.* **2019**, *68*, 741–749.
- Price, E.; Guo, Y.; Wang, C.; MOFFITT, M. Block Copolymer Strands with Internal Microphase Separation Structure via Self-Assembly at the Air-Water Interface. *Langmuir* **2009**, *25*, 6398-6406.
- Qi, Y.; Chilkoti, A. Protein-Polymer Conjugation-Moving beyond PEGylation. *Curr. Opin. Chem. Biol.* **2015**, *28*, 181–193.
- Qian, S.; Liu, R.; Han, G.; Shi, K.; Zhang, W. Star Amphiphilic Block Copolymers: Synthesis: Via Polymerization-Induced Self-Assembly and Crosslinking within Nanoparticles, and Solution and Interfacial Properties. *Polym. Chem.* **2020**, *11*, 2532–2541.

- Raffa, P.; Brandenburg, P.; Wever, D. A. Z.; Broekhuis, A. A.; Picchioni, F. Polystyrene-Poly(Sodium Methacrylate) Amphiphilic Block Copolymers by ATRP: Effect of Structure, PH, and Ionic Strength on Rheology of Aqueous Solutions. *Macromolecules* **2013**, *46*, 7106–7111.
- Rahikkala, A.; Aseyev, V.; Tenhu, H.; Kauppinen, E. I.; Raula, J. Thermoresponsive Nanoparticles of Self-Assembled Block Copolymers as Potential Carriers for Drug Delivery and Diagnostics. *Biomacromolecules* **2015**, *16*, 2750–2756.
- Rainbolt, E. A.; Miller, J. B.; Washington, K. E.; Senevirathne, S. A.; Biewer, M. C.; Siegwart, D. J.; Stefan, M. C. Fine-Tuning Thermoresponsive Functional Poly( $\epsilon$ -Caprolactone)s to Enhance Micelle Stability and Drug Loading. *J. Mater. Chem. B* **2015**, *3*, 1779–1787.
- Rajput, S. D.; Hundiwale, D. G.; Mahulikar, P. P.; Gite, V. V. Fatty Acids Based Transparent Polyurethane Films and Coatings. *Prog. Org. Coat.* **2014**, *77*, 1360–1368.
- Raza, A.; Hayat, U.; Rasheed, T.; Bilal, M.; Iqbal, H. M. N. Redox-Responsive Nano-Carriers as Tumor-Targeted Drug Delivery Systems. *Eur. J. Med. Chem.* **2018**, *157*, 705–715.
- Raza, A.; Rasheed, T.; Nabeel, F.; Hayat, U.; Bilal, M.; Iqbal, H. M. N. Endogenous and Exogenous Stimuli-Responsive Drug Delivery Systems for Programmed Site-Specific Release. *Molecules* **2019**, *24*, 1117.
- Reynhout, I. C.; Cornelissen, J. J. L. M.; Nolte, R. J. M. Self-Assembled Architectures from Biohybrid Triblock Copolymers. *J. Am. Chem. Soc.* **2007**, *129*, 2327–2332.
- Rivankar, S. An Overview of Doxorubicin Formulations in Cancer Therapy. *Journal of Cancer Research and Therapeutics. J. Cancer Res. Ther.* **2014**, *10*, 853–858.
- Rizzardo, E.; Chen, M.; Chong, B.; Moad, G.; Skidmore, M.; Thang, S.H. RAFT Polymerization: Adding to the Picture. *Macromolecules* **2007**, *248*, 104–116.

- Rizzardo, E.; Chen, M.; Chong, B.; Moad, G.; Skidmore, M.; Thang, S. H. RAFT Polymerization: Adding to the Picture. *Macromol. Symp.* **2007**, *248*, 104–116.
- Roy, D.; Brooks, W. L. A.; Sumerlin, B. S. New Directions in Thermoresponsive Polymers. *Chem. Soc. Rev.* **2013**, *42*, 7214–7243.
- Roy, D.; Ullah, A.; Sumerlin, B. S. Rapid Block Copolymer Synthesis by Microwave-Assisted RAFT Polymerization. *Macromolecules* **2009**, *42*, 7701–7708.
- Ruxandra Volovat, S.; Ciuleanu, T.-E.; Koralewski, P.; Olson, J. E. G.; Croitoru, A.; Koynov, K.; Stabile, S.; Cerea, G.; Osada, A.; Bobe, I.; Volovat, C. A Multicenter, Single-Arm, Basket Design, Phase II Study of NC-6004 plus Gemcitabine in Patients with Advanced Unresectable Lung, Biliary Tract, or Bladder Cancer. *Oncotarget* **2020**, *11*, 3105-3117.
- Ryan, S. M.; Wang, X.; Mantovani, G.; Sayers, C. T.; Haddleton, D. M.; Brayden, D. J. Conjugation of Salmon Calcitonin to a Combed-Shaped End Functionalized Poly(Poly(Ethylene Glycol) Methyl Ether Methacrylate) Yields a Bioactive Stable Conjugate. *J. Controlled Release* **2009**, *135*, 51–59.
- Saha, B.; Ruidas, B.; Mete, S.; Mukhopadhyay, C.; Bauri, K.; De, P. AIE-active Non-conjugated Poly(N-vinylcaprolactam) as a Fluorescent Thermometer for Intracellular Temperature Imaging. *Chem. Sci.* **2020**, *11*, 141–147.
- Sajjad, H.; Tolman, W. B.; Reineke, T. M. Block Copolymer Pressure-Sensitive Adhesives Derived from Fatty Acids and Triacetic Acid Lactone. *ACS Appl. Polym. Mater.* **2020**, *2*, 2719–2728.
- Saleem, M.; Wang, L.; Yu, H.; Zain-ul-Abdin; Akram, M.; Ullah, R. S. Synthesis of Amphiphilic Block Copolymers Containing Ferrocene–Boronic Acid and Their Micellization, Redox-Responsive Properties and Glucose Sensing. *Colloid Polym. Sci.* **2017**, *295*, 995–1006.

- Salvi, V. R.; Pawar, P. Nanostructured Lipid Carriers (NLC) System: A Novel Drug Targeting Carrier. *J. Drug Delivery Sci. Technol.* **2019**, *51*, 255–267.
- Sandoval, R. W.; Williams, D. E.; Kim, J.; Roth, C. B.; Torkelson, J. M. Critical Micelle Concentrations of Block and Gradient Copolymers in Homopolymer: Effects of Sequence Distribution, Composition, and Molecular Weight. *J. Polym. Sci. B: Polym. Phys.* **2008**, *46*, 2672–2682.
- Sawant, R. M.; Hurley, J. P.; Salmaso, S.; Kale, A.; Tolcheva, E.; Levchenko, T. S.; Torchilin, V. P. “SMART” Drug Delivery Systems: Double-Targeted PH-Responsive Pharmaceutical Nanocarriers. *Bioconjugate Chem.* **2006**, *17*, 943–949.
- Schmelz, J.; Schedl, A. E.; Steinlein, C.; Manners, I.; Schmalz, H. Length Control and Block-Type Architectures in Worm-like Micelles with Polyethylene Cores. *J. Am. Chem. Soc.* **2012**, *134*, 14217–14225.
- Seuring, J.; Agarwal, S. Polymers with Upper Critical Solution Temperature in Aqueous Solution: Unexpected Properties from Known Building Blocks. *ACS Macro Lett.* **2013**, *2*, 597–600.
- Shahin, M.; Safaei-Nikouei, N.; Lavasanifar, A. Polymeric Micelles for PH-Responsive Delivery of Cisplatin. *J Drug Target.* **2014**, *22*, 629–637.
- Shahriari, M.; Zahiri, M.; Abnous, K.; Taghdisi, S. M.; Ramezani, M.; Alibolandi, M. Enzyme Responsive Drug Delivery Systems in Cancer Treatment. *J. Controlled Release* **2019**, *308*, 172–189.
- Shao, K.; Huang, R.; Li, J.; Han, L.; Ye, L.; Lou, J.; Jiang, C. Angiopep-2 Modified PE-PEG Based Polymeric Micelles for Amphotericin B Delivery Targeted to the Brain. *J. Controlled Release* **2010**, *147*, 118–126.

- Shen, B.; Ma, Y.; Yu, S.; Ji, C. Smart Multifunctional Magnetic Nanoparticle-Based Drug Delivery System for Cancer Thermo-Chemotherapy and Intracellular Imaging. *ACS Appl. Mater. Interfaces* **2016**, *8*, 24502–24508.
- Shim, G.; Kim, D.; Park, G. T.; Jin, H.; Suh, S. K.; Oh, Y. K. Therapeutic Gene Editing: Delivery and Regulatory Perspectives. *Acta Pharmacol. Sin.* **2017**, *38*, 738–753.
- Siepmann, J.; Faham, A.; Clas, S. D.; Boyd, B. J.; Jannin, V.; Bernkop-Schnürch, A.; Zhao, H.; Lecommandoux, S.; Evans, J. C.; Allen, C.; Merkel, O. M.; Costabile, G.; Alexander, M. R.; Wildman, R. D.; Roberts, C. J.; Leroux, J. C. Lipids and Polymers in Pharmaceutical Technology: Lifelong Companions. *Int. J. Pharm.* **2019**, *558*, 128–142.
- Singh, A. P.; Gunasekaran, G.; Suryanarayana, C.; Baloji Naik, R. Fatty Acid Based Waterborne Air Drying Epoxy Ester Resin for Coating Applications. *Prog. Org. Coat.* **2015**, *87*, 95–105.
- Singh, P.; Srivastava, A.; Kumar, R. Synthesis and Characterization of Nano Micelles of Poly(N-Acrylamidohexanoic Acid)-b-Poly(N-Vinylcaprolactam) via RAFT Process: Solubilizing and Releasing of Hydrophobic Molecules. *Polymer* **2015**, *57*, 51–61.
- Singh, R.; Lillard, J. W. Nanoparticle-Based Targeted Drug Delivery. *Exp. Mol. Pathol.* **2009**, *86*, 215–223.
- Singla, P.; Kaur, P.; Mehta, R.; Berek, D.; Upadhyay, S. N. Ring-Opening Polymerization of Lactide Using Microwave and Conventional Heating. *Procedia Chem.* **2012**, *4*, 179–185.
- Smart, T.; Lomas, H.; Massignani, M.; Flores-Merino, M. V.; Perez, L. R.; Battaglia, G. Block Copolymer Nanostructures. *Nano Today* **2008**, *3*, 38–46.
- Smith, A. E.; Xu, X.; McCormick, C. L. Stimuli-Responsive Amphiphilic (Co)Polymers via RAFT Polymerization. *Prog. Polym. Sci.* **2010**, *35*, 45–93.

- Sponchioni, M.; Capasso Palmiero, U.; Moscatelli, D. Thermo-Responsive Polymers: Applications of Smart Materials in Drug Delivery and Tissue Engineering. *Mater. Sci. Eng. C* **2019**, *102*, 589–605.
- Srinivasarao, M.; Low, P. S. Ligand-Targeted Drug Delivery. *Chem. Rev.* **2017**, *117*, 12133–12164.
- Stenzel, M. H. Bioconjugation Using Thiols: Old Chemistry Rediscovered to Connect Polymers with Nature's Building Blocks. *ACS Macro Lett.* **2013**, *2*, 14–18.
- Stevens, C. A.; Kaur, K.; Klok, H. A. Self-Assembly of Protein-Polymer Conjugates for Drug Delivery. *Adv. Drug Delivery Rev.* **2021**, *174*, 447–460.
- Suguri, T.; Olsen, B. D. Topology Effects on Protein-Polymer Block Copolymer Self-Assembly. *Polym. Chem.* **2019**, *10*, 1751–1761.
- Sumerlin, B. S.; Lowe, A. B.; Thomas, D. B.; Convertine, A. J.; Donovan, M. S.; McCormick, C. L. Aqueous Solution Properties of PH-Responsive AB Diblock Acrylamido-Styrenic Copolymers Synthesized via Aqueous Reversible Addition-Fragmentation Chain Transfer. *J. Polym. Sci., Part A: Polym. Chem.* **2004**, *42*, 1724–1734.
- Sutton, D.; Nasongkla, N.; Blanco, E.; Gao, J. Functionalized Micellar Systems for Cancer Targeted Drug Delivery. *Pharm. Res.* **2007**, *24*, 1029–1046.
- Tabatabaei Rezaei, S. J.; Nabid, M. R.; Niknejad, H.; Entezami, A. A. Multifunctional and Thermoresponsive Unimolecular Micelles for Tumor-Targeted Delivery and Site-Specifically Release of Anticancer Drugs. *Polymer* **2012**, *53*, 3485–3497.
- Taguchi, K.; Lu, H.; Jiang, Y.; Hung, T. T.; Stenzel, M. H. Safety of Nanoparticles Based on Albumin-Polymer Conjugates as a Carrier of Nucleotides for Pancreatic Cancer Therapy. *J. Mater. Chem. B* **2018**, *6*, 6278–6287.

- Tao, L.; Liu, J.; Davis, T. P. Branched Polymer-Protein Conjugates Made from Mid-Chain-Functional P(HPMA). *Biomacromolecules* **2009**, *10*, 2847–2851.
- Taubert, A.; Napoli, A.; Meier, W. Self-Assembly of Reactive Amphiphilic Block Copolymers as Mimetics for Biological Membranes. *Curr. Opin. Chem. Biol.* **2004**, *8*, 598–603.
- Taymaz-Nikerel, H.; Karabekmez, M. E.; Eraslan, S.; Kırdar, B. Doxorubicin Induces an Extensive Transcriptional and Metabolic Rewiring in Yeast Cells. *Sci. Rep.* **2018**, *8*, 13672.
- Tenchov, R.; Bird, R.; Curtze, A. E.; Zhou, Q. Lipid Nanoparticles from Liposomes to mRNA Vaccine Delivery, a Landscape of Research Diversity and Advancement. *ACS Nano* **2021**, *15*, 16982–17015.
- Torchilin, V. Tumor Delivery of Macromolecular Drugs Based on the EPR Effect. *Adv. Drug Delivery Rev.* **2011**, *63*, 131–135.
- Town, J. S.; Jones, G. R.; Haddleton, D. M. MALDI-LID-ToF/ToF Analysis of Statistical and Diblock Polyacrylate Copolymers. *Polym. Chem.* **2018**, *9*, 4631–4641.
- Trzebicka, B.; Szweda, R.; Kosowski, D.; Szweda, D.; Otulakowski, Ł.; Haladjova, E.; Dworak, A. Thermoresponsive Polymer-Peptide/Protein Conjugates. *Prog. Polym. Sci.* **2017**, *68*, 35–76.
- Uemukai, T.; Hioki, T.; Ishifune, M. Thermoresponsive and Redox Behaviors of Poly(N - Isopropylacrylamide)-Based Block Copolymers Having TEMPO Groups as Their Side Chains. *Int. J. Polym. Sci.* **2013**, *2013*, 196145.
- Vanparijs, N.; Maji, S.; Louage, B.; Voorhaar, L.; Laplace, D.; Zhang, Q.; Shi, Y.; Hennink, W. E.; Hoogenboom, R.; De Geest, B. G. Polymer-Protein Conjugation via a “grafting to” Approach—a Comparative Study of the Performance of Protein-Reactive RAFT Chain Transfer Agents. *Polym. Chem.* **2015**, *6*, 5602–5614.

- Vanparijs, N.; Nuhn, L.; De Geest, B. G. Transiently Thermoresponsive Polymers and Their Applications in Biomedicine. *Chem. Soc. Rev.* **2017**, *46*, 1193–1239.
- Vargason, A. M.; Anselmo, A. C.; Mitragotri, S. The Evolution of Commercial Drug Delivery Technologies. *Nat. Biomed. Eng.* **2021**, *5*, 951–967.
- Varlas, S.; Lawrenson, S. B.; Arkinstall, L. A.; O'Reilly, R. K.; Foster, J. C. Self-Assembled Nanostructures from Amphiphilic Block Copolymers Prepared via Ring-Opening Metathesis Polymerization (ROMP). *Prog. Polym. Sci.* **2020**, *107*, 101278.
- Vazaios, A.; Touris, A.; Echeverria, M.; Zorba, G.; Pitsikalis, M. Micellization Behaviour of Linear and Nonlinear Block Copolymers Based on Poly(n-Hexyl Isocyanate) in Selective Solvents. *Polymers* **2020**, *12*, 1678.
- Vega-Rios, A.; Licea-Claverie, A. Controlled Synthesis of Block Copolymers Containing N-Isopropylacrylamide by RAFT Polymerization. *J. Mex. Chem. Soc.* **2011**, *55*, 21–32.
- Vendamme, R.; Olaerts, K.; Gomes, M.; Degens, M.; Shigematsu, T.; Eevers, W. Interplay between Viscoelastic and Chemical Tunings in Fatty-Acid-Based Polyester Adhesives: Engineering Biomass toward Functionalized Step-Growth Polymers and Soft Networks. *Biomacromolecules* **2012**, *13*, 1933–1944.
- Veronese, F. M.; Mero, A. The Impact of PEGylation on Biological Therapies. *Biodrugs* **2008**, *22*, 315–329.
- Vihola H, Laukkanen A, Valtola L, Tenhu H, Hirvonen J. Cytotoxicity of thermosensitive polymers poly(N-isopropylacrylamide), poly(N-vinylcaprolactam) and amphiphilically modified poly(N-vinylcaprolactam). *Biomaterials* **2005**, *26*, 3055-64.

- Vukovic, I.; Voortman, T.; Merino, D.; Portale, G.; Hiekkataipale, P.; Ruokolainen, J.; Brinke, G.; Loos, K. Double Gyroid Network Morphology in Supramolecular Diblock Copolymer Complexes. *Macromolecules* **2012**, *45*, 3503–3512.
- Wadajkar, A. S.; Bhavsar, Z.; Ko, C. Y.; Koppolu, B.; Cui, W.; Tang, L.; Nguyen, K. T. Multifunctional Particles for Melanoma-Targeted Drug Delivery. *Acta Biomater.* **2012**, *8*, 2996–3004.
- Wan, D.; Zhou, Q.; Pu, H.; Yang, G. Controlled Radical Polymerization of N-Vinylcaprolactam Mediated by Xanthate or Dithiocarbamate. *Polym. Sci., Part A: Polym. Chem.* **2008**, *46*, 3756–3765.
- Wan, W. M.; Hong, C. Y.; Pan, C. Y. One-Pot Synthesis of Nanomaterials via RAFT Polymerization Induced Self-Assembly and Morphology Transition. *Chem. Commun.* **2009**, *39*, 5883–5885.
- Wan, X.; Liu, T.; Liu, S. Synthesis of Amphiphilic Tadpole-Shaped Linear-Cyclic Diblock Copolymers via Ring-Opening Polymerization Directly Initiating from Cyclic Precursors and Their Application as Drug Nanocarriers. *Biomacromolecules* **2011**, *12*, 1146–1154.
- Wang, C.; Wang, Z.; Zhang, X. Amphiphilic Building Blocks for Self-Assembly: From Amphiphiles to Supra-Amphiphiles. *Acc. Chem. Res.* **2012**, *45*, 608–618.
- Wang, J.; Li, Y.; Dong, X.; Wang, Y.; Chong, X.; Yu, T.; Zhang, F.; Chen, D.; Zhang, L.; Gao, J.; Yang, C.; Han, J.; Li, W. A Micelle Self-Assembled from Doxorubicin-Arabinoside Conjugates with PH-Cleavable Bond for Synergistic Antitumor Therapy. *Nanoscale Res. Lett.* **2017**, *12*, 73.
- Wang, L.; Wen, P.; Liu, X.; Zhou, Y.; Li, M.; Huang, Y.; Geng, L.; Mann, S.; Huang, X. Single-Step Fabrication of Multi-Compartmentalized Biphasic Proteinosomes. *Chem. Commun.* **2017**, *53*, 8537–8540.

- Wang, S.; Vajjala Kesava, S.; Gomez, E. D.; Robertson, M. L. Sustainable Thermoplastic Elastomers Derived from Fatty Acids. *Macromolecules* **2013**, *46*, 7202–7212.
- Wang, Y.; Wu, C. Site-Specific Conjugation of Polymers to Proteins. *Biomacromolecules* **2018**, *19*, 1804–1825.
- Wang, Z.; Chen, J.; Little, N.; Lu, J. Self-Assembling Prodrug Nanotherapeutics for Synergistic Tumor Targeted Drug Delivery. *Acta Biomater.* **2020**, *111*, 20–28.
- Weber, C.; Hoogenboom, R.; Schubert, U. S. Temperature Responsive Bio-Compatible Polymers Based on Poly(Ethylene Oxide) and Poly(2-Oxazoline)s. *Prog. Polym. Sci.* **2012**, *37*, 686–714.
- Welch, R. P.; Lee, H.; Luzuriaga, M. A.; Brohlin, O. R.; Gassensmith, J. J. Protein-Polymer Delivery: Chemistry from the Cold Chain to the Clinic. *Bioconjugate Chem.* **2018**, *29*, 2867–2883.
- Wong, C. K.; Laos, A. J.; Soeriyadi, A. H.; Wiedenmann, J.; Curmi, P. M. G.; Gooding, J. J.; Marquis, C. P.; Stenzel, M. H.; Thordarson, P. Polymersomes Prepared from Thermoresponsive Fluorescent Protein–Polymer Bioconjugates: Capture of and Report on Drug and Protein Payloads. *Angew. Chem.* **2015**, *127*, 5407–5412.
- Wu, Q.; Yi, J.; Wang, S.; Liu, D.; Song, X.; Zhang, G. Synthesis and Self-Assembly of New Amphiphilic Thermosensitive Poly(N-Vinylcaprolactam)/Poly(d,l-Lactide) Block Copolymers via the Combination of Ring-Opening Polymerization and Click Chemistry. *Polym. Bull.* **2015**, *72*, 1449–1466.
- Wu, Q.; Yi, J.; Yin, Z.; Wang, S.; Yang, Q.; Wu, S.; Song, X.; Zhang, G. Synthesis and Self-Assembly of New Amphiphilic Thermosensitive Poly(N-Vinylcaprolactam)/Poly( $\epsilon$ -

- Caprolactone) Block Copolymers via the Combination of Ring-Opening Polymerization and Click Chemistry. *J. Polym. Res.* **2013**, *20*, 262.
- Xia, X. X.; Wang, M.; Lin, Y.; Xu, Q.; Kaplan, D. L. Hydrophobic Drug-Triggered Self-Assembly of Nanoparticles from Silk-Elastin-like Protein Polymers for Drug Delivery. *Biomacromolecules* **2014**, *15*, 908–914.
- Xiao, L.; Huang, L.; Moingeon, F.; Gauthier, M.; Yang, G. PH-Responsive Poly(Ethylene Glycol)-Block-Polylactide Micelles for Tumor-Targeted Drug Delivery. *Biomacromolecules* **2017**, *18*, 2711–2722.
- Xiong, X. B.; Binkhathlan, Z.; Molavi, O.; Lavasanifar, A. Amphiphilic Block Co-Polymers: Preparation and Application in Nanodrug and Gene Delivery. *Acta Biomater.* **2012**, *8*, 2017–2033.
- Xue, X.; Liang, X. J. Overcoming Drug Efflux-Based Multidrug Resistance in Cancer with Nanotechnology. *Chin. J. Cancer.* **2012**, *31*, 100–109.
- Yang, P.; Ning, Y.; Neal, T. J.; Jones, E. R.; Parker, B. R.; Armes, S. P. Block Copolymer Microparticles Comprising Inverse Bicontinuous Phases Prepared via Polymerization-Induced Self-Assembly. *Chem. Sci.* **2019**, *10*, 4200–4208.
- Yang, Y.; Alford, A.; Kozlovskaya, V.; Zhao, S.; Joshi, H.; Kim, E.; Qian, S.; Urban, V.; Cropek, D.; Aksimentiev, A.; Kharlampieva, E. Effect of Temperature and Hydrophilic Ratio on the Structure of Poly(N-Vinylcaprolactam)-Block-Poly(Dimethylsiloxane)-Block-Poly(N-Vinylcaprolactam) Polymersomes. *ACS Appl. Polym. Mater.* **2019**, *1*, 722–736.
- Yokoyama, M. Polymeric Micelles as Drug Carriers: Their Lights and Shadows. *J. Drug Targeting* **2014**, *22*, 576–583.

- York, A. W.; Kirkland, S. E.; McCormick, C. L. Advances in the Synthesis of Amphiphilic Block Copolymers via RAFT Polymerization: Stimuli-Responsive Drug and Gene Delivery. *Adv. Drug Delivery Rev.* **2008**, *60*, 1018-1036.
- Yousefpour Marzbali, M.; Yari Khosroushahi, A. Polymeric Micelles as Mighty Nanocarriers for Cancer Gene Therapy: A Review. *Cancer Chemother. Pharmacol.* **2017**, *79*, 637–649.
- Yu, J.; Lu, C.; Wang, C.; Wang, J.; Fan, Y.; Chu, F. Sustainable Thermoplastic Elastomers Derived from Cellulose, Fatty Acid and Furfural via ATRP and Click Chemistry. *Carbohydr. Polym.* **2017**, *176*, 83–90.
- Zeng, J.; Lv, C.; Liu, G.; Zhang, Z.; Dong, Z.; Liu, J. Y.; Wang, Y. A Novel Ion-Imprinted Membrane Induced by Amphiphilic Block Copolymer for Selective Separation of Pt(IV) from Aqueous Solutions. *J. Memb. Sci.* **2019**, *572*, 428–441.
- Zhai, S.; Ma, Y.; Chen, Y.; Li, D.; Cao, J.; Liu, Y.; Cai, M.; Xie, X.; Chen, Y.; Luo, X. Synthesis of an Amphiphilic Block Copolymer Containing Zwitterionic Sulfobetaine as a Novel PH-Sensitive Drug Carrier. *Polym. Chem.* **2014**, *5*, 1285–1297.
- Zhang, C.; Madbouly, S. A.; Kessler, M. R. Biobased Polyurethanes Prepared from Different Vegetable Oils. *ACS Appl. Mater. Interfaces* **2015**, *7*, 1226–1233.
- Zhang, H. Controlled/"living" Radical Precipitation Polymerization: A Versatile Polymerization Technique for Advanced Functional Polymers. *Eur. Polym. J.* **2013**, *49*, 579-600.
- Zhang, J.; Chen, X. F.; Wei, H. B.; Wan, X. H. Tunable Assembly of Amphiphilic Rod-Coil Block Copolymers in Solution. *Chem. Soc. Rev.* **2013**, *42*, 9127–9154.
- Zhang, J.; Zhang, C.; Madbouly, S. A. In Situ Polymerization of Bio-Based Thermosetting Polyurethane/Graphene Oxide Nanocomposites. *J. Appl. Polym. Sci.* **2015**, *132*, 41751.

- Zhang, L.; Guo, R.; Yang, M.; Jiang, X.; Liu, B. Thermo and PH Dual-Responsive Nanoparticles for Anti-Cancer Drug Delivery. *Adv. Mater.* **2007**, *19*, 2988–2992.
- Zhang, S.; Arshad, M.; Ullah, A. Drug Encapsulation and Release Behavior of Telechelic Nanoparticles. *Nanotechnology* **2015**, *26*, 415703.
- Zhang, Y.; Chan, H. F.; Leong, K. W. Advanced Materials and Processing for Drug Delivery: The Past and the Future. *Adv. Drug Delivery Rev.* **2013**, *65*, 104–120.
- Zhao, H.; Ibarboure, E.; Ibrahimova, V.; Xiao, Y.; Garanger, E.; Lecommandoux, S. Spatiotemporal Dynamic Assembly/Disassembly of Organelle-Mimics Based on Intrinsically Disordered Protein-Polymer Conjugates. *Adv. Sci.* **2021**, *8*, 2102508.
- Zhao, W.; Liu, F.; Chen, Y.; Bai, J.; Gao, W. Synthesis of Well-Defined Protein-Polymer Conjugates for Biomedicine. *Polymer* **2015**, *66*, A1–A10.
- Zhao, X. Q.; Wang, T. X.; Liu, W.; Wang, C. D.; Wang, D.; Shang, T.; Shen, L. H.; Ren, L. Multifunctional Au@IPN-PNIPAAm Nanogels for Cancer Cell Imaging and Combined Chemo-Photothermal Treatment. *J. Mater. Chem.* **2011**, *21*, 7240–7247.
- Zhao, X.; Shan, G. PSMA-*b*-PNIPAM Copolymer Micelles with Both a Hydrophobic Segment and a Hydrophilic Terminal Group: Synthesis, Micelle Formation, and Characterization. *Colloid Polym. Sci.* **2019**, *297*, 1353–1363.
- Zhou, P.; Wu, S.; Hegazy, M.; Li, H.; Xu, X.; Lu, H.; Huang, X. Engineered Borate Ester Conjugated Protein-Polymer Nanoconjugates for PH-Responsive Drug Delivery. *Mater. Sci. Eng. C* **2019**, *104*, 109914.
- Zong, L.; Zhou, S.; Sgriccia, N.; Hawley, M. C.; Kempel, L. C. A Review of Microwave-Assisted Polymer Chemistry (MAPC). *J. Microw. Power Electromag. Energy* **2003**, *38*, 49–74.

## APPENDIX A: Supplementary Information of Chapter 3

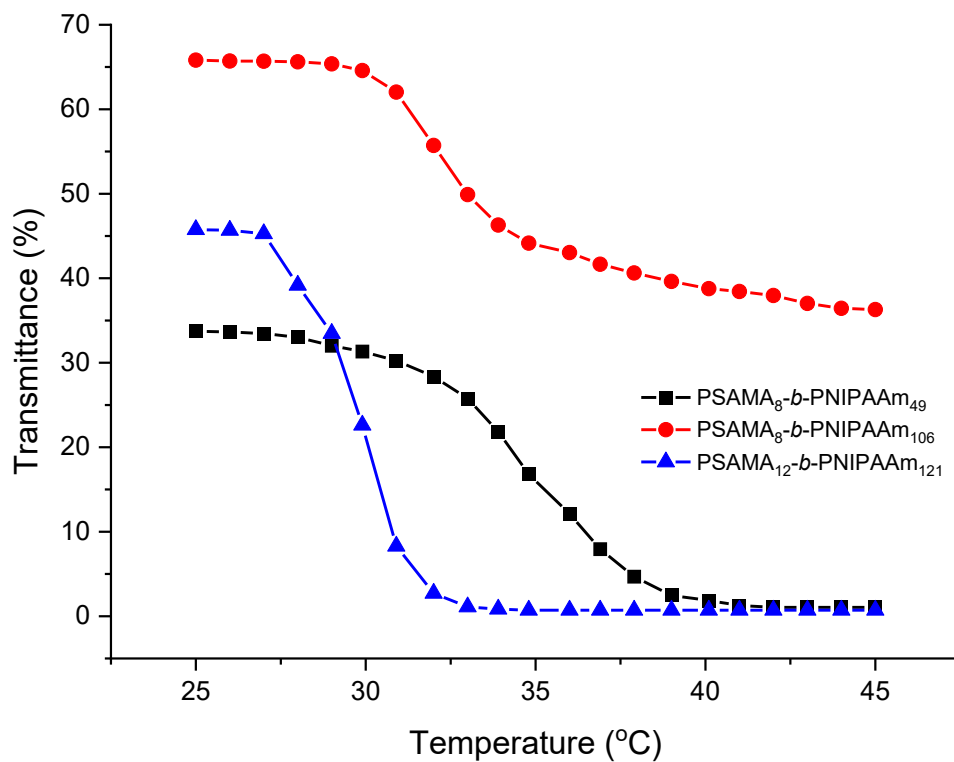


Figure S3.1. Temperature-dependent transmittance of PSAMA-*b*-PNIPAM in aqueous solution

## APPENDIX B: Supplementary Information of Chapter 4

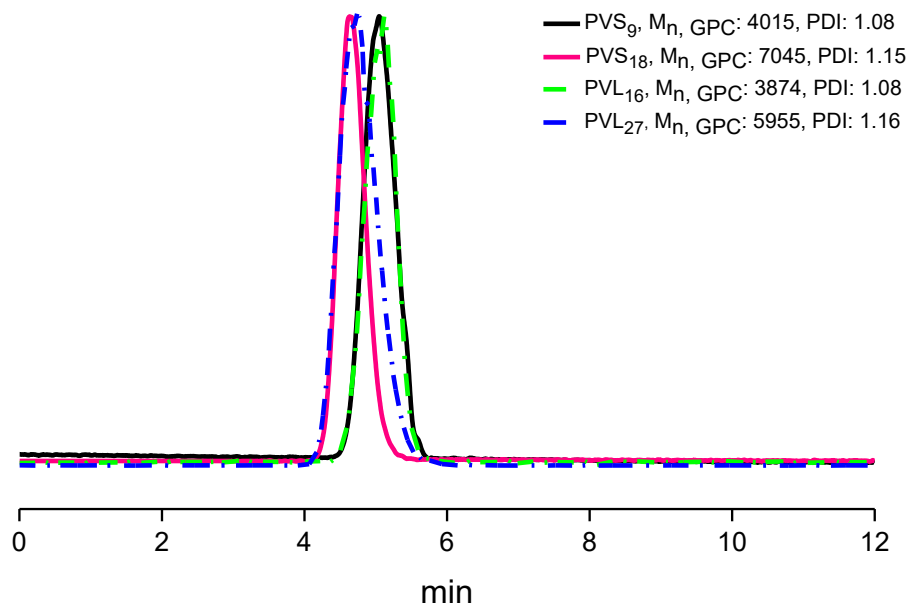


Figure S4.1. GPC traces of PVS and PVL homopolymers.

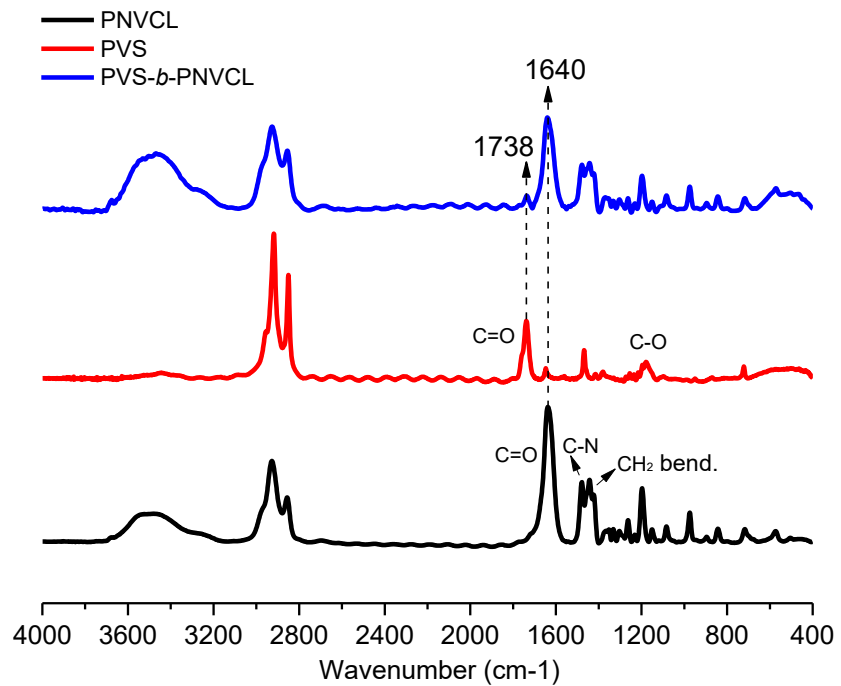


Figure S4.2. FTIR spectrum of PVS, PNVCL and PVS-*b*-PNVCL.

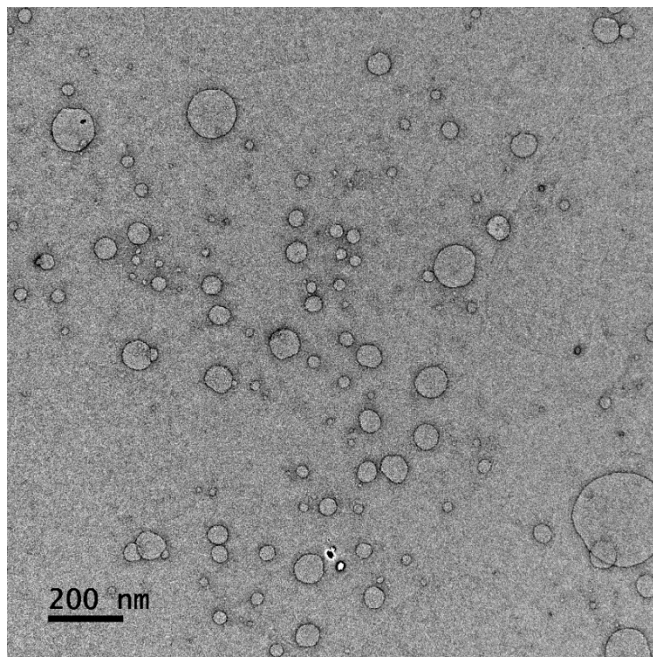


Figure S4.3. TEM images of PVL<sub>16</sub>-*b*-PNVCL<sub>54</sub>.

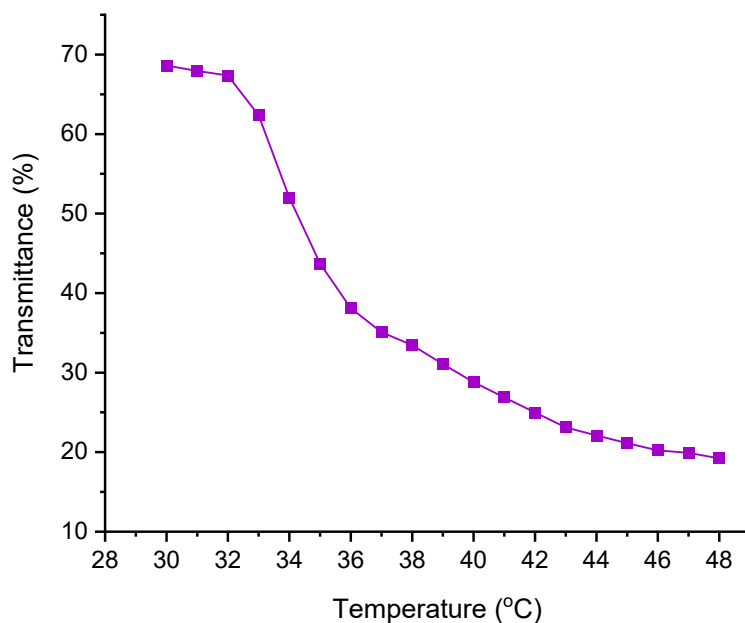


Figure S4.4. Temperature-dependent transmittance of PVS<sub>18</sub>-*b*-PNVCL<sub>95</sub> (1 mg/mL) in aqueous solution at 500 nm (LCST was defined as the temperature corresponding to a 10% decrease in optical transmittance)

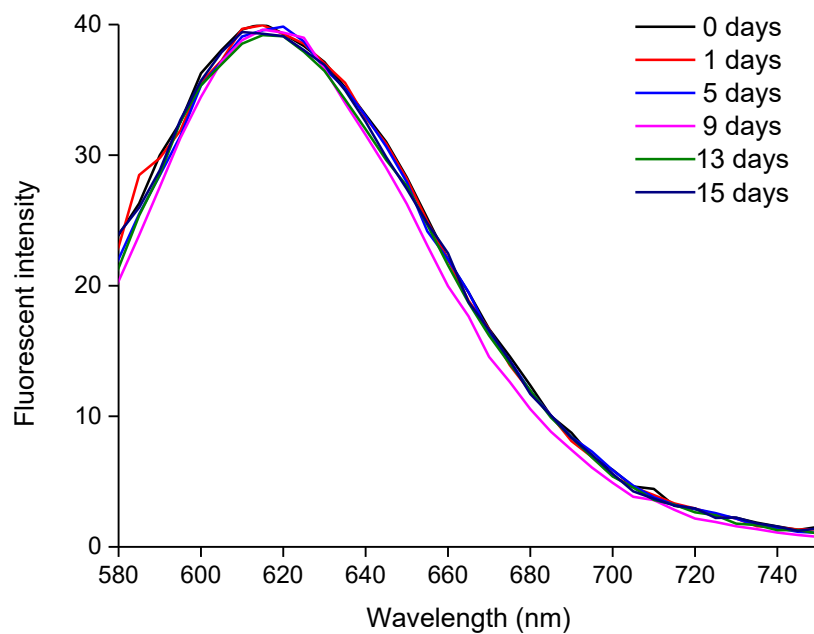


Figure S4.5. Fluorescence emission spectra (excitation at 570 nm) of NR-loaded PVS<sub>18</sub>-*b*-PNVCL<sub>35</sub> micelles incubated in PBS solution

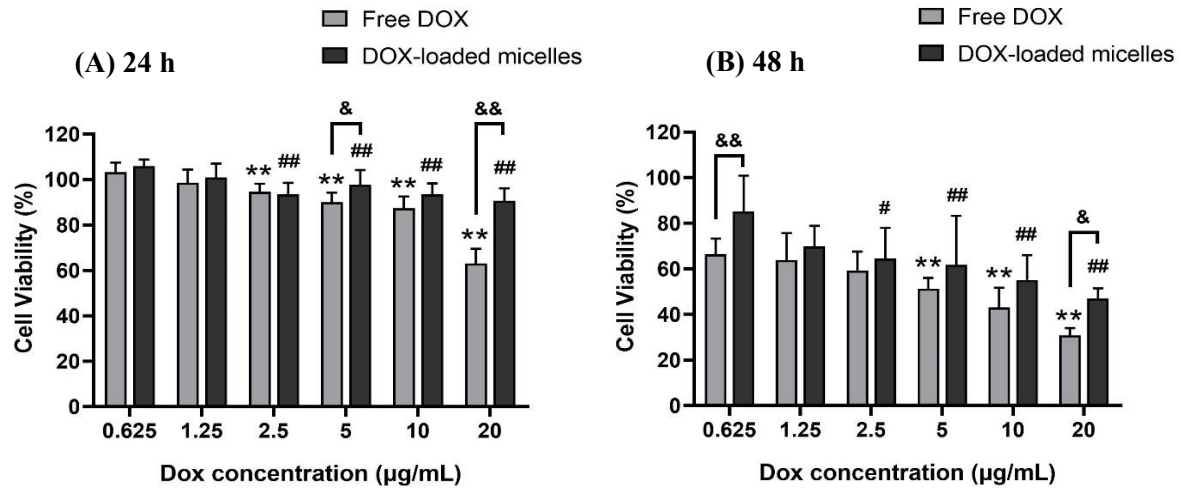


Figure S4.6. Effect of DOX-loaded PVS<sub>18-b</sub>-PNVCL<sub>35</sub> micelles on HEK 293T cell viability. HEK 293T cells were incubated with free DOX and DOX-loaded micelles for 24 h (A) or 48 h (B). Data were presented as mean  $\pm$  SD and obtained from three independent experiments. \*\* $p$ <0.01, comparing with DOX concentration at 0.625  $\mu$ g/mL (Free Dox group); # $p$ <0.05, ## $p$ <0.01, comparing with DOX concentration at 0.625  $\mu$ g/mL (DOX-loaded micelles group); & $p$ <0.05, && $p$ <0.01.

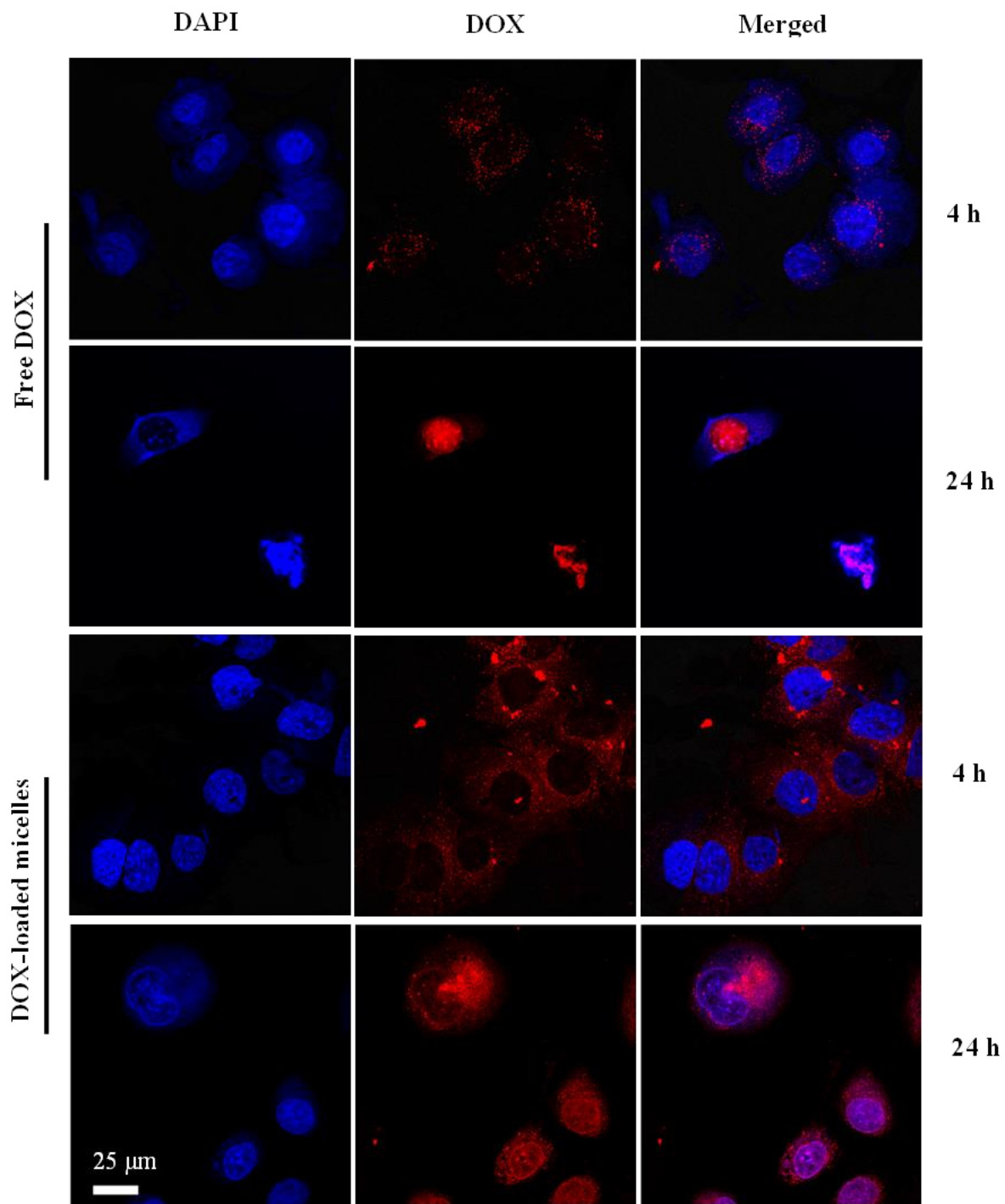


Figure S4.7. CLSM images (1000  $\times$ ) of HeLa cells treated with DOX encapsulated into PVS<sub>18</sub>-b-PNVCL<sub>35</sub> micelles and free DOX for 4 h or 24h.

## APPENDIX C: Supplementary Information of Chapter 5

### Supplemental Method 5.1. Synthesis of 3-(2-pyridinyldisulfanyl)propanol

The synthesis of 3-(2-pyridinyldisulfanyl)propanol was conducted following standard reported procedure with slight modification.<sup>35</sup> Briefly, in a 100 mL round-bottom flask, 5 g (22.7 mmol) of 2,2'-dithiopyridine, 0.33 mL of glacial acetic acid, and 30 mL of methanol were combined. Simultaneously, 1 g (11.2 mmol) of mercaptopropanol was dissolved in 4 mL of methanol and added dropwise via a syringe. The reaction mixture was stirred for 3 h at room temperature and the reaction progress was monitored by TLC (ethyl acetate/hexane:1/1, v/v). Subsequently, the reaction solution was concentrated using a rotary evaporator, resulting in a green oil. The crude product was purified by silica gel column chromatography, employing a gradient of 15-25% ethyl acetate in hexane for elution. This process was repeated twice to completely remove the impurities, specifically unreacted 2,2'-dithiopyridine. The final yield of the purified product was determined to be 57%.

The <sup>1</sup>H NMR spectrum (500 MHz, CDCl<sub>3</sub>, d, ppm) revealed characteristic peaks at 1.94 (pentet, 2H, C-CH<sub>2</sub>-C-O), 2.32 (broad, singlet, 1H, OH), 2.96 (triplet, 2H, S-S-CH<sub>2</sub>), 3.78 (triplet, 2H, C-CH<sub>2</sub>-O), 7.10 (multiplet, 1H, aromatic hydrogen meta to nitrogen), 7.63 (multiplet, 2H, aromatic hydrogens para to nitrogen and ortho to thiol derivatized carbon), 8.46 (quartet, 1H, aromatic hydrogen ortho to nitrogen).

### Supplemental Method 5.2. Synthesis of S-(2-Propionic acid)-O-ethyl xanthate (X1)

A solution was prepared by dissolving 2.2 mL of 2-bromopropionic acid (24.0 mmol) in 35 mL of dry anhydrous methanol. The resulting solution was then cooled in an ice bath.

Subsequently, 5 g of potassium ethyl xanthogenate (31.2 mmol) was slowly added to the solution over a 30-minute period with continuous stirring. After complete dissolution of potassium ethyl xanthogenate, the ice bath was removed, and the reaction was allowed to proceed at room temperature for 24 hours. Following the reaction, the mixture was filtered to eliminate the by-product KBr. The filtrate was then subjected to extraction using diethyl ether/ hexane mixture (2/1, v/v). The organic phase was washed three times with water and dried over anhydrous Na<sub>2</sub>SO<sub>4</sub>. The final product, a pale-yellow solid, was obtained after the solvent evaporation with a yield of 78%.

The characterization of the product by, <sup>1</sup>H NMR (300 MHz, CDCl<sub>3</sub>, d, ppm) revealed the following peaks: 1.41 (triplet, 3H, -CH<sub>3</sub>-CH<sub>2</sub>-), 1.60 (doublet, 3H, -CH<sub>3</sub>-CH-), 4.41 (quartet, 1H, -CH<sub>3</sub>-CH-S-), 4.65 (2 quartet, 2H, O-CH<sub>2</sub>-), 11.10, (broad, 1H, COOH).

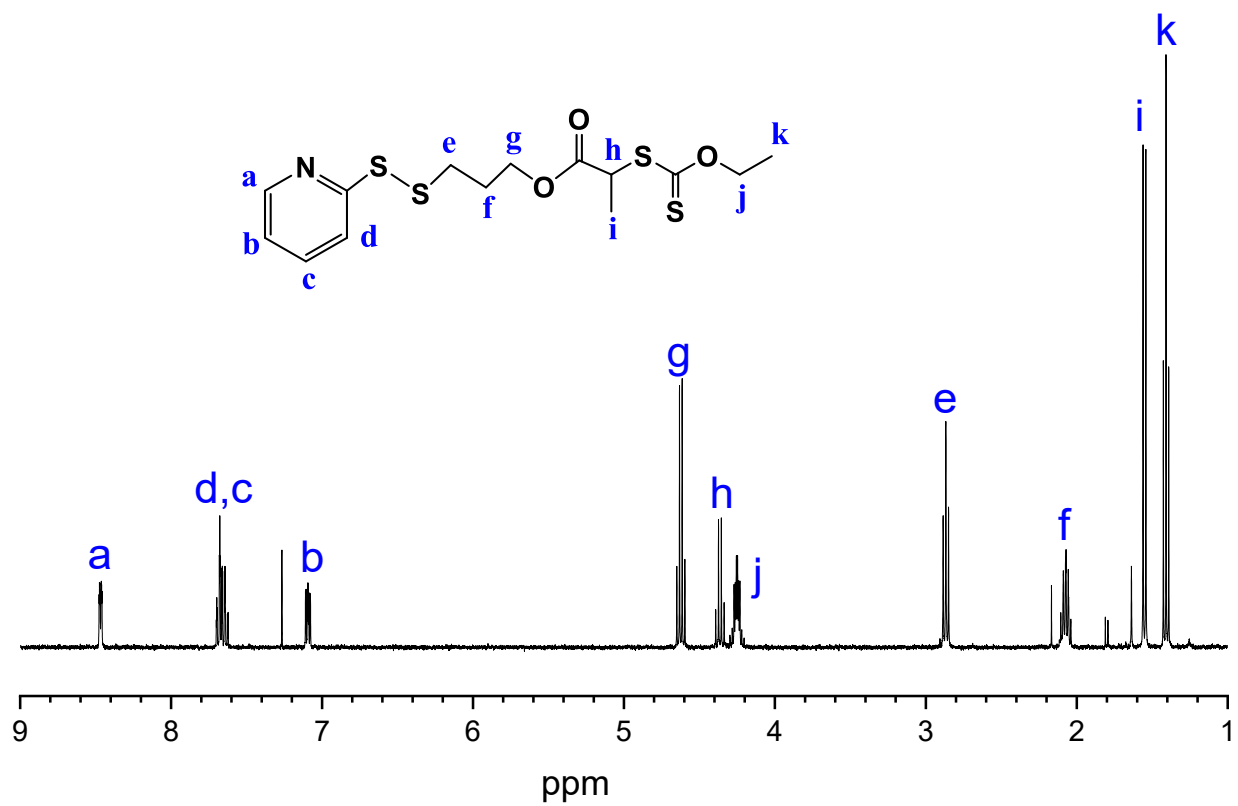


Figure S5.1. <sup>1</sup>H NMR spectrum of S-2-(3-(pyridin-2-yl)propyl) propanoate)-O-ethyl xanthate (X2)

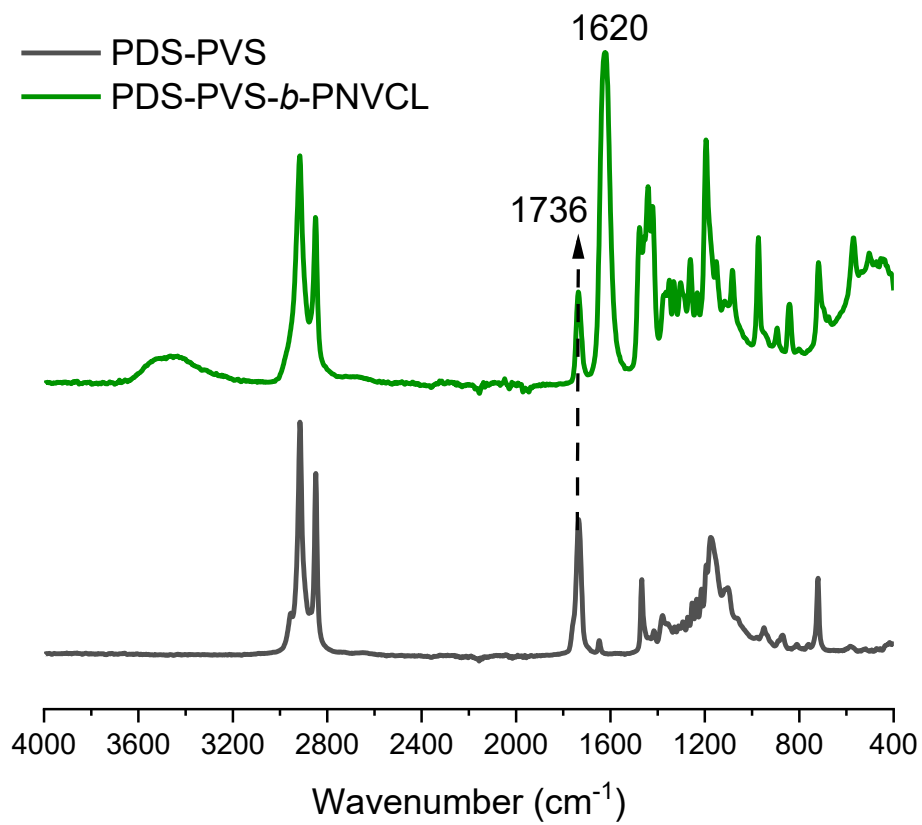


Figure S5.2. ATR-FTIR spectra of PDS-PVS and PDS-PVS-*b*-PNVCL

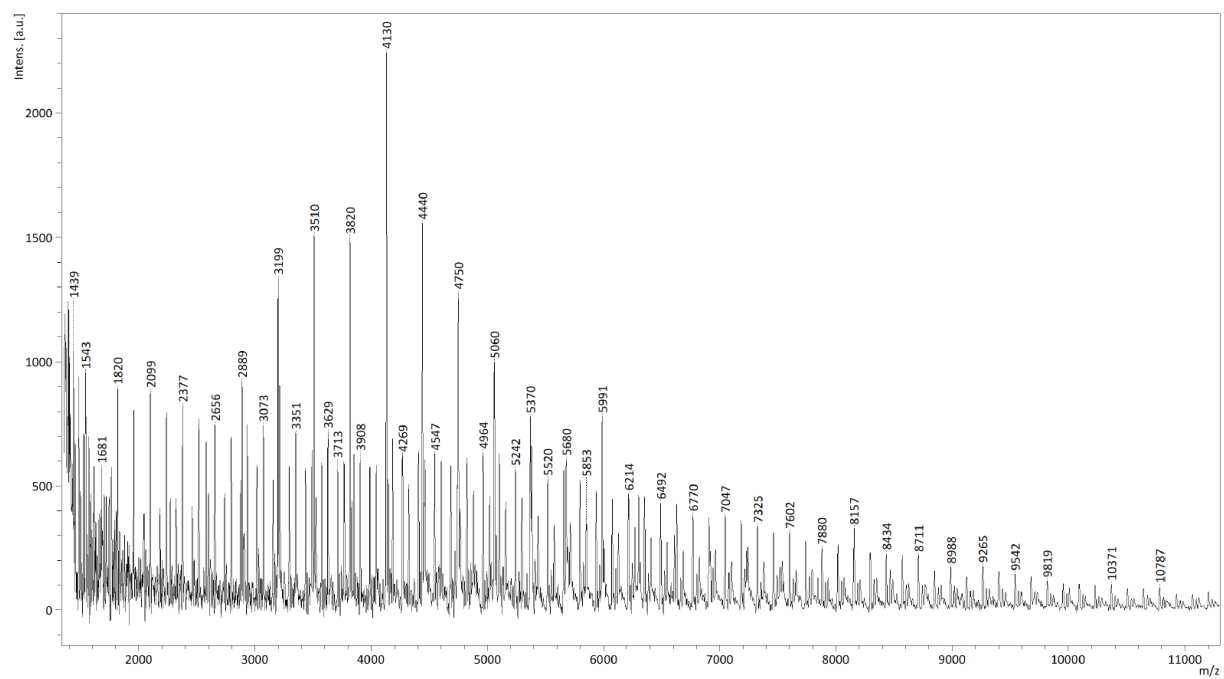


Figure S5.3. MALDI-TOF spectrum of PVS<sub>15</sub>-*b*-PNVCL<sub>55</sub>